Urban hierarchy and the analysis of spatial patterns : towards explicit fractal modelling

Kofi Bonsu

Urban hierarchy and the analysis of spatial patterns: towards explicit fractal modelling

Thèse de doctorat de l'Université Gustave Eiffel

École doctorale n° 528, École doctorale Ville Transports et Territoires – VTT

Spécialité de doctorat : Géographie

Unité de recherche : LVMT

Thèse présentée et soutenue à l'Université Gustave Eiffel, le 18/06/2024, par :

Kofi BONSU

Composition du Jury

Christiane WEBER Directrice de recherche CNRS, UMR TETIS, Montpellier	Président du jury/Rapportrice
Giovanni FUSCO Directeur de recherche CNRS, Université Côte d'Azur	Rapporteur
John ÖSTH Professor, Oslo Metropolitan University	Examinateur
Liu LIU Maîtresse de conférences, CY Cergy Paris Université	Examinatrice
Bernard KUMI-BOATENG Professor, University of Mines and Technology	Examinateur

Encadrement de la thèse

Olivier BONIN Chercheur HDR, Université Gustave Eiffel	Directeur de thèse

Declaration

I declare that this thesis is my own work. It is being submitted for the degree of Doctor of Philosophy in Geography in Université Gustave Eiffel. It has not been submitted for any degree or examination in any other University.

.....

Abstract

The thesis aims to explore the potential of empirical results in identifying urban centers and subcenters by utilizing built-up data extracted from freely-available remote sensing images and fractal analyses. It addresses the challenge of data unavailability in this context. While various methods have been employed in literature, such as minimum cut-off point, spatial statistical methods, and hedonic price method, these are predominantly based on the local context of developed nations, with limited studies focused on developing nations due to data scarcity. This research seeks to fill this gap by investigating the effectiveness of fractal geometry in explicitly identifying urban centers and subcenters, characterizing their spatial organization for urban growth analysis, and delineating urban growth patterns based on the spatial arrangement of urban centers, subcenters, and primary transportation networks. Understanding these dynamics is crucial for informed urban planning and infrastructure decisions. Using the Greater Accra Metropolitan Area (GAMA) as a case study, freely available satellite images spanning from 1991 to 2022 were downloaded and classified using various techniques including random forest, support vector machine, and simple linear iterative cluster (SLIC) with K-Means to extract built-up patterns. A longitudinal analysis was conducted to assess the impact of urban growth on biodiversity, revealing shifts in land cover composition with built-up areas increasingly dominating over vegetation, leading to habitat fragmentation. Land cover and landscape patterns for 2030 were successfully predicted, emphasizing the importance of landscape connectivity and habitat fragmentation in evaluating ecological processes and urban development impacts. Furthermore, multi-radial fractal analysis and mathematical morphology were employed to identify urban centers and subcenters from remote sensing data, based on fractal dimensions and spatial organization. A conceptual urban growth model was developed to visualize expected urban expansion patterns. These findings contribute significantly to the identification and spatial organization of urban centers and subcenters, particularly in cities lacking adequate statistical or geospatial data, espe-

cially in developing countries. Replicating this methodology could contribute to a more comprehensive global database on cities.

Résumé en Français

Introduction

Les villes sont des organismes dynamiques qui évoluent constamment pour s'adapter à des circonstances changeantes. Les centres et sous-centres urbains jouent un rôle crucial dans la croissance et le développement des villes. Ils offrent des opportunités économiques, des expériences culturelles et des interactions sociales qui enrichissent la vie des citadins. L'une des principales caractéristiques des centres et sous-centres urbains est la forte concentration d'activités humaines qu'on y trouve par rapport aux zones environnantes. Il est évident que les centres urbains et les sous-centres sont différents, mais ils sont similaires à certains égards. Les centres urbains sont des zones densément peuplées qui servent de pôles d'activités économiques, culturelles et sociales. Les sous-centres, quant à eux, sont des versions à plus petite échelle des centres urbains, situés en dehors du quartier central des affaires (CBD). Ils sont conçus pour offrir les mêmes avantages que les centres urbains, mais à un niveau plus local. Les centres urbains et les sous-centres offrent de nombreux avantages aux habitants et aux entreprises. En concentrant les activités économiques dans une zone plus restreinte, ces centres peuvent favoriser une croissance économique significative en offrant davantage d'opportunités d'emploi, en particulier dans des secteurs tels que la finance, la technologie et les soins de santé. L'amélioration de la qualité de vie des habitants constitue un autre avantage majeur des centres et sous-centres urbains. En donnant accès à une série d'équipements tels que des parcs, des restaurants, des centres commerciaux, des institutions culturelles, etc., ces centres et sous-centres offrent un cadre de vie plus vivant et plus attrayant aux résidents.

Mais on peut se demander pourquoi il est nécessaire d'identifier les centres et les sous-centres urbains?

L'identification des centres et sous-centres urbains peut aider à planifier un équilibre entre les emplois et les logements. Elle peut également aider à estimer la capacité

écologique des centres-villes. Un bon équilibre entre les emplois et les logements au niveau local permettrait de raccourcir le temps de trajet des travailleurs, de réduire les embouteillages, de diminuer la pollution atmosphérique et sonore due à la circulation automobile et d'améliorer le bien-être général des habitants. Ces éléments contribueraient grandement à rendre une ville plus durable. Deux approches principales sont généralement utilisées pour l'identification des centres et sous-centres urbains : l'approche morphologique et l'approche fonctionnelle. L'approche morphologique s'intéresse à la taille et à la distribution spatiale des centres et des sous-centres, tandis que l'approche fonctionnelle s'intéresse aux connexions entre les différents centres. Dans cette thèse, l'approche morphologique a été utilisée. Dans la littérature, plusieurs méthodes, telles que le point de coupure minimum, les méthodes statistiques spatiales et la méthode des prix hédoniques, ont été adoptées pour l'identification des centres et sous-centres urbains en utilisant des données provenant de diverses sources telles que les statistiques officielles, la télédétection et les systèmes de big data géospatiaux. Cependant, la plupart de ces études sur l'identification des centres et sous-centres urbains sont basées sur le contexte local des nations développées. Les études sur l'identification des centres et sous-centres urbains dans le contexte des pays en développement sont encore rares. Certains chercheurs expliquent cette situation par l'absence probable ou la disponibilité partielle de données statistiques officielles ou de big data géospatiales, telles que les POI et les inscriptions sur les médias sociaux, que les chercheurs peuvent utiliser pour identifier les centres et sous-centres urbains dans les villes des pays en développement.

Étant donné que les centres et sous-centres urbains se caractérisent par une forte concentration d'activités humaines par rapport aux zones environnantes, certains chercheurs ont fait valoir que les images de télédétection, l'imagerie nocturne et les enregistrements sur les médias sociaux pouvaient raisonnablement remplacer la population ou les activités humaines dans l'identification des centres et sous-centres urbains. En effet, grâce à la bonne résolution spatiale et temporelle des images de télédétection disponibles gratuitement, telles que Landsat et Sentinel, qui sont généralement la seule source de données spatialement cohérentes couvrant de vastes zones avec un niveau élevé de détail spatial et de fréquence dans la plupart des pays en développement, le problème des données inadéquates peut être résolu dans une certaine mesure. C'est dans ce contexte que cette thèse a exploré le potentiel des résultats empiriques dans l'identification des centres et sous-centres urbains en proposant une nouvelle approche qui utilise des données sur le bâti extraites d'images de télédétection librement disponibles; et des analyses fractales,

couplées à la morphologie mathématique pour traiter le problème de l'indisponibilité des données dans l'identification des centres et sous-centres urbains, en particulier dans les pays en voie de développement. Les questions de recherche suivantes ont été posées:

1. La géométrie fractale peut-elle être utilisée pour identifier explicitement les centres et sous-centres urbains et leur organisation spatiale à partir de données de télédétection?

2. Est-il possible de caractériser l'organisation spatiale des centres et sous-centres urbains au regard de l'objectif d'analyse de la croissance urbaine?

3. Est-il possible d'esquisser le processus de croissance urbaine à partir de l'organisation spatiale des centres et sous-centres urbains et de la localisation de la forme des principaux réseaux de transport?

Ces questions ont été posées parce que les objectifs de la thèse sont de:

1. Concevoir des modèles de croissance urbaine plus informatifs que les modèles en "tache d'huile"; et

2. Identifier les centres et sous-centres urbains et leur organisation spatiale à partir de données de télédétection uniquement en utilisant des fractales.

Zone d'étude

La région métropolitaine du Grand Accra (GAMA) a été choisie comme zone d'étude pour cette thèse. Il s'agit de la capitale administrative du Ghana, un pays en développement d'Afrique de l'Ouest, et de la principale ville économique du pays. En tant que capitale administrative, GAMA a bénéficié d'investissements considérables, tant publics que privés, dans le développement de ses infrastructures et de ses services. Grâce à ces investissements massifs, un ensemble d'activités économiques a prospéré dans la région, entraînant une augmentation de la population et une pression sur les ressources foncières à l'intérieur de la ville et à sa périphérie. Plusieurs études ont souligné les implications négatives de l'urbanisation incontrôlée dans la région GAMA sur l'environnement et les régions voisines. Cependant, à ce jour, aucune recherche n'a été menée pour identifier les centres et sous-centres urbains de la GAMA, malgré leur rôle central dans la facilitation d'une planification spatiale efficace, d'une allocation optimale des ressources, de l'avancement des infrastructures et d'interventions politiques ciblées visant à favoriser une croissance équilibrée et à améliorer la qualité de vie des résidents. GAMA étant la ville la plus grande et à la croissance la plus rapide du Ghana, un pays en développement

d'Afrique de l'Ouest, où il n'existe pas de données statistiques officielles adéquates pour l'identification des centres et sous-centres urbains, elle a été identifiée comme l'endroit idéal pour mener à bien ce travail. La réussite de ce travail permettra non seulement de combler le manque d'études sur l'identification des centres et sous-centres urbains dans les villes des pays en développement, mais aussi d'aborder la question de la non-disponibilité des données nécessaires à cette fin.

Classification des images satellites

La classification des images satellite est une technique de vision par ordinateur utilisée pour classer les pixels d'une image satellite dans leurs types d'occupation du sol respectifs sur la base de leur contenu visuel. Il existe deux types de classification : la classification supervisée et la classification non supervisée. La classification non supervisée est automatisée et ne nécessite aucune entrée de la part de l'utilisateur (hormis la spécification du nombre de classes). Cependant, la classification supervisée donne à l'utilisateur plus de contrôle sur le processus de classification, car l'utilisateur sélectionne manuellement les données d'apprentissage et les affecte à la classe appropriée. Cette méthode est plus robuste et permet généralement d'obtenir une plus grande précision que la méthode non supervisée. Afin de résoudre le problème de l'absence ou de la disponibilité partielle de données statistiques officielles pour l'identification des centres et sous-centres urbains, la classification d'images satellite librement disponibles a été utilisée pour préparer des cartes d'occupation du sol qui ont servi de données primaires pour l'identification des centres et sous-centres urbains.

Des images satellites librement disponibles de la zone d'étude pour 1991, 2002, 2013 et 2022 ont été téléchargées à partir du site web de l'United States Geological Survey (USGS). Le fichier de forme des limites de la zone d'étude a également été téléchargé gratuitement à partir d'OpenStreetMap. Goole Earth pro a été utilisé avec différentes combinaisons de couleurs pour créer des données de vérité terrain pour la classification supervisée. Certaines des bibliothèques python utilisées sont sk-learn, sk-image, gdal, numpy, geopandas et matplotlib. Fractalyse 3-0.8.1 a été utilisé pour déterminer les dimensions fractales des différents types d'occupation du sol, et Fragstats 4.2 a été utilisé pour calculer les métriques du paysage. Trois méthodes de classification d'images ont été comparées : Random Forest (RF), Support Vector Machine (SVM) et un hybride de Simple Linear Iterative Cluster and K-Means (SLIC K-Means). Random Forest et Support Vector Machine sont des méthodes de classification supervisée, ce qui signi-

fie que des échantillons d'entraînement ont été utilisés pour définir les différents types d'occupation du sol (végétation, bâti, transition et eau), contrairement à SLIC K-Means, où l'algorithme affecte automatiquement les pixels dans les différentes classes spécifiées par l'utilisateur.

La classification d'images est très orientée ; chaque projet a un objectif spécifique pour lequel la classification est effectuée. Cet objectif influence le type de méthode de classification d'images à utiliser, qu'elle soit supervisée ou non supervisée. Lors de la comparaison des méthodes de classification supervisée, la comparaison est souvent basée sur les scores kappa (c'est-à-dire une évaluation de la performance de la classification par rapport à l'attribution aléatoire de valeurs aux cellules). Le score de Kappa est compris entre -1 et 1. Une valeur de 0 indique que la classification n'est pas meilleure qu'une classification aléatoire, un nombre négatif indique que la classification est nettement moins bonne qu'une classification aléatoire, et une valeur proche de 1 indique que la classification est nettement meilleure qu'une classification aléatoire). Une valeur de 0,8 ou plus est généralement considérée comme une classification forte. Lorsque différentes méthodes de classification ont des scores kappa globaux similaires, il devient difficile de choisir l'une plutôt que l'autre.

Une nouvelle approche est proposée, une approche qualitative qui implique la mesure de caractéristiques supplémentaires représentant la forme des types de couverture terrestre classifiés. Ces mesures sont : la dimension fractale, la bordure totale et le nombre de taches. La dimension fractale est un indicateur du caractère lacunaire des types d'occupation du sol. Elle est comprise entre 0 et 2. Plus la valeur est proche de 2, plus le type d'occupation du sol est homogène, et plus elle est éloignée de 2, plus il est faiblement réparti. La lisière totale est une mesure du paysage qui est généralement utilisée en écologie du paysage pour quantifier les structures du paysage. Il s'agit de la somme de toutes les arêtes horizontales et verticales entre les cellules de différents types de couverture terrestre. Elle indique la quantité de détails capturés dans la classification de chaque type de couverture terrestre. Plus la valeur de l'arête totale est élevée, plus les détails ont été pris en compte dans la classification. Un patch peut être défini comme les quatre cellules les plus proches (c'est-à-dire les voisins horizontaux et verticaux uniquement) adjacentes à une cellule ou les huit cellules les plus proches (c'est-à-dire les voisins horizontaux, verticaux et diagonaux) adjacentes à une cellule. Contrairement à la comparaison quantitative basée sur les scores kappa, cette nouvelle approche est une comparaison qualitative basée sur la quantité de détails qu'une méthode de classification est capable de

produire. Il convient de noter que cette approche ne cherche pas à remplacer les mesures quantitatives existantes déjà utilisées, mais à servir de mesure supplémentaire pour aider les analystes à décider quelle méthode est la mieux adaptée à quel projet. Les scores kappa des classifications RF et SVM de GAMA 2022 étaient respectivement de 0,933 et 0,929. Il s'agit d'un scénario typique dans lequel deux méthodes de classification d'images produisent des scores kappa similaires, ce qui rend difficile le choix de l'une par rapport à l'autre. Nous allons donc un peu plus loin en les comparant sur la base de la forme des types d'occupation du sol classés en mesurant les dimensions fractales, le bord total et le nombre de parcelles des types d'occupation du sol classés. Il s'agit d'indicateurs que la précision globale et les scores kappa ne sont pas en mesure d'évaluer. En utilisant les cartes d'occupation du sol GAMA 2022, nous avons observé que les types d'occupation du sol identifiés par RF et SVM étaient très similaires. RF a généralement produit un plus grand nombre de patchs que SVM et SLIC pour tous les types d'occupation du sol. Une fois de plus, RF a produit des valeurs de bordures totales plus élevées que SVM pour tous les types d'occupation du sol identifiés. Cela indique que les cartes d'occupation du sol produites par RF sont plus détaillées que celles produites par SLIC K-Means et SVM. Pour l'objectif d'étude de la croissance urbaine, la RF a été choisie car elle est capable de capturer plus de détails.

Analyse longitudinale du paysage

La mesure de l'état de l'expansion urbaine est cruciale pour l'établissement d'une base de référence qui peut contribuer à des préparations appropriées pour les événements futurs. À l'aide des cartes de l'occupation du sol de la GAMA de 1991 à 2022, obtenues par RF, et de diverses techniques telles que l'analyse des changements de l'occupation du sol, la mesure métrique du paysage et le calcul de la dimension fractale, des informations extraites uniquement d'images satellite librement disponibles ont été utilisées pour réaliser une analyse longitudinale complète et fondée sur des données de la croissance urbaine de la GAMA, et de ses effets sur la biodiversité. L'objectif était de saisir les changements dans l'occupation des sols et les modèles de paysage dans la région GAMA entre 1991 et 2022 et de prédire les modèles de paysage pour 2030. La méthodologie mise en œuvre a été divisée en trois phases. La première phase consistait à analyser les changements de l'occupation du sol dans la région GAMA entre 1991 et 2022, et à déterminer le taux de croissance urbaine au cours de cette période. La deuxième phase, la modélisation de la croissance urbaine et la prédiction de l'occupation du sol de la GAMA pour 2030 en utilisant Land Change Modeler (LCM), Markov Chain Cellular Automata (MCCA), et

un modèle basé sur des agents implémenté dans NetLogo (ABM). La troisième et dernière phase a consisté à quantifier l'évolution des modèles paysagers dans la région GAMA en calculant des métriques paysagères.

Au cours de la première phase, l'étude a réussi à saisir les changements de la couverture terrestre et le taux de croissance urbaine de la région GAMA. Les résultats ont révélé une transformation significative de la composition de la couverture terrestre de la région, la couverture terrestre bâtie dominant désormais la couverture terrestre végétale qui était auparavant dominante. Un changement notable a été observé de la végétation à la transition, avec un pic de 2002 à 2013 et une stabilisation par la suite. Le passage de Transition à Bâti a connu une croissance constante, indiquant une conversion continue des zones de transition en couverture terrestre bâtie. À l'inverse, la tendance du passage de la végétation au bâti a diminué, ce qui suggère une réduction de la conversion des zones de végétation au fil du temps. Les changements de transition vers la végétation et de bâti vers la transition ont présenté des schémas variables, reflétant le dynamisme et l'incohérence. Dans l'ensemble, les changements de couverture terrestre de l'étude GAMA décrivent un paysage complexe et dynamique, avec des taux et des directions de transformation variés entre les différents types de couverture terrestre. L'analyse du taux de croissance urbaine a montré une augmentation de 0,15% (1991 à 2002) à 0,17% (2002 à 2013), puis une diminution à 0,14 % de 2013 à 2022. Un taux de croissance de 0,19% est prévu pour 2030. La fluctuation du taux de croissance entre 2013 et 2030 pourrait être attribuée à plusieurs facteurs dont l'identification nécessiterait une analyse approfondie. Malheureusement, une telle analyse exhaustive dépasse le cadre de cette thèse.

Dans la deuxième phase, le LCM a été utilisé pour modéliser et prédire la croissance urbaine de GAMA pour l'année 2030. Le score de kappa obtenu pour la prédiction était de 0,8, ce qui est un bon score. Elle présente également l'avantage de produire à la fois une prédiction douce, qui donne la probabilité ou la vraisemblance de chaque classe de couverture terrestre à un endroit ou un pixel donné, et une prédiction dure, qui attribue une classe de couverture terrestre unique et définie à chaque endroit ou pixel. L'automate cellulaire à chaîne de Markov (MCCA) combine la théorie de la chaîne de Markov et l'automate cellulaire, représentant les entités spatiales dans une grille et utilisant les probabilités de transition pour simuler la dynamique de la croissance urbaine. MCCA a été utilisé pour modéliser et prédire la croissance urbaine de GAMA pour l'année 2030. Le score de kappa obtenu pour la prédiction était de 0,83, ce qui est légèrement supérieur à celui de LCM. Cependant, contrairement au LCM, le MCCA ne produit pas

de prédiction douce et ne serait donc pas aussi utile que le LCM en cas d'incertitude dans les processus de changement de l'occupation du sol. Les prédictions douces permettent aux décideurs de comprendre le niveau de confiance associé à chaque classe prédite, ce qui facilite l'évaluation des risques et la prise de décision. En revanche, les prédictions dures sont souvent utilisées lorsqu'une classification spécifique et sans ambiguïté est nécessaire et que la capacité du modèle à attribuer avec précision les classes d'occupation du sol fait l'objet d'un niveau de confiance élevé. Cependant, ils peuvent ne pas saisir l'incertitude inhérente aux processus de changement de l'occupation du sol. Le modèle basé sur les agents, mis en œuvre dans NetLogo, offre une plateforme conviviale pour créer et observer le comportement des agents dans un environnement simulé, ce qui le rend polyvalent pour explorer les phénomènes émergents dans les simulations de croissance urbaine. L'avantage de ce modèle est que la simulation de la prédiction peut être analysée en temps réel grâce à ses puissants outils de visualisation intégrés.

Au cours de la troisième phase, l'étude s'est également penchée sur les structures paysagères de la région GAMA à l'aide d'indicateurs paysagers. Les métriques paysagères ont révélé une fragmentation importante du type de couverture végétale, indiquant un impact négatif sur la conservation de la biodiversité, les mouvements d'espèces, le fonctionnement des écosystèmes et la résilience écologique à long terme. En outre, l'étude a permis de prédire avec succès l'occupation des sols et la configuration du paysage de la région GAMA pour l'année 2030 à l'aide d'informations dérivées d'images satellitaires librement accessibles. Les tendances ont mis en évidence l'importance de prendre en compte la connectivité du paysage, la fragmentation de l'habitat et la disposition spatiale des types de couverture terrestre pour évaluer les processus écologiques et les impacts du développement urbain sur l'environnement. Il est essentiel de comprendre et d'identifier les zones à forte fragmentation pour hiérarchiser les efforts de conservation. Cette connaissance peut aider les planificateurs et les gestionnaires du paysage à prendre des décisions éclairées concernant l'aménagement du territoire, la restauration des habitats et les stratégies de conservation. En s'attaquant à la fragmentation dans la région GAMA et en favorisant la connectivité des habitats, il est possible de maintenir l'intégrité et la valeur écologique des paysages tout en soutenant la conservation de la biodiversité et la gestion durable des écosystèmes.

Identification des centres et sous-centres urbains

Sur la base de la définition des centres urbains comme des zones à forte concentration d'activités humaines par rapport aux zones environnantes, nous avions besoin d'une

mesure qui capturait correctement la concentration de la couverture terrestre bâtie. Certaines études utilisent la densité pour déterminer cette concentration, mais il a été observé que la densité peut conduire à des résultats trompeurs. L'urbanisation se caractérisant par des grappes de bâtiments entrecoupées d'espaces ouverts, les fractales constituent un descripteur idéal pour ce type de phénomène. En effet, les fractales possèdent des caractéristiques hiérarchiques inhérentes similaires aux modèles urbains. Elles sont donc bien adaptées pour capturer la distribution complexe observée dans les paysages urbains. Une forme fractale est une structure géométrique qui présente des détails quelle que soit l'échelle à laquelle elle est observée. Sur une carte bidimensionnelle, la dimension fractale est comprise entre 1 et 2. Il s'agit d'un objet qui est moins qu'un plan, plus qu'une ligne, et qui possède des éléments auto-similaires. Ainsi, une ligne a une dimension de 1, ce qui signifie que lorsqu'on la double, on obtient exactement le double de sa taille d'origine. Un carré plein a une dimension de 2, ce qui signifie qu'en le doublant, on obtient quatre fois sa taille d'origine. Que se passe-t-il donc lorsqu'une ligne s'enroule tellement qu'elle commence à remplir une surface, tout comme le carré, mais qu'elle n'est pas aussi solide que le carré solide parce qu'il y a des espaces à l'intérieur de la surface qu'elle a remplie? Nous ne pouvons pas dire que la dimension d'une telle ligne est 1, car elle occupe une surface dont la longueur et la largeur peuvent être déterminées. Nous ne pouvons pas non plus dire qu'elle a une dimension de 2, en raison des espaces dans la zone qu'elle occupe. On peut donc dire que cette ligne a une dimension comprise entre 1 et 2. La dimension d'un tel objet peut être beaucoup mieux décrite par la géométrie fractale que par la géométrie euclidienne. Plus la dimension est proche de 2, plus elle est saturée, et plus elle est proche de 1, moins elle est saturée. Cela peut être comparé à un modèle de construction extrait d'une image satellite classifiée, où divers groupes de bâtiments alternent avec des espaces vides, formant des centres et des sous-centres.

Deux méthodes de détermination des dimensions fractales ont été utilisées ici : la méthode de comptage des boîtes et la méthode multiradiale. La dimension fractale dérivée des méthodes de comptage de boîtes donne une idée globale de la manière dont l'espace est rempli dans une zone donnée. La zone bâtie est couverte par une grille uniforme composée de carrés de taille $\boldsymbol{S}$, et les carrés non vides, $\boldsymbol{N}$ (carrés qui sont complètement ou partiellement remplis par les pixels représentant la zone bâtie) sont comptés. La taille des carrés $\boldsymbol{S}$ qui forment la grille est modifiée progressivement et le nombre de carrés $\boldsymbol{N}$ requis pour couvrir la zone bâtie dans chaque scénario est déterminé. Les séries de points $\boldsymbol{(Si,\ Ni)}$ sont représentées sur un graphique à deux dimensions, où l'axe Y correspond

au nombre de carrés, ***Ni***, et l'axe X à la taille des carrés, ***Si***, qui changent tous deux à chaque étape. Il est donné par: $N = CS^{-D}$

La méthode de comptage des boîtes a été utilisée pour estimer la dimension fractale de la zone bâtie de GAMA pour 1991, 2002, 2013 et 2022 ; voici les résultats obtenus. En 1991, la dimension fractale était de 1,581, elle est passée à 1,687 en 2002, à 1,738 en 2013 et enfin à 1,777 en 2022. Considérant que sur une carte bidimensionnelle, la dimension fractale a une limite supérieure et une limite inférieure définies, avec un taux de croissance non uniforme, la croissance pourrait être modélisée par une courbe de croissance logistique. On estime que la limite maximale de la dimension fractale pour GAMA sera atteinte en 2232.

Il y a ensuite l'analyse fractale multiradiale. Elle est utilisée pour obtenir des informations sur le comportement fractal local et l'organisation spatiale autour d'un point sélectionné. Pour effectuer une analyse radiale, un cercle de rayon r est tracé autour du point sélectionné et le nombre de points N à l'intérieur du cercle est déterminé. Le rayon, ***r***, est progressivement augmenté tout en comptant le nombre de points, ***N***, à l'intérieur du cercle à chaque étape. Ensuite, les séries de points ***(ri, Ni)*** sont représentées sur un graphique à deux dimensions, où l'axe Y correspond au nombre de points ***(Ni)*** et l'axe X à la taille du rayon ***(ri)***, qui changent tous deux à chaque étape. La relation entre les deux variables est similaire à celle exprimée pour la méthode de comptage de boîtes, ***S*** étant remplacé par ***r***.

L'analyse multiradiale a été appliquée avec un rayon de 300 mètres et a généré des cartes dont chaque pixel est caractérisé par sa dimension fractale locale. Cela a permis d'obtenir des estimations correctes de la loi de puissance, même dans les zones peu denses, ce qui constitue une information importante à traiter pour révéler des structures spatiales significatives. Avec une taille de pixel au sol de 30 m, chaque analyse radiale locale a été effectuée sur environ 196 pixels, ce qui a permis d'estimer correctement chaque loi de puissance. Dans la présente étude, une classification manuelle des dimensions fractales locales a été adoptée, avec des seuils déterminés sur la base de l'avis d'experts. Les pixels du motif construit ont été regroupés en quatre classes en fonction de la dimension fractale de chaque pixel. Les pixels dont les dimensions étaient comprises entre 0 et 1,25 ont été classés au stade 1, car ils étaient considérés comme se trouvant au premier stade du processus d'urbanisation. Au stade 1, les constructions sont peu nombreuses et la couverture végétale prédomine dans la zone. Les pixels dont les dimensions fractales sont

comprises entre 1,25 et 1,5 ont été classés dans le stade 2, représentant la deuxième étape du processus d'urbanisation. Ce stade se caractérise par la transition entre le modèle de construction peu dense et la croissance urbaine, généralement le long des réseaux de transport, reliant les centres et les sous-centres. Les pixels dont les dimensions fractales sont comprises entre 1,5 et 1,75 ont été classés au stade 3. Ces pixels sont principalement situés à la périphérie des zones saturées, qui n'ont plus d'espace pour s'étendre, c'est-à-dire au stade 4. Les zones de stade 4 comprenaient des pixels dont les dimensions fractales étaient comprises entre 1,75 et 2. Ces zones sont les plus saturées et dominent dans les centres et sous-centres de la ville.

La morphologie mathématique offre des outils précieux pour l'analyse d'images, en particulier dans le contexte de la classification des images de télédétection. Cette théorie facilite la suppression des détails indésirables tout en conservant les caractéristiques essentielles de la forme. Son avantage réside dans l'utilisation d'opérations axées sur la forme, qui simplifient efficacement les données d'image. Les deux opérations fondamentales de la morphologie mathématique sont l'érosion et la dilatation. L'érosion consiste à retirer des pixels des limites de l'objet, tandis que la dilatation ajoute des pixels aux limites de l'objet.

Les pixels de niveau 4, c'est-à-dire les pixels dont la dimension fractale est comprise entre 1,75 et 2 pour chaque année (1991, 2002, 2013 et 2022), ont été extraits et traités à l'aide de la morphologie mathématique afin de mettre en évidence les centres/sous-centres urbains en éliminant les détails indésirables. Sur la base de la définition d'un centre/sous-centre urbain comme un lieu à forte concentration d'activités humaines, les zones présentant de grands groupes de pixels de niveau 4 ont été classées comme centres/sous-centres urbains. En utilisant les deux principaux noyaux urbains de la GAMA observés pour l'année 1991, Accra Metropolitan Area (AMA) et Tema Metropolitan Area (TMA) comme normes, les amas plus petits que ces centres ont été classés comme sous-centres, tandis que les amas plus grands ou égaux à ces normes ont été classés comme centres.

Conclusion

La présente étude a combiné avec succès des analyses fractales multiradiales avec des opérations de morphologie mathématique pour révéler les centres et sous-centres urbains qui étaient autrement cachés dans les modèles de construction extraits des images de télédétection. La modélisation de la croissance logistique des dimensions fractales et l'analyse de la région GAMA ont révélé qu'en moins de 10 ans, l'ensemble de la région est

susceptible d'atteindre le type de modèle urbain habituellement présent dans les centres-villes, tant en termes de densité que d'organisation spatiale. En outre, l'analyse fractale locale a révélé des changements significatifs dans la hiérarchie des centres et des sous-centres, avec l'émergence d'une grande région connectée le long du bord de mer et de centres secondaires situés de plus en plus loin au nord. Enfin, l'urbanisation le long des routes semble être le nouveau modèle émergent en ce qui concerne la saturation des terres. Le processus de remplissage de la croissance urbaine semble avoir atteint un point de saturation. Par rapport aux études précédentes dans ce domaine, cette étude apporte une contribution unique en intégrant des analyses fractales multiradiales à la morphologie mathématique pour identifier les centres et sous-centres urbains à partir d'images de télédétection uniquement. À ma connaissance, aucune recherche n'a été effectuée et publiée en utilisant la télédétection, les dimensions fractales et la morphologie mathématique pour identifier l'organisation spatiale des centres et sous-centres urbains. Les futures recherches sur la prévision de la croissance urbaine utiliseront toutes les informations structurelles extraites dans de nouvelles méthodes combinant des changements continus et des événements discrets, tels que l'émergence de nouveaux centres et sous-centres.

Mesurer l'homogénéité du développement urbain et identifier les centres et sous-centres urbains sont des étapes cruciales pour comprendre la croissance et le développement des villes. Cependant, l'identification de ces informations structurelles peut s'avérer difficile, en particulier dans les villes où la disponibilité des données est limitée. L'objectif de cette étude était de relever le défi de la disponibilité limitée des données dans l'identification des centres et sous-centres urbains en proposant une nouvelle approche qui utilise des données de télédétection librement disponibles et l'analyse fractale. Alors que plusieurs études antérieures se sont penchées sur la croissance et le développement urbains dans la région GAMA, la présente étude se distingue par le fait qu'elle se concentre spécifiquement sur l'identification des centres et sous-centres urbains à l'aide de fractales et de données de télédétection. Contrairement aux études précédentes qui ont pu utiliser des méthodes différentes ou se concentrer sur d'autres aspects de l'urbanisation, cette recherche visait à combler une lacune dans la littérature sur l'identification des centres et des sous-centres dans les villes des pays en développement et à fournir des informations plus complètes pour la modélisation de la croissance urbaine tout en relevant le défi de la disponibilité limitée des données. Pour combler cette lacune, seules des données de télédétection librement accessibles ont été utilisées pour identifier les centres et sous-centres urbains. La

méthodologie utilisée est facile à reproduire et ne nécessite pas une connaissance approfondie de la zone d'étude. Les résultats de cette recherche apportent des contributions significatives non seulement à l'identification mais aussi à l'organisation spatiale des centres et sous-centres urbains dans les villes qui ne disposent pas de données statistiques adéquates telles que le recensement de la population, les données économiques ou les big data géospatiales, en particulier dans les pays en voie de développement. La reproduction de la méthodologie utilisée permettrait de contribuer à la constitution d'une base de données solide et complète sur les villes du monde.

Acknowledgements

I wish to express my deepest gratitude to all who contributed to the successful completion of this thesis.

First and foremost, I extend my heartfelt appreciation to my supervisor, Prof. Olivier Bonin. His unwavering support, invaluable guidance, and insightful feedback have been foundational throughout this journey. His mentorship shaped not only the trajectory of my research but also nurtured my growth as a scholar. I am profoundly grateful for his expertise and dedication, without which this thesis would not have been possible.

I am deeply thankful to all members of the Laboratoire Ville Mobilité Transport (LVMT), especially Angèle Brachet, Xavier Lehmann, Alberica Bozzi, Maya El Khawand, Léa Zachariou, and Lucile Bauchard. Your warm welcome, friendly atmosphere, and supportive environment have been invaluable since I joined in December 2020. Your kindness and support have made this journey memorable, and I will always be grateful.

My heartfelt appreciation goes to my friends and colleagues who stood by me, offering encouragement and moral support during challenging times. Special thanks to Raphael, Sercan, Zofia, Miriam, Nethra, Zaheer, Katja, Michelle, Anique, Luc, and Chloé. Your belief in me has been a constant source of motivation, lifting my spirits when I needed it most.

I extend my deepest gratitude to my family for their unconditional love, encouragement, and understanding throughout this journey. Your steadfast support has been my rock, providing me with the strength to persevere.

Finally, I dedicate this thesis to my dear father, Dr. George Bonsu. Your guidance, wisdom, and sacrifices have been a solid source of inspiration. Thank you for always believing in me and for being my guiding light. This achievement is as much yours as it is mine.

Contents

List of Figures

List of Tables

Chapter 1

Introduction

1.1 Background

Cities are market places, and thus central for economic development, but also host essential functions linked to residential, health, education, culture, among many others. They are the most dominant mode of housing on earth, and it is predicted by the United Nations (UN) that by 2050 70% of the world's population would live in cities. This could be attributed to factors such as changes in economic structures, rural exodus, uniformity of lifestyles, etc. [151, 63]. The growth of cities, i.e. urbanization, is the key to modernization, economic growth, and development of any country, however, it also affects the livelihoods of people and the environment. Recent studies have shown a strong correlation between physical growth of cities and ecological consequences [128, 77].

The high rate of uncontrolled urbanization which is being experienced all over the world has given rise to increased automobile travel and congestion, elevated levels of pollution, loss of farmlands, duplicative infrastructure at high cost to society, limited employment accessibility and concentrated poverty [77, 76]. However, since urbanization is inevitable in the economic development of any country, especially, when one considers the several benefits that are associated with it such as: convenience, efficiency, economic improvement, better social integration and overall improvement in the standard of living of inhabitants, it is essential that efforts are made to make the urbanization process sustainable. This is because the benefits of urbanization such as the social and economic development of a country can only be achieved if the positive effects far outweigh the negative effects [79, 110, 52]. As urbanization occurs, more often than not, the functions of urban areas become different from what they were originally planned to be. These changes increasingly

put pressure on the natural environment as well as human welfare; and this is a major global concern [128, 110]. It is therefore very prudent to have an in-depth understanding of the changes that occur in the functions of urban areas that lead to urban growth. This would be beneficial for effective urban development planning, natural resources allocation and ecosystem management [62]. To understand the changes in the functions of urban areas, an appreciation of the structure of the urban area and its evolution is vital.

There are at least three main forms of urban growth: infilling, extension and leapfrog. Infilling refers to new developments in areas that were previously unused or being re-developed to new uses within an urban area. Extension refers to developments directly adjacent to existing urban areas. Leapfrog refers to new developments occurring at a distance from an existing urban area, bypassing vacant parcels located closer to already urbanized areas. Monitoring urban growth, studying it, and understanding the dynamics associated with it is an important step in appreciating the urban structure of any city. Unfortunately, monitoring urban growth is not an easy task because the concept of city itself is not so clearly defined. Since many countries lack adequate statistical systems which provide information on population, employment or mobility, which can be used to study urban growth, landuse and land cover information derived from satellite imagery (remote sensing) is the only dependable data source for urban growth analysis in such countries. Landcover, i.e., the way land is occupied (buildings, roads, forests, pastures, etc.) is only a characteristic of urban development, and is partly correlated with landuse, i.e., the way land is used by humans and ecosystems (populations, employment, mobility, ecosystemic services, etc.).

Analyzing urban growth from satellite images requires first to extract landuse/landcover information, and then model the arrangement and evolution of the urban patterns. This is what is performed in several landcover databases such as Corine Land Cover, an European database created by human photo interpretation of remote sensing images, and contains several classes describing urbanization, or in the Urban Atlas, constituted with similar techniques but focusing only on cities. However, these databases are expensive to produce, they do not cover the entire world, and they provide little information on the way cities are structured. For instance, they lack explicit information on how a city center is spatially connected to suburban areas and to industrial areas. Nevertheless, the capacity of a city to withstand further development depends on its structure. The 11th goal of the UN sustainable development goals is to make cities and human settlements inclusive, safe, resilient and sustainable. A sustainably developed city would provide access to utility

services, energy, transportation, housing, and green public spaces for all, while minimizing resource consumption and negative environmental impacts [17].

Geographic information system (GIS) and remote sensing have been successfully incorporated in urban modelling processes and have improved the analytical capabilities of GIS techniques as well as provided modelers with a platform for data management and visualization [92, 110]. Remote sensing provides a rich source of spatially consistent data that covers large areas with both high spatial detail and frequency. With the availability of remote sensing data coupled with GIS techniques, various land covers such as settlement, industrial, recreational and agricultural can be identified. The morphology of an urban area refers to the main physical elements that structure its shape and size. Using GIS and remote sensing to model the morphology of an urban area, certain key concepts in spatial analysis, such as: boundary (to define the extent of the study area); density (number of built-up pixels per area); centrality (identification of large clusters of built-up pixels); and proximity (the distance between built-up clusters) are used to formalize the concept of urban morphology. The morphological evolution of a city can therefore be observed on a remotely sensed image as a sprawl, i.e., growth towards the peripheries of the city, leapfrog or as densification, i.e., space filling within the boundary. By performing a land cover change analysis using historical data from remotely sensed images, metrics such as the rate of urban growth (to determine the speed of the urban growth), the evolution of fractal dimension over the years (to have an idea of how space is being filled in the growth process) and the conversion of non-urban land cover types to urban landcover can be calculated. Urban growth trends can also be studied to identify the possible social processes that led to such growth. Armed with this knowledge, policymakers can make well informed decisions when putting in measures to direct future development towards sustainability, especially, where there is inadequate statistical data to provide vital information for decision making [53]. Consequently, remote sensing has been used extensively in mapping urban areas and as a data source for the analysis and modelling of urban growth and land cover change [69, 128, 121, 122]. The challenge, however, is that at a city scale it becomes quite difficult to use classical image classification techniques to explicitly identify different urban structures [30]. This thesis makes the hypothesis that, to be effective and informative to policy makers, the analysis and the simulation of urban growth from remote sensing data requires an explicit modeling of urban structures. This explicit modeling needs to be across scales, and simple enough to be adapted to different contexts of urbanization.

Cities are not just randomly distributed buildings and people in a defined area. There is some kind of uniformity, an inherent structure, in the way various land uses are arranged and function in a city. The spatial arrangement of the functions of an urban area is referred to as its urban structure. Although every city is unique in its own way, there are some fundamental similarities in the way cities are structured all over the world. This has made possible for the application of the several models that have been developed over the years to help in understanding the urban structure of cities and their evolution in different urban settings.

Some of the most popular models are:

i. the concentric ring model by Burges (1925) - it is made up of a series of concentric circles that vary in size and expand away from the city center. Burgess used this model to describe how different social groups are located in a metropolitan area. **Figure 1.1** is an image of the concentric ring model.

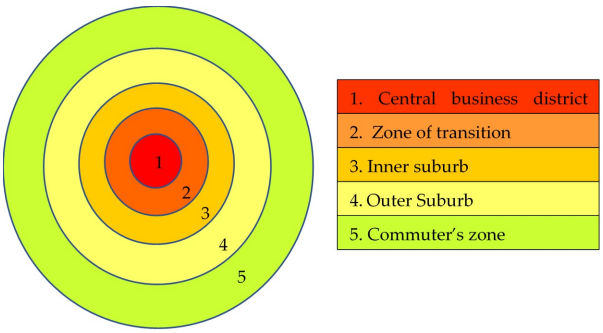

Figure 1.1: Concentric zone model

The innermost circle (1), around which the city grows, the urban core, is known as the central business district (CBD). There are usually only a few residential activities in this zone because of the high commercial activities concentrated there. The second circle (2), transition zone, has mixed residential and commercial characteristics. Because of the proximity of this zone to the CBD, it is continuously experiencing changes due to the expansion of businesses in the CBD. The third circle (3), inner suburb, is also known as the zone of independent workers' home. It is purposely for residential activities as it consists of houses built to accommodate workers, but it has better conditions than the transition zone. Also, it is mostly occupied by single workers. The fourth circle (4), outer suburb, also known as the zone of better residences, has bigger and better housing and developmental facilities. It is mostly occupied by the middle class. Unlike the inner suburb which is mostly occupied by single workers, the residents of the outer suburb are mostly families.

Although there are better facilities available to residents in this zone, such as: parks, open spaces, shops, large gardens, etc., there is an increased commuting cost to the CBD. People who live in this zone appear to have better standards of living. The outermost circle (5), known as the commuter's zone, is the farthest from the CBD. It has the highest commuting cost and lacks public transit options as compared to the other zones, hence its name, "commuter zone". This zone is mostly occupied by the high class, i.e. the highest income group in the society that can afford the high commuting charges, bigger houses, alternative modes of transportation, modern facilities and the highest standards of living to enjoy better quality of life. This ring results in urban expansion. As time passed by and urban areas became more and more complex, the concentric ring model could no longer define the development of existing cities due to limitations such as:

- the ability of many CBDs to exist in a city;
- the non-existence of distinct boundaries that define urban zones. In reality, there are overlaps in the zones in every city;
- political and government interference which can tailor urban growth in a particular direction for better living conditions; and
- as transportation and communication technology advanced, the way people commuted changed and the preference of people living in particular zones also changed.

Nevertheless, it still gives a simplified and generalized insight into the development of cities.

ii. the sectorial model by Hoyt (1939) was built on the basis that the development of cities were not in the form of simple rings as described by Burges (1925), rather, they do so in the form of sectors which grow along the main travel links. Transport routes were very important in the development of urban land use for Hoyt. In the Hoyt's model, activities within a sector were assumed to be the same throughout the sector because of the function they served. This assumption was based on the notion that land use within a sector would remain the same because similar functions attracted one another, i.e., the high class sector would remain high class throughout because it would be the most sought after sector to reside, which would make it expensive, such that, only the rich could afford to live there. The industrial sector

would also remain industrial throughout because of the strategic advantage of a railway or a river. Hoyt's model has five components: the central business district (CBD), factories/industry, low class residential, middle class residential and high class residential.**Figure 1.2** is an image of the Hoyt's sector model.

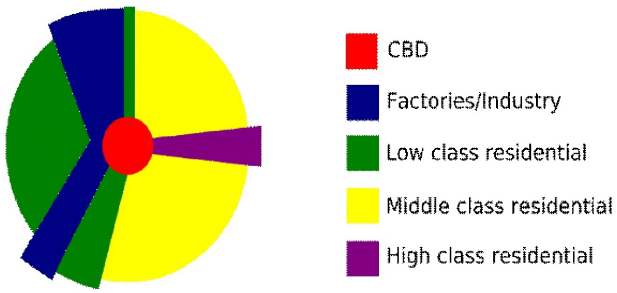

Figure 1.2: Hoyt's Sector Model

The CBD is the located geographically at the center of the city, and it is characterized by high rise buildings. It represents historic growth of many generations, city development and culture. Factories/industries are represented in the form of sectors radiating out of the center. This is so because of transport networks along which the activities emanate. Low class residential sector is where the low-income groups reside. In this sector, roads are narrower and often connects to the industries where most of the people work. They choose to live in this sector because of the proximity to their workplace, which translates into lower commuting cost and high air and noise pollution. The middle class residential sector is a spacious, green and clean environment. Middle income groups who can afford relatively higher commuting cost and prefer better living conditions reside in this area. The activities of the people who reside here are mixed, and are not dominated by the industry as the low class residential sector. The roads connects mostly to the CBD along with some branches to the industries. The high class residential sector is the most desirable part of the city. Wealthy people and people who are well-off reside in this area. The area is clean, there is less traffic, quiet and has bigger houses. The best housing in the city can be found in this sector and the road network leads to the CBD. In as much as Hoyt's model represents urban growth to some extent and builds on the concentric zone model, there are still limitations such as:

- multiple CBDs were not represented;
- physical features may restrict direct growth of the sectors; and

- only railway lines were considered, as there were no room for privately owned cars or other modes of transportation in the model.

iii. independently from the two previous models, the central place theory by Christaller (1933) explains why urban centers are geographically located where they are and how they serve the surrounding smaller settlements (subcenters) with specialized goods and services. It makes the assumption that: all areas have flat surfaces; population and resources are evenly distributed; consumers have similar purchasing power and would purchase at the nearest market; transportation cost is proportional to travel distance; and there are uniform travel networks that allow transportation from one settlement to the other. These assumptions were used to create a place where different types of services, i.e. higher order and lower order services, were offered. Basic services such as groceries were considered to be lower order services whereas specialized services such as universities were considered to be higher order services. Consequently, settlements that provided lower order services were said to be lower order settlements and settlements that provided higher order services were said to be higher order settlements. The services, whether higher or lower order, were distributed on the basis of a population threshold. This is because a minimum number of people were required to sustain a particular service. Although the central place theory is widely appreciated, it has certain limitations such as: the unrealistic nature of its assumptions. Resources are never equally distributed, people do not have the same purchasing power, and it is highly impossible to have a large flat terrain in reality. **Figure 1.3** is an image depicting the rank order of the central places.

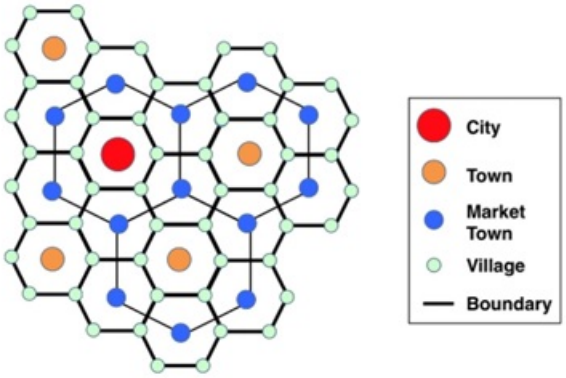

Figure 1.3: Rank order of central places

iv. the multiple nuclei model by Harris and Ullman (1945), explained that contrary to the monocentric models developed by Burgess (1925) and Hoyt (1939), cities grow

and evolve based on the presence of multiple nuclei or centers of activity rather than a single CBD. This is a widely accepted model since it is much more applicable to modern cities than the previous models. It suggests that cities have multiple specialized nuclei or activity centers, each with its distinct functions and land use patterns. These nuclei interact and evolve based on transportation networks, accessibility, and economic dynamics. Unlike the traditional concentric zone model, this theory acknowledges that cities adapt and change over time, with various nuclei driving growth and development. It offers a more flexible framework for understanding the complexity of urban land use and the interactions among different city elements, fostering a richer and more accurate portrayal of urban structure and evolution. The urban activities listed under this model are: CBD, light manufacturing, low-class residential, upper-class residential, heavy manufacturing, outlying business district, residential suburb and industrial suburb. In this model, while some business activities are attracted to other businesses, others try to avoid some businesses, and some similar activities also form clusters in particular areas. Although the multiple nuclei model was considered better than the previous models, it also has its limitations since it could not be applied to many cities; and did not entirely explain the structure of urban areas. **Figure 1.4** is an image of the multiple nuclei model.

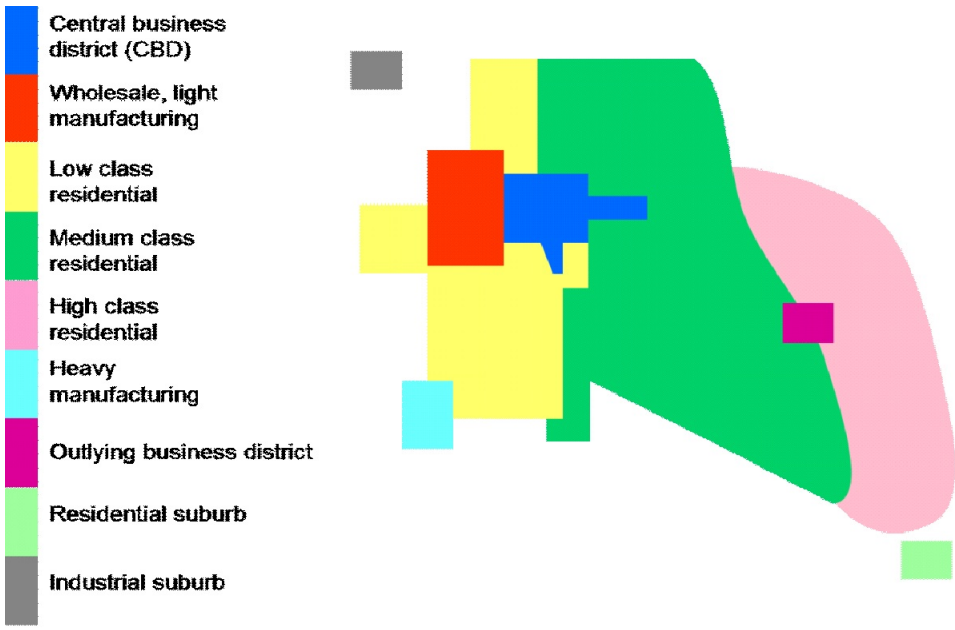

Figure 1.4: Multiple Nuclei Model

Cities typically start with a central hub where administrative, religious, economic, and educational functions converge in their early development. Over time, this central area,

often referred to as the central business district (CBD), can shift away from its historical core, evolving into a focal point for administrative and economic activities. This CBD is intricately connected to the surrounding suburbs, where residents live and commute to the center for their daily needs. When a city revolves around only one such center or CBD, it's termed a monocentric city. However, as economic growth and population swell, the central core of a monocentric city can expand, giving rise to new suburban settlements. These suburbs, in turn, develop their own centers as businesses naturally spring up nearby, catering to the needs of the local residents. This localized service provision not only reduces commuting expenses but also strengthens the link between the suburbs and the primary center. This phenomenon leads to the emergence of polycentric urbanization, where multiple centers take shape and grow into conurbations. While earlier urban development typically followed a monocentric pattern, the current trend is leaning towards polycentricity. This shift occurs as smaller neighboring settlements naturally integrate into expanding cities. Urban geographers are avidly studying this trend, employing various approaches to gain deeper insights into this evolving urban landscape.

Kloosterman and Musterd [78] were concerned with the diverse views on the concept of polycentrism based on the backgrounds of practitioners. They stated that while spatial planners had a particular way of looking at it, human and economic geographers also had another way of looking at it. Volgmann and Munter [141] were particularly interested in how urbanization externalities, i.e., size, density and diversity, take effect in German polycentric urban regions and how they influence the growth of metropolitan functions. Wang [144] examined the relationship between polycentricity and the provision of urban amenities by asking questions such as: whether polycentric cities provided more quantities of urban consumption amenities. The research concluded that a higher degree of intra-urban polycentricity is associated with a larger number of urban amenities.

There are conflicting views on the impacts of polycentricity on the society. Some studies claim that it is advantageous to the society because socioeconomic competitiveness and environmental sustainability are associated with polycentricity. This is because there is strong correlation between increased levels of productivity, per capita income and urban size. Again, the expansion of spatial layout could ease congestion, reduce environmental pollution, control pricing of houses, reduce the frequency of crime occurrences and increase urban vibrancy. On the other hand, certain studies also suggest that it is not so advantageous because of the poor developmental foundation of these newly formed centers, the lack of infrastructural facilities and the lagging behind of public services. All these factors

reduce the attraction of highly skilled labor in newly formed centers [145, 93]. In order to have an in-depth understanding of the advantages and disadvantages of polycentricity, there should be a system to facilitate its identification for it to be easily studied. Identifying and studying it would enable city/urban planners to make the most out of the positive impacts and reduce its negative impacts. Studying the causes of the formation of centers and subcenters in a city, the sizes of these centers and subcenters, their locations, and how they relate with one another, will provide a clear and detailed understanding of the spatial structure of the city [78, 147, 91]. The knowledge obtained will serve as a reference for a rational and optimized urban development model [145].

There are two perspectives when it comes to the identification of centers and subcenters, functional or morphological [88, 154]. From the functional perspective, centers and subcenters are identified by the mobility of people, exchange of goods and services, communication and cooperation from one location to the other within the city [83]. This requires the collection of data that represents the connections and interactions between different spatial units in the urban system. This kind of data is however difficult to obtain with good quality. Some researchers have used diverse data sources such as GPS data from taxis, check-ins on social media and knowledge cooperation among different urban units in a given urban system [106, 34, 145]. For example, Roth et al. [123] used data collected from the Oyster Card, an electronic ticketing system used to record public transport passenger movement and fare tariffs within London to reveal the polycentric structure of the city. The morphological perspective also focuses on the size and spatial distribution of urban areas in the identification of centers and subcenters [93, 120]. Census and socioeconomic statistical data have been used in certain studies to determine morphological centers and subcenters. Unfortunately, statistical data can only depict urban distribution to a certain spatiotemporal scale and are often limited to administrative boundaries. This leads to modifiable areal unit problem (MAUP) which results in questionable identification of urban spatial characteristics [145]. Burger and Meijers [33] explored the relationship between morphological and functional polycentricity and concluded that most cities are more morphologically polycentric than functionally polycentric, using Netherlands as a case study.

1.2 Problem Statement

In modelling built-up areas, traditional measures used in urban planning considers built-up areas as homogeneous surfaces, which are not so, because in reality, built-up areas exhibit some kind of continuity and fragmentation as diverse clusters of buildings alternate with empty spaces, forming centers and subcenters with different levels of "densities" [27, 57, 31]. In the field of spatial analysis, density as a measure is not able to adequately capture the spatial distribution of elements in space. For example, **Figure 1.5** [31] is an image depicting areas of the same size and of the same density but having different spatial distributions.

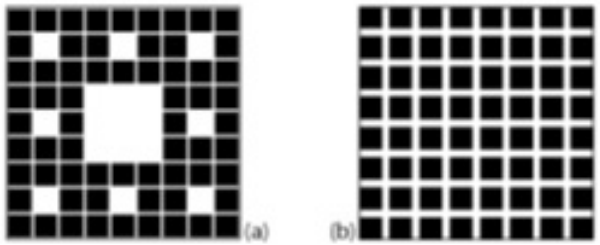

Figure 1.5: a and b have the same density but different mass distributions

Even though **Figure 1.5** shows different blocks with the same density, it is clear that the spatial distribution of the elements in both cases are different.Therefore, relying solely on the density measure is not sufficient, particularly when the spatial distribution of elements in space is integral to understanding the phenomenon under study. When this is related to the morphology of built-up areas, it is evident that such complex forms that result from the heterogeneity existing in the spatial distribution of urban activities are characterized by alternating patterns of continuity, fragmentation, and varying degrees of concentration. The same can be observed on any land use map, demonstrating that the density measure alone cannot be used to suitably describe such complex forms since it does not consider the spatial distribution of elements in the built-up pattern. Such complex forms may, however, be described using fractal dimensions due to the inherent hierarchical features of fractals that are also exhibited in urban patterns [59, 102, 73].

Fractal measures have been used for a long time to characterize urban forms, with Batty [27] and Frankhauser [56, 59] known for pioneering this field of study, among others. Since then, the approach has developed further, although limited to the academic sphere. According to McAdams [103], this could be because the application of fractal methods in investigating actual urbanizations is a complex process, which results in conflicting measurements in certain instances. Nonetheless, fractal analysis has been recognized as

a relevant method for analyzing urban forms [26]. The idea of this thesis to use remote sensing data and GIS techniques to: measure the phenomenon of urban growth by finding suitable methods and indicators to put this phenomenon into evidence from the data; characterize the phenomenon by giving indicators to help understand its extent, its pace, its homogeneity, its direction, etc.; interpret the phenomenon by introducing meaningful concepts that are not directly present in the data, such as the city center, fringes, etc.; typify the phenomenon by raising the level of generality of the analysis by proposing mechanisms, regularities in the process itself, etc.; and finally, model the phenomenon. This research aims to come up with novel techniques to explicitly classify remotely sensed data at a city scale for the purpose of urban modelling. Particular attention will be paid to the analysis of the urban hierarchy in centers and sub-centers, as well as to the spatial organization of these elements. The semantic analysis of urban patterns will eventually make it possible to model them with a multi-scale primitive such as fractals.

1.3 Research Questions

The research questions this thesis seeks to address are:

i. can fractal geometry be used to explicitly identify urban centers, sub-centers and their spatial organization from remote sensing data?

   So far, fractal geometry has been used to estimate the fractal dimension of cities by analysis of the spatial distribution of buildings [130, 39] to develop multiscale cellular automata [134], or to support land planning design [57]. In this thesis, the idea is to use the fractal decomposition used in the computation of dimensions to identify urban hierarchies and help to add structure to patterns obtained by classification of remote sensing imagery;

ii. is it possible to characterize the spatial organization of urban centers and sub-centers with respect to the objective of analyzing urban growth?

   Most urban growth models focus on the consumption of natural and agricultural areas by the urbanization process, leading to the ubiquitous urban sprawl model where a city is an oil stain that diffuses everywhere. These models are created mainly because of the lack of information on the structure of cities. Explicit fractal models should enable the proposal of fractal growth models in which cities do have differentiated functions; and

iii. is it possible to sketch urban growth processes based on the spatial organization of urban centers and sub-centers and the localization of the shape of the main transport networks?

Sketching the urban growth process in a simple and generalized manner would facilitate the communication of findings, especially, to non-technical audience.

1.4 Objectives

The objectives of this thesis are to:

i. design urban growth models that are more informative than "oil stain" models; and

ii. identify urban centers, subcenters and their spatial organization from only remote sensing data using fractals.

1.5 Methodology

The methodology used in this thesis are:

i. identification of classification algorithms that can adequately classify built-up and non-built-up areas for the analysis of urban growth;

ii. longitudinal analysis of urban growth;

iii. fractal analysis of urban patterns; and

iv. identification of centers and subcenters.

1.6 Significance of Thesis

Urban centers and subcenters are very significant in the future development of any city [106]. They are essential policy tools in the decentralization of population and improving standards of living with better environmental quality [147]. Identifying urban centers and subcenters is important because it helps in planning jobs-housing balance and the ecological capacity of city centers [147]. Proper local jobs-housing balance can shorten commuting time for workers, reduce traffic congestion, decrease air and noise pollution caused by automobile movement, and improve the overall well-being of inhabitants [89]. It also helps in better understanding urban expansion and provides town planners with in-

formation needed to evaluate effectiveness of planning layouts [34]. Unfortunately, there is not enough studies on the identification of urban centers and subcenters of cities in developing countries as most studies on the topic are based on the local context of developed countries [154]. This could probably be due to the lack or partial availability of official statistical data or geospatial big data such as POIs and social media check ins that have been used by several researchers in identifying urban centers and subcenters [101, 94].

To bridge this gap, this thesis rely on only freely available remote sensing data, which is usually the only source of consistent spatial data that covers large areas with high spatial detail and frequency in most developing nations, to identify urban centers and subcenters. The methodology used is easy to replicate and it does not require one to have ample knowledge of the study area. The findings in this research provides significant contributions to not only the identification but also the spatial organization of urban centers and subcenters in cities that do not have adequate statistical data such as: population census, economic data or geospatial big data, especially in developing counties. Replication of the methodology used would help contribute to a robust and comprehensive database on the cities in the world.

Compared with previous studies in this field, this thesis makes the unique contribution of integrating multiradial fractal analyses with mathematical morphology to identify urban centers and subcenters from only remote sensing images. To the best of my knowledge, no research has been done and published using remote sensing, fractal dimensions and mathematical morphology to identify the spatial organization of urban centers and subcenters.

1.7 Facilities Used

The facilities used in this thesis are:

i. library and internet facilities at Université Gustave Eiffel;

ii. landsat images from United States Geological Surveys (USGS);

iii. ArcGIS Desktop from Laboratoire Ville Mobilité Transport (LVMT);

iv. Google Earth;

v. Fractalyse 3 – 0.81;

vi. Fragstats 4.2; and

vii python libraries such as: Scikit-learn, SciPy, OpenCV, gdal, geopandas, matpotlib, numpy.

1.8 Organisation of Thesis

The thesis is organized into six chapters. Chapter 1 is the introduction, where a general overview of the entire thesis is presented: the background, problem statement, research questions, objectives, methodology, significance of the thesis and the facilities used. Chapter 2 is a brief history and description of the study area chosen for the application of the methodology. The land tenure system of the study area and its effect on the planning of the city is discussed. Urban sprawl in the region is also discussed as well as a literature review on some previous studies concerning urban growth in the region. Finally a justification of why the study area was chosen is presented. Chapter 3 is a review of the image classification methods used in this thesis. How the satellite images used in the thesis were acquired, preprocessed, classified, assessment of the accuracy of the classification and the preparation of land cover maps of the study area are demonstrated with a case study. In Chapter 4, the future growth of the study area is predicted using Markov's chain cellular automata, Land change modeler (LCM), and an agent based model in NetLogo. A longitudinal analysis of some landscape metrics on the evolution of urban growth of the study area and another coastal region in Ghana, Sekondi Takoradi Metropolitan Area (STMA) are compared. Chapter 5 is on the characterization of the land cover maps produced in chapter 3. The spatial organization of the built-up areas are analyzed using fractal methods. Mathematical morphology is used to extract inherent functions such as centers and subcenters within the built up area which otherwise would have been hidden within the built-up pixels. A schematic diagram is used to represent the urban growth process of the study area based on the concept of chorems. Chapter 6 is a conclusion of the entire thesis and some recommendations.

Chapter 2

Relevant Information on Study Area

2.1 Location and Size

Ghana is a very fast growing country in West Africa. It shares borders with Togo to the East, La Cote d'Ivoire to the West, Burkina Faso to the North and Gulf of Guinea to the South. With over 30 million inhabitants, Ghana is the second most populous country in West Africa, after Nigeria. Currently divided into 16 administrative regions, Greater Accra Region, which is the smallest, is also the densest among all the regions. The length of Ghana's coastline is approximately 550 km [21], and Greater Accra Region occupies approximately 121.73 km, i.e. roughly a third of the country's coastline. This makes the region a very important one for the country. Situated between longitudes 0°30′ W and 0°45′ E; and latitudes 5°30′ N and 6°10′ N, it has a total land surface area of 3 548 km^2. **Figure 2.1** is a map showing the Greater Accra Region of Ghana.

The topography of the region varies from flat to gently undulating lowlands with pockets of inselbergs. There are coastal savannah shrubs interspersed with thickets, coastal scrubs, grassland and mangrove swamp. Small portions of guinea savannah and moist semi-deciduous forest mainly cover the region. The grasses are short and barely grow beyond one meter, with the trees growing to an average height of five meters. Sadly, all of these vegetation are currently being threatened by urban land expansion. It is believed that much of the area was once covered with dense forest, but has been lost due to climate change and human activities [9, 10].

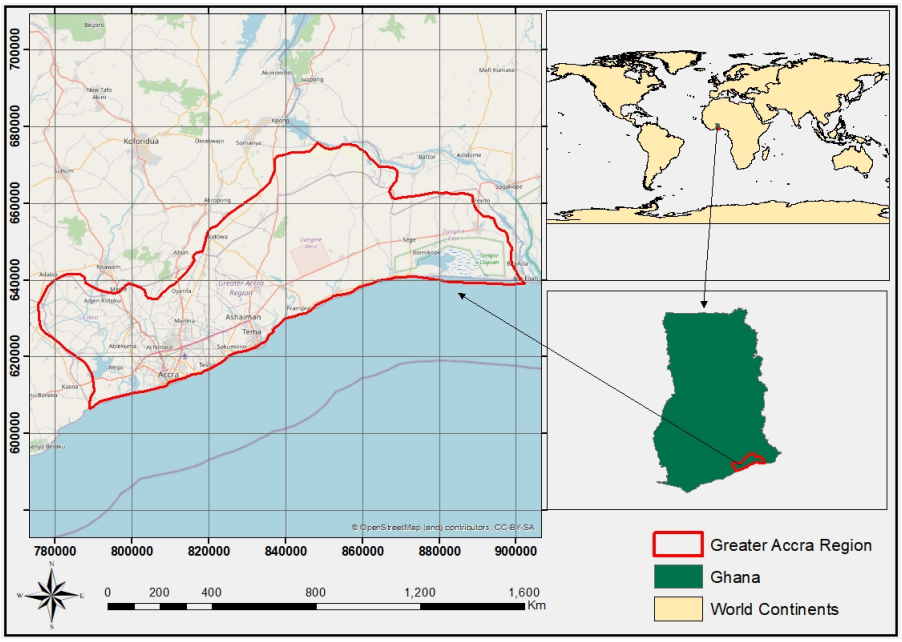

Figure 2.1: Greater Accra Region of Ghana

There is wide variation in communities and living standards in the region, which ranges from reasonably high and middle-income urban communities to deprived urban slums and typically deprived rural farming communities. **Figure 2.2** are photos of some areas in Greater Accra Region. The photos, obtained on google images, were chosen to represent the diversity of landscapes in the region. They show highly urbanised areas (**Figure 2.2a and 2.2b**), infrastructure such as airport, roads, harbor and market (**Figure 2.2c, 2.2d, 2.2e and 2.2f**), deprived communities (**Figure 2.2g, 2.2h, 2.2i**) and residential new districts (**Figure 2.2j**). They demonstrate how steep the urbanisation in Greater Accra Region is, and the different forms it manifests itself. Like most urbanizations, the diversity in the urbanisation of Greater Accra Region can be attributed to economic, socio-cultural and technological factors.

For development planning and administrative purposes, 12 municipalities within the Greater Accra Region (Accra Metropolitan Area (AMA), Tema Metropolitan Area (TMA), Ga South, Ga East, Ga West, Sowutuom, La Dadekotopon, Madina, Adenta, LEKMA, Ashiaman, Kpone Katamaso), together referred to as Greater Accra Metropolitan Area (GAMA), which is the study area for this thesis, is referred to as the administrative capital of Ghana. The spatial extent of the study area, based on the WGS 1984 UTM Zone 30 N coordinate system and Transverse Mercator projection is: 650095.255310 m North; 605158.239929 m South; 841614.953308 m East; and 774978.788696 m West. As the administrative capital and also the major economic hub of the country, GAMA has

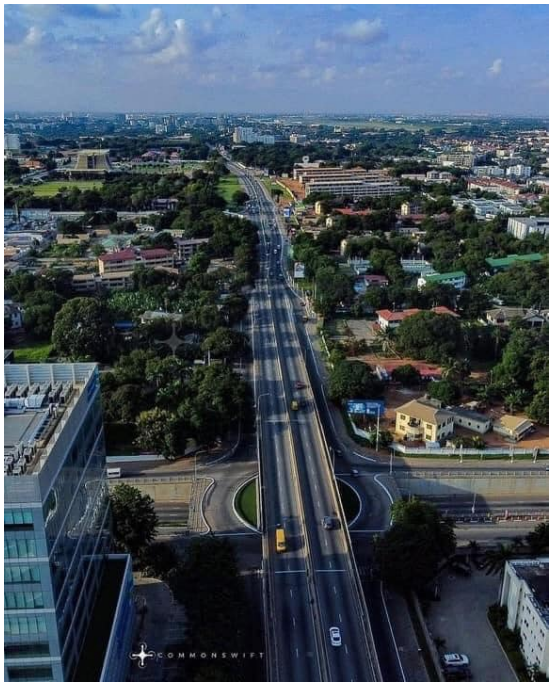

(a) North Ridge

(b) Cantoments

(c) Airport City

(d) Kwame Nkrumah Circle

been the beneficiary of a lot of investments (both public and private) in infrastructural and service developments [119]. Due to these massive investments, there is a cluster of economic activities in the region, which has resulted in increased population and pressure on land resources within and at the peripheries of GAMA, causing an urban sprawl. **Figure 2.3** is a map of the study area, GAMA.

The evidence of urban sprawl in the study area is revealed through the results of NDVI (normalized differential vegetation index) and NDBI (normalized differential built-up index) calculation of the study area (**figure 2.4a and 2.4b**). Basically, NDVI indicates the presence of vegetation in a specific area, while NDBI represents the presence of built-up structures in a specific area. Both indicators range from +1 to -1. For NDVI, a value of +1 signifies highly vegetated areas, whereas a value of -1 indicates areas with less vegetation. On the other hand, a value of +1 for NDBI corresponds to highly urbanized areas, whereas a value of -1 indicates less urbanized areas. These two indicators complement each other and confirm the transition from vegetation to urbanization in the study area. In terms

(e) Tema Harbor

(f) Tudu

(g) Teshie

(h) Ashaiman

(i) Nungua

(j) Community 1, Tema

Figure 2.2: Photos of some areas in Greater Accra Region

of biodiversity conservation, the analysis of NDVI values reveals a significant amount of vegetated areas, particularly in the northern sector of GAMA, in 1991. However, over the years (1991, 2002, 2013, and 2022), these vegetated areas have progressively decreased. The loss of vegetation can be attributed to several factors. However, in this case, based on the NDBI values observed, it can be stated that the land previously covered with vegetation has been transformed into built-up areas. The results from NDBI highlight the alarming expansion of built-up structures in GAMA. By comparing the NDBI values of 1991 and 2022, it becomes evident that almost the entire surface of GAMA is now covered by built-up areas.

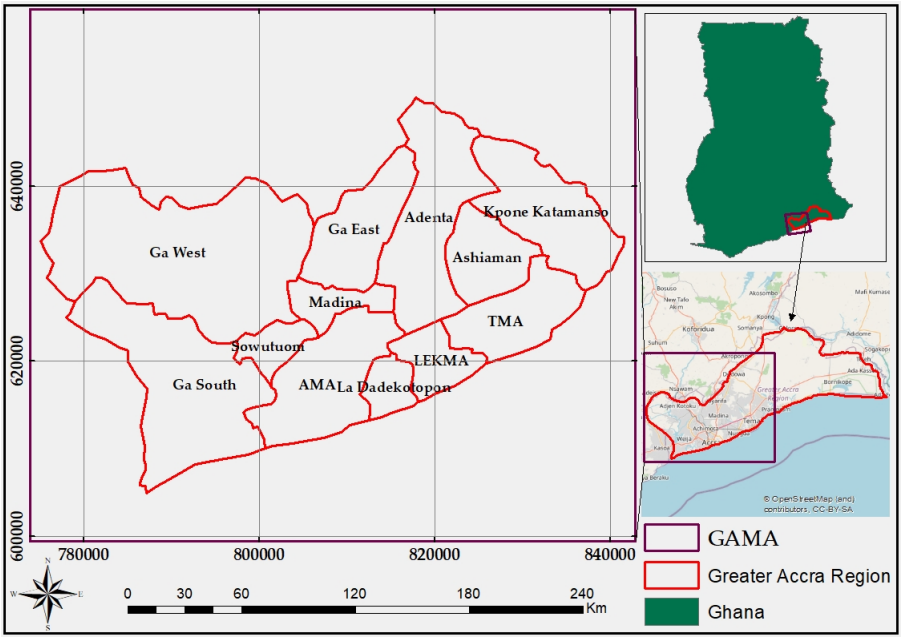

Figure 2.3: Map of study area, GAMA

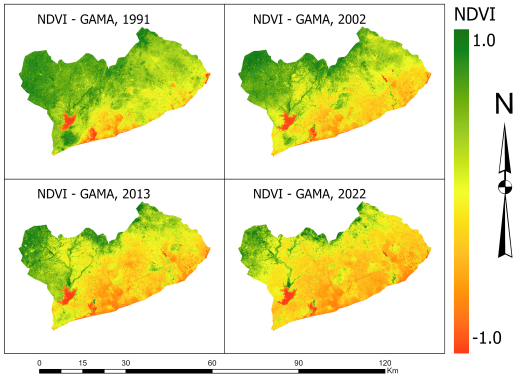

(a) GAMA NDVI 1991-2022

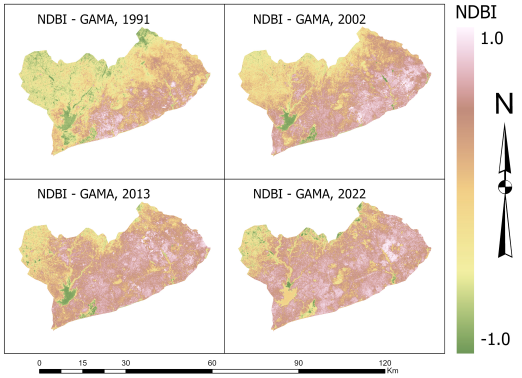

(b) GAMA NDVI 1991-2022

Figure 2.4: Evidence of urban sprawl in GAMA

Although administratively defined as independent, the municipalities that make up GAMA, which a few decades ago were purely rural, are now geographically, economically and functionally part and parcel of the built-up area of the Accra Metropolis. Studies have shown that the built-up in the surrounding municipalities is largely attributed to the spillover of the population of the Accra Metropolis [119, 81].

2.2 Brief History and Description

Strategically situated along the coast, the sea facilitated the transaction of business with European merchants. This made Accra gain a reputation as a trade post, where the indigenous merchants acted as middlemen between European merchants and inland residents. The booming maritime trade with Europeans from the 15th century and the

subsequent establishment of castles and forts caused the then fishing village, Accra, to rise from a trading post to a major urban center [7].

The decision by the colonial British government to relocate the administrative capital of Ghana (then Gold Coast) from Cape Coast to Accra is one of the most important factors in the development of GAMA. Accra's reputation as a business center and its dominance over other Ghanaian towns was asserted in 1877 when it became the headquarters of the British colonial administration, and subsequently the capital of the British Crown Colony, Gold Coast, which later became known as Ghana. In effect, missionary organizations, government agencies, as well as international and private firms established their headquarters there, gradually transforming it into the center of trade and consular businesses in the country. Accra has gone on to attract significant public and private investments towards its infrastructural and services development over the years, making it the 'most developed' region in Ghana [119]. By 1962, Tema, located some 25 km east of Accra had been developed into the country's largest seaport and industrial node. The development of the Tema seaport drew rural migrants to the new Accra-Tema corridor, that became the new economic center, as is evidenced by the rapid increase in population from 0.14 million in 1948 to 1.07 million in 1984 [61].

Much of Accra's growth align with the introduction of liberalization policies in 1983. During this time the economic efforts of the urban economy shifted from the old colonial city to a diffused spatial organization form which is also associated with uneven economic and residential development [67, 119]. Accra and Tema not only emerged as the economic nuclei of the region but also became the industrial and service hubs of the country, attracting both domestic and foreign investments. Successive governments prioritized infrastructure development in the region with the aim of making it a growth pole in anticipation to trickle down the benefits to other parts of the country [67]. However, the region continuously plays an increasingly dominant role as the preferred destination of rural-urban migration in Ghana.

Present day Accra is characterized by fragmented economic and residential geographies which are developing independently of any spatial urban planning. Thus, development is happening at such a fast rate that it has overwhelmed the planning department of the city. Individual housing developments typically take place even before infrastructural and service provision are implemented because there are no laid out plans to guide the development processes. This puts the sustainable urban development of the city into

question [109].

2.3 Evolution of the Demographic and Territorial Characteristics of GAMA

After the Second World War, rural-urban migration intensified. This resulted in the emergence of squatter settlements and slums in the region. Even though Accra's growth dates back several decades, the growth of the city picked up steam during the last three decades of economic liberalization and increased the intensity of engagement with global capital. Like many cities in Sub-Saharan Africa, Accra is experiencing a very rapid urban growth in terms of both spatial extent and population [108].

The population of the region increased from 491 817 to 1 431 099 from 1960 to 1984. Then it moved up from 2 905 726 in 2000 to 4 010 054 in 2010. **Figure 2.5** is a map showing a population distribution of the 12 municipalities in 2010 and 2021. A table showing the population of each municipality in 2010 and 2021 is presented in **Appendix A** [20].

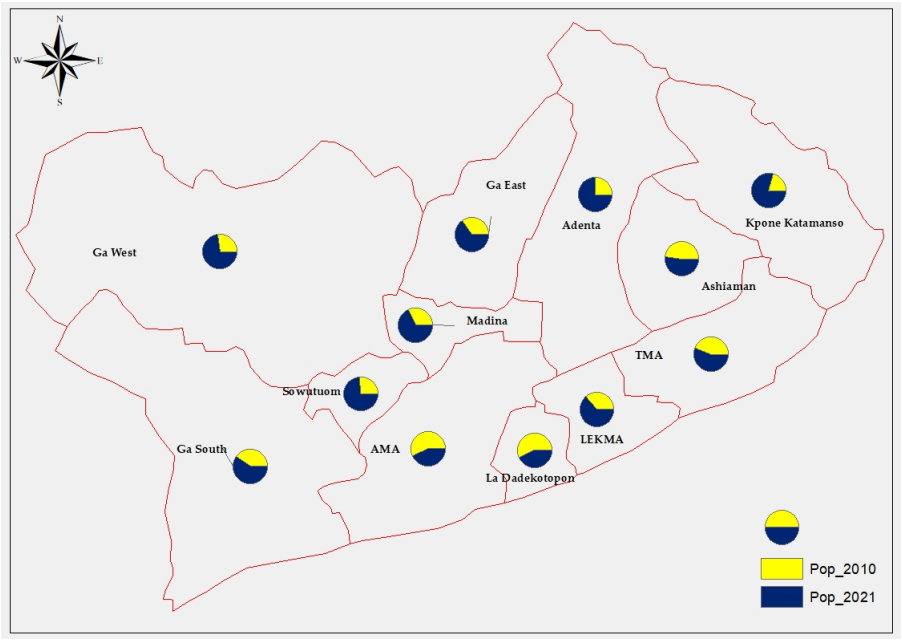

Figure 2.5: Map showing the population distribution of GAMA in 2010 and 2021.

Greater Accra Region is the second most populous region in Ghana, behind Ashanti Region, however, it is the region with the highest population density. With an average growth rate of 3.5% per annum, the projected growth shows that by 2040, the population of GAMA will increase to 10.5 million [119]. While the population of the Accra Metropolis was about 77% of the total population of GAMA in 1970, it declined to 72% in 1984 and

about 50% in 2010. The growth rate of the metropolis was just 1.1% for the period 2000-2010, compared to 3.3% for 1984-2000. In 2010, approximately 41% of the residents who lived in the Accra were migrants [61]. Increasingly, much of the population of the region is settling outside the Accra Metropolis. The built-up of the surrounding municipalities is largely attributed to the spillover of the population of the Accra Metropolis hence the urban sprawl being experienced in the metropolitan area [119, 10, 7].

GAMA covers a total area of 1 583.8 km^2 and houses the capital city of Ghana (Accra), the country's most prominent seaport (Tema), and the country's only international airport, Kotoka International Airport; making it the major economic and political hub of the country [10]. As the most economically significant metropolitan area in Ghana, GAMA accounts for almost a quarter of the national gross domestic product (GDP). It also serves as the headquarters of several national and international industries such as manufacturing, banking and finance, telecommunication, oil and gas, health, education, etc. Although manufacturing is the most dominant industrial type in GAMA, recent economic growth is accelerated by service sectors.

As a result of the economic liberalization in the 1980s, investment-friendly environments have been created in Ghana and the vast majority of the foreign direct investments (FDI) have been directed to GAMA. Central government policies such as the Accra Gateway Project and the Ghana Free Zones Programme (GFZP) strengthened the influx of FDI into GAMA. These initiatives facilitated infrastructure construction such as upgrading the Tema seaport and the Kotoka International Airport (KIA); and promoted export-led production through tax incentives and administrative advancement in licensing and customs procedures, all of which further encouraged FDI inflows [67, 61]. According to the Ghana Investment Promotion Center (GIPC) quarterly report for 2020, GAMA was the beneficiary of 85.51% of registered projects during the first half of the year, i.e., January to June 2020 [23]. Economic growth in GAMA is also characterized by an explosion of commercial and retail businesses. Since the growth in the retail sector has largely been in the informal sector, this has not demonstrated any drastic changes in the traditional CBD. New retail spaces have been concentrated along major roads, a phenomenon, partly driven by and partly influencing urban sprawl in GAMA [81, 61]. The traditional CBD contains old markets for petty trading (including Makola and Kantamanto markets), small craft businesses, and established companies. However, the district largely contains old structures with residential functions owned communally by families who wish for them to remain as "family houses". With new businesses and other organizations coming to

Accra to leverage agglomeration economies and benefit from proximity to the Kotoka International Airport, new economic centers are emerging. These new centers contain large firms capable of affording the high land value areas, particularly, along the Oxford Street in Osu and Cantonments.

The government's creation of the Accra Airport City, aimed at promoting a high-density mixed-use development zone with the intention of addressing political problems associated with the redevelopment of the traditional Central Business District (CBD), has encouraged the establishment of a new center. Gradually, the airport city is becoming the financial hub of the country: major banking, finance and insurance companies, hotels, entertainment, and mega shopping centers can be found there. Generally, these investments have brought positive economic outcomes in the region, as seen in the decline in the poverty rate from 25.8% in 1992 to 2.5% in 2017 [41, 61]. Unfortunately, in spite of the positive economic outlook, governance in GAMA has not been very effective at handling the urban issues associated with economic growth such as: environmental hazards, exponential growth of informal settlements, infrastructural problems, uncoordinated development and urban sprawl.

2.4 Land Tenure System in GAMA (Ghana)

Land tenure refers the rules, regulations and institutional structures, both customary and enacted legislations, which influence the holding and appropriation of land and its resources for socioeconomic development. Generally, it is the set of relations among people concerning the use of land [107]. Land tenure in Ghana is generally communal in nature; and this has determined the nature of land administration over the years. Prior to the arrival of European settlers in Ghana, the land tenure system that was practiced was the customary land tenure system. Customary land tenure system is a land relation in which the ownership of land is vested in the whole family, lineage or a clan, while individuals enjoy unrestricted rights of usage. The main idea of customary tenure is that the land belongs to the whole social group and not just an individual. There is a belief that land is an ancestral trust committed to the living for the benefit of themselves and the unborn generation yet to come [13]. Initially, local leaders often received substantial revenues from granting land concessions to European settlers while they retained their inalienable rights under the local tradition. However, when the Europeans became colonial rulers, they found the communal ownership to one tract of land intolerable and decided to regularize

what they saw as a chaotic state of affairs.

These attempts were fiercely opposed by the chiefs and the people because of the influence of land on the concepts of kinship, the family system and the entire field of social relationships to them. The first attempt by government to intervene in the customary system of land tenure was made in 1894 when the Crown's Lands Bill was introduced by the colonial government with the intention of vesting all lands of the then Gold Coast Colony (now Ghana) in the English Crown. The chiefs and people of the colony constituted themselves into the Aborigines Right Protection Society to serve as a pressure group against the enforcement of the law. The idea was therefore abandoned on the direction of the Queen of England. This was subsequently followed by several other attempts and by 1927, the colonial government, realizing the strong opposition of the chiefs and people against any attempt to intervene in the system of land holding, had to greatly modify its land policy into one of minimal government intervention. Towards the end of the colonial period, indigenous land tenure systems were operating in parallel with the European based system, which has led to a dual system of land tenure - this has created a lot of ambiguity surrounding land policies and objectives [66, 107, 29]. The colonial trace of legal duality is prominently reflected in the customary and statutory legal land systems in Ghana [29]. Today, the land tenure system in Ghana is defined by the 1992 Constitution of the Republic of Ghana. The Constitution recognizes two tenure systems namely: customary and public lands [107, 13, 80].

2.4.0.1 Customary Lands

Section 36 (8) of the 1992 Constitution of the Republic of Ghana recognizes customary ownership of land. Customary lands consist of all the various interests and rights held under the traditional system involving skin lands, stool lands, clan lands, and family lands. Customary lands are communally owned and are vested in chiefs and family heads who act as custodians on behalf of their subjects including the living, the dead, and the unborn. Customary lands account for about 80% of all lands in Ghana and constitute the main source of land released for development in GAMA [13, 96, 80]. Private ownership of customary land can be acquired by way of a grant, sale, lease, gift or marriage. Ownership is by way of outright purchase from customary land owners or private individuals. For land tenure security, the title of this land must be registered under the statutory law after acquisition.

2.4.1 Public Lands

Public lands belong to the state and are managed on the principle that the market may not always be effective in terms of safeguarding public interest. They are vested in the President, on behalf of, and in trust for the people of Ghana based on the relevant provisions of the Administration of Lands Act, 1962 (Act 123). Public lands also include any other land acquired through the State Lands Act, 1962 (Act 125) or through any other statutes, in the public interest. Public lands are administered by the Lands Commission and its secretariats, as provided in the Lands Commission Act, 1994 (Act 483) [13].

2.4.1.1 State Lands

State lands refer to lands that the Government has compulsorily acquired for a specific public purpose or in the interest of the general public - such as: road construction, urban planning, military installation, health facilities and schools - by the lawful exercise of its constitutional or statutory power of eminent domain. All previous interests in such lands are extinguished and persons who previously held recognizable interests in the lands are entitled by law to compensation, either monetary or replacement with land of equivalent value. Many a time, the compensation does not happen, and this undermines the equity, fairness and tenure security for those affected. This makes the people question the state's legitimacy to exercise control over acquired lands and emboldens the people to encroach on state lands [13, 42, 80].

2.4.1.2 Vested Lands

Vested lands are a hybrid of public lands and customary lands. Vested lands are customary lands which are held by the state in trust for the land-owning family or community. While the state manages such lands, the family or community retain their interest in the land and enjoy the proceeds that may accrue in the form of rent or lease. The management responsibilities cover legal (e.g. prosecution), financial (e.g. rent assessment, collection, disbursement) and estate management e.g. physical planning and its enforcement and administration of the property. Vested lands are administered under the Administration of Lands Act, 1962 (Act 123) and the Lands Commission Act, 2008 (Act 767) [42, 80].

2.4.2 Urban Developmental Planning in GAMA

In Ghana, urban planning is primarily the responsibility of local government authorities, including the metropolitan, municipal, and district assemblies (MMDAs). These bodies are responsible for developing and implementing plans for their respective areas. Each municipality has an independent physical planning office that is in charge of preparing plans and controlling physical development by processing developmental permit applications. There is a municipal chief executive officer in each municipality, who is responsible for overseeing the day-to-day operations of the municipality, and approves development projects and programs in the municipality. The independence of the municipalities of GAMA has a significant impact on urban planning. It creates challenges for coordinated urban planning across the entire metropolitan area as each municipality has its own plans and priorities. This makes it difficult to implement regional plans and to address cross-municipality issues such as transportation and environmental management. Additionally, the financial and human resource capacities of the different municipalities vary, which leads to disparities in the quality of urban planning and service delivery across the metropolitan area.

In spite of these challenges, projects such as the Greater Accra Metropolitan Area - Sanitation and Water Project has been developed in an effort to support coordinated planning and management of water and sanitation services across the metropolitan area [15]. There is also the GAMA Structure Plan, a twenty-year African Development Bank Project that is meant to develop a spatial plan to guide the development of GAMA. The final draft report on the project indicated that the plan would transform Accra into an economic powerhouse. It includes policies and strategies to promote sustainable land use, transportation, housing, and environmental management in Accra [112]. However, there have always been challenges in the implementation of developmental plans in Accra. Some of these challenges are: inadequate participation of the public in the planning process, the lack of political will, and limited financial and human resources. There is therefore the need for concerted efforts to address the challenges in the implementation of plans so as to promote sustainable urban development in the city [7].

2.4.3 Effects of Land Tenure System in GAMA on Urban Developmental Planning

The existence of contradictory legal land systems in Ghana engenders conflict within the land delivery system; individuals who are aware of this conflict exploit subsequent opportunities in their land use actions. Boamah and Walker [29] argued that the dualism of legal land systems in Accra offers the opportunity to make land use decisions which are paradoxically legal and illegal at the same time. In spite of all the modernizations in GAMA, traditional rule and authority play an integral role in the evolution of the city, i.e., directing how the city grows and what form that growth takes. Because there is no data readily available on how much land in the city is still owned by the community until the point of purchase, there is difficulty when it comes to land acquisition in GAMA through chiefs or family heads. One has to go through a lot of hurdles to get a land title that reflects the buyer's details without any petitions from the community. This has contributed to Accra being among the regions with the highest number of land disputes in the country [96].

Ghana's land tenure system, which comprises of a blend of customary and state tenure systems, is viewed as complex networks of interrelationships characterized by social, political and human activities [42]. There is no doubt that the plural and complex nature of land ownership in Ghana has influenced the spatial planning and development outcomes in GAMA. Planning has become a complicated process due to the presence of conflicting interests, the promotion of self-serving ideas, involvement of diverse stakeholders, and ongoing power struggles. There is therefore always the need for a greater collaboration in order for a consensus to be reached in designing plans for developmental purposes. GAMA's unique land tenure system makes the implementation of land use policies a bit of a challenge. The typical models of land use policies under the English common law system do not necessarily fit the customary land tenure system, and they were not designed to do so either [137]. There is a clear disconnect between spatial plans and local land use decisions. Planning schemes of the city which are prepared by metropolitan assemblies are expected to be implemented on customary lands which are administered by chiefs and family heads. This creates enforcement challenges. For example, many plans become outdated before implementation, resulting in fragmented and unsustainable urban development patterns [80].

2.4.4 Urban Development and Sprawl in GAMA

As the administrative capital of Ghana, GAMA has been the beneficiary of a lot of investments (both public and private) in infrastructural and service developments. Due to these investments, there has been a cluster of economic activities in the region, which has resulted in increased population and pressure on land resources within and also at its peripheries, resulting in an urban sprawl [118, 82]. Urban planning in GAMA has not been able to keep up with the rapid rate of development, resulting in an uncoordinated growth of the city. The rapid outward expansion of the city has engulfed rural areas and encroached on agricultural lands for the development of residential and commercial services which are characterized by low density buildings [119, 2]. Low density housing brews urban sprawl. According to Adam-Smith [8], every farm that is converted to a building reduces the possibilities of growing food, and food is needed to live. While low density neighborhoods give an assurance of privacy, quietness and less traffic to residents, it is essential to bear in mind that land is a finite commodity, hence the efficiency of its usage is very vital. Currently, the segregation between rural and urban areas in GAMA has disappeared due to urban sprawl. This has significant implications on the livelihood of inhabitants, especially, when it comes to food security and other ripple effects such as issues relating to the environment, climate, public health, transport and energy [151].

According to Owusu [119], containment strategies were developed by Accra Planning and Development Programme (APDP) in association with the United Nations Development Programme (UNDP) and the United Nations Center for Human Settlement (UN-Habitat) for GAMA. The strategic plan looked at five options:

i. urban consolidation – putting a hold on all developmental projects at the peripheries of the city to focus on developing lands effectively within the existing boundaries;

ii. multi-city structure – establishment of several cities within the metropolitan area, each with its own central business district and servicing population of 250 000 – 300 000 to bring about decentralisation;

iii. twin city - the development of Accra and Tema was to be coordinated and harmonised. The strategy envisaged merging of Accra and Tema by making the two cities grow towards each other;

iv. satellite towns - restrict the growth of Accra by directing future urban development

consciously to potential growth centers such as: Dodowa, Nsawam, Amasaman, Kasoa, etc. (all within commuting distance from Accra); and

v. laissez-faire - continue with what is already happening until natural or economic constraints prevent further expansion.

After several deliberations on the advantages and disadvantages of each of the options as well as taking into consideration social and environmental impacts, transport inefficiencies, administrative difficulties, cost effectiveness, land economics and flexibility to meet future needs, it was concluded that no single concept would be able to contain the sprawl of GAMA, instead, a mixed-concept plan involving three concepts (urban consolidation, twin-city and multi-city structure) was proposed for GAMA [119]. Decades after the formulation of the GAMA Strategic Plan, the shape and size of GAMA has been seen to be growing and expanding in all directions except to the south which is occupied by the ocean. The failure of the strategies could be attributed to:

i. existing land management systems where land is held under customary institutions and planning is done by the local government. The custodians of the lands often give lands out for purposes not intended by the planners. This is due to the fact that there is no coordination between the land owners and the town planners;

ii. weak planning and development control institutions due to the inadequate number and quality of staff. Many of the municipalities do not have planning schemes and where they exist, they are outdated because development is happening at a faster pace than implementation of the plans; and

iii. GAMA is fragmented into separate autonomous local government areas. When the GAMA strategic plan was being prepared, the region consisted of Accra Metropolitan Assembly (AMA), Tema Municipal Assembly and the Ga District but now they have been subdivided into 12 municipal assemblies (**Section 2.1**). Because of the independence and autonomous nature of all these municipal assemblies, there is little cooperation between them and they all develop their lands as they see fit.

2.5 Literature Review on Urban Growth in GAMA

Several studies have been conducted concerning the urban growth in GAMA. Yankson and Gough [149] studied the impact of the rapid urbanization on the physical and residential environment of peri-urban Accra and the implications of these changes on the

environmental management of the urban fringe areas. They pointed out that the peri-urban areas are being ignored by the planning agencies which is not advantageous to the environment. Forests are increasingly being converted for residential purposes, which is leading to the diversion of water courses, drying up of ponds and an increase in soil erosion. According to the study, a resident lamented in an interview, saying...

"... in the past there was forest and big trees but now the forest is no longer here. The big trees too are missing. The land is becoming grassland. The strangers who have acquired the land also develop their sites and have cut the trees to build their houses. Bush fires are also destroying the forests. There is pressure on farmers. In the past the farmers were shifting from place to place thus leaving the land to fallow because there was more land. The place was left for 6 to 7 years so that by the time you returned to the old place, the trees had grown and there was always forests. Now more farmers are using the same site continuously."

They recommended to the then district assemblies, the various communities in the peri-urban areas and NGOs to help deal with the environmental degradation by embarking on educational campaigns to address the need to protect the environment. Another research by Osei et al. [118] also attempted to identify and quantify the urban sprawl in Greater Accra Region between 1985 and 2014 based on Shannon's entropy indices of the various years. They concluded that the urban area is mainly sprawled around city centers and along the main road, which means the major road that cuts across the region as well as the city centers were the main causes of sprawl in the region. Owusu, [119] attributed the urban sprawl and uncoordinated development in the region to the land tenure system, the lack of cooperation between the various municipalities that make up the region, and failure of institutions in charge of planning.

Oduro et al. [115] used sustainable livelihood framework as an analytical tool to explore the livelihood strategies adopted by the residents of peri-urban Accra as a response to the city's physical expansion. It was established that while some of the indigenous people benefited from the urban growth and took advantage of the economic opportunities created by it, others were also unfavorably affected by it. Those who benefit from the physical expansion of the region were the chiefs and family heads who capitalize on the increasing demand for land by allocating plots of land to developers. Other wealthy people also acquire lands at a cheaper rate from the chiefs and later sell their leasehold interests to developers at higher rates. Those who are affected the most are the resource-

poor indigenes and long term settlers whose main source of livelihood is farming on these lands. They lose their farmlands to developers as a result of tenure insecurity, especially, in the customary land tenure system; and they do not have the means to acquire new lands nor invest in alternative livelihoods. It was recommended in the study that local government authorities should incorporate peri-urban livelihood issues into their planning activities.

Addae and Oppelt [9] analyzed the land-use/land-cover change in GAMA and modelled its urban growth. Their objective was to provide a better understanding of the extent, rate and pattern of urban land use change within the region in order to obtain an overview of the factors that influence the urban expansion. Landsat images from 1991 to 2015 were classified using maximum likelihood image classification algorithm and predicted the urban extent of 2025 using a hybrid of neural network and markov's chain. At the end of the studies, they concluded that main land cover change in the region was the expansion of built-up area at the expense of vegetation. It was also anticipated that urban extent would spill to the adjoining districts, mainly to the western and eastern sides of the region by 2025. Akubia and Bruns [11], also did similar research by analyzing the spatiotemporal dynamics of landuse change and urban expansion in GAMA using Quickbird/Worldview-2 images of 2008 and 2017. The objectives of the research were to: analyze the spatio-temporal patterns of land-use change; quantify the rate, intensity and spatial patterns of urban expansion at sub-regional and district levels; and explore the implications of land use change dynamics and patterns of urban expansion for regional spatial planning development. The study revealed that the expansion in GAMA occurred in municipalities located within the peripheries, particularly, the western and eastern directions, which turned out to be the hotspots of the urbanization.

In an attempt to get more understanding on the impacts of the rapid urban growth in GAMA on the environment and nearby regions, Yiran et al. [151] analyzed the household energy consumption patterns in relation to land-use change in peri-urban Accra. They concluded that majority of the populace relied on wood as the main source of energy for cooking. Owing to the rapid conversion of vegetation to built-up areas within the region, it had become necessary to import wood from other parts of the country. They cautioned that if this trend persists, it could lead to deforestation in the source regions, potentially resulting in desertification. Thus, the uncontrolled urbanization in GAMA is not just a GAMA problem but has negative implications in nearby regions and other parts of the country as a whole.

2.6 Justification of Chosen Study Area

The thesis focuses on using the concept of fractals and remote sensing data to detect the spatial arrangement of urban centers and subcenters. It aims to create urban growth models that provide more comprehensive insights compared to traditional models like the oil stain model. The study is motivated by the lack of research on the identification of urban centers and subcenters in developing countries, as highlighted by Yu et al. [154] and the challenge posed by the absence or partial availability of official statistical data to do so, as noted by [101, 94].

The choice of the Greater Accra Metropolitan Area (GAMA) in Ghana, the largest and fastest-growing city in the country, was deliberate. GAMA serves as an ideal location for this research due to its status as the fastest-growing city in a developing country with limited official statistical data for the identification of urban centers and subcenters. This study aims to bridge the research gap in the identification of urban centers and subcenters in developing countries while addressing the challenge of data unavailability. This would help to contribute to a better understanding of urban growth in such contexts.

Chapter 3

Satellite Image Classification

3.1 Introduction

Land is a non-renewable resource, and as such, it must be used sustainably. One way to go about this is to incorporate better land use planning and land management strategies in the utilization of land [74]. To develop better land use plans and land management strategies which are geared towards sustainability, information on land use and land cover (LULC) cannot be left out of the equation. This is because, fundamentally, the way land is distributed, owned, and utilized is a defining characteristic of modern societies, as it involves the idea of ownership and how space is partitioned for various functions. Land use refers to how land is used by humans while land cover refers to what lies on the surface of the land as a result of land use [4]. Land use usually results in land cover changes, which can alter water quality, soil quality, air quality, etc.; and all these in turn affect the quality of human lives. This is the reason why it is important that LULC changes are studied, quantified and incorporated into land planning and management strategies.

Although information on LULC can be obtained from traditional field surveys and aerial surveys, these approaches have been found to become time consuming and expensive as the size of the study area increases. However, with remote sensing, which is the art and science of measuring the reflective response of the earth's surface after it has been hit with a source of light, LULC data can be collected in a relatively less expensive and timely manner [45]. Data obtained from remote sensing has proven to be spatially consistent, and covers large areas with both high spatial detail and frequency at a relatively lower cost. The downside is that it can only be used to make direct observations on land cover and not land use, and also there is only so much information one can obtain on the third dimension. To

obtain information on the third dimension or on land use from remote sensing, it must be inferred by associating the measured land cover information obtained with supplementary information such as: already established vertical datums, socio-economic data or expert knowledge [132]. Once remote sensing data has been obtained, the individual pixels in the data need to be classified into their respective land cover types according to their visual content and the purpose of the classification. Manually checking and classifying images can be a difficult task, especially, when the number of pixels involved is huge. It is therefore very practical that the entire process is automated using a computer vision technique like image classification. This is one of the reasons why image classification is considered a very important task in the field of computer vision [126]. There are several image classification techniques such as maximum likelihood, random forest, support vector machine, artificial neural network, etc. that can be used to classify the individual pixels in the data into their respective land cover types [132, 98, 1].

Generally, image classification methods can be categorized into two: supervised and unsupervised. Unsupervised image classification is where each pixel in an image is identified to be a member of one of the inherent categories present in the image without the use of labeled training samples; and is based on machine learning algorithms for its implementation. Abass et al. [116] acknowledged clustering algorithms and dimension reduction algorithms as the two main classes of unsupervised machine learning algorithms needed for unsupervised image classification. Their review discussed the applications of these algorithms in the context of unsupervised image classification. On the other hand, supervised image classification requires training samples (i.e., representative data points collected from a known class of interest to the analyst) for each class. The classification is based on how similar a pixel is to each point in the training sample [14]. There is also another category called object based image classification. In this category, individual pixels are aggregated into spectrally homogenous objects using image segmentation algorithms. These spectrally homogeneous objects are then classified using either supervised or unsupervised techniques [90].

Image classification is very purpose oriented, hence, there is no such thing as a universal classification scheme. Even deciding on which classification method is better than the other is very subjective because one must be able to establish in what way, say, method A is better than method B. It all boils down to the purpose for which the classification is being carried out. The purpose of this research is to utilize satellite image classification techniques in the studying of urban growth. Therefore, the main interests of the classifica-

tion that would be done in this research would be on the urban extent of newly urbanized areas, evolution of the boundaries of the urbanization front, and transformations in already urbanized areas. Hence, the image classification as applied here would consider fewer classes (basically, urban and non-urban) than most applications, while particular attention is paid to the form of the identified objects, not just the area they cover.

Several studies have been done on the applications and comparisons of different image classification methods for detecting LULC changes. Smiths and Schowengerdt [131] assessed the quality of image classification algorithms and the economic effects of misclassification. Lui and Xia [90] published a paper on the advantages and limitations of object-based classification algorithms relative to pixel based algorithms. Ma et al. [97] reviewed some object-based supervised land cover image classification methods and concluded that Random Forest shows the best performance in object-based image classification. Aburas et al. [4] reviewed some conventional and machine learning models for modelling, simulating, and predicting land use change to determine the best approach that can accurately simulate land use changes. Przemyslaw [85] compared different methods of texture analysis for their efficacy in land use classification of satellite imagery. Toosi et al. [138] evaluated and compared four supervised classification algorithms for the monitoring of mangrove cover changes. Basheer et al. [25] evaluated some satellite image classification methods as implemented in ArcGIS Pro and Google Earth Engine. What all these studies had in common is that the comparison of the classification methods were based on overall accuracies and kappa scores. Overall accuracy and kappa score are widely used quantitative measures that serve as indicators of the predictive ability of a classification method. They are derived from confusion matrices, which rely on the existence of a so-called ground truth that is difficult to define, especially, for a relatively fuzzy concept such as urbanization. For instance, one can't really tell when an inhabited rural area becomes an urbanized area: is it the number of inhabitants; the built up density; or the infrastructure present there? Also, in instances where different classification methods have similar overall accuracies and kappa scores, so far, there are no scientific basis for selecting one over the other.

Although different classification methods are compared in this chapter, the aim is not just to check the accuracies of the various methods, but to also identify their effects on land cover maps. The objective of this chapter is to investigate the effects of a chosen classification method on resulting land cover maps in spite of similar overall accuracies and kappa scores. This would involve measuring additional characteristics that represent the

form and shape of the classified land cover types, characteristics that are not accounted for by the overall accuracy and kappa score. Unlike the usual quantitative comparison of the overall accuracies and kappa scores, this novel approach is a qualitative comparison which is based on the how much details the classification method is able to produce. This approach does not seek to replace the existing quantitative measures already used in comparing different classification methods but to serve as supplementary measures to help analysts decide on which method is best suited for specific projects.

3.2 Materials Used

The boundary of the study area was freely downloaded from OpenStreetMap (https://www.openstreetmap.org/relation/1991849#map=10/5.8524/0.1978; retrieved on 13/01/2022). Landsat images of the study area for the years 1991, 2002, 2013, and 2022 were also freely downloaded from the United States Geological Survey (USGS) website, spanning from Landsat 4 to Landsat 9. With a spatial resolution of 30 m, extra care was taken to certify that all the downloaded images had cloud cover of less than 5%. This was done to reduce issues of misclassification. The downloaded images were then processed to convert them from digital numbers to top of atmosphere (TOA) reflectance. It is important to covert digital number values to TOA reflectance values so that the atmospheric impacts on the reflected wavelengths are removed for desired indices to be obtained and used for analysis [16]. The variables used for the conversions were obtained from the calibration coefficients provided in the metadata file that comes along with the Landsat image when it is downloaded. These computations were implemented with the raster calculator tool from the spatial analyst toolbox in ArcMap. ArcMap was used to prepare the images for classification. The bands in each downloaded image were clipped to the boundary of the study area and stacked together to create a composite band, i.e., single raster dataset from the multiple bands [153]. This was done using the "composite bands" and "extract by mask" tools in ArcMap to enable visualization of the image in different color combinations.

By visualizing it in different color combinations, it becomes easier to identify different land cover types when creating ground truth data for supervised classification. Ground truth data refers to accurate and reliable reference data that serves as a benchmark for evaluating the performance of automated classification algorithms. It typically involves manually labeling or annotating specific objects or land cover types in satellite images, allowing for the validation of the algorithm's results. Ground truth data plays a crucial

role in assessing the accuracy and effectiveness of satellite image classification models. Ground truth data was carefully selected based on firsthand knowledge of the region. This selection involved visual interpretation of the satellite images through several color combinations and comparison with Google Earth imagery and Atlas of urban expansion maps of Accra (http://www.atlasofurbanexpansion.org/cities/view/Accra) to represent the following land cover types: 'Vegetation,' 'Built-up,' 'Transition,' and 'Water.' Vegetation refers to thick forest cover with trees, dense bushes and grass lands. Built-up area refers to all man-made features such as: buildings, roads, bridges, ports and harbor, etc. Transition refers to vegetated areas gradually changing into built-up areas. They represent mixed land cover comprising bare lands, areas cleared for construction purposes, isolated buildings, and shrubs. Water refers to all water bodies such as: streams, lakes, rivers, lagoons etc. The cell values at the location of each ground truth point for all the bands in the composite bands were extracted and attached to their respective ground truth points in the attribute table using the "extract multi values to point" tool in ArcMap. 70% of the ground truth data were randomly selected as train data and the remaining were kept as test data to check the accuracy of the results that were obtained. The data and software used are presented in **Table 3.1**.

Table 3.1: Data and Software Used

DATA			
Product ID	**Spacecraft ID**	**Date Acquired**	**Source**
LT04_L1TP_193056_19910110_20200915_02_T1	Landsat 4	10/01/1991	USGS
LE07_L1TP_193056_20021226_20200916_02_T1	Landsat 7	26/12/2002	USGS
LE07_L1TP_193056_20131224_20200906_02_T1	Landsat 7	24/12/2013	USGS
LC09_L2SP_193056_20220131_20220202_02_T1	Landsat 9	31/01/2022	USGS
GAMA Boundary Shapefile			OpenStreetMap
SOFTWARE			
ArcMap 10.8			
Python Libraries: Scikit-learn, GDAL			
Google Earth			
Fractalyse 3 - 0.8.1			
Fragstats 4.2			

3.3 Methods Used

Two supervised image classification methods, Random Forest and Support Vector Machine, were employed. Additionally, a hybrid approach using simple linear iterative clustering (SLIC) and K-Means was used for unsupervised object-based image classification. These methods were used to assess the impact of the chosen classification technique on

the resulting land cover map. Apart from the fact that random forest and support vector machine are popular choices for supervised land cover modelling, Random forest was chosen due to its multi-scale robustness. It is well suited for multi class problems, and works well with features of different scales, which makes it interesting for studying urban forms. Support vector machine was chosen because it is most suited for binary classification problems, performs well on sparse data, and introduces the concept of distance between points. The issue of urban growth is likewise mostly binary (urban/ non-urban) and the data can be sparse at certain places. SLIC is also known to be good at preserving the contours of features. The contours would represent the urbanization front, which is important in studying urban sprawl.

For the supervised classification methods, confusion matrices were generated, with which their overall accuracies, recall, precision, f1 scores and kappa scores were determined. This was not done for the unsupervised classification because there were no ground truth data with which to generate a confusion matrix. In measuring the additional characteristics that represented the form and shape of the classified land cover types but were not accounted for by the overall accuracy and kappa score, several methods were employed. The box counting method was used to assess the lacunarity of each land cover type. The total edge of each land cover type was calculated to determine the limits of its perimeter, and the number of patches of each land cover type was calculated to assess the level of heterogeneity in the spatial distribution of the land cover types.

3.3.1 Random Forest

Random forest (RF) is a classification algorithm that consists of a large number of decision trees that function together. Decision trees are building blocks of the random forest algorithm. They consider all the possible features of an object and select one that produces the most separation between the observations to classify them, such that, the resulting classes are as different form each other as possible while the members of each class are as similar to each other as possible. However, decision trees are very sensitive to training data as very little changes in the training data can result in a significantly different tree structure. This inconsistency makes it impossible for the algorithm to make generalizations [152]. To resolve this problem, random forest is used [70]. Random forest is a group of decision tree classifiers that are individually trained on different random subsets of the training data to ensure diversity in the classifiers. The random subsets of the training data are obtained by either bootstrap aggregation (bagging) or pasting. Bag-

ging is the process where samples uniformly taken from the training data for training the classifiers are done with replacement whereas with pasting, the sampling is done without replacement. This creates an uncorrelated forest of trees whose collective prediction is more accurate than that of any individual decision tree. After the classifiers have been trained, each decision tree in the random forest produces a class prediction. The class with the highest vote, which could be hard voting or soft voting, becomes the model's prediction. In hard voting, the predicted class is the class most predicted class by the individual decision trees; if there is a tie, a random one is picked. In soft voting the individual class probabilities are averaged over individual classifiers. The class with the highest probability is the predicted class. Random Forest is much less sensitive to the training data as compared to individual decision trees [136, 152, 138].

3.3.2 Support Vector Machine

A Support Vector Machine (SVM) is a powerful, yet flexible supervised machine learning algorithm that can detect patterns and information in data for classification and regression. This is achieved by categorizing the dataset into various classes by constructing margins (hyperplanes) between the classes obtained to find a maximum marginal hyperplane. The hyperplane is generated in an iterative manner so that the error can be minimized. The real power of this algorithm depends on the kernel function being used. The kernel function plays an important role in SVM, i.e., it makes it possible to solve non-linear problem using linear classifiers [138]. It provides shortcuts to avoid complex mathematical computations as one goes up to a higher dimension where it is impossible to have a hyperplane [19]. The most commonly used kernels are: linear kernel, Gaussian kernel, polynomial kernel and radial base function (RBF) [124, 126]. SVM has been successfully applied in several land-use applications such as: land use modelling, land used classification, land slide susceptibility studies and flood susceptibility studies [4]. The primary advantage of SVM is that it has good generalization capabilities with limited training samples, i.e., they can handle outliers and overlapping classes very well [129, 45].

3.3.3 SLIC K-Means

Simple linear iterative clustering (SLIC) is an algorithm used to generate superpixels by clustering pixels based on the similarity of their color and proximity in the image plane. Superpixels contain more information than pixels since they are made up of several

pixels; and they provide convenient and compact representation of images. Generating superpixels is very useful for object detection, cutting images and for reducing the amount of data to be processed to help reduce computational time. According to Achanta et al. [6] SLIC operates in a five-dimensional [labxy] space, where [lab] is the pixel color vector in CIELAB color space and [xy] is the color pixel position. For an image with N pixels, if the desired number of superpixels is K, the approximate size of each superpixel will be N/K pixels. Using the centers of the superpixels as grid intervals, for approximately equal sized superpixels, the grid interval can be given by $S = \sqrt{N/K}$. To generate the superpixels, a special method of distance estimation, D_s, is used, **equation 3.3**. This is because regular Euclidean distance in this 5D space would not suffice without normalizing the spatial distances. D_s is given by the sum of the lab distance, **equation 3.1**, and xy plane distance, **equation 3.2**, normalized by the grid interval, S.

$$d_{lab} = \sqrt{(l_k - l_i) + (a_k - a_i)^2 + (b_k - b_i)^2} \tag{3.1}$$

$$d_{xy} = \sqrt{(x_k - x_i)^2 + (y_k - y_i)^2} \tag{3.2}$$

$$D_s = D_{lab} + \frac{m}{s} d_{xy} \tag{3.3}$$

Where m is a variable which controls the compactness of the superpixels. The higher the value of m, the more spatial proximity is emphasized, making the cluster more compact. D_s enforces color similarity as well as pixel proximity in the 5D space such that the expected cluster sizes and their spatial extent are approximately equal. After the image has been segmented into superpixels, similar superpixels are further grouped into various classes using K-Means clustering method. K-Means partitions n observations into k clusters based on Euclidean mean value. It is fast and simple to use, however, it requires the analyst to have prior knowledge of the number of classes. Using K-Means, the number of clusters, K, is defined in advance, and the algorithm assigns each observation to exactly one of these clusters. The objective of the K-Means clustering is to minimize the inertia, i.e., the within cluster variation, such that the sum of the inertia across all the clusters is as small as possible.

3.4 Case Study

To ascertain the effects of a chosen image classification method on the resulting land cover model, the methods discussed in **Section 3.3** were used to determine the land cover changes in GAMA from 1991 to 2022. The study area was classified in to four classes: "Vegetation", "Built-up", "Transition", and "Water". The same training dataset was used to train models for the supervised classifications, i.e., random forest and support vector machine. Confusion matrices were calculated, with which the overall accuracies and kappa scores were derived to make a quantitative comparison. For each classification method, the global fractal dimension, the total edge values and the number of patches of the classified land cover types were determined. These metrics (fractal dimension, total edge and number of patches) were the basis on which the qualitative comparison of the classification methods were made.

3.4.1 Image Classification Using Random Forest (RF) - GAMA

The following python libraries were used: numpy, matplotlib, gdal, geopandas and sklearn. Geopandas was used to read the ground truth data as a geodataframe. The land cover names (class names) were extracted and assigned class ids. The class ids were added to the geodataframe and the data was divided into two: 70% for training the model and 30% to test the model. Gdal was used to open the composite band as a gdal dataset. The gdal dataset was read as an array, stacked and then reshaped into a 2d array to match the training data. From sklearn, random forest was used to train and fit a model to classify each cell in the satellite image into its associated land cover type. The results were written as tiff files using gdal and exported to ArcMap to prepare the land cover maps of GAMA. **Figure 3.1** are the land cover maps of GAMA for 1991, 2002, 2013 and 2022 obtained using random forest. The python script for the RF classification can be found in **Appendix B.1**.

3.4.2 Image Classification Using Support Vector Machine (SVM) - GAMA

The same procedure that was used to read the images, the ground truth data and assign class ids for the RF classification was used for the SVM. However, here, the classifier used was support vector machine with a linear kernel from sklearn. The result was written as a tiff file using gdal and exported to ArcMap to prepare the land cover maps of GAMA.

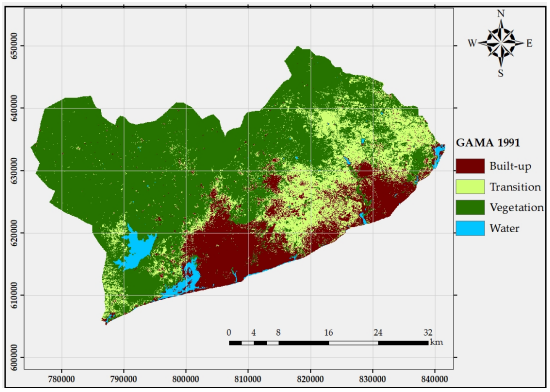

(a) RF GAMA 1991

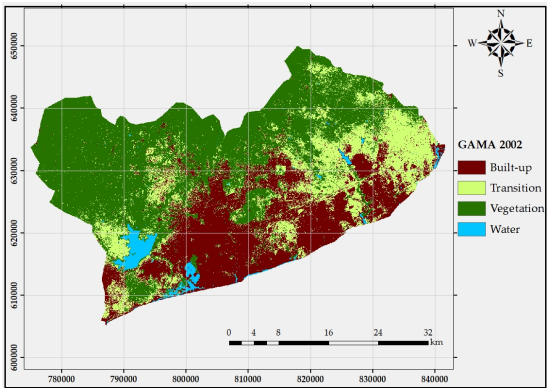

(b) RF GAMA 2002

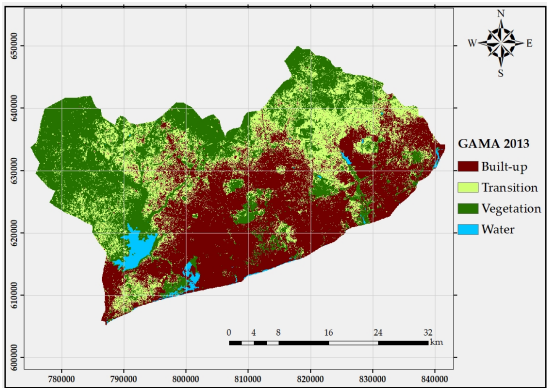

(c) RF GAMA 2013

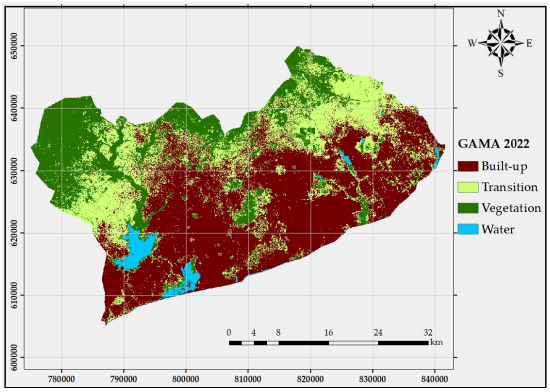

(d) RF GAMA 2022

Figure 3.1: RF land cover maps of GAMA (1991, 2002, 2013 and 2022)

Figure 3.2 are the land cover maps of GAMA for 1991, 2002, 2013 and 2022 obtained using support vector machine. The python script for the SVM image classification can be found in **Appendix B.2**.

3.4.3 Image Classification Using SLIC K-Means (SLIC) - GAMA

Gdal was used to open the composite bands for the various years as gdal datasets. The images appeared darker, so a histogram was computed using skimage to know the limits of the RGB bands. The RGB bands were then stretched to their limits, to enhance the image brightness. Gamma adjustments were also done to further enhance the image brightness. The images were then converted to grayscale and smoothened to reduce noise in them. The smoothened images were then segmented into superpixels using the simple linear iterative clustering (SLIC) algorithm by clustering the pixels based on their color similarity and proximity in the image plane. Region properties of the superpixels were measured to determine the intensity of the superpixels. The mean intensities of the superpixels were computed and plotted on a histogram to get an idea of the range of variation of the various intensities. K-means was then used to create a model of 5 clusters to fit the mean intensities. The model was then used to predict labels for the

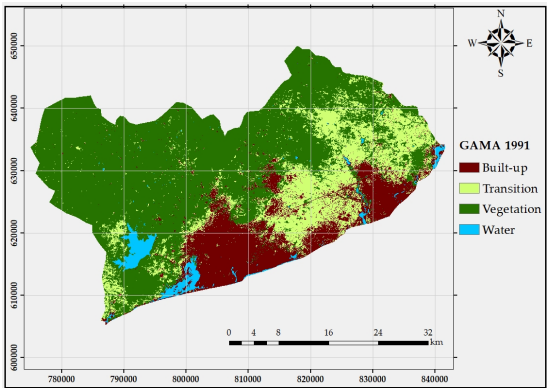

(a) SVM GAMA 1991

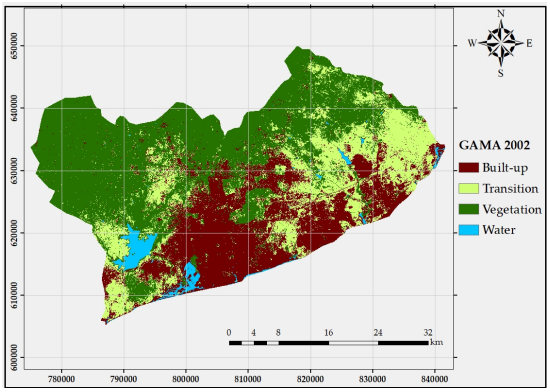

(b) SVM GAMA 2002

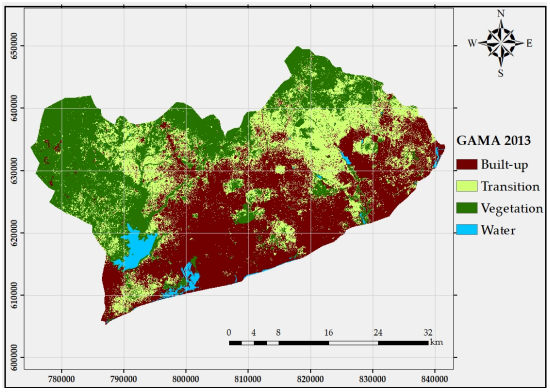

(c) SVM GAMA 2013

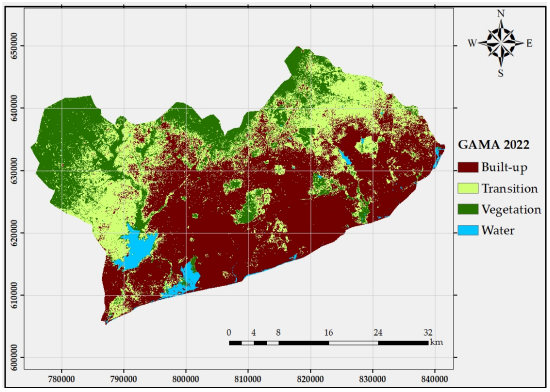

(d) SVM GAMA 2022

Figure 3.2: SVM land cover maps of GAMA (1991, 2002, 2013 and 2022)

clusters. The images were then labeled appropriately by taking a combination of the predicted labels of the different clusters to relabel them according to the coordinates of each cluster. The results were written as tiff files using gdal and exported to ArcMap. The tiff files were reclassified into four classes to match the land cover types chosen for this thesis ("Vegetation", "Built-up", "Transition", and "Water"). SLIC K-Means could not identify water bodies, as it misclassified them as vegetation. To address this, a shapefile of the water bodies was rasterized and mosaicked into the reclassified tiff files to obtain the water bodies on the resulting land cover maps. **Figure 3.3** are the land cover maps of GAMA for 1991, 2002, 2013 and 2022 obtained using SLIC K-Means. The python script for the SLIC image classification can be found in **Appendix B.3**.

3.4.4 Comparison of Image Classification Methods

In comparing different classification methods, what most researchers use is the accuracy assessment. They do this by analyzing confusion matrices to ascertain how well the algorithms performed [39]. A confusion matrix is a table that defines the correspondence between land cover types classified by a classifier and the ground truth data. From the confusion matrix, accuracy indicators such as the overall accuracy, recall, precision,

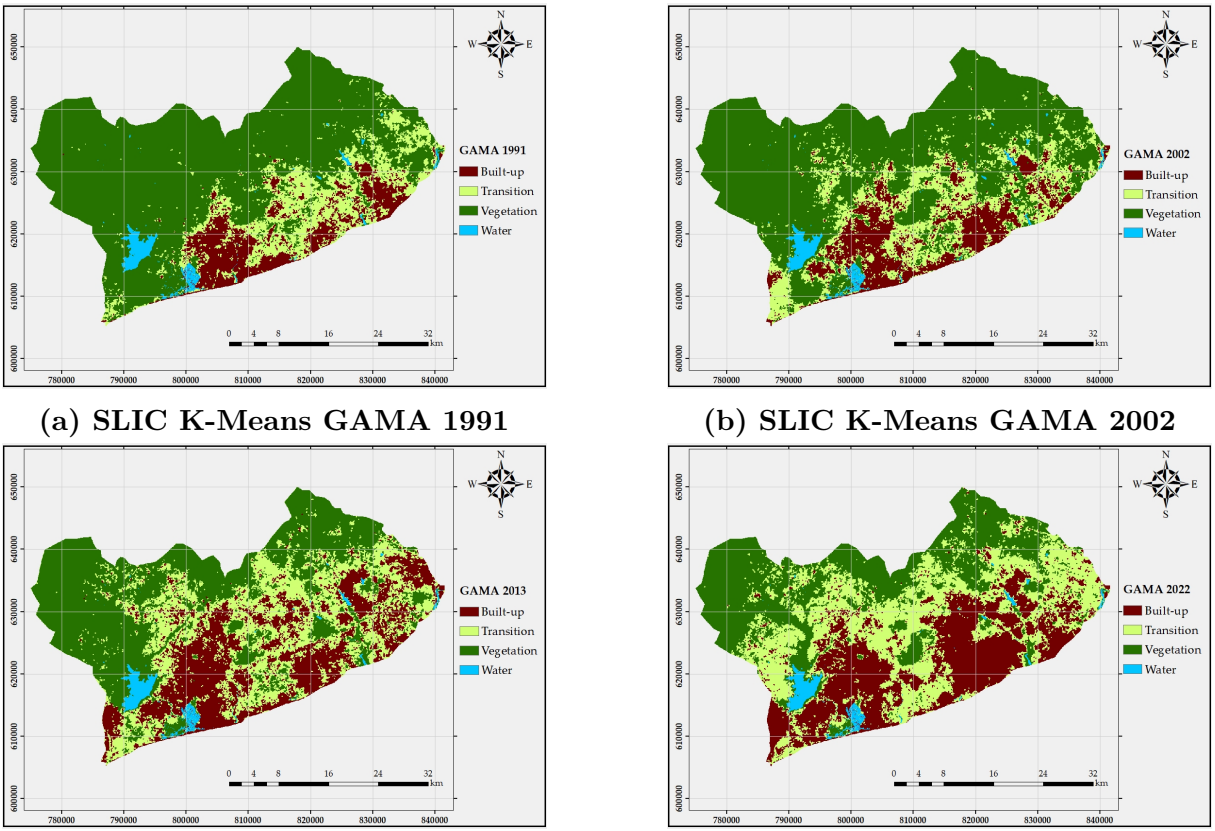

(a) SLIC K-Means GAMA 1991 **(b) SLIC K-Means GAMA 2002**

(c) SLIC K-Means GAMA 2013 **(d) SLIC K-Means GAMA 2022**

Figure 3.3: SLIC K-Means land cover maps of GAMA (1991, 2002, 2013 and 2022)

f1 score and kappa score can be computed. Overall accuracy is a ratio of the total number of correctly classified observations to the total number of observations. It is a measure of how well the classifier performed. This is a general measure of the classification accuracy, however, it does not indicate which classes were poorly classified. To know how well the classification worked on each class, recall (producer accuracy) and precision (user accuracy) are used. Recall is the ratio of the correctly predicted observations of a particular land cover type to total observations of that land cover type. It is a measure of how many points in the test data that actually belong a to a particular land cover type are predicted to belong to that land cover type. On the other hand, precision is the ratio of correctly predicted observations of a particular land cover type to the total predicted observations of that land cover type. It is a measure of how many points in the test data that have been predicted to belong to a particular land cover type actually belong to that land cover type. Both precision and recall measure the predictive performance of the model in different ways. Precision measures the extent to which predictions made by the classifier are correct whereas recall measures the extent to which actual observations made are predicted correctly. These two measures can be combined to form a single metric

called F1 score. F1-Score is the harmonic mean of the performance of the model on each land cover type based on the precision and recall. It is used to assess the relative impact of recall and precision on the model. F1 score ranges between 0 and 1, the closer it is to 1 the better the model. Another important accuracy indicator is the kappa score. It essentially evaluates how well the classification performed as compared to just randomly assigning values to cells, i.e., whether or not the classification did better than randomly assigning values to cells in the image. The kappa score can range from -1 to 1. A value of 0 indicates that the classification is no better than a random classification. A negative number indicates the classification is significantly worse than a random classification. A value close to 1 indicates that the classification is significantly better than a random classification [140]. The standard scale follows the following set of rules: a value of 0.8 or higher is considered strong, 0.4–0.8 is moderate, and less than 0.4 suggests a poor agreement. The overall accuracy, recall, precision, f1 score and kappa score are given by **equation 3.4**, **equation 3.5**, **equation 3.6**, **equation 3.7** and **equation 3.8** respectively.

$$Overall\ Accuracy = \frac{Number\ of\ correctly\ predicted\ pixels}{Number\ of\ reference\ pixels} \tag{3.4}$$

$$Recall = \frac{Number\ of\ correctly\ classified\ samples\ of\ a\ class}{Column\ total} \tag{3.5}$$

$$Precision = \frac{Number\ of\ classified\ samples\ of\ a\ class}{Row\ total} \tag{3.6}$$

$$F1\ Score = 2 \times \frac{precision \times recall}{precision + recall} \tag{3.7}$$

$$kappa\ Coefficient = \frac{(TS \times TCS) - \sum(Column\ Total \times Row\ Total)}{TS^2 - \sum(Column\ Total \times Row\ Total)} \tag{3.8}$$

where:

$TS = Total\ Sample$

$TCS = Total\ Correct\ Samples$

The confusion matrices and classification reports for GAMA 1991, 2002, 2013 and 2022, indicating the overall accuracy, precision, recall, f1-score and kappa score of the RF and SVM classifications are presented in **Appendix C.1 and C.2** respectively. From the kappa scores, it was observed that both RF and SVM performed very well. They all had kappa scores of more than 0.8 for all the years considered. **Table 3.2** is a table showing the kappa scores obtained when RF and SVM were used to model the land cover of GAMA for 1991, 2002, 2013 and 2022. No kappa score was computed for SLIC K-Means because it is an unsupervised classification, hence there was no reference data with which to make the comparison.

Table 3.2: Kappa scores for RF and SVM, GAMA 1991, 2002, 2013 and 2022

	Kappa Score RF	**Kappa Score SVM**
1991	0.928	0.925
2002	0.906	0.913
2013	0.881	0.849
2022	0.933	0.929

Both RF and SVM produced satisfactory results. This is a typical scenario of two image classification methods producing similar overall accuracies and kappa scores, making it difficult to choose one over the other. However, the interest of this chapter is not just to compare classification methods based on only overall accuracies and kappa scores, but also based on the form and shape of the classified land cover types. These are indicators which the overall accuracies and kappa scores are unable to assess. In this chapter, fractal dimension, total edge and number of patches are proposed as measures to quantify the shape and form of classified land cover types. Fractal dimension is an indicator of the lacunarity of the land cover types. It is used in landscape ecology to measure the complexity of landscape patterns [139]. Several definitions for fractal dimension exist: Hausdorff dimension, Minkowski dimension, correlation dimension, etc., but in this thesis, the Minkowski dimension, also known as the box counting dimension is what would be used. On a two dimensional surface, fractal dimension ranges from 0 to 2, the closer the value is to 2, the more regular the land cover type. Total edge is a landscape metric that is typically used in landscape ecology in quantifying landscape patterns. It is the sum of all the horizontal and vertical edges between cells of different land cover types

[139, 105]. It is an indicator of how much details were captured in the classification of each land cover type. The higher the value of the total edge, the more details there are in the land cover type. A patch could be defined as the four nearest neighbor cells (i.e., horizontal and vertical neighbors only) adjoining a cell or the eight nearest neighbor cells (i.e., horizontal, vertical and diagonal neighbors) adjoining a cell. Based on the definition of a patch by the analyst, PN refers to the total number of patches in the landscape [139, 105]. Fractal dimension, total edge and patch number are given by **equation 3.9, equation 3.10 and equation 3.11** respectively.

$$N = S^{-D} \tag{3.9}$$

where:

N= Number of boxes

S= Scale

D= Fractal Dimension

$$Total\ Edge = \sum_{k=1}^{m} e_{ik} \tag{3.10}$$

where:

e_{ik}= edge length in meters between land cover type i and k

$$Number\ of\ Patches = N \tag{3.11}$$

Table 3.3, 3.4, 3.5 and 3.6 are tables comparing random forest, support vector machine and SLIC K-Means based on the fractal dimension, total edge values and number of patches of the various land cover types classified for GAMA 1991, 2002, 2013 and 2022.

Appendix D is a map comparing the land cover maps obtained with each method for each year considered in this study. Since the aim of this thesis is to study urban growth,

Table 3.3: Comparison between RF, SVM, and SLIC, GAMA 1991

Landcover	Random Forest			Support Vector Machine			SLIC K-Means		
	FD	TE	PN	FD	TE	PN	FD	TE	PN
Built-up	1.590	5 228 100	8 250	1.581	4 718 820	7 675	1.547	1 412 760	268
Transition	1.636	10 067 910	15 021	1.625	7 551 090	9 416	1.583	2 163 030	573
Vegetation	1.814	7 643 910	7 555	1.807	5 939 010	5 429	1.821	1 061 640	420
Water	1.205	378 060	440	1.225	534 180	879	1.227	333 990	173

Table 3.4: Comparison between RF, SVM, and SLIC, GAMA 2002

Landcover	Random Forest			Support Vector Machine			SLIC K-Means		
	FD	TE	PN	FD	TE	PN	FD	TE	PN
Built-up	1.683	7 864 860	10 941	1.681	7 260 480	10 410	1.567	2 040 870	502
Transition	1.679	11 576 190	20 142	1.671	8 986 020	13 647	1.625	1 441 770	466
Vegetation	1.777	7 840 920	7 765	1.771	6 696 570	5 967	1.802	3 085 410	790
Water	1.188	399 270	521	1.19	373 590	391	1.227	333 990	173

Table 3.5: Comparison between RF, SVM, and SLIC, GAMA 2013

Landcover	Random Forest			Support Vector Machine			SLIC K-Means		
	FD	TE	PN	FD	TE	PN	FD	TE	PN
Built-up	1.743	9 258 480	9 161	1.743	9 243 900	9 783	1.654	4 062 270	1 115
Transition	1.703	14 851 290	20 963	1.704	13 379 520	17 784	1.682	2 079 870	499
Vegetation	1.721	8 601 810	9 325	1.708	6 841 920	7 291	1.728	2 340 120	648
Water	1.194	276 780	264	1.197	295 260	237	1.227	333 990	173

Table 3.6: Comparison between RF, SVM, and SLIC, GAMA 2022

Landcover	Random Forest			Support Vector Machine			SLIC K-Means		
	FD	TE	PN	FD	TE	PN	FD	TE	PN
Built-up	1.772	8 972 370	10 618	1.775	7 241 040	6 998	1.667	3 485 550	613
Transition	1.704	12 769 860	14 382	1.705	11 844 030	12 512	1.709	1 871 160	431
Vegetation	1.646	5 360 040	6 400	1.631	5 122 500	6 332	1.688	1 855 680	615
Water	1.199	306 150	215	1.216	364 470	452	1.227	333 990	173

the focus of the analysis would be on the built-up area. The other land cover types, i.e.: transition, vegetation and water, would be classified as non-built-up areas.

From **Table 3.3, 3.4, 3.5, and 3.6**, it was observed that the difference between the values obtained for fractal dimensions of the built-up area with respect to RF and SVM were not significant. This means that fractal dimension could not clearly distinguish between RF and SVM. The fractal dimension values obtained for SLIC, however, were lower than those of RF and SVM. Typically, if there are more patches in a particular land cover type, automatically, the total edge values would be high. This was confirmed by the similar trend observed in the total edge values and patch numbers obtained for RF, SVM and SLIC. Generally the built-up areas identified with RF had the highest patch number and total edge values, followed by SVM and then SLIC. **Appendix E** are charts summarizing the fractal dimension, total edge and patch number values of the various land cover types classified using RF, SVM and SLIC K-Means for GAMA 1991, 2002, 2013 and 2022 respectively.

The high TE and PN values observed on the built-up areas classified with RF indicates that RF is able to show more details in a land cover map than SVM and SLIC. The TE and PN values observed on the SLIC land cover maps were the least among the three methods. This was not very surprising because SLIC is a cluster of pixels based on the similarity of their color and proximity in the image plane. What this implies is that if the interest of the analyst is to obtain a detailed land cover map, the best option among the three methods used in this case study is RF. Also if the interest of the analyst is to produce a more generalized land cover map, SLIC is the best method to use.

3.4.4.1 Subsections

Since urbanization in GAMA is not uniformly distributed, the study area was divided into three subsections (Section A, Section B and Section C), as shown in **Figure 3.4**, to get a closer look at the differences between the land cover maps obtained with the different classification methods at the various sections. From the land cover maps obtained with the different classification methods for all the years under study, Section A, Section B and Section C were extracted and studied by calculating their fractal dimension, total edge and patch numbers. **Appendix F** are maps showing Section A, Section B and Section C respectively. **Appendix G** are tables showing the fractal dimension, total edge and patch numbers of Section A, Section B and Section C.

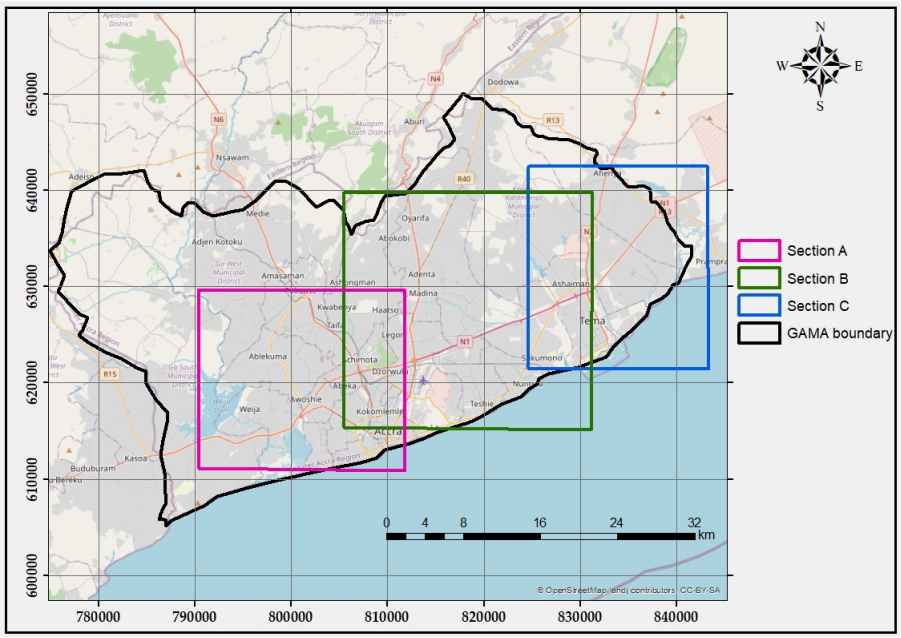

Figure 3.4: Map of GAMA divided into three sections, Section A, B and C

Section A: Based on visual inspection of **Appendix F.1**, with emphasis on the built-up areas, it was observed that the results obtained with RF and SVM were quite similar for all the years, in terms of the spatial distribution of the built-up pixels. Visually, SLIC was very different from RF and SVM as it appears to amplify the spaces in the built-up areas identified by RF and SVM. While the fractal dimensions of the built-up areas classified with RF and SVM were fairly the same, the total edge values of RF were slightly higher than those of SVM from 1991 to 2013, but were more pronounced in 2022. This difference can be seen when the top right corner of the built up area is observed. The patch numbers of the built-up areas classified with RF and SVM were also fairly the same for all the years until 2022 where RF was significantly higher than SVM. **Appendix H.1, H.2 and H.3** are charts showing the fractal dimensions, total edge values and patch numbers of the land cover maps obtained with RF, SVM and SLIC of section A in 1991, 2002, 2013 and 2022.

Section B: Based on visual inspection of **Appendix F.2**, with emphasis on the built-up areas, it was observed that the results obtained with RF and SVM were not as similar as what was observed in *Section A*. In 1991, some built-up areas were identified in the central parts of the map obtained with RF which were not present on the map obtained with SVM. As the years progressed, the differences became smaller. The built-up areas identified with SLIC appeared scattered because of the exaggeration of the spaces in the built-up areas, however, in 2022, the built-up area identified in the central part was similar to what was identified with RF and SVM. This could be because the central part

was very saturated, such that, there was very little space to be exaggerated. The fractal dimensions and total edge values showed the same trend as what was observed in *section A*. The patch numbers of RF from 1991 to 2013 were slightly higher than SVM, but was quite pronounced on 2022. As compared to the patch numbers obtained with RF and SVM, those of SLIC were very low. **Appendix H.4, H.5 and H.6** are charts showing the fractal dimensions, total edge values and patch numbers of the land cover maps obtained with RF, SVM and SLIC of section B in 1991, 2002, 2013 and 2022.

Section C: Based on visual inspection of **Appendix F.3**, with emphasis on the built-up areas, it was observed that the results obtained with RF and SVM were very similar in terms of the spatial distribution of the built-up areas. The fractal dimensions showed the same trend as what was observed in *section A* and *Section B*. The total edge values of RF were higher than those of SVM and SLIC, except in 2013 where the total edge value of the built up identified with SVM was slightly higher than that of the RF. In 1991 and 2002, the patch number for RF was higher than that of SVM. In 2013 and 2022, the patch numbers for SVM was slightly higher than RF. The total edge values and patch number for SLIC were the least throughout. **Appendix H.7, H.8 and H.9** are charts showing the fractal dimensions, total edge values and patch numbers of the land cover maps obtained with RF, SVM and SLIC of section C in 1991, 2002, 2013 and 2022.

3.5 Conclusion and Recommendations

The aim of this chapter was to analyze how a particular classification method impacts the spatial distribution of identified land cover types in land cover maps, even when accuracy and kappa scores are similar. Upon conclusion of the study, it was observed that although different classification methods may possess similar overall accuracies and kappa scores, subtle differences in qualities such as lacunarity and edge length of identified land cover types can be detected. These differences serve as important factors in guiding analysts to choose a more suitable classification method for their specific project requirements. Along with commonly used quantitative measures such as overall accuracy, recall, precision, f1 score, and kappa score, additional qualitative measures were proposed such as fractal dimension, total edge, and patch number. These measures are not meant to replace the quantitative measures, but rather to supplement them and enhance the comparison of classification algorithms.

Three classification methods were tested: random forest (RF), support vector machine

(SVM) and SLIC K-Means. RF and SVM classification methods displayed similar overall accuracy, recall, precision, f1 score, and kappa score values. On the other hand, as an unsupervised classification method, SLIC K-Means had no confusion matrix to compute these measures. The fractal dimensions, total edge values, and patch numbers of the different land cover types resulting from each classification method were computed and compared.

Despite the similarities in accuracy measures, the qualitative measures, particularly total edge values and patch numbers, revealed that land cover maps resulting from RF classification were more detailed than those of SVM and SLIC K-Means. However, for those interested in obtaining a more generalized land cover map, SLIC K-Means would be the optimal choice. By incorporating qualitative measures such as fractal dimensions, total edge, and patch number into studies for comparing image classification methods, analysts will be able to select classification methods based on both accuracy and texture of resulting land cover maps.

Future research can focus on developing and evaluating additional qualitative measures beyond fractal dimension, total edge, and patch number to enhance the assessment of land cover mapping methods. This could involve investigating other textural, structural, or spatial characteristics of land cover maps for a more comprehensive understanding of their quality. Researchers can explore ways to effectively integrate these qualitative measures with traditional quantitative metrics, such as overall accuracy and kappa scores, to create a more robust evaluation framework. This integrated approach provides a more holistic view of classification method performance. Since visualisation plays a crucial role in conveying the richness of the land cover data, additionally, researchers could investigate advanced visualisation techniques for land cover maps, highlighting the unique features and information provided by different classification methods. Additionally, researchers should investigate advanced visualization techniques for land cover maps, highlighting the unique features and information provided by different classification methods. Visualization plays a crucial role in conveying the richness of land cover data.

Chapter 4

Longitudinal Landscape Analysis of Urban Growth in GAMA

4.1 Introduction

Urbanization offers improved living standards and access to various services such as education and recreation, however, it also exposes people to various environmental challenges such as air pollution, noise, water contamination, waste disposal problems, and excessive heat [71, 104]. According to Dong et al. [46], the United Nations' World Charter for Nature from 1982 emphasized the importance of considering the sustainable capacity of ecosystems in long-term economic development planning, so as to prevent irreversible damage. It is therefore very essential that effective spatial governance measures are put in place to promote regional sustainable development while urbanizing. It is also important to monitor the state of urban growth over time to facilitate natural resource management, ecosystem protection, and mitigate unbalanced regional development [46].

Urbanization is significantly linked to industrialization, modernization, and the sociological process of rationalization, all of which are important factors for regional economies [128]. Measuring the state of urban expansion is crucial to the establishment of a baseline which can aid in appropriate preparations for future occurrences. This has significant effects on the ecosystem [77, 110]. According to McGarigal [105], a landscape refers to a varied land area consisting of a collection of interconnected ecosystems that repeat in a similar pattern throughout the observed region. As the backdrop for all human activities on earth, landscapes serve as habitats for both human beings and other life forms [72]. Due to the interaction between humans and other living organisms, landscapes are con-

stantly evolving. As urban areas develop, landscape patterns are altered, with forest and agricultural uses being transformed into industrial, commercial, and residential uses [71]. Gökyer [65] identified five primary factors that contribute to landscape changes, namely: socio-economic, political, natural, cultural, and technological advancements. Over the years, there have been several small-scale changes in landscapes aimed at improving the living conditions of humans. Although these changes may seem insignificant when viewed individually, their cumulative impact on the ecosystem is substantial.

Generally, a landscape can be modelled as a matrix, corridor, patch, and mosaic [24, 65]. The landscape matrix is typically the most dominant and interconnected land cover type within the landscape. When the landscape composition (i.e., the non-spatial characteristics of the landscape) and the landscape configuration (i.e., the spatial characteristics of the landscape) are disturbed, the landscape matrix becomes fragmented, a process referred to as fragmentation. According to Flowers et al.[55] the process of fragmentation can be summarized into four phases: perforation, dissection, dissipation, and shrinkage as shown in **figure 4.1**.

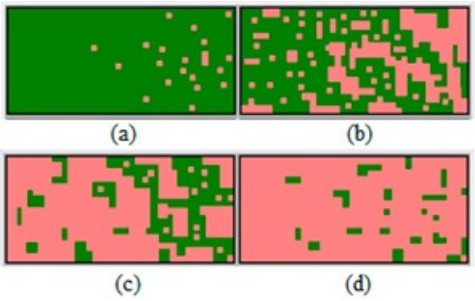

Figure 4.1: The four stages of fragmentation: a) perforation – initial small openings forming patches (i.e., non-linear areas found within the matrix differing from its surroundings) within the matrix; b) dissection – larger intrusions of patches, often along with physical features; c) dissipation – the spread and merging of patches; and d) shrinkage – reduction in patch size and attrition. Source:[55]

Fragmentation can cause negative impacts such as: deforestation; alteration of water courses leading to flooding; reduced availability of food; urban sprawl; and increased pollution from automobile usage including exhaust fumes, noise, and dust [72]. While it may not be possible to completely prevent landscape fragmentation due to the unending human interactions with the environment, understanding the process of fragmentation can help in anticipating and preparing for its effects before it eventually occurs. This knowledge can inform the decisions of land use policy makers and authorities, enabling them to act in the best interests of future generations. Since fragmentation is a spatial

process that occurs over time, a spatiotemporal analysis can be employed to measure it. Simply examining land cover maps is insufficient for measuring fragmentation. Additional quantitative information is required. Such information can be derived from the numerous landscape metrics that have been developed to describe landscape patterns [148, 125, 105].

Landscape metrics are measurable units that allow for the qualitative and quantitative description of spatial patterns and ecological processes over time in space. The qualitative description of the land cover types present in the landscape is provided by the landscape composition, whereas the quantitative description of the spatial arrangements of the land cover types present in the landscape is provided by the landscape configuration. Many landscape metrics are strongly correlated, which makes them redundant if they all are chosen for a particular analysis. Selecting a relevant subset from the numerous metrics available can be quite challenging. According to Turner et al. [139], landscape metrics must be chosen to achieve specific objectives, minimize redundancy, explain pattern variability across the landscape, and cover a substantial portion of the range of their potential values. Flowers et al. [55], also stated that when utilizing landscape metrics to analyze urban growth patterns, it is recommended to select metrics that capture the characteristics of the landscape area, its edge effects, and shape complexity. In this chapter, drawing inspiration from previous works on the quantification of landscape patterns for urban growth management [68, 3, 143, 5, 113, 99, 91, 35], Class Area (CA), Number of Patches (NUMP), Edge Density (ED), and Proportion of like Adjacency (PLADJ) have been chosen for the quantification of the fragmentation process of Greater Accra Metropolitan Area (GAMA) from 1991 to 2022.

The aim of this chapter is to provide a comprehensive and data-driven longitudinal analysis on the urban growth of GAMA, and its effects on biodiversity. Using the land cover maps of GAMA from 1991-2022 that were obtained with RF in Chapter 3, and various techniques such as land cover change analysis, landscape metric measurement, and multiradial fractal dimension calculation, information extracted solely from freely available satellite images are used to achieve this objective. The idea is to capture the changes in land cover and landscape patterns in GAMA from 1991 to 2022 and predict the landscape patterns for 2030. The results of this analysis can be used to understand the drivers and impacts of urban growth in GAMA and to inform urban planning and management strategies for the region's future development. Additionally, the prediction of future land cover and landscape metrics can provide valuable insights for decision-makers in terms of

managing and adapting to the region's urban growth.

4.2 Materials and Methodology

4.2.1 Materials used

The data and software used in this chapter are presented in **table 4.1**

Table 4.1: Data and software used

Data used	
Land cover maps of GAMA	1991, 2002, 2013 and 2022
Software used	
ArcGIS Desktop	
Fragstats 4.2	
Python Libraries: SciPy	
IDRISI 17.0 The Selva Edition	
Fractalyse 3 - 0.81	
Netlogo 6.3.0	

4.2.2 Methodology

The methodology implemented in this chapter is categorized into three phases. The initial phase involves analyzing the land cover changes in GAMA from 1991 to 2022, and determining the rate of urban growth during this period. The second phase is urban growth modelling and prediction of the land cover of GAMA for 2030 using Land Change Modeler (LCM), Markov Chain Cellular Automata (MCCA), and an Agent Based Model implemented in NetLogo (ABM). The third and final phase is a quantification of the evolution of the landscape patterns in GAMA by calculating landscape metrics. Additionally, the evolution of the landscape pattern of Sekondi Takoradi Metropolitan Area (STMA), a coastal city about 280 km west of GAMA, would be analysed.

4.2.2.1 Phase 1 - GAMA land cover change analysis (1991-2022)

The land cover maps of GAMA were converted from raster to polygon using 'From Raster' from the 'Conversion Tools' in the ArcToolbox. To ensure distinct codes for each land cover type, the attribute table was accessed. Next, the 'Dissolve' function from the geoprocessing tab was utilized to merge similar features into a single feature using 'gridcode' as the dissolve field. The different classes were labeled within the attribute table, and the area covered by each class was computed using the 'calculate geometry' option. This

process was carried out for all the years under examination, namely 1991, 2002, 2013, and 2022. To identify changes that have occurred over time, the 'Intersect' tool from the geoprocessing tab was employed. This operation involved calculating the geometric intersection between consecutive years (1991-2002, 2002-2013, and 2013-2022). The more recent land cover map was superimposed on the previous one, adopting the changes where they occurred while keeping unchanged areas consistent. To facilitate this analysis, a new field named 'Change' with a text data type was added to the attribute table. A VB Script was composed in the field calculator to label the changes according to the format "Change = Land cover type Yr 1 + '-' + Land cover type Yr 2". Additionally, another field named 'Area_Change' with a double data type was created to calculate the area affected by each land cover change. The area calculations were performed using the 'calculate geometry' function within the attribute table. Finally, the attribute table was exported to Excel in order to generate charts illustrating the various changes that occurred over the specified period.

4.2.2.1.1 Rate of urban growth The calculation of urban growth rate involves comparing the land cover classification of a specific area during different time periods. This analysis focused on examining the changes in the extent of land categorized as "Built-up" over time. To determine the rate of urban growth, the area occupied by urban land cover (i.e., Built-up) was calculated for each time period. Subsequently, the difference in area between the two consecutive periods was determined. Dividing the change in area by the time period yielded the annual rate of change in urban land cover. The growth rate is given by **equation 4.1**.

$$Morphological\ growth\ rate = \frac{((UrbanArea(t_2) - UrbanArea(t_1))}{Year(t_2) - Year(t_1)} \times 0.01 \qquad (4.1)$$

4.2.2.2 Phase 2 - Urban growth modelling and prediction

Three urban growth models (Land Change Modeler, Markov Chain Cellular Automata and NetLogo) were used to model and predict the future land cover of GAMA. The best model was determined by comparing the Kappa score of the result of each model and how much details it was able to capture.

4.2.2.2.1 Land change modeler The Land Change Modeler (LCM) in Idrisi is a tool used for land change modeling and prediction. It integrates data sources, performs statistical and spatial analysis, and simulates land cover changes over time. LCM follows a stepwise approach, starting with change analysis and transition potential modeling, and progressing to change prediction based on historical data. In change analysis, alterations between two land cover maps are identified as transitions from one state to another. Transition potential modeling groups these transitions into sub-models with transition variables. The transition variables provide valuable information about the conditions and characteristics associated with the transitions between different land cover states. By incorporating transition variables into the modeling process, LCM enables a more accurate representation of the relationships between explanatory factors and land cover change patterns. This process generates a transition potential map indicating change potential at a specific time. The transition sub-models are modeled using the multi-layer perceptron (MLP) neural network, which automatically adjusts parameters and learning rates to improve the model. Markov chain analysis is employed during change prediction to quantify the amount of change in each transition, considering an end date. The resulting models include a hard prediction model that provides a single realization of predicted change based on competitive land allocation, and a soft prediction model that assesses vulnerability to change for selected transitions, offering a comprehensive understanding of change potential. LCM is valuable for land management, urban planning, and environmental assessment purposes.

4.2.2.2.1.1 Transition variables This study employed specific transition variables, namely evidence likelihood (evlilkelihood), multiradial fractal dimensions (frac), distance from vegetation (Dist_veg), and distance from the central business district (Dist_CBD).

i. Evidence likelihood: In IDRISI, the evidence likelihood is obtained by combining a changes map and a land cover map. The changes map represents the transitions between land cover classes over time, while the land cover map shows the initial state of the landscape. Using a probabilistic approach, the conditional probabilities of transitioning between land cover classes are calculated from the changes map. These probabilities are then applied to the land cover map to assign evidence likelihood values to each pixel based on the neighboring pixel's conditional probabilities. This process considers spatial relationships to estimate the likelihood of a pixel belonging to a specific land cover class. The evidence likelihood approach in IDRISI

provides a more accurate and probabilistic assessment of land cover classification by incorporating observed changes and their spatial patterns.

ii. Multiradial fractal dimension: Multiradial fractal dimension is a measure used to quantify the complexity or irregularity of a shape or pattern. It is derived from the concept of fractals, which are mathematical objects that exhibit self-similarity at different scales. The multiradial fractal dimension specifically focuses on the dimensionality of a shape or pattern when viewed from different radial directions [58]. In the context of land cover analysis, the multiradial fractal dimension is often applied to quantify the complexity of built-up areas or urban landscapes. By calculating the fractal dimension at multiple radial directions around a point or region, it provides insights into the spatial structure and arrangement of built-up features. Higher values of the multiradial fractal dimension indicate more regular or homogeneous patterns while lower values indicate greater complexity or irregularity in the distribution of built-up areas. The multiradial fractal dimension is a useful tool in understanding urban morphology and spatial patterns, as it captures the inherent complexity and heterogeneity of urban landscapes. It can be employed to analyze the changes in urban form over time, compare different urban areas, or assess the impact of urbanization on the landscape. The multiradial fractal dimension of the built-up area of GAMA was calculated using Fractalyse 3 - 0.8.1 after the built-up area was extracted from the land cover map using ArcMap 10.8.

iii. Distance from Vegetation: The distance from Vegetation refers to the spatial proximity from areas with natural or planted vegetation, such as forests, parks, gardens, or green spaces. It is a measure used to understand the relationship between built-up areas and vegetated areas. The distance from vegetation can be an important factor in various environmental and ecological studies. It can provide insights into the availability of green spaces and natural habitats, urban heat island effects, air quality, biodiversity, and overall ecosystem health in urban environments. Analyzing the distance from vegetation can help researchers and policymakers assess the accessibility and distribution of green spaces within a city, identify areas with limited access to nature, and evaluate the potential impacts of urbanization on natural habitats and wildlife. The distance from vegetation was calculated using the Euclidean distance tool in ArcMap 10.8.

iv. Distance from CBD: The distance from CBD refers to the physical distance between

a particular location and the central commercial and economic hub of a city or urban area. The CBD is typically characterized by a concentration of commercial activities, office buildings, retail centers, and transportation hubs. The distance from the CBD is an important factor in urban planning, transportation, and land use studies as it can influence various aspects of urban development. The distance from the CBD can impact land values, with properties closer to the CBD often being more expensive due to their proximity to business and employment opportunities. It can also affect transportation patterns, as areas closer to the CBD may experience higher traffic volumes and greater accessibility to public transportation options. Additionally, the distance from the CBD can influence the distribution of land uses and the intensity of development. Typically, areas closer to the CBD tend to have a higher concentration of commercial and residential buildings, while areas farther away may consist of more suburban or rural land uses. Understanding the distance from the CBD is crucial for urban planners, policymakers, and researchers to assess patterns of urban growth, plan transportation networks, allocate resources, and develop strategies to manage urban development effectively. It helps in identifying areas of potential urban expansion, determining the need for infrastructure development, and implementing policies to promote balanced growth and sustainable development across the city or urban area. The distance from CBD was computed from the center of the identified CBD to the edge of the study area.

These transition variables were derived exclusively from land cover maps prepared by the classification of freely available satellite images.

4.2.2.2.2 Markov Chain Cellular Automata (MCCA) Markov Chain Cellular Automata is another approach used for predictive modelling. It utilizes a Markovian process where the future state of a system at a particular time can be predicted based on the present state of the system and the matrix of transition probabilities between each land cover class. The MARKOV module in IDRISI enables the generation of a transition probability matrix. This matrix allows for the estimation of the probability of land cover class changes or persistence between two specific time periods. This module requires two land cover maps as input and generates the following outputs:

i. Transition probability matrix: this indicates the probability of a pixel in a particular class changing to any other class or staying the same in the subsequent time period.

ii. Transition areas matrix: this provides the expected total area in cells that will undergo change in the next time period.

A cellular automaton is a type of cellular entity that alters its state autonomously based on its previous state and the states of its adjacent neighbors, following a defined set of rules. The CA_MARKOV module requires three inputs to project changes in land cover: the current landcover map, the transition areas file generated by the MARKOV analysis of the current and an earlier map, and a collection of suitability images indicating the suitability of each pixel for different land cover types. The module performs an iterative reallocation of land cover to match the predicted area totals from the MARKOV analysis. The iteration process is determined by a user-defined number of time steps. In each iteration, land cover classes lose and gain land, and suitability is adjusted by a filtering stage to reduce suitability away from existing areas of that type. The Cellular Automaton component arises from both the iterative reallocation process and the suitability filtering stage.

4.2.2.2.3 Agent Based Model NetLogo is a programming language and integrated modeling environment that is widely used to simulate complex systems, including urban growth. In the context of urban growth modeling, NetLogo provides a range of tools for simulating land use changes, population dynamics, transportation systems, and other factors that influence the spatial structure of cities. The software provides an interface for building and running simulations, and offers a wide range of visualization and analysis tools to explore the results of the simulations. One common approach to using NetLogo for urban growth modeling is to develop agent-based models (ABMs) that simulate the behavior of individual actors (such as households, businesses, or local governments) within a larger system. These models can incorporate a range of spatial and non-spatial variables that influence urban growth, such as land use regulations, transportation infrastructure, and demographic changes. ABMs developed using NetLogo can be calibrated and validated using real-world data, and used to explore different scenarios for urban growth under various policy and environmental conditions. For example, a NetLogo-based model of urban growth could be used to evaluate the impact of zoning regulations on land use patterns, or to explore the potential consequences of different transportation investment strategies. Overall, NetLogo is a powerful tool for simulating urban growth and exploring the complex dynamics that drive the evolution of cities over time. The model simulates urban growth with rules for spontaneous, new spreading center, edge, and road-influenced

growth. It initializes by loading raster datasets for slope, urban areas, roads, excluded zones, and land use. Suitability for urbanization is determined based on slope and exclusion criteria. During growth processes, patches randomly urbanize, initiate new growth around spreading centers, expand at edges, and extend along road networks. Suitability is checked, and the model visualizes results through various displays. Key parameters include dispersion, road gravity, and search distance. The rules collectively emulate urbanization influenced by terrain, roads, and land suitability.

4.2.2.3 Phase 3 - Landscape metrics of GAMA

In this thesis, Fragstats 4.2 was used to analyse the spatial pattern of the landscapes of STMA and GAMA by computing various landscape metrics. The landscape metrics that were chosen for the analysis are:

i. Class Area (CA): CA is a fundamental measure of landscape composition which indicates how much of the landscape is comprised of a particular patch type. It is the sum of the areas (m^2) of all patches of a particular patch type, divided by 10 000 to convert it to hectares. It is calculated using **equation 4.2** [105].

$$CA = \sum_{j=1}^{n} a_{ij} \left(\frac{1}{10000} \right) \tag{4.2}$$

Where, a_ij = area (m^2)

ii. Number of Patches (NP): A patch could be defined as the four nearest neighbor cells (i.e., horizontal and vertical neighbors only) adjoining a cell or the eight nearest neighbor cells (i.e., horizontal, vertical and diagonal neighbors) adjoining a cell. Based on the definition of a patch by an analyst, NP refers to the total number of patches in the landscape. The number of patches provides valuable information about habitat fragmentation, species diversity, and habitat quality within a landscape. Understanding this metric aids in evaluating the spatial distribution of habitats, assessing the impacts of fragmentation on biodiversity, and guiding conservation and land management decisions to promote ecological integrity and sustainable use of landscapes. It is calculated using **equation 4.3** [139, 105].

$$NP = N \tag{4.3}$$

Where, N = Total number of patches in the landscape

iii. Edge Density (ED): ED is the sum of all horizontal and vertical edges between cells of corresponding patch types multiplied by the length unit of the cell divided by the total area of the landscape. Edge density is crucial for assessing landscape structure, habitat fragmentation, and their implications for biodiversity conservation and ecosystem functioning. It aids in making informed decisions regarding land-use planning, habitat restoration, and conservation strategies aimed at maintaining the integrity and ecological value of landscapes. It is calculated using **equation 4.4** [139, 105].

$$ED = \frac{\sum_{k=1}^{m} e_{ik}}{A} \times 10000 \tag{4.4}$$

Where, e_{ik} = Total length of all edges of a particular cover type A = Total landscape area

iv. Proportion of Like Adjacencies (PLADJ): PLADJ equals the number of like adjacencies involving the focal class, divided by the total number of cell adjacencies involving the focal class; multiplied by 100 (to convert to a percentage). Assessing the proportion of like adjacency is valuable for land management and conservation planning. It helps identify areas with high or low proportions of like adjacency, guiding decisions on habitat restoration, creation of corridors, and prioritization of conservation efforts. By promoting connectivity and appropriate spatial arrangements of land cover types, land managers can enhance habitat quality, maintain ecological processes, and support sustainable land use practices. PLADJ is given by **equation 4.5** [105].

$$PLADJ = \left[\frac{g_{ii}}{\sum_{k=1}^{m} g_{ik}}\right] \times 100 \tag{4.5}$$

Where, g_{ii} = number of like adjacencies between pixels of a particular patch type

g_{ik} = number of adjacencies between pixels of different patch types

4.3 Results and Discussion

4.3.1 Phase 1- GAMA Land cover change analysis (1991-2022)

The trend observed in the land cover changes of GAMA from 1991 to 2022 indicates several patterns. The most notable change is the increasing trend in the change from Vegetation to Transition, with a peak at 224.79 km^2 from 2002 to 2013; and a slight decrease to 169.83 km^2 from 2013 to 2022. This suggests a conversion of Vegetation areas into Transition land cover during the earlier period, followed by a relatively stable Transition in the later years. Similarly, the Transition to Built-up change demonstrates an increasing trend from 102.05 km^2 (1991 to 2002) to 151.54 km^2 (2002 to 2013), remaining relatively stable at 147.54 km^2 (2013 to 2022). This indicates a consistent growth in Transition areas converting into Built-up land cover, which then maintains its extent in the later years. On the other hand, the Vegetation to Built-up change shows a declining trend, decreasing from 107.54 km^2 (1991 to 2002) to 77.56 km^2 (2002 to 2013) and further decreasing to 46.37 km^2 (2013 to 2022). This suggests a reduction in the conversion of Vegetation areas into Built-up land cover over time. The Transition to Vegetation and Built-up to Transition changes exhibit varying patterns with fluctuating values across the three time periods, indicating some level of dynamism and inconsistency in these specific land cover changes. Overall, the trend in land cover changes highlights the dynamic nature of the studied area, with varying rates of changes between different land cover types over the analyzed time span. **Figure 4.2** is chart comparing the land cover changes between 1991 and 2022.

4.3.2 Phase 2 – Urban growth modelling and prediction of GAMA

4.3.2.1 Land Change Modeller

Initially, the required data, including land cover maps of GAMA 1991-2022 (shown in **figure 3.1**), the transition variables, and excluded areas were prepared in ArcMap 10.8 and converted to ASCII for easy importation into IDRISI 17.0. The transition variables and excluded areas are shown in **Appendix J.1** and **Appendix J.2** respectively. The land cover images of GAMA for 2002 and 2013 were used as inputs to predict the land cover of 2022 using the LCM model, which included modeling transition variables using MLP to

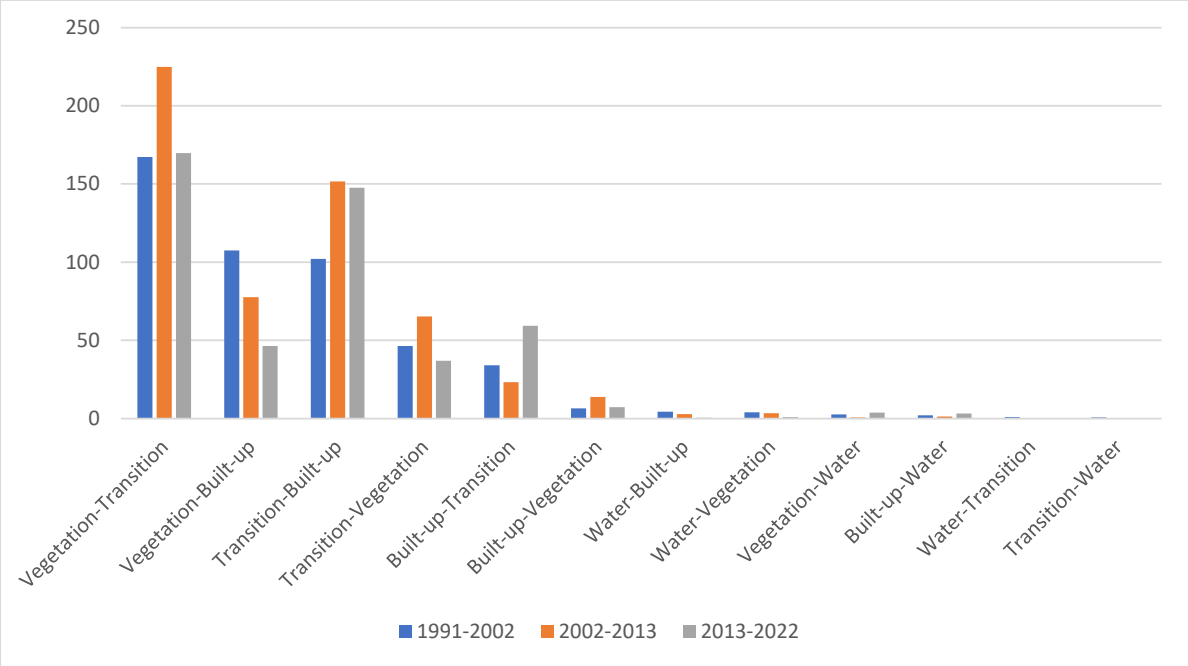

Figure 4.2: A chart comparing the various land cover changes between 1991 and 2022

determine transition potentials. Two sub-models, namely "urbanization" and "afforestation" were developed to model land use change. The "urbanization" sub-model accounted for land use changes from Vegetation to Transition, Vegetation to Built-up, and Transition to Built-up. On the other hand, the "afforestation" sub-model represented land use changes from Transition to Vegetation and Built-up to Transition. These changes were the most dominant changes in GAMA from 1991 to 2022 based on the land cover change analysis. The MLP for modelling the transition potential of the 2022 land cover of GAMA produced an accuracy of 93.83% and 85.03% for "urbanization" and "afforestation," respectively. The MLP results are shown in **Appendix K**. Transition potential maps were created and a Markov chain was used to predict the land cover map of GAMA for 2022. The predicted map was compared with the actual land cover map of 2022, resulting in a kappa score of 0.80. **Figure 4.3a and figure 4.3b** depict the hard and soft prediction of the land cover map of GAMA 2022. The high kappa score obtained instilled confidence in forecasting the land cover map of GAMA for 2030 using the 2013 and 2022 land cover maps of GAMA. **Figure 4.4a and figure 4.4b** showcases the hard and soft predicted land cover maps of GAMA for 2030.

4.3.2.2 Markov Chain Cellular Automata (MCCA)

First, the land cover maps of GAMA for 2002 and 2013 were used as inputs in the Markovian transition estimator. The number of time period between them, i.e, 11 years,

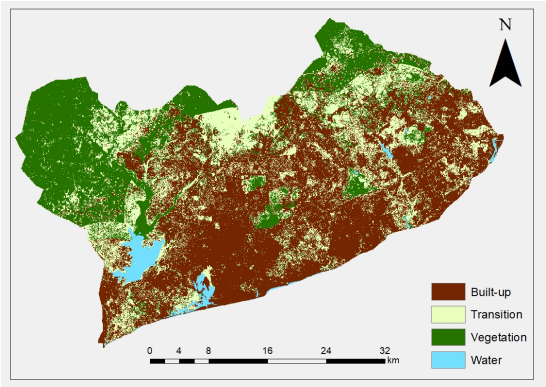

(a) Hard Prediction GAMA 2022

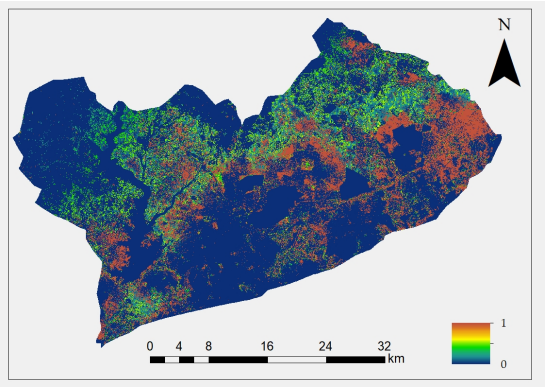

(b) Soft Prediction GAMA 2022

Figure 4.3: Hard and soft prediction of GAMA 2022 using LCM

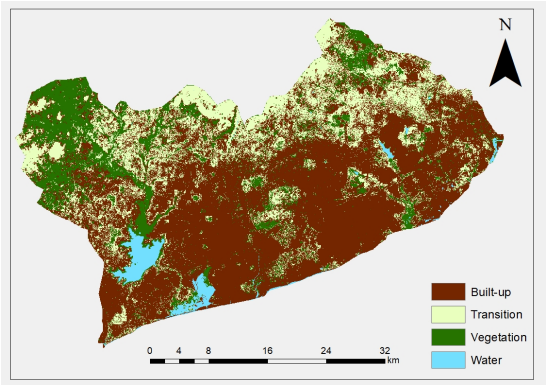

(a) Hard Prediction GAMA 2030

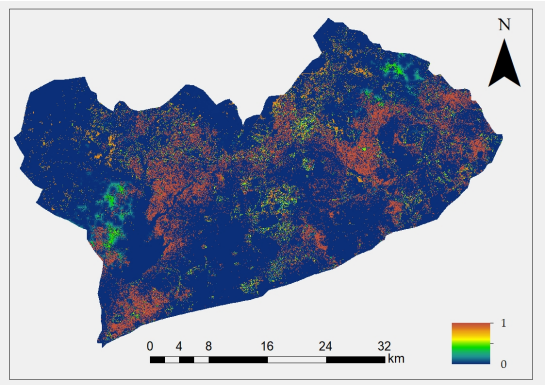

(b) Soft Prediction GAMA 2030

Figure 4.4: Hard and soft prediction of GAMA 2030 using LCM

and the number of time periods to project forward from the latest land cover map, i.e., 8 years, were specified. A transition probability matrix and a transition area matrix were then produced. Using the 2013 land cover map of GAMA as the basis land cover image, the land cover of GAMA for 2022 was predicted with the help of the transition area matrix and a transition suitability image collection. The transition suitability image collection was made up of evlilkelihood, multiradial fractal dimensions, distance from vegetation, and distance from the central business district. The number of cellular automata iterations were set to 10; and a 5×5 contiguity filter was used as the cellular automata filter type. The predicted land cover map of 2022 was compared with the actual landcover map of GAMA for 2022. The validation produced a kappa score of 0.83. The high kappa score obtained instilled confidence in forecasting the land cover map of GAMA for 2030 using the original land cover maps of GAMA for 2022 as the basis land cover image. **Figure 4.5a and figure 4.5b** are the predicted landcover maps of GAMA for 2022 and 2030 respectively.

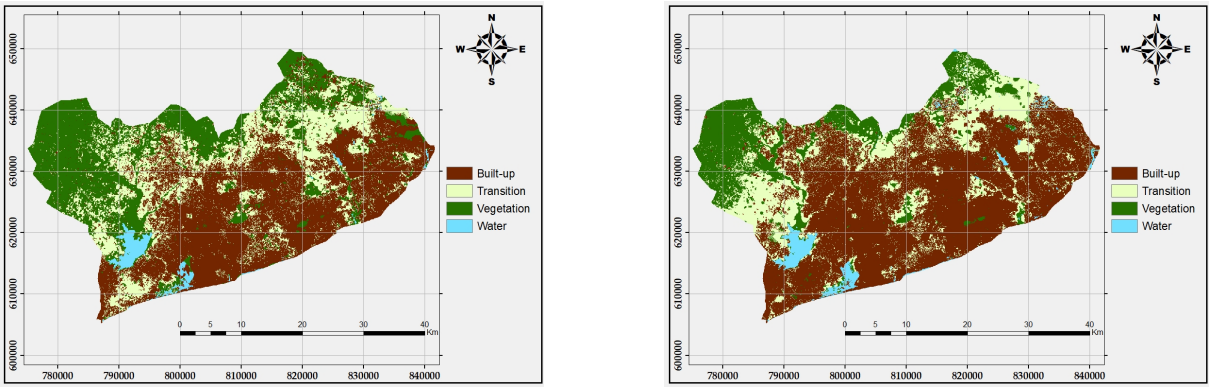

(a) MCCA GAMA 2022 Prediction **(b) MCCA GAMA 2030 Prediction**

Figure 4.5: Land cover prediction of GAMA Using MCCA

4.3.2.3 Agent Based Model in Netlogo

The Netlogo model for simulating the urban growth of GAMA was fashioned from the partial re-implementation of the SLEUTH Urban Growth Model (UGM) that was developed by Clarke, Hoppen and Gaydos [155]. It is a work done by Yang Zhou, who has made the code available on GitHub (https://github.com/YangZhouCSS/Urban_Growth_Model). It represents a complex spatial simulation model designed for studying urban growth and land-use changes. It operates as an agent-based simulation of urban growth, focusing on the interplay between terrain characteristics, road networks, and land suitability. The code defines several global variables, including datasets for slope, urbanization, road networks, land use, and exclusion criteria. The 'setup' procedure initializes the model by loading raster datasets for slope, urban areas, roads, excluded zones, and land use. It also processes these spatial datasets and setting up the simulation environment. It checks the suitability of patches for urbanization and displays road patches if required. Suitability for urbanization is determined by checking slope conditions and exclusion criteria. It also establishes parameters such as dispersion values, road gravity values, and probability tables based on slope. The 'go' procedure is the main simulation loop and orchestrates different growth processes, including spontaneous growth, new spreading center growth, edge growth, and road-influenced growth. Spontaneous growth randomly urbanizes patches based on a dispersion value. New spreading center growth initiates urbanization around patches marked as newly urbanized. Edge growth induces urbanization on the edges of existing urban areas, dependent on certain probabilities. The road-influenced growth process simulates urban expansion along road networks. During this, the model seeks nearby road pixels and extends urbanization based on road connectivity. Suitability is continuously checked, and the model visualizes the results through various displays. It updates the

visualization of the patches to represent urbanized and non-urbanized areas and roads. The 'load_data' procedure loads various spatial datasets and applies them to patches, while the other procedures like 'spontaneous_growth', 'new_spreading_center_growth', and 'road_influenced_growth' handle different aspects of urban growth based on the defined parameters and conditions. One advantage of this model is the built-in visualization tools that allow researchers to observe and analyze simulation results in real-time. This feature is invaluable for gaining insights into the evolving urban landscape and patterns. This makes NetLogo model is a valuable tool for analyzing urbanization processes and their dependencies on factors such as slope, road networks, and exclusion criteria. It allows for the exploration of urban growth patterns and can provide insights into urban planning and land-use management. Key parameters such as dispersion, road gravity, and search distance influence the growth dynamics, collectively emulating the complexity of urbanization patterns influenced by topography, roads, and land suitability.

Figure 4.6 and **Figure 4.7** are maps showing the simulation results after 8 periods, i.e., 2022 to 2030.

Figure 4.6: UGM Model in Netlogo GAMA 2022

Urban growth modeling involves various approaches to simulate and predict changes in land cover and spatial configurations over time. The Land Change Modeler (LCM), part of the TerrSet software suite, integrates statistical and machine learning algorithms for comprehensive landscape analysis. LCM was used to model and predict the urban growth of GAMA for the year 2030. The kappa score achieved for the prediction was 0.8, which is a good score. It also has the advantage of producing both a soft prediction, which

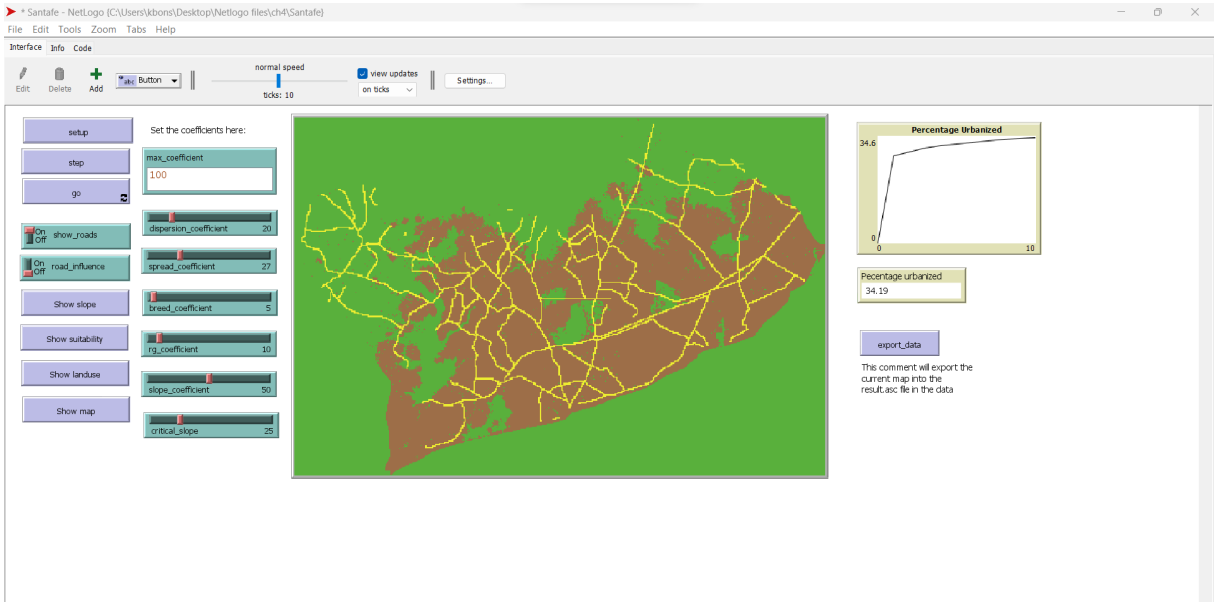

Figure 4.7: UGM Model in Netlogo GAMA 2030

gives the probability or likelihood for each land cover class at a given location and hard prediction, which assigns a single, definite land cover class to each location or pixel. Markov Chain Cellular Automata (MCCA) combines Markov chain theory with Cellular Automata, representing spatial entities in a grid and utilizing transition probabilities to simulate urban growth dynamics. MCCA was used to model and predict the urban growth of GAMA for the year 2030. The kappa score achieved for the prediction was 0.83, which is slightly higher than that of LCM. However, unlike LCM, MCCA does not produce a soft prediction, therefore it would not be as useful as LCM when dealing uncertainty in land cover change processes. Soft prediction allows decision makers to understand the level of confidence associated with each predicted class, aiding in risk assessment and decision making. Hard predictions on the other hand are often used when a specific, unambiguous classification is required, and there is a high level of confidence in the model's ability to accurately assign land cover classes. However, they may not capture the inherent uncertainty in land cover change processes. Agent based model implemented in NetLogo, offers a user-friendly platform for creating and observing the behavior of agents within a simulated environment, making it versatile for exploring emergent phenomena in urban growth simulations. The advantage of this model is that simulation of the prediction can be analyzed in real time due to its powerful built in visualization tools.

4.3.3 Phase 3 - Landscape metrics, GAMA 1991-2022

4.3.3.1 Class area (CA)

Class area demonstrates changes in the extent and distribution of land cover types within the landscape over time. From the results obtained, it was observed that the class area varied for each land cover type over time. In 1991, Vegetation had the highest class area (983.40 km^2), followed by Transition (287.98 km^2), Built-up (271.05 km^2), and Water (41.46 km^2). Between 1991 and 2022, Built up experienced a significant increase at the expense of vegetation. There was a steady reduction in the class area for Vegetation (from 983.40 km^2 to 369.56 km^2) as well as a steady increase in the class area for Built-up land cover class (from 271.05 km^2 to 758.69 km^2). Transition also showed slight increases in class area (from 287.98 km^2 to 417.19 km^2), while Water exhibited relative stability in class area. Looking ahead to the projected year of 2030, Vegetation and Built-up are expected to continue on the same trend. The class area for Transition on the other hand is expected to reduce to 355.5 km^2. Water is also projected to increase in class area (from 32.99 km^2 to 43.10 km^2). The fluctuations in class area indicate shifts in land use, land cover changes, and potential impacts on ecosystem services and biodiversity. The decrease in vegetation and the expansion of built-up areas reflect ongoing urbanization and land transformation processes. This emphasizes the need for sustainable land management practices to mitigate further land cover changes and promote ecosystem conservation. **Table 4.2** provides information on the class area for the different land cover types (Vegetation, Transition, Built-up, and Water) in the years under study (1991, 2002, 2013, 2022, and predicted 2030). **Figure 4.8** is a chart showing the area covered by the various land cover types in GAMA from 1991-2030 (predicted).

Table 4.2: Table showing the area covered by each land cover type

Class Area (km^2)					
	1991	2002	2013	2022	2030 (Predicted)
Vegetation	983.40	761.81	543.77	369.56	274.53
Transition	287.98	343.37	374.73	417.19	355.50
Built-up	271.05	440.98	632.41	758.69	909.88
Water	41.46	37.73	32.99	38.46	43.10

4.3.3.2 Number of patches (NP)

Increase or decrease in number of patches causes disruption in the landscape matrix. This typically occurs as a result of anthropogenic activities. If the number of patches of a landcover increases, it is an indication of fragmentation, whereas if it decreases, it indicates

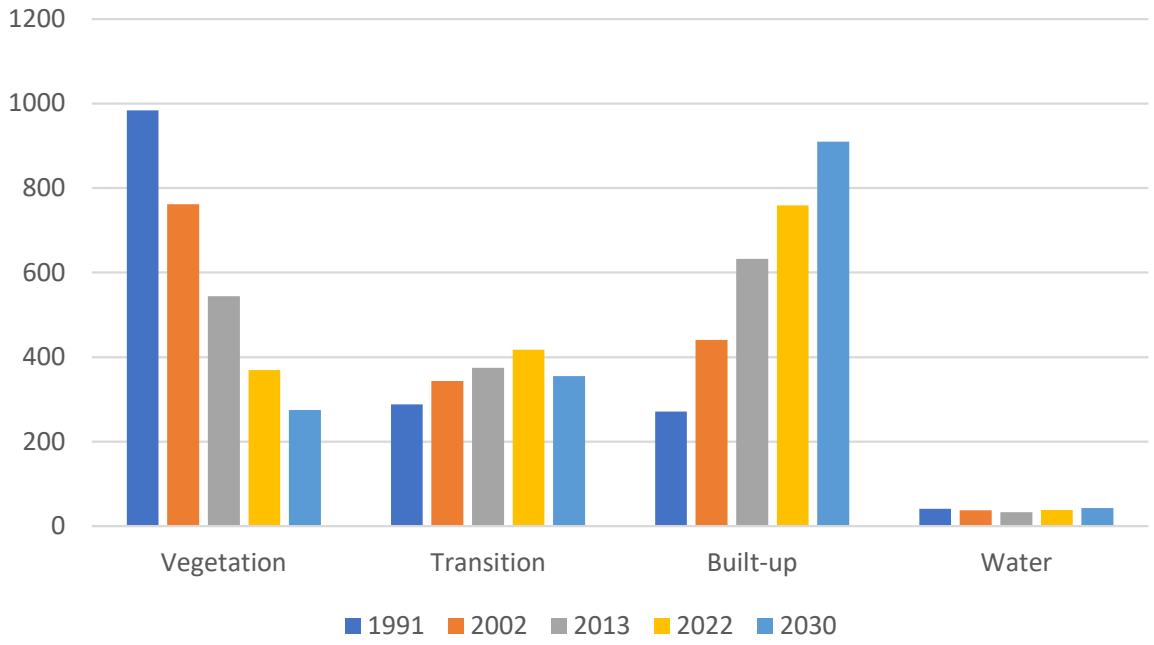

Figure 4.8: Chart showing the area covered by various land cover types from 1991 to 2030 (predicted)

uniformity or a reduction in the area it covers due to land cover change. Analyzing the obtained results, it becomes evident that the number of patches varies for each land cover type over time. In 1991, Transition had the highest number of patches (15 021), followed by Built-up (8 250), Vegetation (7 555), and Water (440). However, significant fluctuations were observed in these values over the years. Between 1991 and 2013, there were changes in the number of patches for each land cover type. Vegetation experienced an increase in the number of patches (from 7 555 to 9 325), indicating potential fragmentation or subdivision of vegetated areas. Transition and Built-up areas also showed increases in the number of patches, suggesting increased subdivision and expansion of these land cover types. Water, on the other hand, exhibited a decrease in the number of patches (from 440 to 264), indicating potential amalgamation or reduction in the number of distinct water bodies. Looking ahead to the projected year of 2030, changes are expected in the number of patches. Vegetation is projected to decrease significantly (from 6 400 to 2 300), indicating a potential reduction in the number of vegetated patches. Built-up is projected to experience a significant reduction in the number of patches (from 10 618 to 1 848). On the other hand, the number of patches for Transition are expected to increase from 14 382 to 18 354 and those of Water are also expected to increase from 311 to 1 172. The results highlight changes in the spatial configuration and fragmentation of land cover types within the landscape over time. The fluctuations in the number of patches suggest alterations in the size, shape, and distribution of patches, which can impact ecological processes, habitat

connectivity, and biodiversity patterns. **Table 4.3** provides information on the number of patches for the different land cover types (Vegetation, Transition, Built-up, and Water) in the years under study (1991, 2002, 2013, 2022, and predicted 2030). **Figure 4.9** is a chart showing the number of patches of the various land cover types in GAMA from 1991 – 2030 (predicted).

Table 4.3: Table showing the number of patches for each land cover type in GAMA

Number of Patches					
	1991	2002	2013	2022	2030 (predicted)
Vegetation	7555	7765	9325	6400	2300
Transition	15021	20142	20963	14382	18354
Built-up	8250	10941	9161	10618	1848
Water	440	521	264	311	1172

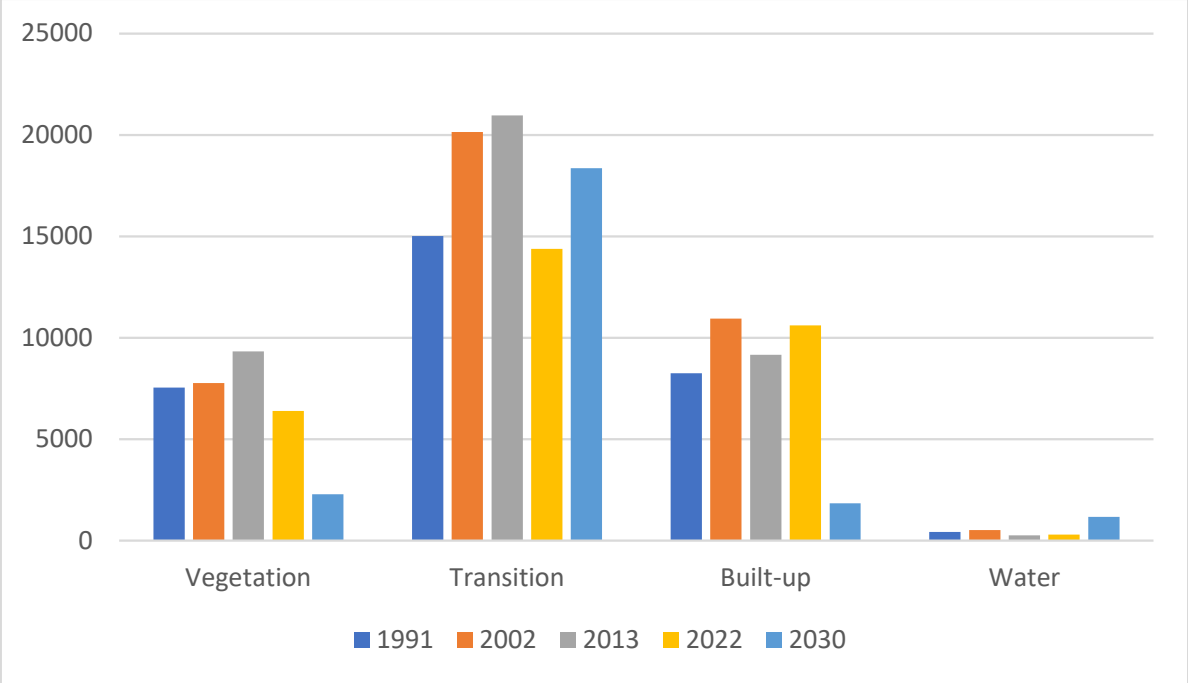

Figure 4.9: Chart showing the number of patches of land cover types from 1991 2030 (predicted)

4.3.3.3 Edge Density

Edge density refers to the amount of edge or boundary between different land cover types relative to the total area. Edge density for different land cover types over time provides insights into the spatial patterns and fragmentation of the landscape. As landscapes become more and more patchy, the edge density value increases, indicating that the landscape is becoming more fragmented. However, edge density is equal to 0 when there is only one patch, i.e, only one land cover type. From the results obtained, it was observed

that in 1991, Transition had the highest edge density value (33.67), followed by Vegetation (25.56), Built-up (17.48), and then Water (1.26). As the years progressed, significant fluctuations were observed in these values. Between 1991 and 2013, there was an increase in edge density for Vegetation (from 25.56 to 28.77) and Transition (from 33.67 to 49.66), indicating a higher fragmentation or subdivision of these land cover types. Built-up areas also experienced an increase in edge density (from 17.48 to 30.96), suggesting increased fragmentation of urban areas. On the other hand, Water exhibited a decrease in edge density (from 1.26 to 0.93), indicating a reduction in the extent of water edges within the landscape. Looking ahead to the projected year of 2030, there are expected changes in edge density values. Vegetation is projected to decrease significantly (from 17.92 to 8.43), indicating a potential decrease in fragmentation or aggregation of vegetated areas. Transition and Built-up are also expected to decrease (from 42.70 to 30.76) and (from 30.96 to 27.70) respectively. Water is projected to have relatively stable edge density values. The results reveal changes in the fragmentation and connectivity of land cover types within the landscape over time. The fluctuations in edge density values suggest alterations in the spatial configuration of patches, which can have implications for habitat fragmentation, ecological processes, and biodiversity patterns. **Table 4.4** provides information on the edge density values for different land cover types (Vegetation, Transition, Built-up, and Water) for the years 1991, 2002, 2013, 2022, and predicted 2030. **Figure 4.10** is a chart showing the edge density of the various land cover types in GAMA from 1991 – 2030 (predicted).

Table 4.4: Table showing the edge density of each land cover type

Edge Density					
	1991	2002	2013	2022	2030 (predicted)
Vegetation	25.56	26.22	28.77	17.92	8.43
Transition	33.67	38.71	49.66	42.70	30.76
Built-up	17.48	26.30	30.96	30.00	27.67
Water	1.26	1.34	0.93	1.02	1.89

4.3.3.4 Proportion of like adjacency

The Proportion of Like Adjacency metric measures the proportion of like adjacent pixels in a given land cover type, with higher values indicating greater clustering of patches. From the results obtained, it can be observed that the proportion of like adjacency varies across the different land cover classes and time periods. In 1991, the highest proportion of like adjacency was observed for Vegetation (94.05%), followed by Water (92.55%), Built-up

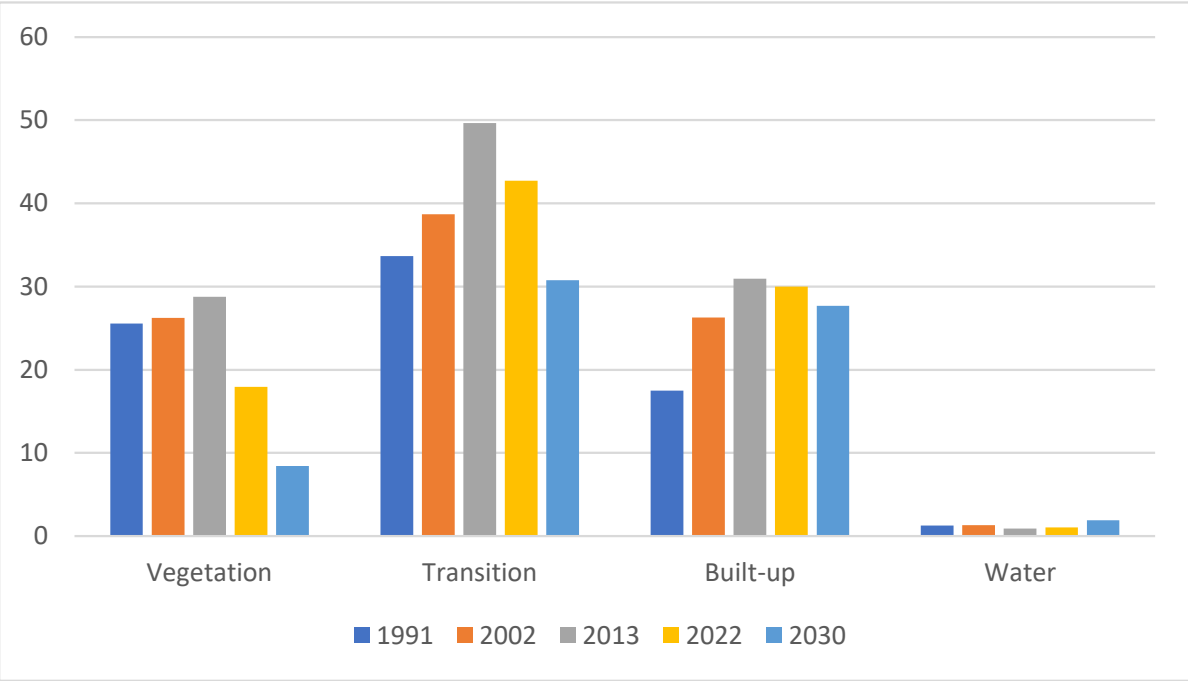

Figure 4.10: Chart showing the edge density of the various land cover types from 1991 to 2022

(85.39%), and Transition (73.74%). However, over the years, there have been fluctuations in these values. Between 1991 and 2013, all land cover types experienced a decline in the proportion of like adjacency with the exception of Transition, which experienced a slight increase of 0.93% from 1991 to 2002; and Built-up which experienced steady increment throughout the years observed. Vegetation decreased from 94.05% to 87.97%, Transition decreased from 73.74% to 70.21% and Water increased insignificantly from 92.55% to 92.95%. However, from 2013 to the projected year of 2030, there was an overall increase in the proportion of like adjacency for all the land cover classes with the exception of Water. From the projections, Vegetation is expected to increase to 92.84%, Transition to 80.51%, Built-up to 93.11%, however, Water is expected to decrease to 89.51%. The results suggest that there have been changes in the spatial configuration of land cover types within the landscape over time. The proportion of like adjacency provides insights into the degree of aggregation or dispersion of patches of the same land cover class. The fluctuations in these values indicate potential changes in landscape fragmentation, connectivity, and potential impacts on ecological processes and biodiversity. **Table 4.5** provides information on the proportion of like adjacency for the different land cover types (Vegetation, Transition, Built-up, and Water) for the years 1991, 2002, 2013, 2022, and predicted 2030. **Figure 4.11** is a chart showing the proportion of like adjacency of the various land cover types in GAMA from 1991 – 2030 (predicted).

Table 4.5: Table showing the proportion of like adjacency of each land cover type

Proportion of Like Adjacency (%)					
	1991	2002	2013	2022	2030 (predicted)
Vegetation	94.05	92.14	87.97	88.91	92.84
Transition	73.74	74.66	70.21	76.96	80.51
Built-up	85.39	86.52	88.94	91.06	93.11
Water	92.55	91.44	92.95	93.36	89.51

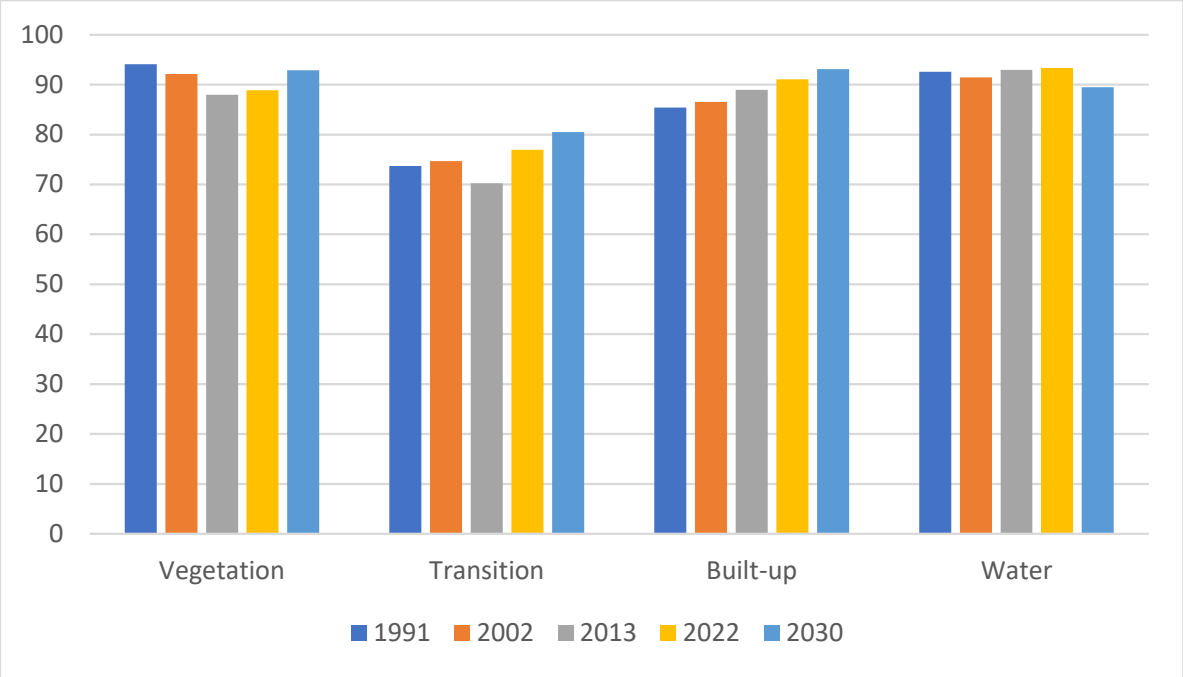

Figure 4.11: Chart showing the proportion of like adjacency of the various land cover types from 1991 to 2022

4.3.3.4.1 Rate of Urban Growth

The initial urban area in 1991 measured 271.05 km^2 indicating a relatively moderate level of urbanization. Over the following years, the rate of urban growth increased significantly. By 2002, the urban area had risen to 440.98 km^2, representing a growth rate of 0.15, indicating a rapid pace of urban development. Between 2002 and 2013, there was a continuation of the upward trend in urban growth, with the urban area reaching 632.41 km^2, corresponding to a growth rate of 0.17. This indicates that urbanization was progressing at a relatively fast pace during this period as well. However, in 2022, there was a notable reduction in the urban growth rate, which decreased to 0.14. It suggests that the rate of urban expansion slowed down as compared to previous years, indicating a relatively less rapid pace of urbanization. This reduction could be attributed to several factors such as economic fluctuations, government policies, demographic changes, or other local circumstances. Looking ahead to the predicted year 2030, the data indicates an in-

crease in the urban growth rate. The projected growth rate for 2030 is 0.19, corresponding to an urban area of 909.88 km^2. This suggests a resurgence in the rate of urbanization, indicating a faster pace of urban growth compared to the reduced rate observed in 2022. The increase in the predicted urban growth rate for 2030 could be influenced by various factors such as population growth, economic development, infrastructure investments, urban planning strategies, and government policies aimed at promoting urban expansion. It's important to note that these deductions are based solely on the analysis of satellite images, a comprehensive analysis of the specific context and factors influencing urban growth would require a more in-depth examination.**Table 4.6** shows the area and the rate of urban growth from 1991-2022.

Table 4.6: Table showing the rate of urban growth in GAMA from 1991-2022.

Rate of Urban Growth		
Year	Area (km2)	Rate (%)
1991	271.05	
2002	440.98	0.15
2013	632.41	0.17
2022	758.69	0.14
2030 (predicted)	909.88	0.19

4.4 Conclusion

The study successfully captured the land cover changes and the urban growth rate of the GAMA region. The findings revealed a significant transformation in the land cover composition of the region, with the Built-up land cover now dominating over the previously dominant Vegetation land cover. A notable shift was observed from Vegetation to Transition, peaking from 2002 to 2013 and stabilizing thereafter. The Transition to Built-up change showed consistent growth, indicating an ongoing conversion of Transition areas into Built-up land cover. Conversely, the trend from Vegetation to Built-up demonstrated a decline, suggesting a reduction in the conversion of Vegetation areas over time. The Transition to Vegetation and Built-up to Transition changes exhibit varying patterns, reflecting dynamism and inconsistency. Overall, GAMA's land cover changes depict a complex and dynamic landscape with diverse rates and directions of transformation between different land cover types. The analysis of urban growth rate showed an increase from 0.15% (1991 to 2002) to 0.17% (2002 to 2013), but then a decrease to 0.14% from 2013 to 2022. A projected growth rate of 0.19% is expected in 2030. The fluctuation in growth rate from 2013 to 2030 could be attributed to several factors which would

require a comprehensive analysis to identify. Unfortunately, such comprehensive analysis is beyond the scope of this thesis. The study also captured the landscape patterns of the GAMA region using landscape metrics. The landscape metrics further revealed extensive fragmentation of the Vegetation land cover type, indicating a negative impact on biodiversity conservation, species movements, ecosystem functioning, and long-term ecological resilience. Additionally, the study successfully predicted the land cover and landscape pattern of GAMA for the year 2030 using information derived from freely available satellite imagery. The trends highlight the importance of considering landscape connectivity, habitat fragmentation and spatial arrangement of land cover types for assessing ecological processes and urban development impacts on the environment. Understanding and identifying areas with high fragmentation is crucial for prioritizing conservation efforts. This knowledge can assist landscape planners and managers in making informed decisions regarding land-use planning, habitat restoration, and conservation strategies. By addressing fragmentation in GAMA and promoting habitat connectivity, the integrity and ecological value of the landscapes can be maintained while supporting biodiversity conservation and sustainable ecosystem management.

GAMA was selected as the study area due to its rapid growth in a developing country where data for urban center identification is limited. Sekondi Takoradi Metropolitan Area (STMA), while smaller and not as fast-paced than GAMA, bears similarities and has the potential for similar growth. With a national airport, harbor, and proximity to mining and petroleum companies, STMA offers an intriguing comparative study to understand its relation to GAMA, given their coastal city nature.

4.5 Landscape Pattern Analysis of STMA

Another important coastal city in Ghana is Sekondi Takoradi Metropolitan Area (STMA). STMA is located between latitudes 4°52′30″ N and 5°4′0″ N; and longitudes 1°37′0″ W and 1°52′30″ W at the southern part of the Western Region of Ghana. It is about 280 km west from Accra and 130 km east from La Cote d'Ivoire. It is bordered to the north by Mpohor District, Shama District to the east, Effia-Kwesimintsim Municipal to the west and south by the Gulf of Guinea. The capital of the Metropolis is the Twin-City, Sekondi/Takoradi, which is also the capital of the Western Region [18]. Its coastal location, proximity to mining towns, presence of a commercial airport and the role of Sekondi-Takoradi as a port city makes it an important city in Ghana [49].

The discovery of oil in commercial quantities off the coast of the Western Region in 2007 has significantly impacted the spatial and socio-economic profile of STMA, making it the most industrialized urban settlement closest to the oil fields [54]. As a result, influx of migrants as well as the presence of international oil companies have boosted investments in the city's real estate market and other major commercial developments [48]. With the Takoradi port expanding strategically to accommodate the demands of the oil industry, there have been accelerated economic development and population increase in the region. These have caused some changes in the landcover patterns of STMA which are worth studying [84]. One of the effects of these accelerated developments is that residential buildings in STMA are being lost to commercial and civic activities as more offices are coming in due to the oil discovery [114]. This situation has led to the creation of new sites outside the limits of the existing built-up area; and increased development of more informal settlements. Most ejected tenants find their way into already existing slum areas in parts of Efiekuma, New Takoradi and Kwesimintsim because they do not want to live so far away from the central business district (CBD) [114, 54, 150]. This is a source of worry for urban managers as these areas are already characterized by high population densities, substandard housing and poor infrastructural services. **Figure 4.12** is a map of the STMA.

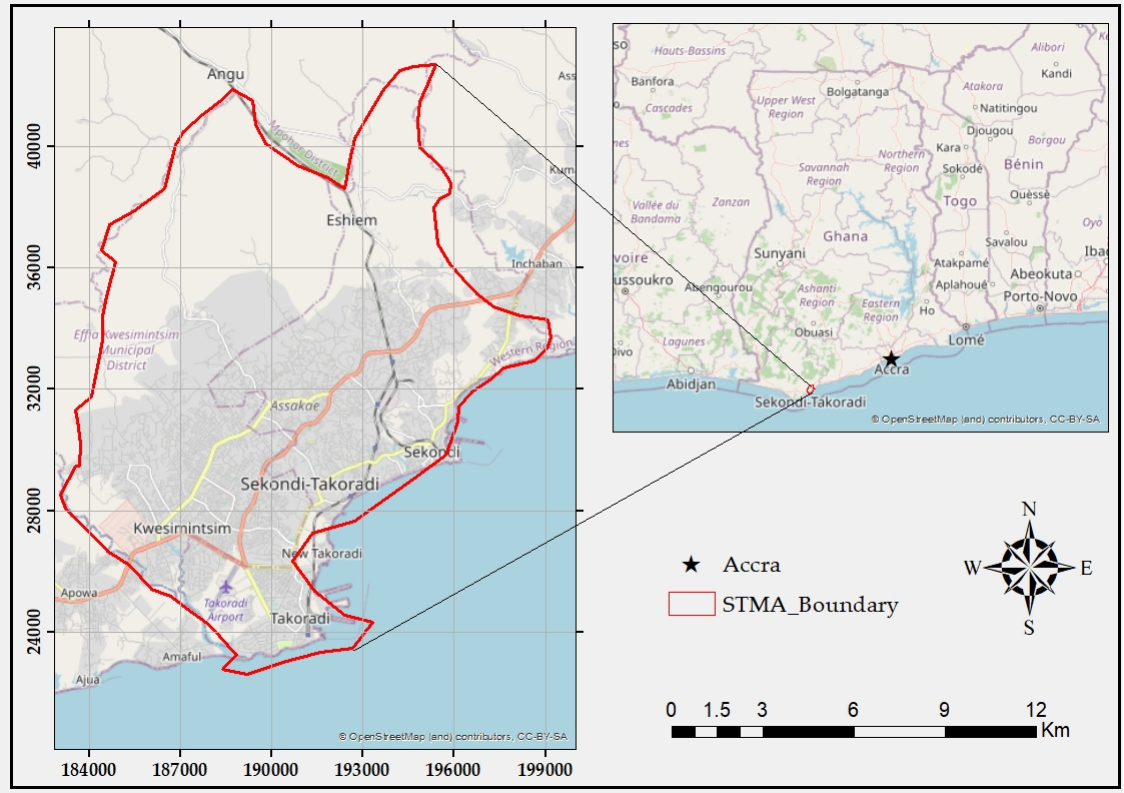

Figure 4.12: Map of STMA

STMA and GAMA share coastal locations, providing economic opportunities tied to maritime activities. While GAMA is larger and serves as the capital region with a higher population, STMA, though smaller, plays a crucial role in Ghana's economy, focusing on mining and petroleum. Both areas are influenced by national and regional policies affecting urban planning and economic development.

To study the evolution of the landscape pattern of STMA, and predict its future state (2030), satellite images of STMA for the years 2016 and 2022 were downloaded from United States Geological Surveys (USGS) to achieve this objective. The satellite image classification was done using Random Forest; and the resulting land cover maps of STMA for 2016 and 2022 are shown in **figure 4.13a and figure 4.13b** respectively. The error matrix, showing the accuracy obtained can also be found in **Appendix L**. Information on the downloaded satellite images are presented in **Table 4.7**. MCCA was used to predict the land cover of STMA for 2030 using the land cover maps of STMA 2016 and 2022 with a 5×5 contiguity filter. **Figure 4.14** is a map showing the 2030 predicted land cover map of STMA.

Table 4.7: Satellite Images of STMA

DATA			
Product ID	Spacecraft ID	Date Acquired	Source
LE07_L2SP_194057_20160106_20200903_02_T1	Landsat 7	06/01/2016	USGS
LC09_L2SP_194057_20220122_20220124_02_T1	Landsat 9	22/01/2022	USGS

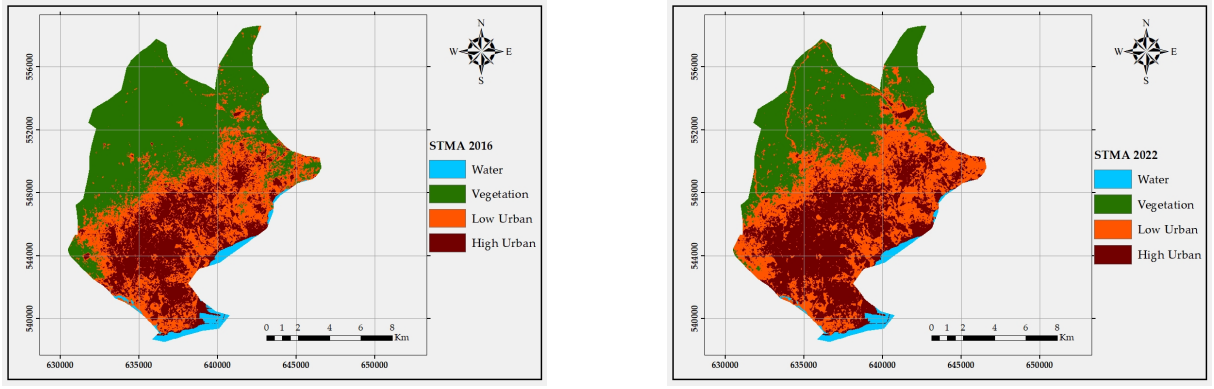

(a) Land cover map of STMA, 2016 **(b) Land cover map of STMA, 2022**

Figure 4.13: Land cover maps of STMA 2016-2022

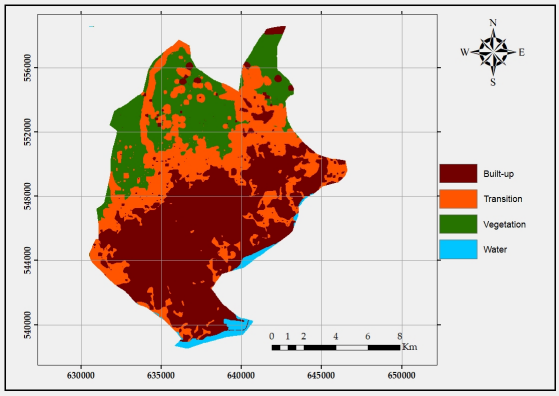

Figure 4.14: Land cover of map of STMA,2030 (Predicted)

4.5.1 Landscape Metrics, STMA

4.5.1.1 Class Area

In 2016, Vegetation had the highest class area (80.51 km^2), followed by Transition (47.34 km^2), Built-up (42.19 km^2), and Water (4.70 km^2). However, there were notable changes in these values over the years. Between 2016 and 2030 (projected), Vegetation experienced a significant reduction, decreasing from 80.51 km^2 to 37.78 km^2, indicating potential loss or conversion of vegetated areas. Transition areas showed relatively stable or slight changes in class area over the years while Built-up showed a steady increase from 42.19 km^2 to 81.05 km^2. Water exhibited only a slight decrease in class area, from 4.70 km^2 to 3.64 km^2. The decreasing class area values for Vegetation land cover and the increasing class area values for Built-up land cover indicate potential land use changes such as urbanization, or other factors leading to the increase in Built-up at the expense of Vegetation. These changes can have implications for ecosystem services, biodiversity, and the overall landscape composition and function. **Table 4.8** provides information on the area occupied by different land cover types (Vegetation, Transition, Built-up, and Water) for various years (2016, 2022, and predicted 2030). **Figure 4.15** is a chart showing the area occupied by the various land cover types in GAMA from 2016 – 2030 (predicted).

Table 4.8: Table showing the area covered by each land cover type, STMA

Class Area ($km\hat{2}$)			
	2016	2022	2030 (predicted)
Vegetation	80.5104	58.2165	37.7775
Transition	47.3373	53.9316	52.2765
Built-up	42.1884	58.3893	81.0522
Water	4.7025	4.2012	3.6423

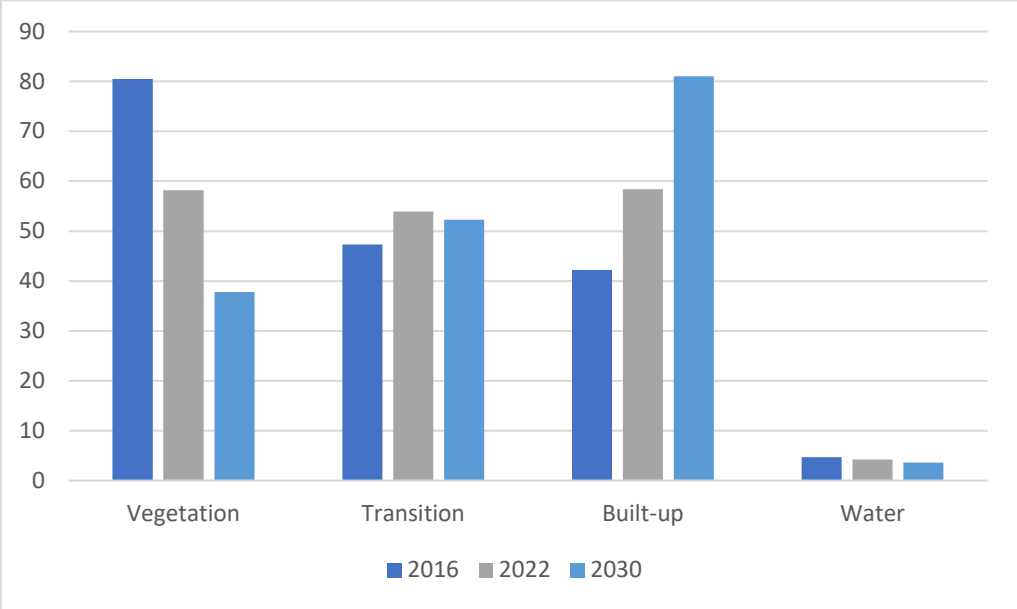

Figure 4.15: Chart showing the area covered by the various land cover types from 2016 to 2030 (predicted)

4.5.1.2 Number of patches

Analyzing the data, it is evident that the number of patches varies for each land cover type over time. In 2016, Transition had the highest number of patches (1 133), followed by Built-up (642), Vegetation (388), and Water (25). Between 2016 and 2030 (predicted), there was a substantial decrease in the number of patches for most land cover Types. Vegetation experienced a drastic reduction, decreasing from 388 patches to 23 patches, indicating potential loss or conversion of vegetated areas. Transition also showed a notable decrease from 1 133 patches to 138 patches, while Built-up and Water exhibited relatively smaller reductions in the number of patches. The substantial reduction in the number of patches suggests a decrease in the size, shape, and distribution of patches, potentially indicating land conversion, urbanization, or other land use changes. These changes can have implications for habitat fragmentation, biodiversity, and ecological processes within the landscape. **Table 4.9** provides information on the number of patches of the different land cover types (Vegetation, Transition, Built-up, and Water) for various years (2016, 2022, and predicted 2030). **Figure 4.16** is a chart showing the number of patches of the various land cover types in GAMA from 2016 – 2030 (predicted).

4.5.1.3 Edge Density

In 2016, Transition had the highest edge density value (40.25), followed by Built-up (25.52), Vegetation (14.99), and Water (1.05). However, there were notable changes in

Table 4.9: Table showing the number of patches for each land cover types in STMA

Number of Patches			
	2016	2022	2030 (predicted)
Vegetation	388	142	23
Transition	1133	1019	138
Built-up	642	525	165
Water	25	20	15

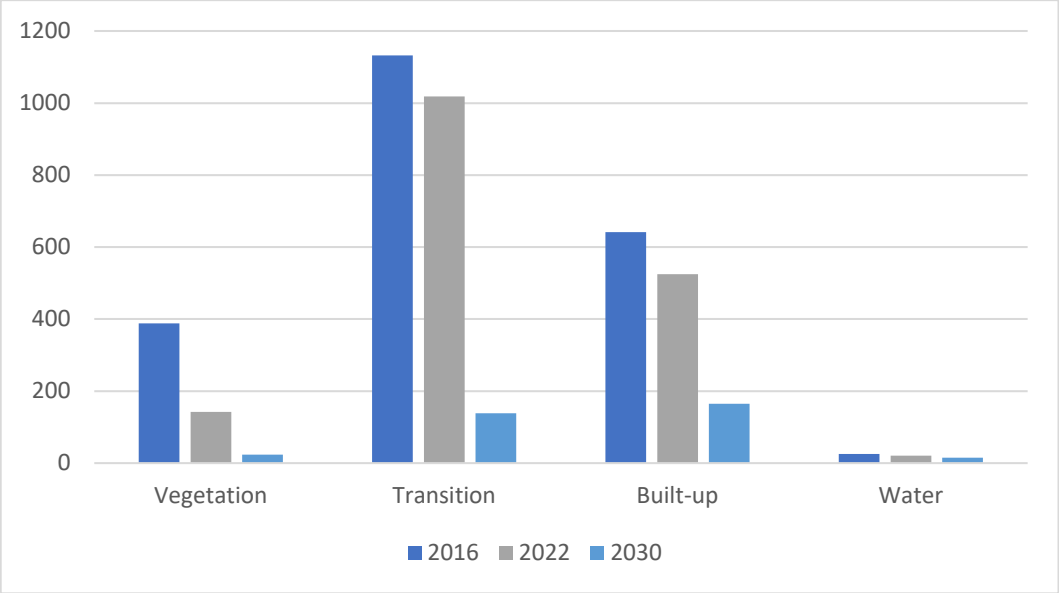

Figure 4.16: Chart showing the number of patches of land cover types from 2016 to 2030 (predicted)

these values over the years. Between 2016 and 2030 (predicted), there was an overall decreasing trend in edge density for most land cover types. Vegetation showed a substantial decrease from 14.99 to 4.80, indicating a potential reduction in the fragmentation of vegetated areas. Transition also exhibited a decrease from 40.25 to 11.90, suggesting improved connectivity or reduced fragmentation within this land cover type. Built-up areas showed relatively stable edge density values for 2016 and 2022 indicating a consistent level of fragmentation or aggregation. However, the edge density values of built-up showed a sharp decrease from 25 to 8 in 2030 (predicted). Water exhibited a slight decrease in edge density from 1.05 to 0.70 throughout the period studied, indicating potential changes in the extent or shape of water bodies. The decreasing edge density values indicate a reduction in fragmentation and potentially increased aggregation or connectivity of land cover patches. **Table 4.10** provides information on the edge density of different land cover types (Vegetation, Transition, Built-up, and Water) for various years (2016, 2022, and predicted 2030). **Figure 4.17** is a chart showing the edge density of the various land cover types in GAMA from 2016 – 2030 (predicted).

Table 4.10: Table showing the edge density for each land cover types in STMA

Edge Density			
	2016	2022	2030 (predicted)
Vegetation	14.9969	10.2741	4.7998
Transition	40.2493	35.4903	11.8951
Built-up	25.5168	25.6421	8.7125
Water	1.0475	0.9269	0.7024

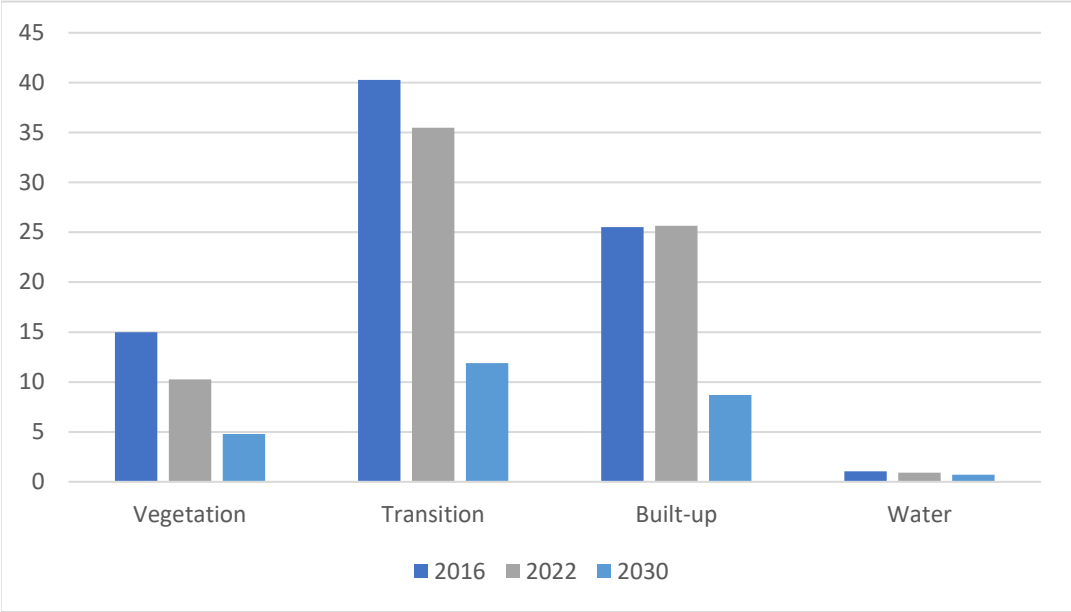

Figure 4.17: Chart showing the edge density of land cover types from 2016 to 2030 (predicted)

4.5.1.4 Proportion of Like Adjacency

In 2016, Vegetation had the highest proportion of like adjacency (95.03%), followed by Water (91.16%), Built-up (85.23%), and Transition (79.18%). Between 2016 and 2030 (predicted), there was an overall increasing trend in the proportion of like adjacency for most land cover types. Vegetation showed a gradual increase from 95.03% to 96.31%, indicating potential aggregation or clustering of vegetated areas. Transition experienced a significant increase from 79.18% to 94.16%, suggesting a substantial improvement in the adjacency of patches within this land cover class. Built-up areas also showed a notable increase in the proportion of like adjacency from 85.23% to 97.23%, indicating increased connectivity or aggregation of built-up patches. Water exhibited relatively stable values, remaining around 91% for the entire period. The increasing proportion of like adjacency indicates a potential reduction in fragmentation and improved patch aggregation within the land cover classes. This can have implications for habitat quality, ecological processes, and biodiversity patterns, with potential positive effects on ecosystem functioning and resilience. **Table 4.11** provides information on the proportion of like adjacency of the

various land cover types (Vegetation, Transition, Built-up, and Water) for the years 2016, 2022, and predicted 2030. **Figure 4.18** is a chart showing the proportion of like adjacency of the various land cover types in GAMA from 2016 – 2030 (predicted).

Table 4.11: Table showing the proportion of like adjacency for each land cover types in STMA

Proportion of Like Adjacency (%)			
	2016	2022	2030 (predicted)
Vegetation	95.0322	95.1844	96.3085
Transition	79.1804	83.8128	94.1603
Built-up	85.2312	89.2096	97.234
Water	91.1579	91.2061	91.4752

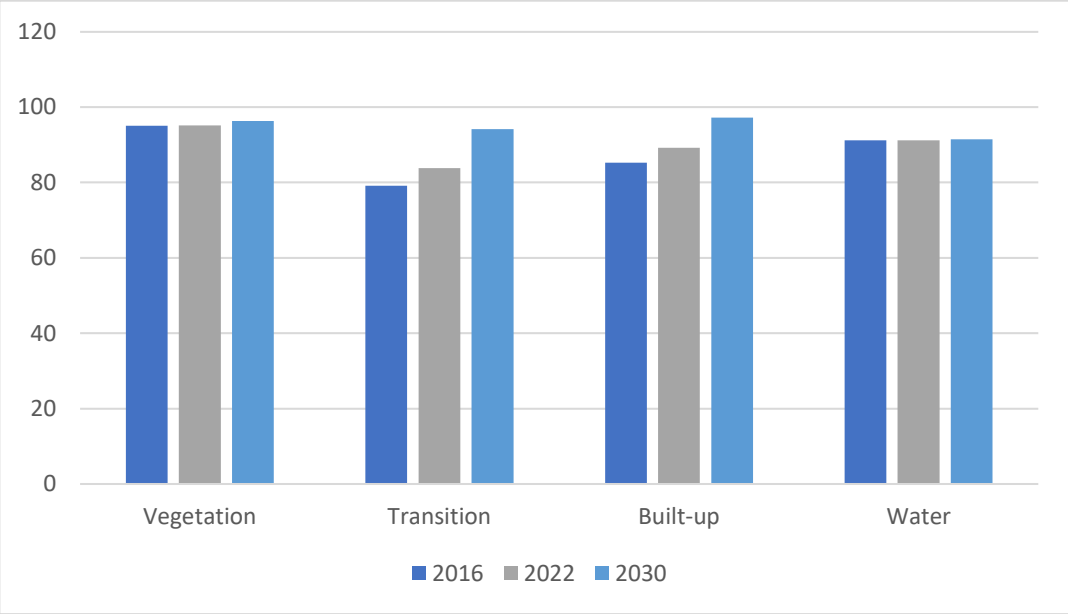

Figure 4.18: Chart showing the proportion of like adjacency of land cover types from 2016 to 2030 (predicted)

4.5.2 Conclusion of the STMA Study

In STMA, the various landscape metrics calculated provide insights into the changes in land cover dynamics over time. In terms of class area, Vegetation dominated in 2016 with 80.51 km^2, followed by Transition (47.34 km^2), Built-up (42.19 km^2), and Water (4.70 km^2). However, by the projected year 2030, there is a significant reduction in Vegetation class area, potentially indicating land use changes such as urbanization, with Built-up showing a steady increase. The number of patches for each land cover type reduced over the years, reflecting potential changes in the size, shape, and distribution of patches. Similarly, edge density values demonstrated variations, suggesting alterations in landscape fragmentation and connectivity. Proportion of like adjacency increased for

most land cover types, confirming the potential reduction in fragmentation and increased patch aggregation. These changes have implications for ecosystem services, biodiversity, and overall landscape structure.

STMA holds a pivotal position within Ghana, distinct from the Greater Accra Metropolitan Area (GAMA), which is approaching urban saturation. STMA represents a city with the potential to experience substantial growth and development in the near future. Therefore, it is crucial to manage this expansion with great care to avoid compromising sustainability standards, particularly with regards to biodiversity conservation. The impending saturation of STMA underscores the need for a comprehensive, multifaceted approach to control urban sprawl, given the intricate interplay of social, economic, and environmental factors that drive urban growth.

Several strategies can be employed to manage and control urban sprawl in STMA effectively:

i. Comprehensive Urban Planning: A well-thought-out urban development plan is essential to guide the city's growth, ensuring that land is allocated for various purposes efficiently, and infrastructure is developed in a sustainable manner.

ii. Strengthening Land Use Regulations: Enforcing and enhancing land use regulations can prevent haphazard development and ensure that land is used in ways that align with the city's long-term goals.

iii. Investment in Public Transport: Developing and improving public transportation options can reduce the reliance on private vehicles, curbing the need for extensive road networks and lowering the environmental impact of urban sprawl.

iv. Encouragement of Green Infrastructure: Incorporating green spaces, parks, and urban forests into the city's fabric can mitigate the environmental effects of urban expansion, preserve natural habitats, and enhance the quality of life for residents.

v. Promotion of Sustainable Housing: Encouraging the construction of eco-friendly and energy-efficient housing options not only reduces the environmental footprint but also provides residents with sustainable and comfortable living environments.

vi. Strengthening Community Participation: Involving the local community in the decision-making process can help ensure that development aligns with their needs and values, fostering a sense of ownership and accountability.

By employing these strategies, STMA can manage its urban growth in a sustainable and responsible manner, ensuring that the city's potential for development is harnessed without compromising the long-term well-being of its residents and the surrounding environment.

Chapter 5

Characterization of Land Cover Maps: Towards the Identification of Urban Centers and Sub-centers

5.1 Introduction

Urban form is defined as the patterns and layout in the space of physical urban features. It has an influence on the typology of buildings, mobility, and other urban functions, thereby becoming a potential cause of a huge impact on the environmental footprint of a city. Such impacts are becoming increasingly preeminent as most cities develop further. Most of the existing urban growth models focus on the consumption of natural and agricultural areas through the urbanization process, which leads to the ubiquitous urban sprawl model, where a city is an oil stain that diffuses everywhere. In this modeling approach, the spatial extent, i.e., the size of the city, is used as the main parameter.

The compact city model, which was introduced by Dantzig and Saaty [43], largely favors higher density for urban areas. That notwithstanding, in order to have cities with higher sustainability, the morphology of the city has to be understood and described much better beyond density. The morphology of built-up areas is usually intertwined with developmental factors, such as the cultural, economic, political, and technological conditions of the period in which these areas were constructed. However, these factors do not remain constant and are always changing due to several reasons [26, 102, 58].

Density and fractal dimensions are two distinct concepts used in different contexts, includ-

ing urban planning and spatial analysis. Density refers to the concentration or amount of something within a given area. In the context of urban planning, density commonly refers to the number of people or buildings per unit of land area [47]. It is a measure of how closely packed or concentrated a population or urban development is within a specific space. Density is an important consideration in urban planning as it influences various aspects of urban life, including transportation, infrastructure, resource consumption, and social dynamics. High density often indicates a higher number of people or buildings within a given area, while low density suggests a more spread-out or less populated environment [60]. Higher population densities generally require more efficient public transportation systems, compact development patterns, and mixed land uses to promote walkability and reduce car dependence [12]. A fractal form, on the other hand, is geometric structure that presents details at whichever scale it is observed. A usual class of fractals comprises self-similar objects, i.e., objects that replicate themselves at finer scales through iterative function systems. All fractal objects can be characterized by a non-integer fractal dimension which describes the rate as well as the degree to which space is being filled by the fractal object. This reveals important aspects of the structure through quantification of the degree of irregularity or fragmentation within the object being modeled [26, 86, 73]. It is noteworthy that fractal objects are abstract idealized shapes that are not actually observed in reality, similar to a square or a circle. In measuring the fractality of a built-up area, the objective is to determine its fractal dimension (in fact, several definitions for fractal dimension exist: Hausdorff dimension, Minkowski dimension, correlation dimension, etc.), which can be obtained by using several methods, such as: box counting, dilation analysis, and correlation analysis. These methods are used to obtain global information on a built-up pattern to understand how it occupies space. They are applied to an urban pattern, considering it as one texture during the analysis. Another method for determining fractal dimension is radial analysis. Unlike the methods mentioned earlier (box counting, dilation analysis, and correlation analysis), this method is used for obtaining local information on the spatial organization around a selected point within the built-up pattern. It is therefore more of a local than a global approach for the determination of fractal dimensions [56, 86, 58, 39]. A higher fractal dimension corresponds to a highly dense built-up area with very few open spaces interspersed within the urban fabric, therefore, it is associated with poor environmental conditions. On the contrary, a lower fractal dimension corresponds to a sparsely distributed built-up area. Since built-up areas with open green spaces contribute positively to the health of cities

and their residents, lower fractal dimension of a city is indicative of its good environmental conditions [100, 73]. While both density and fractal dimensions are valuable for analyzing built-up areas, fractal dimensions are better suited for studying the spatial organization of clusters of buildings in an area because of their inherent hierarchical properties. Fractal analysis explores the complexity, irregularity, and self-similar patterns within a system, enabling an understanding of the spatial organization and relationships among its elements. On the contrary, density provides a vague indication of the amount of space occupied per unit area, as illustrated in **Figure 1.5**.

Land cover maps aid in land use planning by conveying information on current land use patterns and guiding future land use decisions. Analyzing the spatial organization of land use patterns can help in the identification of suitable areas for specific land uses like residential, commercial, or industrial zones. This information is crucial for formulating zoning regulations, determining infrastructure requirements, and advancing sustainable development practices. Analyzing the spatial organization of land cover maps offers valuable insights for urban planning, environmental management, and sustainable development. Understanding patterns, fragmentation, connectivity, and distribution of land cover categories empowers planners to make informed decisions, enhancing ecological integrity, optimizing land use, and promoting livable, resilient cities [28]. There are several benefits for studying the spatial organization of urban forms. Regarding environmental management, spatial organization aids in identifying areas where proposed development projects may pose risks to sensitive ecosystems, critical habitats, or natural resources [50]. By understanding the spatial relationships between land cover categories and their ecological significance, planners can minimize environmental impacts and encourage sustainable land management. Spatial organization analysis also facilitates the examination of patterns and arrangements of various land cover categories within a landscape. By studying the distribution and adjacency of land cover types, important insights can be gained about urban form, ecological connectivity, and the impact of human activities on landscape and biodiversity [87]. Furthermore, spatial organization assessment enables the evaluation of fragmentation or connectivity in land cover. Fragmentation refers to the division of continuous natural areas into smaller, isolated patches, which can have adverse ecological consequences. Conversely, connectivity refers to the extent to which different land cover patches are connected, facilitating species movement and ecological processes. Understanding these characteristics helps identify areas that may require interventions to enhance connectivity or mitigate fragmentation effects [127]. Within the

context of studying urban sprawl, spatial organization analysis assists in assessing the extent and spatial patterns of the sprawl. Urban sprawl denotes the uncontrolled expansion of urban areas into surrounding rural or undeveloped land. By examining land cover maps over a period, urban planners can identify the direction, rate, and form of urban growth, enabling informed decisions regarding infrastructure development, resource allocation, and environmental conservation to be made [75]. Also, green spaces such as parks, forests, and recreational areas provide significant ecological, social, and aesthetic benefits to cities. Analyzing the distribution and accessibility of green spaces on land cover maps helps in the identification of areas with limited access to nature, guiding efforts to improve equitable distribution and enhance urban livability.

Besides their complex morphology, cities have a spatial organization that reflects functions such as urban centers and subcenters and implies another kind of spatial heterogeneity than the one captured using global fractal dimensions. Batty and Xie [26] concluded that the ultimate objective of their work was to provide a certain means of classifying cities according to their physical forms in terms of urban and land use development. The authors argued that the geometry of urban residential development was fractal since both the degree and the rate at which space is filled in an urban setting followed the scaling laws, which implied self-similarity of the urban forms across different scales. However, these authors restricted their analysis to just one point in the city, the central business district (CBD), and suggested the possibility of treating all points in the city as origins when conducting this kind of analysis. Encarnacao et al. [51] extended this a little further and digitized the built-up area of the metropolitan area of Lisbon into a matrix of square cells of size 1 km^2. The authors then used the box-counting method to determine the fractal dimension of each cell in the matrix. As stated by the authors, this approach was adopted because just a single box-counting analysis would provide global information on the characterization of the built-up area. However, the authors wished to realize the complete characterization of the built-up area to demonstrate the heterogeneous fractal property of the built-up areas. In the end, the matrix was classified into five classes based on the fractal dimension of each cell. The cells with higher fractal dimensions indicated areas closer to saturation, while the cells with lower fractal dimensions indicated isolated areas. This classification enabled the identification of areas requiring immediate planning and regulation based on their urban form.

However, because Encarnacao et al. [51] used the box-counting method, the fractal dimension obtained for each cell described how space had generally been occupied in that

particular cell. In the present study, a method introduced by Frankhauser to classify urban textures [58] that he named the multi-radial approach was adopted. This method does not compute an alternate fractal dimension, but rather attributes a local fractal dimension to each pixel in the analyzed texture. Unlike the box-counting method, the multi-radial approach considers local effects, such as the distance from a point to its neighboring points. This method is used for obtaining information regarding the local fractal behavior and spatial organization around a selected point. This approach would provide greater insight into the urban form than that provided by the traditional density-based measures, as the former measures the hierarchy and describes the structure of the urban patterns. A stronger hierarchy would be a high concentration of mass in large clusters and a large number of buildings with little mass. This kind of local concentration of mass is inconsistent with a homogeneous distribution, in which all elements are assumed to have identical sizes [59]. The areas with a stronger hierarchy would then be classified as urban centers and subcenters.

Urban centers and subcenters are quite significant in the future development of any city [106]. These centers are essential policy tools in the decentralization of the population and improving the standards of living with better environmental quality [147]. One prominent feature of urban centers and subcenters is the high concentration of human activities compared to the surrounding areas [88]. However, the definition of an urban centers and subcenters could be subjective because it is always based on the objective of the research. In any research, urban centers and subcenters may be identified using two main approaches: the morphological approach or the functional approach [88, 83, 154]. The morphological approach is concerned with the size and spatial distribution of the centers and subcenters, while the functional approach is concerned with the linkages between different centers [154]. Various methods, such as minimum cut-off point, spatial statistical methods, and hedonic price method have been adopted to identify urban centers and subcenters using data from official statistics, remote sensing, and geospatial big data systems [106, 89, 34, 88, 95, 154, 94]. The identification of urban centers and subcenters is important because it assists in planning the balance between jobs and housing and the ecological capacity of the city centers [146]. Appropriate local jobs–housing balance would allow for a shortened commuting time of workers, reduced traffic congestion, decreased air and noise pollution due to automobile movement, and improved overall well-being of the inhabitants [89]. In addition, a better understanding of urban expansion would be achieved, which would provide town planners with the information necessary to evaluate

the effectiveness of the planning layouts [34].

However, unfortunately, studies on the identification of urban centers and subcenters in cities are scarce, particularly in developing nations, with most such studies reported so far based on the local context of developed nations only [154]. This could probably be due to the lack or partial availability of official statistical data or geospatial big data, such as POIs and social media check-ins, for use by researchers to identify urban centers and subcenters [101, 94]. Nevertheless, due to the good spatial and temporal resolutions of freely-available remote sensing images, such as Landsat and Sentinel, the challenge of inadequate data for the identification of urban centers and subcenters could be dealt with to a certain extent. Taubenböck et al. [135] used 3D building models derived from remote sensing data and identified urban centers as areas with high urban mass concentration. The authors argued that this could be a reasonable substitute for the density data when identifying the urban centers. Cai et al. [34] combined night-time light imagery with social media check-in data to locate urban centers and also argued that these data could serve as valid substitutes for population or human activities in the identification of urban centers. Li et al. [88] indicated that from empirical results, it is believed that there is much more potential to be explored by examining the built-environment for research related to urban structure. In this context, the present study explored the potential of empirical results in the identification of urban centers and subcenters by attempting to use built-up data extracted from freely-available remote sensing imagery datasets, which are usually the only source of consistent spatial data that covers large areas with high spatial detail and frequency in most developing nations.

The aim of this chapter is to explore the potential of fractal geometry in explicitly identifying urban centers and sub-centers, as well as understanding their spatial organization using remote sensing data. This approach aims to design urban growth models that are more informative compared to the oil-stain models, with GAMA serving as the study area. The idea is to use the fractal decomposition used in the computation of dimensions to identify urban hierarchies and facilitate adding structure to the patterns obtained through the classification of remote-sensing imagery. Morphological image analysis is used as a complementary image processing technique to highlight the identified urban centers and subcenters. It is noteworthy that the present study aims only to describe the evolution of the spatial structure of the built-up patterns and not to explain the underlying reasons for it. This aim requires information and data on population distribution, transport networks, land prices, land use policies, etc., which are partially unavailable, causing the

explanation part to be beyond the scope of the present work.

In comparison to the relevant previous studies, the present study offers the unique contribution of integrating multi-radial fractal analyses with mathematical morphology to identify urban centers and subcenters using only remote sensing images. No study conducted so far, to the best of my knowledge, has used remote sensing, fractal dimensions, and mathematical morphology for the identification of urban centers and subcenters. The findings in this study would contribute significantly to the identification of urban centers and subcenters in cities that do not have adequate statistical data, such as population census, economic data, and geospatial big data, especially in developing nations.

5.2 Methodology

To explicitly identify urban centers and subcenters of GAMA, and understand their spatial organization from remote sensing data, the following methodology was employed.

5.2.1 Global Organization

The box-counting method (estimating the Minkowski dimension) was adopted to obtain global information on the spatial organization of the built-up pattern of GAMA for the years 1991, 2002, 2013, and 2022. Box counting is a grid-based analysis of an object (in this case, the built-up area of GAMA), the fractal dimension of which has to be determined. It provides an estimate of the Minkowski dimension. The built-up area is covered by a uniform grid composed of squares of size $\boldsymbol{S}$, and the non-empty squares, $\boldsymbol{N}$ (squares that are completely or partly filled with the pixels representing the built-up area) are counted. The size of the squares, $\boldsymbol{S}$, that form the grid is varied progressively, and the number of squares, $\boldsymbol{N}$, required to cover the built-up area in each scenario is determined. The series of points, $\boldsymbol{(S_i, N_i)}$, are plotted on a two-dimensional graph, where the Y-axis corresponds to the number of squares, N_i, and the X-axis corresponds to the size of the squares, S_i, both of which change in each step [86, 58, 142]. The relationship between the two variables is then expressed as follows:

$$N = CS^{-D} \tag{5.1}$$

where:

C = Total size of the grid

D = Box counting fractal dimension

The estimation of D is based on a logarithmic transformation of **equation 5.1**, which has the form of an equation of a straight line, where D is the slope of the line.

$$logN = -Dlog(S) + log(C) \tag{5.2}$$

D is then estimated using an ordinary least square (OLS) regression.

5.2.2 The Curve of Scaling Behavior

The curve of scaling behavior is a chart that illustrates the changes in the fractal dimension with scale. This curve is a unique way of visualizing the empirical results of fractal analysis by providing detailed information regarding the spatial organization of urban patterns [38]. In **equation 5.2**, which is the equation of a straight line, the fractal dimension is the value of the slope of the straight line. However, assuming that the fractal dimension D and the constant C depended on the size of the square S, and based on the fact that the real-world phenomena do not strictly obey the fractal law, and rather the fractal relation itself, a sequence of local slope values, $\alpha^{(loc)}$, may be obtained from the relationship, as follows [59, 58]:

$$\alpha^{(loc)} = \frac{logN(S_{i-1}) - logN(S_i)}{log(S_i) - log(S_{i-1})} \tag{5.3}$$

The series of points $(S_i, \alpha_i^{(loc)})$ may then be plotted on a graph to illustrate the scaling behavior of the urban pattern under study.

5.2.3 Logistic Growth Model

A logistic function is a common type of sigmoid function that has applications in numerous fields, including ecology, demography, geoscience, sociology, and artificial neural networks. The function was first proposed as a population growth model by Verhulst in 1838 and

has since been used in several biological and economic growth modeling processes [22]. According to Chen [37], any system with distinct upper and lower limits and a non-uniform growth rate presents a growing course that has an S-shaped curve, which may be abstracted as a logistic function. On a two-dimensional map, the fractal dimension of the built-up area ranges between 0 and 2, and the growth rate is non-uniform, which renders it possible to model the evolution of the fractal dimension with a logistic function. Xiaoming and Chen [100] modeled the fractal dimension values of a time series in Shenzhen using logistic function modeling. According to Chen [36], the logistic function for the evolution of fractal dimension is as follows:

$$D(t) = \frac{D_{max}}{1 + Ae^{k(t-t_0)}} \tag{5.4}$$

where:

t = year

t_0 = first year to be considered

D(t) = fractal dimension at time t

D_0 = fractal dimension at time t = 0

$D_{max} \leq 2$ = maximum fractal dimension

A = $\frac{D_{max}}{D_0} - 1$

k = growth rate of the fractal dimension

5.2.4 Multi-Radial Analysis

Radial analysis is another method for determining fractal dimensions, which plays a particular role in urban pattern analysis [59]. This method provides a local estimate of the correlation dimension and is adopted to obtain information on the local fractal behavior and spatial organization around a selected point. In order to perform a radial analysis, a circle with a radius r is drawn around the selected point, and the number of points, N, within the circle is determined. The radius, r, is gradually increased while counting the number of points, N, inside the circle at each step. Next, the series of points, (r_i, N_i), are plotted on a two-dimensional graph, where the Y-axis corresponds to the number of points N_i, and the X-axis corresponds to the size of the radius, r_i, both of which change in each step. The relationship between the two variables is similar to that expressed in **equation 5.1**, with just S replaced with r [86, 58, 142]. The multi-radial analysis is a

generalization of the radial analysis method, which allows for extracting information on the spatial organization around a selected cell, i.e., basically, a radial analysis performed on each pixel in the built-up pattern over a specified range.

5.2.5 Morphological Image Analysis

Mathematical morphology is a theory that provides useful tools for image analysis. This theory may be applied to eliminate unwanted details from classified remote-sensing images. The advantage of using mathematical morphology is that it comprises shape-oriented operations that simplify image data while preserving their essential shape characteristics and eliminating irrelevances [133]. Erosion and dilation are the two basic operations of mathematical morphology. Basically, erosion removes pixels from the boundaries of objects, while dilation adds pixels to the boundaries of objects. One important element in mathematical morphology operations is the structuring element. The size and shape of the structuring element determine the number of pixels that could be added or removed in a mathematical morphology operation. The two secondary mathematical morphology operations are opening and closing. In order to perform the opening operation, the image is first eroded and then dilated. In the closing operation, the image is first dilated and then eroded. The main difference between the basic operations and the secondary operations is as follows: the basic operations clean the image and leave the image either smaller or larger than its original size; and the secondary operations perform the same function while maintaining the same size of the image as that of the original image prior to the operation [111].

5.3 Results and Discussion

5.3.1 Global Organisation

The box-counting method (estimating the Minkowski dimension) was adopted to obtain global information on the spatial organization of the built-up pattern of GAMA for the years 1991, 2002, 2013, and 2022. The extracted built-up pattern of GAMA for 1991, 2002, 2013 and 2022 is shown in **figure 5.1 a-d** respectively. The obtained results are presented in **Table 5.1**. A general increase in the fractal dimension was observed from 1991 to 2022, as visible in **figure 5.2**. This indicated a continuous decrease in the number of open spaces in GAMA, causing the region to be more saturated as the fractal dimension

approached 2.

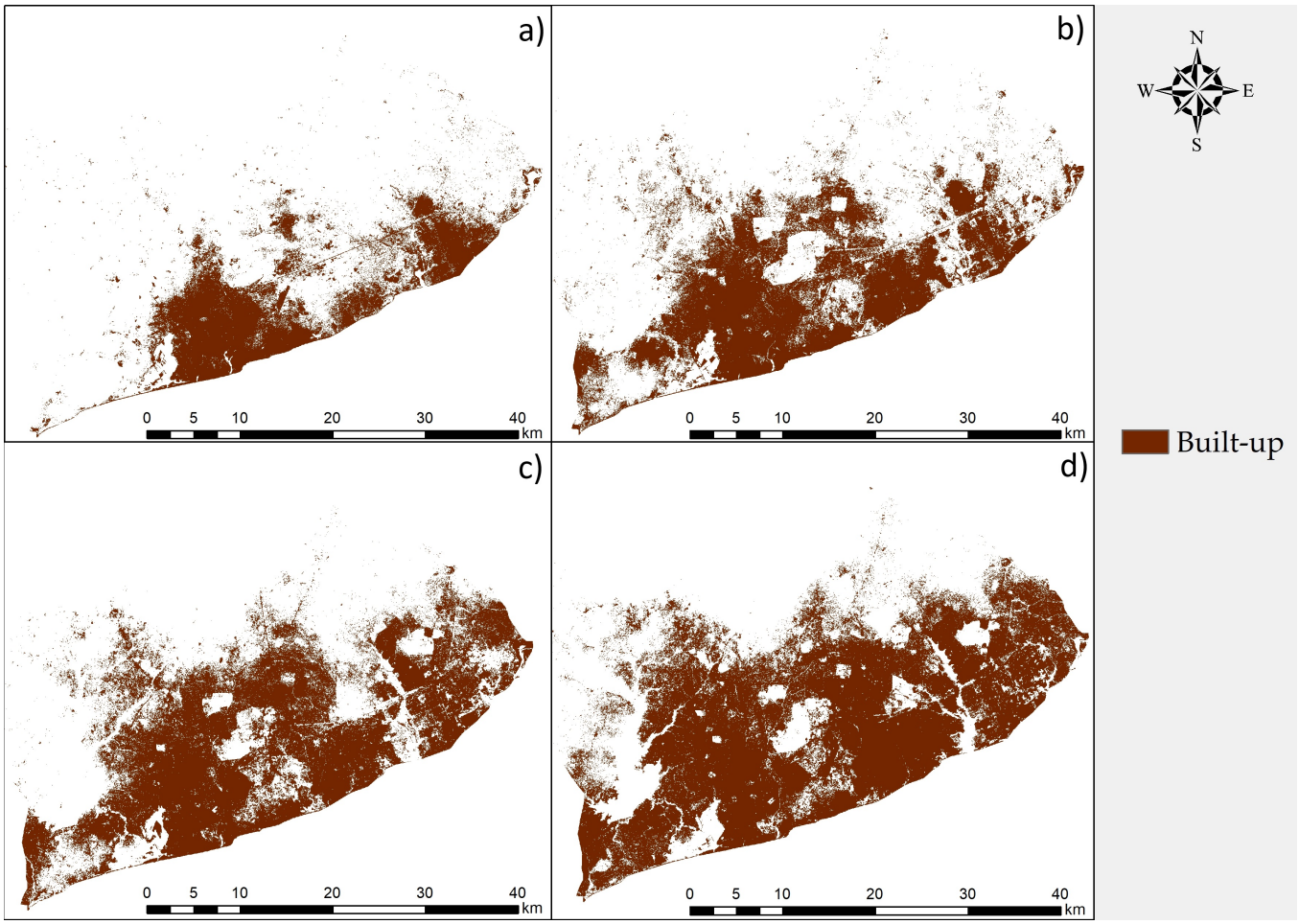

Figure 5.1: Extracted built-up pattern of GAMA from the 1991 to 2022.

Table 5.1: Box counting fractal dimension for GAMA during different years

Year	Fractal Dimension
1991	1.581
2002	1.687
2013	1.738
2022	1.777

5.3.2 The Curve of Scaling Behavior

The box-counting method provides an overall average of the fractal dimension of the built-up pattern in the study region, while the scaling behavior is an average of the fractal dimension at sections along the built-up pattern. In the case of a perfect fractal, the curve of scaling behavior is a straight line as no variations occur in the fractal dimension. **Figure 5.3** depicts a chart representing the curve of scaling behavior of the built-up area of GAMA from the year 1991 to 2022. The intercepts of the curves follow the same increasing order as followed by the fractal dimensions and characterize the repartition of

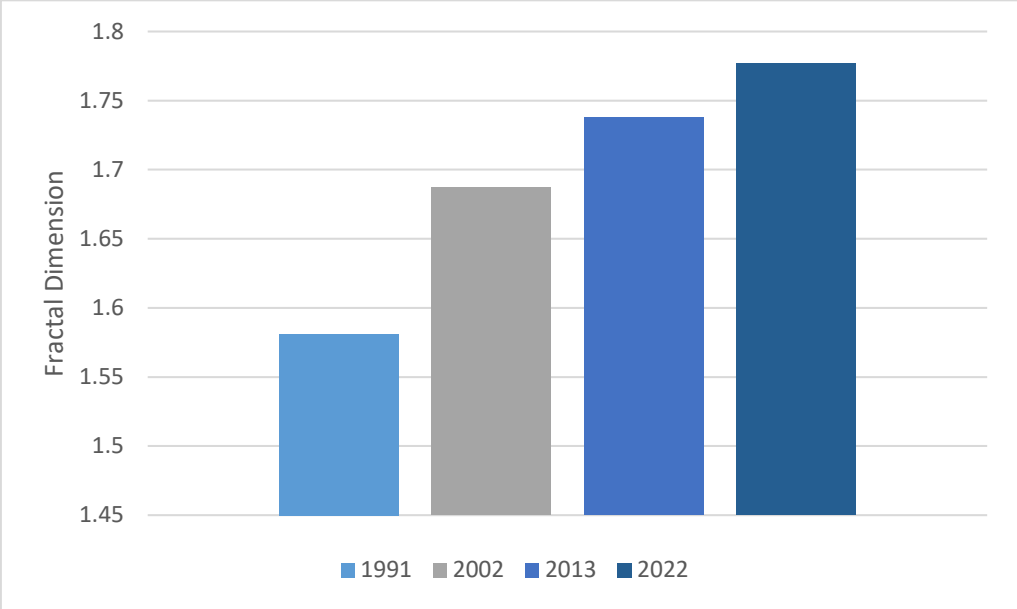

Figure 5.2: Evolution of the fractal dimension of built-up area in GAMA from 1991 to 2022.

the smallest boxes. On the right-hand side, the dramatic drop toward zero is because of the boundary effect, reinforced by the fact that GAMA is a coastal agglomeration. The shapes of the curves revealed meaningful information on the possibility to model the entire agglomeration as a single fractal object, i.e., a horizontal curve, indicating that the texture was homogeneous.

In 1991, the curve of scaling behavior descended gently from 60 m to 330 m and began undulating in the mid-section from 330 m to around 1.74 km, where it began rising again until it leveled and then declined again due to boundary effects. The undulations in the mid-sections on the curve during 1991 were due to the gaps in that section of the study region in 1991. Therefore, the self-similarity of the 1991 texture was not totally observed at all scales, thereby revealing the main scales of urban centers. In 2002, when those gaps were filled, the undulations were not as pronounced as those in the previous year. The curve for 2002 was fairly-straight until it reached 780 m, where it began rising and then declined. The characteristic size of the urban centers had increased, and the centers had begun connecting, resulting in an urban pattern more uniformly covering the entire agglomeration. The curves for 2013 and 2022 were quite similar, while the curve for 2022 was relatively smoother as compared to the curve for the year 2013. The changes in the scaling behavior of the 2022 curve were not that sharp due to the saturation of the built-up pattern this year. The values used for plotting the graph are provided in **Appendix I**.

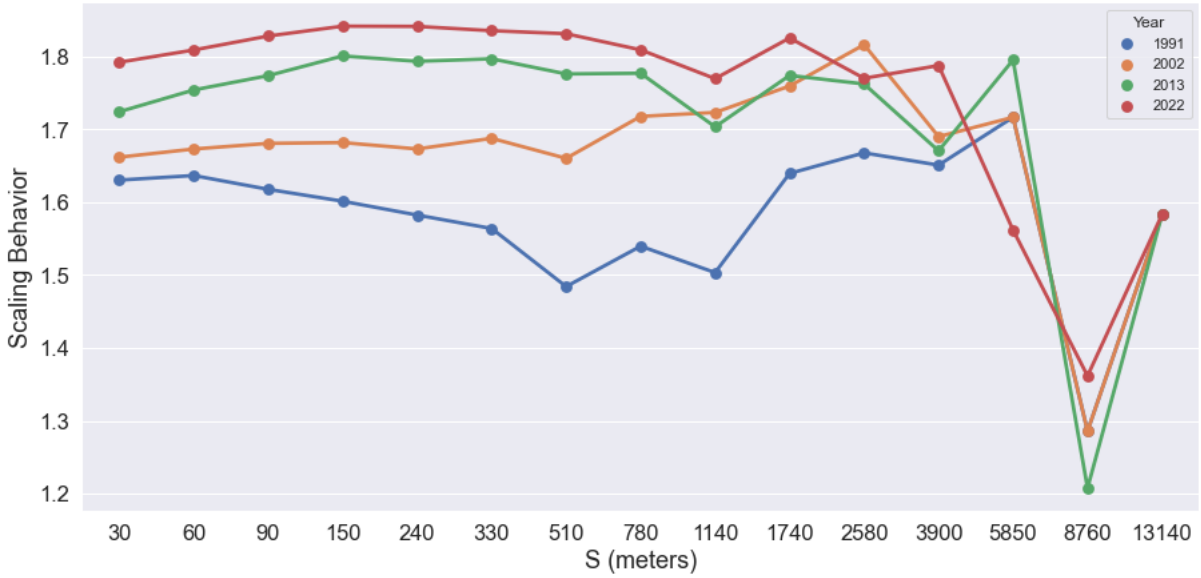

Figure 5.3: The curve of scaling behavior for GAMA fom 1991–2022

5.3.3 Logistic Growth Model

In order to predict the fractal dimension of GAMA in the future, a logistic growth model was developed. As presented in **table 5.1**, the rate of increase in the fractal dimension from the year 1991 to 2002 (0.106) was nearly twice the rate of increase from 2002 to 2013 (0.051). In the 2013–2022 period, the rate of increase reduced again, compared to that during 2002–2013. This non-uniformity in the growth rate, coupled with the distinct upper and lower limits of the fractal dimensions of built-up patterns on a two-dimensional map, made it possible to model the evolution of fractal dimensions over the period with a logistic growth function to facilitate the prediction of the future growth [36, 100]. The evolution of fractal dimension was successfully modeled, and the parameters of the logistic equation were estimated by identifying the set of parameters that minimized the sum of squared residuals using the 'fmin' optimization tool in the Optimize package of SciPy, which is based on the Nelder-Mead Simplex Algorithm [117]. The logistic equation for the evolution of fractal dimension in GAMA is as follows:

$$D(t) = \frac{1.817}{1 + 0.149e^{0.055(t-1991)}} \tag{5.5}$$

With an R^2 value of 0.9981, it was estimated that the maximum limit of the fractal dimension would be reached in 2232. **Figure 5.4** presents a chart depicting the logistic growth pattern of the fractal dimensions in GAMA. Using this model to forecast the

fractal dimension in the year 2032 yielded a dimension of 1.79, which was similar to the one obtained for AMA for the year 2022. With a high rate of growth observed in the GAMA region, the model enabled the assumption that if the urban expansion remains uncontrolled, the entire region would reach the uniformity of the administrative center within 10 years.

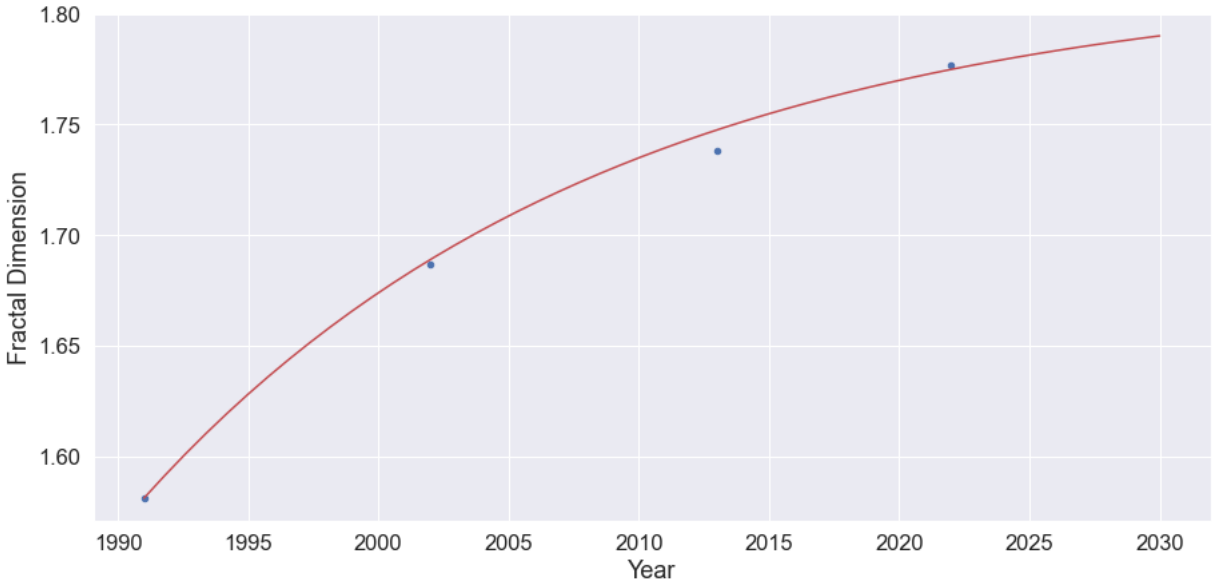

Figure 5.4: Logistic growth pattern of fractal dimensions for GAMA from 1991–2022

5.3.3.1 Multi-Radial Fractal Analysis

Multi-radial analysis was applied with a radius of 300 meters and generated maps with each pixel characterized by its local fractal dimension. This ensured correct estimates of the power law, even in sparse areas, which is important information required to be processed to reveal meaningful spatial structures. With a ground pixel size of 30 m, each local radial analysis was performed on approximately 196 pixels, which ensured that each power law was estimated correctly. In the present study, a manual classification of the local fractal dimensions was adopted, with thresholds determined based on expert opinion.

The pixels in the built-up pattern were grouped into four classes according to the fractal dimension of each pixel. The pixels with dimensions between 0 and 1.25 were classified as stage 1 because they were considered to be in the first stage of the urbanization process. In stage 1, the built-up pattern is sparsely distributed and the land cover predominant in the area is vegetation. The pixels with fractal dimensions between 1.25 and 1.5 were classified as stage 2, representing the second stage in the urbanization process. This stage

is characterized by the transition from the sparsely distributed built-up pattern to urban growth, typically along transport networks, connecting centers and subcenters. The pixels with fractal dimensions between 1.5 and 1.75 were classified as stage 3. These pixels were mostly located on the fringes of the saturated areas, which did not have any further space for expansion, i.e., stage 4. Stage 4 areas comprised pixels with fractal dimensions ranging between 1.75 and 2. These areas were the most saturated and dominant in the centers and subcenters of the city. **Figure 5.5** a, b, c and d present the maps depicting the multi-radial fractal dimensions of the study region for the years 1991, 2002, 2013, and 2022, respectively.

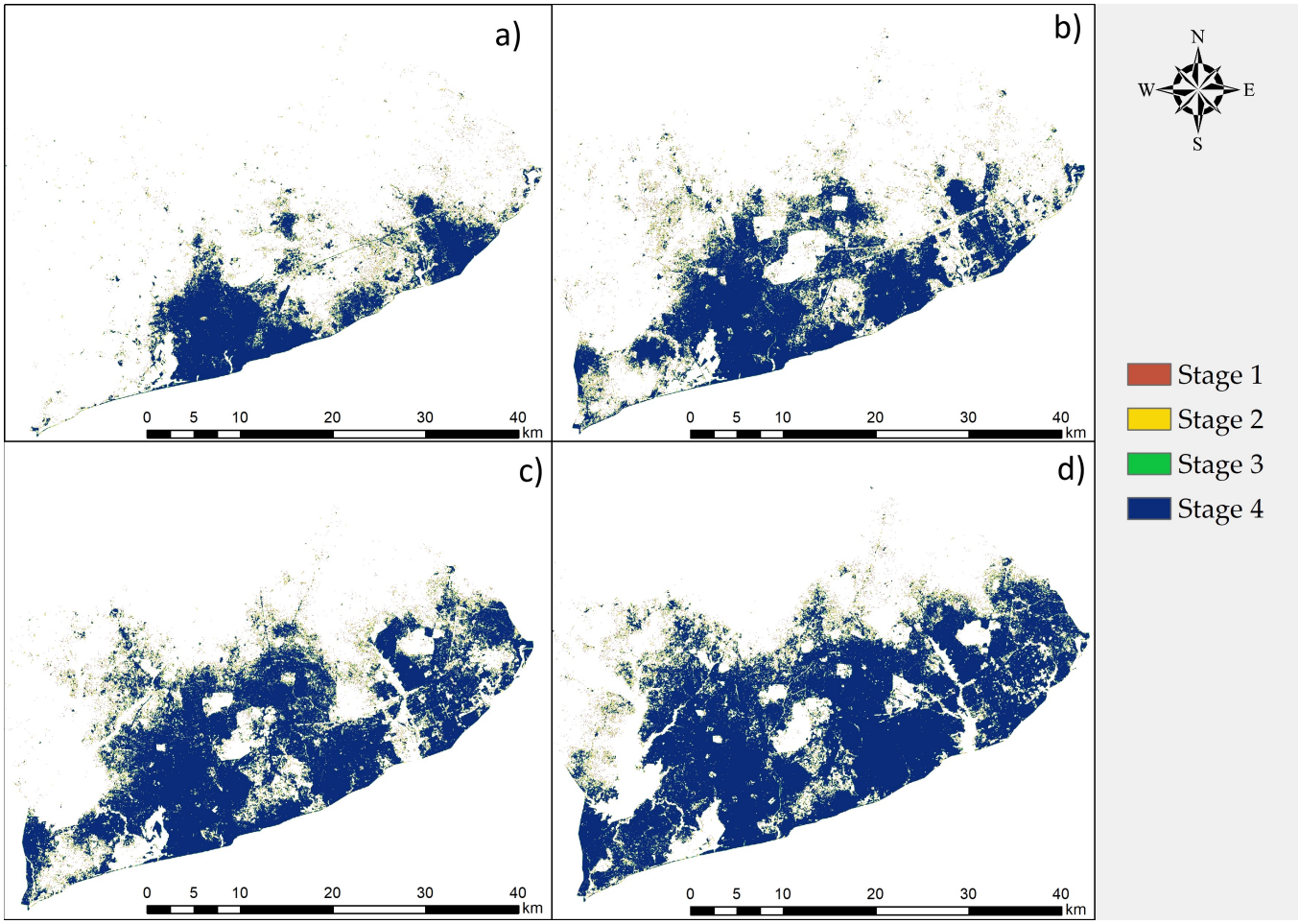

Figure 5.5: Multi-radial Fractal Dimensions of GAMA from 1991–2022

In **figure 5.5**a, which is a map depicting the multi-radial fractal dimensions of the built-up area of GAMA in the year 1991, the two main centers of GAMA, i.e., AMA and TMA, could be explicitly identified along with the two subcenters, Madina and LEKMA depicted in **figure 5.6**a. Until 2002, these centers and subcenters had expanded (**figure 5.6**b) and a new subcenter had emerged in the southwestern corner of the city, GA South. The north of AMA, which has been expanding in the southwestern direction, had a cluster of pixels dominated by Stage 1 and Stage 2. This cluster was referred to as a seed as it was

attracting new settlements due to its proximity to AMA and was thus expected to grow into a subcenter. Until 2013, Madina, LEKMA, and AMA had grown so much toward each other that they had merged to form one big center (**figure 5.6**c). The seed identified in **figure 5.6**b had attracted a lot of settlers and was now considered a subcenter. TMA had also expanded eastward, contrary to 2002, when very little growth was observed. In 2022, the center consisting mainly of AMA, Madina, and LEKMA had engulfed the subcenter at the southwestern corner of the study region to form an even bigger center. TMA had also become further saturated, for the most part, due to in-filling. Two new subcenters and several seeds were observed at the peripheries of the two main centers (**figure 5.6**d).

5.3.3.2 Morphological Image Analysis

The stage 4 pixels, i.e., the pixels with fractal dimensions ranging from 1.75 to 2 for each year (1991, 2002, 2013, and 2022), were extracted and processed further using mathematical morphology to highlight the urban centers and subcenters through the elimination of unwanted details. According to the definition of an urban center/subcenter as a place with a high concentration of human activities [88], the areas with large clusters of stage 4 pixels were classified as urban centers and subcenters. Using the two main urban cores of GAMA observed for the year 1991, AMA and TMA, as standards, clusters smaller than these centers were classified as subcenters, while the clusters bigger or equal to these standards were classified as centers. In each year, an appropriate structuring element was selected for each morphological operation. The morphological operations of opening, closing, and erosion were performed using OpenCV in python. **Figure 5.6**a depicts a map with the centers and subcenters of GAMA in the year 1991. It may be observed that the two main urban centers,i.e. AMA and TMA, could be explicitly identified in the map along with a subcenter LEKMA between them. In 2002, as depicted in **Figure 5.6**b, the centers and subcenter identified in **Figure 5.6**a had increased in size, and a few settlements had emerged in the east of AMA and the north of LEKMA. In 2013, as depicted in **Figure 5.6**c, the centers had increased in size, as usual, while the subcenter observed in **Figure 5.6**a and **Figure 5.6**b had increased so much in size that it was comparable to the two main urban centers. Therefore, it was classified as a center now. New agglomeration settlements were observed toward the east of AMA and the west of TMA, which were identified as subcenters. Until 2022, as depicted in **Figure 5.6**d, the subcenter east of AMA had merged with AMA, forming one big center. The other two

centers had also merged with the subcenter on the west of TMA, forming another big center with quite a little space separating them. The multi-radial fractal analyses and the observed evolution of the urban centers and subcenters in GAMA from 1991 to 2022 revealed a likelihood of the two centers identified in **Figure 5.6**d merging and forming an even bigger center, with its subcenters forming in the north and northeast of AMA.

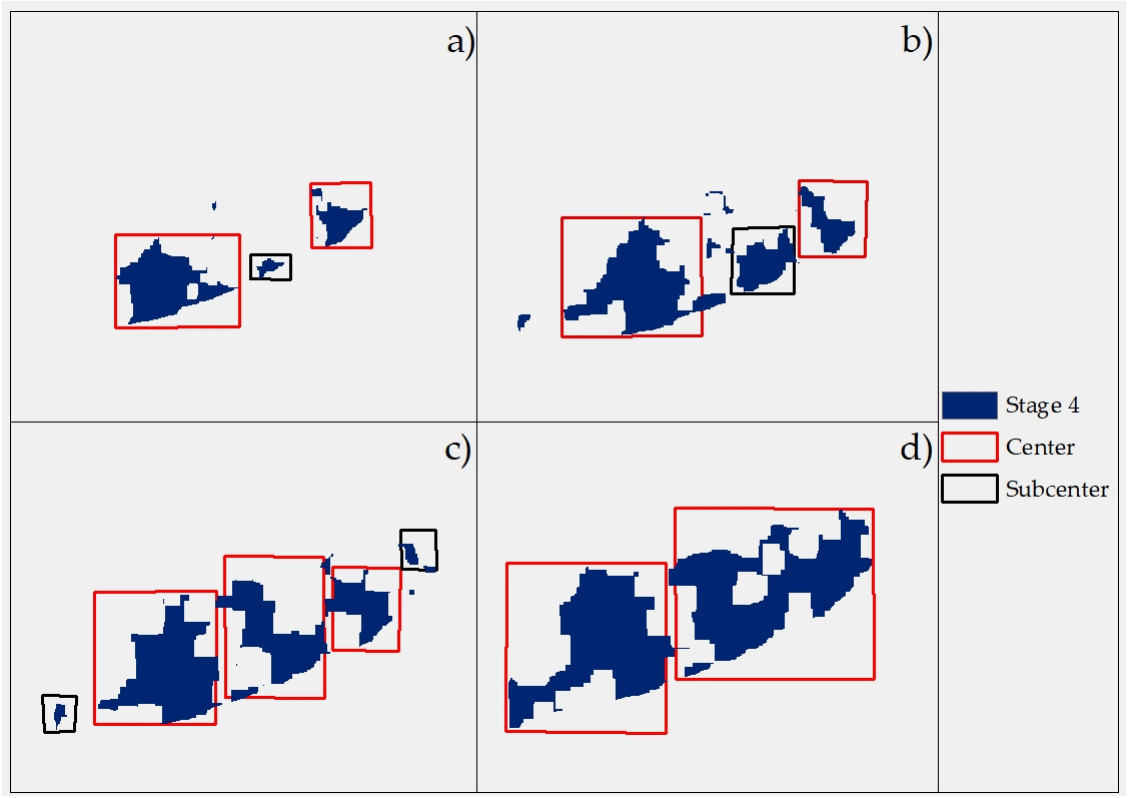

Figure 5.6: Schematic map of Urban Centers and Subcenters in GAMA, 1991–2022

5.3.4 Graphical Modelling with Chorems

A map is a communication tool; and communication is basically a process of successfully getting information from one party to another. For a map to be able to communicate effectively, users must be able to understand the meaning of what the cartographer is sharing. Using symbology closer to how humans reason about commonsense knowledge can help overcome some of the challenges of language barriers that can result from verbal communication or communicating through text [44]. Maps are useful in understanding terrains and the dynamics of events that occur in these terrains, identifying patterns, and making predictions of future occurrences. However, in as much as maps are useful, sometimes not all the details displayed in maps are relevant to decision making. Only sections pertaining to the reason for which the map is being used are useful for decision making at any given time. Therefore in decision making, generalized maps which stress

on the most important aspects relevant to the issue being tackled are more informative to a broader audience than a highly detailed map [40].

In running the affairs of a geographic area, just as business intelligence is helpful in the success of businesses, territorial intelligence is equally helpful in the understanding and governing of geographic areas [40]. Territorial intelligence is a multidisciplinary knowledge that improves the understanding of the connections between socio-ecological transition and growth. It involves communities, stakeholders and researchers with the aim of promoting inclusiveness and coordinated governance to allow territorial actors to elaborate, manage and evaluate projects for sustainable development [64]. Due to its participatory nature which allows several stakeholders to participate in decision making, information that would be shared must be simple enough to be easily understood, yet detailed enough to facilitate effective decision making.

This is where the concept of chorems comes into play. Chorems are schematic representations of geographic spaces which eliminates unwanted details that do not aid in map comprehension [44]. Using chorems in map making makes communication so efficient that even nontechnical users of the map are able to easily understand the message being delivered [32]. Chorems constitute a visual vocabulary for the description of the main characteristics of a territory, and can therefore be a solid basis for decision making because they highlight the salient aspects of the map by leaving aside other aspects not so relevant to the matter being addressed. Visual models based on chorems can interpret and represent spaces, their geographic distributions and their dynamics [40]. **Figure 5.7** is a map showing the schematic representation of the urban growth process of GAMA based on the spatial organization of the urban centers, subcenters, and the localization of the major transport networks.

5.3.5 Conclusion

Measuring the homogeneity of urban development as well as identifying urban centers and subcenters are crucial steps to understand the growth and development of cities. However, identifying such structural information can be challenging, especially in cities where data availability is limited. The objective of this study was to address the challenge of limited data availability in the identification of urban centers and subcenters by proposing a novel approach that utilizes freely available remote sensing data and fractal analysis. While several previous studies have investigated urban growth and development in GAMA, this

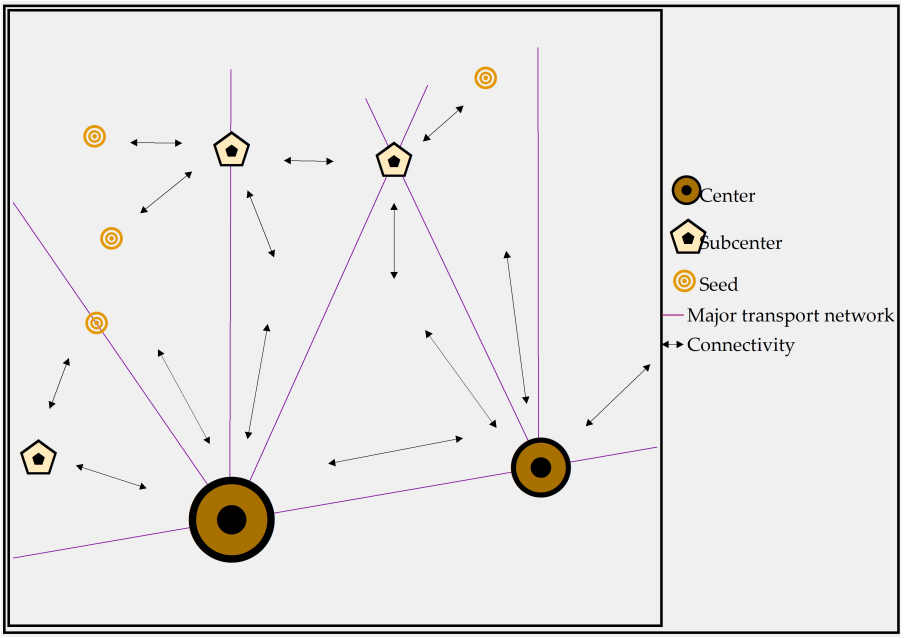

Figure 5.7: Schematic representation of urban growth in GAMA

study differs in its specific focus on the identification of urban centers and subcenters using fractals and remote sensing data. Unlike previous studies that may have used different methods or focused on other aspects of urbanization, this research aims to fill a gap in the literature on identifying centers and subcenters in cities in developing countries and provide more comprehensive insights for urban growth modeling while addressing the challenge of limited data availability.

To bridge this gap, only freely available remote sensing data were used to identify urban centers and subcenters. The methodology used is easy to replicate and it does not require one to have ample knowledge of the study area. The findings in this research provides significant contributions to not only the identification but also the spatial organization of urban centers and subcenters in cities that do not have adequate statistical data such population census, economic data or geospatial big data, especially in developing counties. Replication of the methodology used would help contribute to a robust and comprehensive database on the cities in the world. The present study successfully combined multi-radial fractal analyses with mathematical morphology operations to reveal the urban centers and subcenters that were otherwise hidden in the built-up patterns extracted from remote sensing images.

The logistic growth modelling of the fractal dimensions and analysis of the GAMA region revealed that in less than 10 years, the whole region is likely to reach the kind of urban pattern that is usually present in the city centers, in terms of both density and spatial organization. Moreover, the local fractal analysis revealed significant changes in

the hierarchy of the centers and subcenters, with the emergence of a large connected region along the seashore and secondary centers that are located farther and farther to the north. Lastly, urbanization along the roads appears to be the new emerging pattern as far as land saturation is concerned (**Figure 5.8**). The in-filling process of urban growth appears to have reached a saturation point.

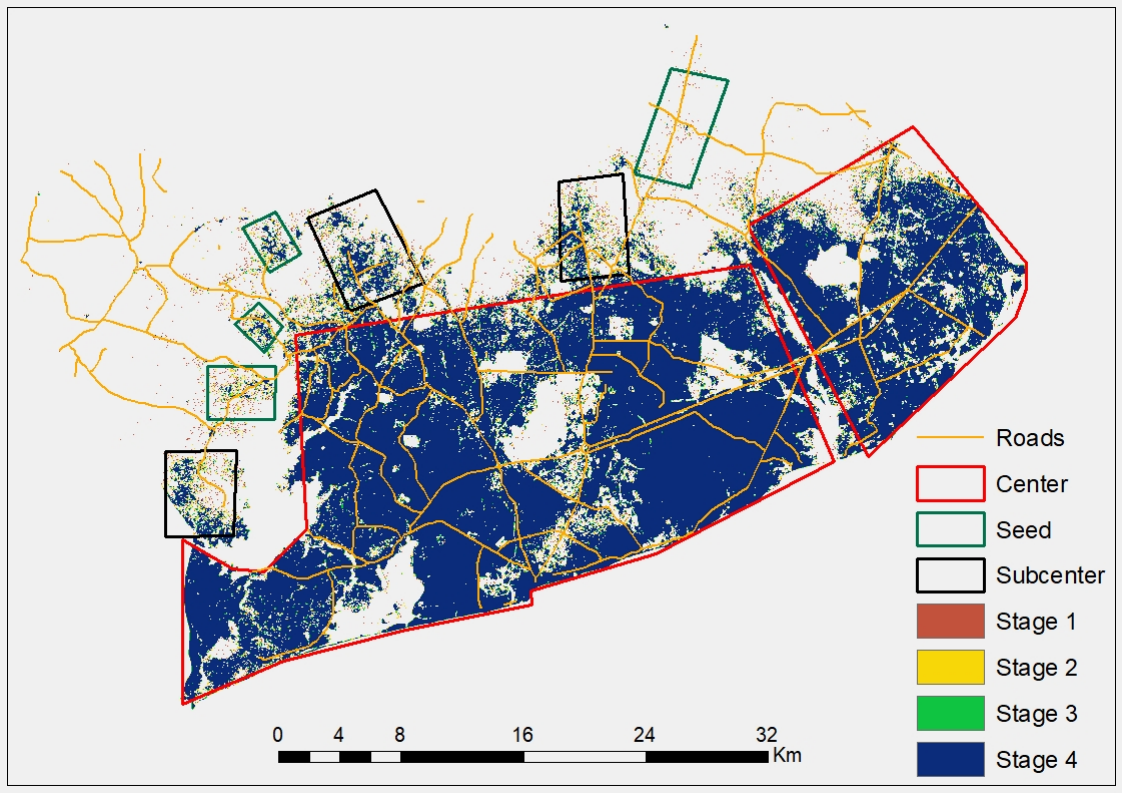

Figure 5.8: Emerging urbanization along the roads in GAMA, 2022

Compared with previous studies in this field, this study makes the unique contribution of integrating multiradial fractal analyses with mathematical morphology to identify urban centers and subcenters from only remote sensing images. To the best of my knowledge, no research has been done and published using remote sensing, fractal dimensions and mathematical morphology to identify the spatial organization of urban centers and subcenters. Future research on urban growth forecasting will use all the structural information extracted in new methods combining continuous change and discrete events, such as the emergence of new centers and subcenters.

Chapter 6

Conclusion and Recommendations

6.1 Conclusion

6.1.1 Methodological

A novel approach was proposed to compare three satellite image classification methods: random forest(RF), support vector machine (SVM), and simple linear iterative clustering (SLIC). This comparison was based primarily on the effects of a classification method on the resulting land cover map, in spite of similarities in their kappa scores and overall accuracies. This was done by measuring certain characteristics of the identified land cover types such as: total edge, number of patches and fractal dimension. These characteristics are not captured by the overall accuracies and kappa scores, yet, they represent the form and shape of the classified land cover types. It was concluded that although different classification methods may possess similar overall accuracies and kappa scores, subtle differences in qualities such as lacunarity and edge length of identified land cover types could be detected. These differences serve as important factors in guiding analysts to choose a more suitable classification method for their specific project requirements. Among the image classification methods compared, it was observed that land cover maps resulting from RF classification produced the most detailed land cover maps. However, for a more generalized land cover map, SLIC was the best option. Using random forest to classify satellite images of GAMA (1991-2022), different forms of urban growth such as:

i. extension - the expansion of the urban area outward, essentially increasing the urban footprint by adding new developments;

ii. leapfrog - urban growth that has occurred sporadically, with certain areas being

developed while leaving gaps or undeveloped spaces in between; and

iii. infilling - urban growth has occurred by filling in or developing areas within the existing urban footprint, rather than expanding outward

were captured in the urban growth pattern of the study area, demonstrating an urban hierarchy.

Urban hierarchy typically refers to a system in which urban areas are ranked or organized based on their size, importance, and functions. The study area, GAMA, being characterized by a mixture of developed areas with buildings and undeveloped or open spaces, kept changing as the years progressed resulting in an evolution of the urban hierarchy. The evolution of the urban hierarchy was successfully tracked by analyzing spatial patterns using landscape metrics. The findings revealed a significant transformation in the land cover composition of the region, with the Built-up land cover type now dominating over the previously dominant Vegetation land cover type. The landscape metrics further revealed extensive fragmentation of the Vegetation land cover type, indicating a negative impact on biodiversity conservation, species movements, ecosystem functioning, and long-term ecological resilience. Additionally, the study successfully predicted the land cover and landscape pattern of GAMA for the year 2030 using information extracted from the satellite images. Information on the urban hierarchy was used as an explanatory variable in conjunction with a predictive modelling techniques such as Land change modeler, Markov chain cellular automata, and Netlogo to forecast how the spatial organization of the landscape pattern of GAMA in the future. The trends observed highlighted the importance of considering landscape connectivity, habitat fragmentation and spatial arrangement of land cover types in assessing ecological processes and urban development impacts on the environment. While the research focused on vegetation, which is a critical component of the natural ecosystem, it is important to note that data on species richness were not incorporated. Unfortunately, data availability constraints and the scope of the work prevented this valuable aspect from being included in the analysis.

The goal of this thesis was to address the challenge of the lack or partial availability of data in the identification of urban centers and subcenters, therefore, no additional data was used aside freely available remote sensing data. That notwithstanding, an additional method, mathematical morphology, was adopted. Mathematical morphology is a field of mathematical theory and image processing that deals with the analysis and processing of images or other spatial structures. It was applied to eliminate unwanted details from the

processed remote sensing images. By successfully combining mathematical morphology with multiradial fractal analysis, a method used to obtain information on the local fractal behavior and spatial organization around a selected point, sections of the built up pattern extracted from the freely available remote sensing data where of higher fractal dimensions were identified and classified as urban centers and subcenters. These centers are morphological centers, which are characterized by high concentration of human activities present there as compared to surrounding areas. The presence of human activities were equated to the presence of built up land cover type. The intensity of the human activities were equated to the fractal dimensions, therefore, the higher the fractal dimension, the higher the intensity of human activities present there.

The urban growth process was sketched based on the spatial organization of urban centers, subcenters, and the localization of the main transport networks. This was done by first identifying the existing urban centers and subcenters within the city. The major transportation networks were then plotted on the sketch. Arrows were used to represent the expected directions of urban growth from the existing centers and subcenters considering how growth is likely to radiate from the city center and how transportation networks might facilitate this expansion. Concentric circles were used to represent potential areas for future urban development. Creating such a sketch, often referred to as an urban growth model or a conceptual diagram, helps visualize and understand how a city or urban area is likely to evolve over time. This kind of sketch can be a valuable tool for urban planners, policymakers, and stakeholders to visualize and communicate expected urban growth process. It can also serve as a foundation for more detailed urban planning and development strategies.

6.1.2 Thematic

Urban growth refers to the expansion of urban areas, which includes an increase in the physical size and population of cities and towns. It is a fundamental aspect of urban development and is often measured in terms of the expansion of built-up areas, the increase in the number of buildings and infrastructure, and the growth of the urban population. Urban growth can result from various factors, including natural population growth (births exceeding deaths), rural-to-urban migration, and the reclassification of rural areas into urban ones. In this thesis, urban growth was measured based on the expansion of built-up areas as identified on freely available remote sensing data (satellite images). The current research aimed to design urban growth models that were more informative than

"oil stain" models; and identify urban centers, subcenters and their spatial organization from only freely available remote sensing data. This is because, despite the importance of the identification of urban centers and subcenters in the sustainable development of cities, there are not enough studies on the subject within the context of developing countries owing to the lack or partial availability of data to do so. To bridge the gap of there not being enough studies on the subject within the context of developing countries and address the challenge of data unavailability in the identification of urban centers and subcenters, the current research sought to ascertain whether or not:

i. fractal geometry could be used to explicitly identify urban centers, subcenters, and their spatial organization from remote sensing data;

ii. it were possible to characterize the spatial organization of urban centers and subcenters while analyzing urban growth; and

iii. it were possible to sketch urban growth process based it the spatial organization of urban centers, subcenters, and the localization of the shape of main transport networks.

Based on the findings of the research, it can be concluded that while fractal geometry can provide valuable insights into the complexity and organization of urban areas, it is just one component of a broader toolkit for urban analysis. To explicitly identify urban centers, subcenters, and their spatial organization from remote sensing data, additional methods and data sources will be required. Here, urban centers and subcenters were defined as areas with high concentration of human activities as compared to surrounding areas. The difference between them is that urban centers are densely populated areas that serve as hubs for social, cultural and economic activities, whereas subcenters are smaller scale versions of the urban centers, designed to provide many of the same benefits as urban centers but on a more localized level. While urban centers are typically located in the central business district (CBD) of a city, characterized by high rise buildings, busy streets, and a diverse mix of people and businesses, subcenters are located outside of the CBD. Also, the research has demonstrated that it is possible to characterize the spatial organization of urban centers and subcenters with the objective of analyzing urban growth. Characterizing the spatial organization of urban centers and subcenters is a crucial aspect of urban planning and management. With this novel technology, practitioners can easily make preliminary studies of the evolution of urban areas to get an idea of where future growth is likely to happen at a cheaper and faster rate. It helps

in understanding the dynamics of urban growth, infrastructure needs, and the allocation of resources for sustainable development. These analyses are often performed by urban planners, geographers, and researchers to inform policy decisions and urban development strategies. This can be achieved through a combination of geographic information system (GIS) techniques, remote sensing data, and spatial analysis.

6.2 Recommendations

Further research is needed to explore the use of machine learning and artificial intelligence techniques to automate the identification and classification of urban centers and subcenters from remote sensing data. This could involve developing algorithms that can adapt to different urban contexts and improve accuracy. Also, additional case studies should be conducted in different urban areas to validate the methodology developed in this research. This will help assess the applicability of the combination of mathematical morphology and multi-radial fractal analysis in various urban contexts and geographic regions. Comparative studies should be conducted between developed and developing countries to assess the transferability of the methodology and to identify unique challenges and opportunities in different urbanization contexts. Also, interdisciplinary collaboration should be encouraged between urban planners, geographers, remote sensing experts, and data scientists. This can lead to a more comprehensive approach to urban analysis and help bridge the gap between research and practical applications. Open data initiatives and increased accessibility to high resolution remote sensing data should be advocated for in developing countries. Collaboration with local and international organizations to make such data available can facilitate further research in this field. These recommendations will help to build on the findings of the research and contribute to the advancement of urban planning and sustainable development practices, particularly in the context of developing nations.

Bibliography

[1] Sunitha Abburu and Suresh Babu Golla. Satellite image classification methods and techniques: A review. *International journal of computer applications*, 119(8), 2015.

[2] Austin Dziwornu Ablo, Freda Elikplim Asem, GA Yiran, and George Owusu. Urban sprawl, land use change and the changing rural agrarian livelihood in peri-urban accra, ghana. *Rural-urban linkages and sustainable development: Case studies from Africa*, 16:77–100, 2020.

[3] Maher M Aburas, Sabrina H Abdullah, Mohammad F Ramli, and Zulfa H As' shari. Landscape analysis of urban growth patterns in seremban, malaysia, using spatio-temporal data. In *IOP Conference Series: Earth and Environmental Science*, volume 37, page 012055. IOP Publishing, 2016.

[4] Maher Milad Aburas, Mohd Sanusi S Ahamad, and Najat Qader Omar. Spatio-temporal simulation and prediction of land-use change using conventional and machine learning models: A review. *Environmental monitoring and assessment*, 191:1–28, 2019.

[5] Maher Milad Aburas, Yuek Ming Ho, Mohammad Firuz Ramli, and Zulfa Hanan Ash'aari. Monitoring and assessment of urban growth patterns using spatio-temporal built-up area analysis. *Environmental Monitoring and Assessment*, 190:1–26, 2018.

[6] Radhakrishna Achanta, Appu Shaji, Kevin Smith, Aurelien Lucchi, Pascal Fua, and Sabine Süsstrunk. Slic superpixels compared to state-of-the-art superpixel methods. *IEEE transactions on pattern analysis and machine intelligence*, 34(11):2274–2282, 2012.

[7] Ransford A Acheampong. Accra: City scoping study. Technical report, African Cities Research Consortium, 2021.

[8] B Adam-Smith. High or low? the housing density conundrum. https://www.houseplanninghelp.co/housing-density-conundrum/, 2013. Accessed: 2021-08-10.

[9] Bright Addae and Natascha Oppelt. Land-use/land-cover change analysis and urban growth modelling in the greater accra metropolitan area (gama), ghana. *Urban Science*, 3(1):26, 2019.

[10] John EK Akubia, Abubakari Ahmed, and Antje Bruns. Assessing how land-cover change associated with urbanisation affects ecological sustainability in the greater accra metropolitan area, ghana. *Land*, 9(6):182, 2020.

[11] John EK Akubia and Antje Bruns. Unravelling the frontiers of urban growth: spatio-temporal dynamics of land-use change and urban expansion in greater accra metropolitan area, ghana. *Land*, 8(9):131, 2019.

[12] SM Alipour and Khaled Galal Ahmed. Assessing the effect of urban form on social sustainability: A proposed 'integrated measuring tools method'for urban neighborhoods in dubai. *City, Territory and Architecture*, 8(1):1–21, 2021.

[13] Anon. A study on land tenure in urban areas. Technical report, Water Aid, 2009.

[14] Anon. Supervised image classification techniques. https://www.ukessays.com/essays/engineering/supervised-image-classification-9746.php, 2018. Accessed: 2022-02-09.

[15] Anon. Ghana - greater accra metropolitan area sanitation and water project. https://www.worldbank.org/en/news/loans-credits/2020/09/22/ghana-greater-accra-metropolitan-area-sanitation-and-water-project, 2020. Accessed: 2023-04-08.

[16] Anon. Using the usgs landsat level-1 data product. https://www.usgs.gov/landsat-missions/using-usgs-landsat-level-1-data-product, 2021. Accessed: 2021-12-09.

[17] Anon. Sdg 11 - sustainable cities and communities. https://ec.europa.eu/eurostat/statistics-explained/index.php?title=SDG_11_-_Sustainable_cities_and_communities#:~:text=SDG%2011%20aims%20to%20renew,resource%20use%20and%20environmental%20impact., 2022. Accessed: 2023-03-08.

[18] Anon. Sekondi takoradi metropolitan assembly. https://stma.gov.gh/about-us, 2022. Accessed: 2022-08-13.

[19] Anon. Svm kernel functions – 'coz your svm knowledge is incomplete without it. https://www.ukessays.com/essays/engineering/supervised-image-classification-9746.php, 2022. Accessed: 2022-04-10.

[20] Anon. Ghana: Administrative division. https://www.citypopulation.de/, 2023. Accessed: 2023-04-04.

[21] K. A. Appeaning. Ghana's coastline, swallowed by the sea. https://en.unesco.org/courier/2021-1/ghanas-coastline-swallowed-sea#:~:text=With%20a%20coastline%20of%20550,particularly%20affected%20by%20coastal%20erosion., 2021. Accessed: 2023-04-04.

[22] ST Appiah, Albert Buabeng, and B Odoi. Comparative study of mathematical models for ghana's gold production. *Ghana Mining Journal*, 18(1):78–83, 2018.

[23] Anon b. *GIPC Quaterly Investment Report*. Ghana Investment Promotion Center, 2020.

[24] Susan Bannerman and Marvin Eng. *Spatial patterns and landscape ecology: implications for biodiversity*. Ministry of Forests, Research Program, 1997.

[25] Sana Basheer, Xiuquan Wang, Aitazaz A Farooque, Rana Ali Nawaz, Kai Liu, Toyin Adekanmbi, and Suqi Liu. Comparison of land use land cover classifiers using different satellite imagery and machine learning techniques. *Remote Sensing*, 14(19):4978, 2022.

[26] Michael Batty and Yichun Xie. Preliminary evidence for a theory of the fractal city. *Environment and Planning A*, 28(10):1745–1762, 1996.

[27] Mike Batty, Paul Longley, and Stewart Fotheringham. Urban growth and form: scaling, fractal geometry, and diffusion-limited aggregation. *Environment and planning A*, 21(11):1447–1472, 1989.

[28] Thomas Blaschke. The role of the spatial dimension within the framework of sustainable landscapes and natural capital. *Landscape and urban planning*, 75(3-4):198–226, 2006.

[29] Emmanuel Frimpong Boamah and Margath Walker. Legal pluralism, land tenure and the production of "nomotropic urban spaces" in post-colonial accra, ghana. In *Geography Research Forum*, volume 36, pages 86–109, 2016.

[30] O. Bonin, J. Baro, and J. Hubert. *Technological Innovation: Identification of Urban Structures on Regular Squared Grids with the Hhelp of Spatial Calculus*. IGU Urban Commission Annual Conference, 9th - 16th, University College Dublin, Ireland, August 2015.

[31] O. Bonin and P. Frankhauser. *Exploration Trans-échelles d'une Ville Nouvelle à l'Aide de l'Analyse*. Besançon, France: Treizièmes Rencontres de Théo Quant, 2017.

[32] Roger Brunet. La carte-modèle et les chorèmes. *Mappemonde*, 4(4):2–6, 1986.

[33] Martijn Burger and Evert Meijers. Form follows function? linking morphological and functional polycentricity. *Urban studies*, 49(5):1127–1149, 2012.

[34] Jixuan Cai, Bo Huang, and Yimeng Song. Using multi-source geospatial big data to identify the structure of polycentric cities. *Remote Sensing of Environment*, 202:210–221, 2017.

[35] Serhat Cengiz, Sevgi Görmüş, and Dicle Oğuz. Analysis of the urban growth pattern through spatial metrics; ankara city. *Land Use Policy*, 112:105812, 2022.

[36] Yan-Guang Chen. Logistic models of fractal dimension growth of urban morphology. *Fractals*, 26(03):1850033, 2018.

[37] Yanguang Chen. Logistic models of fractal dimension growth for spatio-temporal dynamics of urban morphology. *arXiv preprint arXiv:1606.03538*, 2016.

[38] Yanguang Chen. A study on the curves of scaling behavior of fractal cities. *arXiv preprint arXiv:2112.14032*, 2021.

[39] Yanguang Chen, Jiejing Wang, and Jian Feng. Understanding the fractal dimensions of urban forms through spatial entropy. *Entropy*, 19(11):600, 2017.

[40] Ibtissem Cherni, Seifallah Ouertani, Sami Faiz, Sylvie Servigne, and Robert Laurini. Chorems: A new tool for territorial intelligence. In *29th Urban Data Management Symposium*, pages 67–76, 2013.

[41] Edgar Cooke, Sarah Hague, and Andy McKay. The ghana poverty and inequality report: Using the 6th ghana living standards survey. *University of Sussex*, pages 1–43, 2016.

[42] E Danso and M Barry. Land tenure administration in peri-urban accra: A case study of bortianor. *Customary and Group Land Rights*, pages 1–20, 2012.

[43] George Bernard Dantzig and Thomas L Saaty. *Compact city: a plan for a liveable urban environment*. W. H. Freeman, 1973.

[44] Vincenzo Del Fatto. *Visual summaries of geographic databases by chorems*. PhD thesis, University of Salerno, Italy; INSA of Lyon, France, 2009.

[45] Sakshi Dhingra and Dharminder Kumar. A review of remotely sensed satellite image classification. *International Journal of Electrical and Computer Engineering*, 9(3):1720, 2019.

[46] Jianquan Dong, Hong Jiang, Tianwei Gu, Yanxu Liu, and Jian Peng. Sustainable landscape pattern: a landscape approach to serving spatial planning. *Landscape Ecology*, pages 1–12, 2022.

[47] Gilles Duranton and Diego Puga. The economics of urban density. *Journal of economic perspectives*, 34(3):3–26, 2020.

[48] Alexander Eduful and Michael Hooper. Urban impacts of resource booms: The emergence of oil-led gentrification in sekondi-takoradi, ghana. In *Urban Forum*, volume 26, pages 283–302. Springer, 2015.

[49] Alexander K Eduful and Michael Hooper. Urban migration and housing during resource booms: The case of sekondi-takoradi, ghana. *Habitat International*, 93:102029, 2019.

[50] JI Ellis, MR Clark, HL Rouse, and Geoffroy Lamarche. Environmental management frameworks for offshore mining: the new zealand approach. *Marine Policy*, 84:178–192, 2017.

[51] Sara Encarnação, Marcos Gaudiano, Francisco C Santos, José A Tenedório, and Jorge M Pacheco. Fractal cartography of urban areas. *Scientific Reports*, 2(1):527, 2012.

[52] Kyle Farrell. An inquiry into the nature and causes of nigeria's rapid urban transition. In *Urban Forum*, volume 29, pages 277–298. Springer, 2018.

[53] Kyle Farrell and Hans Westlund. China's rapid urban ascent: An examination into the components of urban growth. *Asian Geographer*, 35(1):85–106, 2018.

[54] Raphael Edem Fiave. Sekondi-takoradi as an oil city. In *Geography Research Forum*, volume 37, pages 61–79, 2017.

[55] Bryon Flowers, Kuo-Tsang Huang, and Gerardo O Aldana. Analysis of the habitat fragmentation of ecosystems in belize using landscape metrics. *Sustainability*, 12(7):3024, 2020.

[56] Pierre Frankhauser. The fractal approach. a new tool for the spatial analysis of urban agglomerations. *Population: an english selection*, pages 205–240, 1998.

[57] Pierre Frankhauser. The fractalopolis model-a sustainable approach for a central place system. *HAL*, 2012.

[58] Pierre Frankhauser. From fractal urban pattern analysis to fractal urban planning concepts. *Computational approaches for urban environments*, pages 13–48, 2015.

[59] Pierre Frankhauser et al. Fractal geometry of urban patterns and their morphogenesis. *Discrete dynamics in nature and society*, 2:127–145, 1998.

[60] Bernard Fosu Frimpong and Frank Molkenthin. Tracking urban expansion using random forests for the classification of landsat imagery (1986–2015) and predicting urban/built-up areas for 2025: A study of the kumasi metropolis, ghana. *Land*, 10(1):44, 2021.

[61] Eric Gaisie, Hyung Min Kim, and Sun Sheng Han. Accra towards a city-region: Devolution, spatial development and urban challenges. *Cities*, 95:102398, 2019.

[62] Qingke Gao, Jianhong Fu, Yang Yu, and Xuehua Tang. Identification of urban regions' functions in chengdu, china, based on vehicle trajectory data. *PloS one*, 14(4):e0215656, 2019.

[63] Alief Bani Ghazi, Helmia Adita Fitra, and Citra Persada. Identification of changes in the morphological space structure of bandar lampung city using overlay geographic information system analysis. In *IOP Conference Series: Earth and Environmental Science*, volume 739, page 012092. IOP Publishing, 2021.

[64] Jean-Jacques Girardot and Evelyne Brunau. Territorial intelligence and innovation for the socio-ecological transition. In *9th International conference of territorial intelligence, ENTI*, 2010.

[65] Ercan Gökyer. Understanding landscape structure using landscape metrics. In *Advances in landscape architecture*. IntechOpen, 2013.

[66] Katherine V Gough and Paul WK Yankson. Land markets in african cities: the case of peri-urban accra, ghana. *Urban studies*, 37(13):2485–2500, 2000.

[67] Richard Grant and Paul Yankson. Accra. *Cities*, 20(1):65–74, 2003.

[68] Christina D Hargis, John A Bissonette, and John L David. The behavior of landscape metrics commonly used in the study of habitat fragmentation. *Landscape ecology*, 13:167–186, 1998.

[69] Martin Herold, Noah C Goldstein, and Keith C Clarke. The spatiotemporal form of urban growth: measurement, analysis and modeling. *Remote sensing of Environment*, 86(3):286–302, 2003.

[70] Tin Kam Ho. Random decision forests. In *Proceedings of 3rd international conference on document analysis and recognition*, volume 1, pages 278–282. IEEE, 1995.

[71] Aigerim Ilyassova, Lakshmi N Kantakumar, and Doreen Boyd. Urban growth analysis and simulations using cellular automata and geo-informatics: comparison between almaty and astana in kazakhstan. *Geocarto International*, 36(5):520–539, 2021.

[72] Jochen AG Jaeger, Tomás Soukup, Christian Schwick, Luis F Madriñán, and Felix Kienast. Landscape fragmentation in europe. *European landscape dynamics–CORINE land cover data*, pages 157–198, 2011.

[73] Fatemeh Jahanmiri and Dawn Cassandra Parker. An overview of fractal geometry applied to urban planning. *Land*, 11(4):475, 2022.

[74] Rajeev Kumar Jaiswal, Rajesh Saxena, and Saumitra Mukherjee. Application of remote sensing technology for land use/land cover change analysis. *Journal of the Indian Society of Remote Sensing*, 27:123–128, 1999.

[75] Michael P Johnson. Environmental impacts of urban sprawl: a survey of the literature and proposed research agenda. *Environment and planning A*, 33(4):717–735, 2001.

[76] Nada Kadhim, Monjur Mourshed, and Michaela Bray. Advances in remote sensing applications for urban sustainability. *Euro-Mediterranean Journal for Environmental Integration*, 1(1):7, 2016.

[77] Andrea Kaim, Anna F Cord, and Martin Volk. A review of multi-criteria optimization techniques for agricultural land use allocation. *Environmental Modelling & Software*, 105:79–93, 2018.

[78] Robert C Kloosterman and Sako Musterd. The polycentric urban region: towards a research agenda. *Urban studies*, 38(4):623–633, 2001.

[79] Liang Kong, Zhengwei He, Zhongsheng Chen, Mingliang Luo, Zhong Du, Fuquan Zhu, and Li He. Spatial distribution and morphological identification of regional urban settlements based on road intersections. *ISPRS International Journal of Geo-Information*, 10(4):201, 2021.

[80] Prosper Issahaku Korah, Tony Matthews, and Natalie Osborne. Assembling accra through new city imaginary: Land ownership, agency, and relational complexity. *Habitat international*, 106:102277, 2020.

[81] Prosper Issahaku Korah, Tony Matthews, and Deanna Tomerini. Characterising spatial and temporal patterns of urban evolution in sub-saharan africa: The case of accra, ghana. *Land Use Policy*, 87:104049, 2019.

[82] Daniel Kpienbaareh and Isaac Luginaah. Modeling the internal structure, dynamics and trends of urban sprawl in ghanaian cities using remote sensing, spatial metrics and spatial analysis. *African Geographical Review*, 39(3):189–207, 2020.

[83] Angelika Krehl and Stefan Siedentop. Towards a typology of urban centers and subcenters–evidence from german city regions. *Urban Geography*, 40(1):58–82, 2019.

[84] B Kumi-Baoteng, Eric Stemn, and A Agyapong. Effect of urban growth on urban thermal environment: a case study of sekondi-takoradi metropolis of ghana. *Journal of environment and earth science*, 5(2):32–41, 2015.

[85] Przemysław Kupidura. The comparison of different methods of texture analysis for their efficacy for land use classification in satellite imagery. *Remote Sensing*, 11(10):1233, 2019.

[86] Apostolos Lagarias. Fractal analysis of the urbanization at the outskirts of the city: models, measurement and explanation. *Cybergeo: European Journal of Geography*, 2007.

[87] Scott LaPoint, Niko Balkenhol, James Hale, Jonathan Sadler, and Rodney van der Ree. Ecological connectivity research in urban areas. *Functional Ecology*, 29(7):868–878, 2015.

[88] Juan Li, Ying Long, and Anrong Dang. Live-work-play centers of chinese cities: Identification and temporal evolution with emerging data. *Computers, Environment and Urban Systems*, 71:58–66, 2018.

[89] Dong Lin, Andrew Allan, and Jianqiang Cui. Sub-centres, socio-economic characteristics and commuting: A case study and its implications. *International Journal of Urban Sciences*, 21(2):147–171, 2017.

[90] Desheng Liu and Fan Xia. Assessing object-based classification: advantages and limitations. *Remote sensing letters*, 1(4):187–194, 2010.

[91] Xudong Liu, Yongzhong Tian, Xueqian Zhang, and Zuyi Wan. Identification of urban functional regions in chengdu based on taxi trajectory time series data. *ISPRS International Journal of Geo-Information*, 9(3):158, 2020.

[92] Yan Liu. *Modelling urban development with geographical information systems and cellular automata*. Crc Press, 2008.

[93] Zhen Liu and Shenghe Liu. Polycentric development and the role of urban polycentric planning in china's mega cities: An examination of beijing's metropolitan area. *Sustainability*, 10(5):1588, 2018.

[94] Ying Long, Yimeng Song, and Long Chen. Identifying subcenters with a nonparametric method and ubiquitous point-of-interest data: A case study of 284 chinese cities. *Environment and Planning B: Urban Analytics and City Science*, 49(1):58–75, 2022.

[95] Ge Lou, Qiuxiao Chen, Kang He, Yue Zhou, and Zhou Shi. Using nighttime light data and poi big data to detect the urban centers of hangzhou. *Remote Sensing*, 11(15):1821, 2019.

[96] J. Lumumba. Land in accra: A clash between tradition and the modern city. https://www.urbanafrica.net/news/land-in-accra-a-clash-between-tradition-and-the-modern-city/, 2015. Accessed: 2015-07-30.

[97] Lei Ma, Manchun Li, Xiaoxue Ma, Liang Cheng, Peijun Du, and Yongxue Liu. A review of supervised object-based land-cover image classification. *ISPRS Journal of Photogrammetry and Remote Sensing*, 130:277–293, 2017.

[98] Nur Anis Mahmon, Norsuzila Ya'acob, and Azita Laily Yusof. Differences of image classification techniques for land use and land cover classification. In *2015 IEEE 11th International Colloquium on Signal Processing & Its Applications (CSPA)*, pages 90–94. IEEE, 2015.

[99] Ramandeep Kaur M Malhi, Akash Anand, Prashant K Srivastava, G Sandhya Kiran, George P. Petropoulos, and Christos Chalkias. An integrated spatiotemporal pattern analysis model to assess and predict the degradation of protected forest areas. *ISPRS International Journal of Geo-Information*, 9(9):530, 2020.

[100] Xiaoming Man and Yanguang Chen. Fractal-based modeling and spatial analysis of urban form and growth: A case study of shenzhen in china. *ISPRS International Journal of Geo-Information*, 9(11):672, 2020.

[101] Francesca Mariani, Ilaria Zambon, and Luca Salvati. Population matters: Identifying metropolitan sub-centers from diachronic density-distance curves, 1960–2010. *Sustainability*, 10(12):4653, 2018.

[102] Michael A McAdams. Applying gis and fractal analysis to the study of the urban morpholgy in istanbul. GEOMED, 2007.

[103] Michael A McAdams. The application of fractal analysis and spatial technologies for urban analysis. *Journal of Applied Functional Analysis*, 4(4):569–579, 2009.

[104] Robert I McDonald, Andressa V Mansur, Fernando Ascensão, M'lisa Colbert, Katie Crossman, Thomas Elmqvist, Andrew Gonzalez, Burak Güneralp, Dagmar Haase, Maike Hamann, et al. Research gaps in knowledge of the impact of urban growth on biodiversity. *Nature Sustainability*, 3(1):16–24, 2020.

[105] Kevin McGarigal. Fragstats help. *University of Massachusetts: Amherst, MA, USA*, 182, 2015.

[106] Daniel P McMillen. Nonparametric employment subcenter identification. *Journal of Urban economics*, 50(3):448–473, 2001.

[107] Theodora Mantebea Mends and Johan De Meijere. A study of the institution of the customary land tenure system in the supply of property rights for urban

development-an example of accra, ghana. In *5th FIG Regional Conference on Promoting Land Administration and Good Governance. Accra, Ghana (FIG)*, volume 14, 2006.

[108] John Victor Mensah, Erika Mamley Osae, and Asare Kofi Yeboah. Emergence of squatter settlements in the greater accra metropolitan area in ghana: An issue of state failure or survival? *Cell*, 233:245626060, 2021.

[109] Lasse Møller-Jensen, Albert N Allotey, Richard Y Kofie, and Paul WK Yankson. A comparison of satellite-based estimates of urban agglomeration size for the accra area. *ISPRS International Journal of Geo-Information*, 9(2):79, 2020.

[110] Sulaiman Ibrahim Musa, Mazlan Hashim, and Mohd Nadzri Md Reba. A review of geospatial-based urban growth models and modelling initiatives. *Geocarto International*, 32(8):813–833, 2017.

[111] Laurent Najman and Hugues Talbot. *Mathematical morphology: from theory to applications*. John Wiley & Sons, 2013.

[112] O. P. Nduzi. Accra to become economic powerhouse - structural plan report. https://gna.org.gh/2023/02/accra-to-become-economic-powerhouse/, 2023. Accessed: 2023-04-08.

[113] Duong H Nong, Christopher A Lepczyk, Tomoaki Miura, and Jefferson M Fox. Quantifying urban growth patterns in hanoi using landscape expansion modes and time series spatial metrics. *PloS one*, 13(5):e0196940, 2018.

[114] Franklin Obeng-Odoom. *Oiling the urban economy: Land, labour, capital, and the state in Sekondi-Takoradi, Ghana*. Routledge, 2014.

[115] Charles Yaw Oduro, Ronald Adamtey, and Kafui Ocloo. Urban growth and livelihood transformations on the fringes of african cities: A case study of changing livelihoods in peri-urban accra. *Environment and Natural Resources Research*, 5(2):81, 2015.

[116] Abass Olaode, Golshah Naghdy, and Catherine Todd. Unsupervised classification of images: a review. *International Journal of Image Processing*, 8(5):325–342, 2014.

[117] Travis. E. Oliphant. Scipy titorial. 2004.

[118] Frimpong Emmanuel Osei, Bolarinwa Olutayo Balogun, and Comfort Gyasiwaa Afrifa. Identifying and quantifying urban sprawl in the greater accra region of

ghana from 1985 to 2014. *International Journal of Science and Research (IJSR)*, 4(1), 2015.

[119] George Owusu. Coping with urban sprawl: A critical discussion of the urban containment strategy in a developing country city, accra. *Planum: The Journal of Urbanism*, 26(1):1–17, 2013.

[120] Joan Perez, Giovanni Fusco, and François Moriconi-Ebrard. Identification and quantification of urban space in india: Defining urban macro-structures. *Urban Studies*, 56(10):1988–2004, 2019.

[121] Lien Poelmans and Anton Van Rompaey. Complexity and performance of urban expansion models. *Computers, Environment and Urban Systems*, 34(1):17–27, 2010.

[122] R. Rafiee, S. A. Malhuny, N. Khorasanoi, A. A. Darvishefat, and A. Danekar. Simulating urban growth in mashad city, iran, through the sleuth model(ugm). *Cities*, 26(1):19–26, 2009.

[123] Camille Roth, Soong Moon Kang, Michael Batty, and Marc Barthélemy. Structure of urban movements: polycentric activity and entangled hierarchical flows. *PloS one*, 6(1):e15923, 2011.

[124] E. Russano. Support vector machines (svms): Definitions & applications. https://study.com/academy/lesson/support-vector-machines-smvs-definitions-applications.html, 2019. Accessed: 2022-02-24.

[125] Mehebub Sahana, Haoyuan Hong, and Haroon Sajjad. Analyzing urban spatial patterns and trend of urban growth using urban sprawl matrix: A study on kolkata urban agglomeration, india. *Science of the Total Environment*, 628:1557–1566, 2018.

[126] K. Sanghvi. Image classification techniques. https://medium.com/analytics-vidhya/image-classification-techniques-83fd87011cac, 2020. Accessed: 2022-05-08.

[127] Rocco Scolozzi and Davide Geneletti. A multi-scale qualitative approach to assess the impact of urbanization on natural habitats and their connectivity. *Environmental Impact Assessment Review*, 36:9–22, 2012.

[128] Vivek Shandas, Yasuyo Makido, and Salim Ferwati. Rapid urban growth and land use patterns in doha, qatar: Opportunities for sustainability. *European Journal of Sustainable Development Research*, 2017.

[129] Yang Shao and Ross S Lunetta. Comparison of support vector machine, neural network, and cart algorithms for the land-cover classification using limited training data points. *ISPRS Journal of Photogrammetry and Remote Sensing*, 70:78–87, 2012.

[130] Guoqiang Shen. Fractal dimension and fractal growth of urbanized areas. *International Journal of Geographical Information Science*, 16(5):419–437, 2002.

[131] PC Smits, SG Dellepiane, and RA Schowengerdt. Quality assessment of image classification algorithms for land-cover mapping: a review and a proposal for a cost-based approach. *International journal of remote sensing*, 20(8):1461–1486, 1999.

[132] Terry Sohl and Benjamin Sleeter. Role of remote sensing for land-use and land-cover change modeling. *Remote Sensing of Land Use and Land Cover*, page 225, 2012.

[133] Pierre Soille and Martino Pesaresi. Advances in mathematical morphology applied to geoscience and remote sensing. *IEEE Transactions on Geoscience and Remote Sensing*, 40(9):2042–2055, 2002.

[134] Cécile Tannier, Gilles Vuidel, Hélène Houot, and Pierre Frankhauser. Spatial accessibility to amenities in fractal and nonfractal urban patterns. *Environment and Planning B: Planning and Design*, 39(5):801–819, 2012.

[135] Hannes Taubenböck, Ines Standfuß, Michael Wurm, Angelika Krehl, and Stefan Siedentop. Measuring morphological polycentricity-a comparative analysis of urban mass concentrations using remote sensing data. *Computers, Environment and Urban Systems*, 64:42–56, 2017.

[136] Phan Thanh Noi and Martin Kappas. Comparison of random forest, k-nearest neighbor, and support vector machine classifiers for land cover classification using sentinel-2 imagery. *Sensors*, 18(1):18, 2017.

[137] Kevin G Thurman. Land use regulations and urban planning initiatives in accra, ghana. *PLAN A6211*, 1, 2010.

[138] Neda Bihamta Toosi, Ali Reza Soffianian, Sima Fakheran, Saeid Pourmanafi, Christian Ginzler, and Lars T Waser. Comparing different classification algorithms for

monitoring mangrove cover changes in southern iran. *Global Ecology and Conservation*, 19:e00662, 2019.

[139] Monica G Turner and Robert H Gardner. *Landscape Ecology in Theory and Practice: Pattern and Process (2nd ed.)*, volume 482. Springer, 2015.

[140] Humboldt State University. Gsp 216 introduction to remote sensing. http://gsp.humboldt.edu/olm/Courses/GSP_216/lessons/accuracy/metrics.html, 2022. Accessed: 2022-08-13.

[141] Kati Volgmann and Angelika Münter. Understanding metropolitan growth in german polycentric urban regions. *Regional Studies*, 56(1):99–112, 2022.

[142] Gilles Vuidel and Cécile Tannier. Fractalyse 3.0 user manual, 2022.

[143] Chengdong Wang, Yutao Wang, Renqing Wang, and Peiming Zheng. Modeling and evaluating land-use/land-cover change for urban planning and sustainability: A case study of dongying city, china. *Journal of Cleaner Production*, 172:1529–1534, 2018.

[144] Tianyu Wang, Wenze Yue, Xinyue Ye, Yong Liu, and Debin Lu. Re-evaluating polycentric urban structure: A functional linkage perspective. *Cities*, 101:102672, 2020.

[145] Lai Wei, Yun Luo, Miao Wang, Yuyang Cai, Shiliang Su, Bozhao Li, and Hangyu Ji. Multiscale identification of urban functional polycentricity for planning implications: An integrated approach using geo-big transport data and complex network modeling. *Habitat International*, 97:102134, 2020.

[146] Tianren Yang, Ying Jin, Longxu Yan, and Pei Pei. Aspirations and realities of polycentric development: Insights from multi-source data into the emerging urban form of shanghai. *Environment and Planning B: Urban Analytics and City Science*, 46(7):1264–1280, 2019.

[147] Tianren Yang, Haozhi Pan, Geoffrey Hewings, and Ying Jin. Understanding urban sub-centers with heterogeneity in agglomeration economies—where do emerging commercial establishments locate? *Cities*, 86:25–36, 2019.

[148] Yuanyuan Yang, Yansui Liu, Yurui Li, and Guoming Du. Quantifying spatio-temporal patterns of urban expansion in beijing during 1985–2013 with rural-urban development transformation. *Land use policy*, 74:220–230, 2018.

[149] Paul William Kojo Yankson and Katherine Venton Gough. The environmental impact of rapid urbanization in the peri-urban area of accra, ghana. *Geografisk Tidsskrift-Danish Journal of Geography*, 99(1):89–100, 1999.

[150] Paul WK Yankson, Katherine V Gough, James Esson, and Ebenezer F Amankwaa. Spatial and social transformations in a secondary city: the role of mobility in sekondi-takoradi, ghana. *Geografisk Tidsskrift-Danish Journal of Geography*, 117(2):82–92, 2017.

[151] Gerald Albert Baeribameng Yiran, Austin Dziwornu Ablo, and Freda Elikplim Asem. Urbanisation and domestic energy trends: Analysis of household energy consumption patterns in relation to land-use change in peri-urban accra, ghana. *Land Use Policy*, 99:105047, 2020.

[152] T. Yiu. Understanding random forest - how the algorithm works and why it is so effective. https://towardsdatascience.com/understanding-random-forest-58381e0602d2, 2019. Accessed: 2022-03-10.

[153] Nicholas E Young, Ryan S Anderson, Stephen M Chignell, Anthony G Vorster, Rick Lawrence, and Paul H Evangelista. A survival guide to landsat preprocessing. *Ecology*, 98(4):920–932, 2017.

[154] Lu Yu, Wei Zheng, Tao Yu, and Yongxiang Wu. How to identify urban centers/subcenters in metropolises? an analytical review. *Habitat International*, 115:102397, 2021.

[155] Yang Zhou. Urban growth model in netlogo. https://www.gisagents.org/2015/09/urban-growth-model-in-netlogo.html, 2015. Accessed: 2024-02-25.

Appendix A

Population of GAMA, 2010 and 2021

A.1 Population of GAMA, 2010 and 2021

Municipality	Population 2010	Population 2021
Ga South	234 191	350 121
Ga West	205 351	549 591
Sowutuom	117 220	332 232
AMA	1 665 086	1 281 570
La Dadekotopon	183 528	140 264
Ga East	147 742	283 379
Madina	111 926	244 676
Adenta	78 215	237 546
LEKMA	125 873	217 304
Ashiaman	190 972	208 060
TMA	292 773	374 148
Kpone Katamanso	109 864	417 334

Appendix B

Python Scripts for Image Classification

B.1 Image Classification Script - RF

```
# write classified image as a tiff file
def createGeotiff(outRaster, data, geo_transform, projection):
    # Create a GeoTIFF file with the given data
    driver = gdal.GetDriverByName('GTiff')
    rows, cols = data.shape
    rasterDS = driver.Create(outRaster, cols, rows, 1, gdal.GDT_Int32)
    rasterDS.SetGeoTransform(geo_transform)
    rasterDS.SetProjection(projection)
    band = rasterDS.GetRasterBand(1)
    band.WriteArray(data)
    rasterDS = None

# Display map
def color_image_show(img, title):
    fig = plt.figure(figsize=(15,15))
    fig.set_facecolor('white')
    plt.imshow(img)
    plt.title(title)
    plt.show()
```

```
import numpy as np
import gdal
import pandas as pd
import geopandas as gpd
import matplotlib.pyplot as plt
from sklearn.ensemble import RandomForestClassifier
from sklearn.metrics import classification_report
from sklearn.metrics import confusion_matrix
from sklearn.metrics import cohen_kappa_score
import joblib

# define input raster and output raster path
inpRaster = 'Images/2013_cmpst_filledc.tif'
outRaster = 'Classified/RF_GAMA_2013.tif'

# Read Raster Data
ds = gdal.Open(inpRaster)

# Retrieve raster attributes
rows = ds.RasterYSize
cols = ds.RasterXSize
bands = ds.RasterCount
gt = ds.GetGeoTransform()
proj = ds.GetProjection()

# Read Raster as Array
array = ds.ReadAsArray() #(bands, rows, cols)

#modify structure by stacking bands to dorm one element
array = np.stack(array,axis=2) #(rows, cols, bands)
# reshape to a 2d array so that it can match with the training data
array = np.reshape(array, [rows*cols,bands])
```

```
# convert array to dataframe to keep both test and training
# data in the same structure

array_df = pd.DataFrame(array, dtype='int16')

# Read  training data
gdf = gpd.read_file("ground_truth/2013_truth.shp")
class_names = gdf['Label'].unique() # get class names
print ("class names", class_names)
class_ids = np.arange(class_names.size)+1 # assign ids to class names
print('class ids', class_ids)

#create a dataframe of the class names and class ids
#df.to_csv("GAMA_2020 data/class_lookup.csv")
# save dataframe as csv for future reference

df = pd.DataFrame({'Label': class_names, 'id': class_ids})
print('gdf without ids', gdf.head())

#add class ids to the shapefile
gdf['class_id'] = gdf['Label'].map(dict(zip(class_names, class_ids)))
print('gdf with ids', gdf.head())

# divide truth data data into test and train data
gdf_train = gdf.sample(frac=0.7)
gdf_test = gdf.drop(gdf_train.index)
print('gdf shape', gdf.shape, 'training shape',
    gdf_train.shape, 'test', gdf_test.shape)
gdf_train.to_file("ground_truth/GAMA_2013_train.shp")
gdf_test.to_file("ground_truth/GAMA_2013_test.shp")



#enter features to used for training according
```

```
#how they are named in the columns of training data

data = gdf_train[['b1_GAMA_13', 'b2_GAMA_13', 'b3_GAMA_13',
                  'b4_GAMA_13', 'b5_GAMA_13','b6_GAMA_13',
                   'b7_GAMA_13', 'b8_GAMA_13', 'b9_GAMA_13']]
#enter training label according to your csv column name
label = gdf_train['class_id']


data_test = gdf_test[['b1_GAMA_13', 'b2_GAMA_13', 'b3_GAMA_13',
             'b4_GAMA_13', 'b5_GAMA_13', 'b6_GAMA_13', 'b7_GAMA_13',
              'b8_GAMA_13', 'b9_GAMA_13']]

label_test = gdf_test['class_id']



####no need to modify the code below###
########################################


#set classifier parameters and train classifier
clf = RandomForestClassifier(n_jobs=-1)
clf.fit(data,label)

#predict classes
y_pred = clf.predict(array_df)

#reshape predicted classes into a 2d array
classification = y_pred.reshape((rows,cols))

#export classified image
createGeotiff(outRaster,classification,gt,proj)
```

```
#Accuracy assessment
#check performance of classifier on test data

clf.score(data_test,label_test)

#check performance of classifier on train data
clf.score(data,label)
# classification report
x_pred= clf.predict(data_test)
print(classification_report(label_test, x_pred,
         target_names=class_names))

#confusion matrix
cm = confusion_matrix(label_test, x_pred)
pd.DataFrame(cm, index=class_names, columns=class_names)

kappa= cohen_kappa_score(label_test, x_pred)
kappa

#joblib.dump(clf, "RF_GAMA_13")

#mj = joblib.load("C:/Users/kbons/Desktop/Classification Scripts/RF_GAMA_13")
```

B.2 Image Classification Script - SVM

```
# write classified image as a tiff file
def createGeotiff(outRaster, data, geo_transform, projection):
    # Create a GeoTIFF file with the given data
    driver = gdal.GetDriverByName('GTiff')
    rows, cols = data.shape
    rasterDS = driver.Create(outRaster, cols, rows, 1, gdal.GDT_Int32)
    rasterDS.SetGeoTransform(geo_transform)
    rasterDS.SetProjection(projection)
```

```
    band = rasterDS.GetRasterBand(1)
    band.WriteArray(data)
    rasterDS = None

# Display map
def color_image_show(img, title):
    fig = plt.figure(figsize=(15,15))
    fig.set_facecolor('white')
    plt.imshow(img)
    plt.title(title)
    plt.show()



# import necessary libraries
import numpy as np
import gdal
import pandas as pd
import geopandas as gpd
import matplotlib.pyplot as plt
from sklearn.svm import SVC
from sklearn.metrics import classification_report
from sklearn.metrics import confusion_matrix
from sklearn.metrics import cohen_kappa_score
import joblib

# define input raster and output raster path
inpRaster = 'Images/2013_cmpst_filledc.tif'
outRaster = 'Classified/SVM_GAMA_2013.tif'

# Read Raster Data
ds = gdal.Open(inpRaster)

# Retrieve raster attributes
rows = ds.RasterYSize
```

```
cols = ds.RasterXSize
bands = ds.RasterCount
gt = ds.GetGeoTransform()
proj = ds.GetProjection()

# Read Raster as Array
array = ds.ReadAsArray() #(bands, rows, cols)

#modify structure by stacking bands to dorm one element
array = np.stack(array,axis=2) #(rows, cols, bands)
# reshape to a 2d array so that it can match with the training data
array = np.reshape(array, [rows*cols,bands])

# convert array to dataframe to keep both test and training
# data in the same structure

array_df = pd.DataFrame(array, dtype='int16')

# Read  training data
gdf = gpd.read_file("ground_truth/2013_truth.shp")
class_names = gdf['Label'].unique() # get class names
print ("class names", class_names)
class_ids = np.arange(class_names.size)+1 # assign ids to class names
print('class ids', class_ids)

#create a dataframe of the class names and class ids
#df.to_csv("GAMA_2020 data/class_lookup.csv")
# save dataframe as csv for future reference

df = pd.DataFrame({'Label': class_names, 'id': class_ids})
print('gdf without ids', gdf.head())

#add class ids to the shapefile
gdf['class_id'] = gdf['Label'].map(dict(zip(class_names, class_ids)))
```

```
print('gdf with ids', gdf.head())

# divide truth data data into test and train data
gdf_train = gdf.sample(frac=0.7)
gdf_test = gdf.drop(gdf_train.index)
print('gdf shape', gdf.shape, 'training shape',
    gdf_train.shape, 'test', gdf_test.shape)
gdf_train.to_file("ground_truth/GAMA_2013_train.shp")
gdf_test.to_file("ground_truth/GAMA_2013_test.shp")



#enter features to used for training according
#how they are named in the columns of training data

data = gdf_train[['b1_GAMA_13', 'b2_GAMA_13', 'b3_GAMA_13',
                 'b4_GAMA_13', 'b5_GAMA_13','b6_GAMA_13',
                  'b7_GAMA_13', 'b8_GAMA_13', 'b9_GAMA_13']]
#enter training label according to your csv column name
label = gdf_train['class_id']


data_test = gdf_test[['b1_GAMA_13', 'b2_GAMA_13', 'b3_GAMA_13',
            'b4_GAMA_13', 'b5_GAMA_13', 'b6_GAMA_13', 'b7_GAMA_13',
             'b8_GAMA_13', 'b9_GAMA_13']]

label_test = gdf_test['class_id']



####no need to modify the code below###
########################################

#set classifier parameters and train classifier
```

```
#set classifier parameters and train classifier
clf = SVC(kernel = 'linear')
clf.fit(data,label)
#predict class
y_pred = clf.predict(array_df)

#reshape predicted classes into a 2d array
classification = y_pred.reshape((rows,cols))

# display image
color_image_show(classification, 'GAMA Support Vector Machine 2022')

#export classified image
createGeotiff(outRaster,classification,gt,proj)

#Accuracy assessment
#check performance of classifier on test data
clf.score(data_test,label_test)

#check performance of classifier on train data
clf.score(data,label)
# classification report
x_pred= clf.predict(data_test)
print(classification_report(label_test, x_pred, target_names=class_names))

#confusion matrix
cm = confusion_matrix(label_test, x_pred)
pd.DataFrame(cm, index=class_names, columns=class_names)

kappa= cohen_kappa_score(label_test, x_pred)
kappa

#joblib.dump(clf, "SVM_GAMA_13")
```

```
#mj = joblib.load("C:/Users/kbons/Desktop/Classification Scripts/SVM_GAMA_13")
```

B.3 Image Classification Script - SLIC K-Means

```
    def color_image_show(img, title):
    fig = plt.figure(figsize=(15,15))
    fig.set_facecolor('white')
    plt.imshow(img)
    plt.title(title)
    plt.show()

import gdal
import numpy as np
import matplotlib.pyplot as plt

img = gdal.Open('C:/Users/kbons/Desktop/Anibere/2020/Corrections/2020_cmpst_ps.tif')
driverTiff = gdal.GetDriverByName("Gtiff")
rows = img.RasterYSize
cols = img.RasterXSize
gt = img.GetGeoTransform()
proj = img.GetProjection()
n = img.RasterCount

import numpy as np
B1m = img.GetRasterBand(4).ReadAsArray()
B2m = img.GetRasterBand(3).ReadAsArray()
B3m = img.GetRasterBand(2).ReadAsArray()

import numpy.ma as ma
B1 = ma.masked_less_equal(B1m,0)
B2 = ma.masked_less_equal(B2m,0)
B3 = ma.masked_less_equal(B3m,0)
```

```
B1 = B1/B1.max()
B2 = B2/B2.max()
B3 = B3/B3.max()

img432 = np.dstack((B1,B2,B3))
color_image_show(img432, "RGB")

from skimage import exposure
fig= plt.figure(figsize= (15,15))
fig.set_facecolor('white')

for color, channel in zip('rgb', np.rollaxis(img432, axis = -1)):
    counts, centers = exposure.histogram(channel)
    plt.plot(centers[1::], counts[1::], color=color)
plt.show()

RGB_ha_m = np.empty(img432.shape,dtype="float32")
lims =[(0.37,0.47),(0.15,0.24),(0.11,0.19)]
for lim, channel in zip(lims, range(3)):
    RGB_ha_m[:, :, channel] = exposure.rescale_intensity(img432[:, :,
                                                    channel], lim)
color_image_show(RGB_ha_m, "RGB Stretched")

RGB_ha_m[:,:,0] = exposure.adjust_gamma(RGB_ha_m[:,:,0], 0.82)
RGB_ha_m[:,:,1] = exposure.adjust_gamma(RGB_ha_m[:,:,1], 0.87)
RGB_ha_m[:,:,2] = exposure.adjust_gamma(RGB_ha_m[:,:,2], 0.92)
RGB_ha = ma.masked_less_equal(RGB_ha_m,0)
color_image_show(RGB_ha, "Stretched RGB gamma adjusted")

from skimage.color import rgb2gray
RGB_graym = rgb2gray(RGB_ha)
plt.figure(figsize=(15,15))
plt.imshow(RGB_graym)
```

```
RGB_gray = RGB_graym
RGB_gray = ma.masked_less_equal(RGB_gray, 0) #mask
plt.figure(figsize=(15,15))
plt.imshow(RGB_gray)

import time
from skimage.segmentation import slic
segments_f = slic(RGB_gray, n_segments= 50000, mask=B1)
start = time.time()
print("it took", ((time.time()-start)), "seconds for segmentation")

from skimage import color
plt.figure(figsize=(15,15))
plt.imshow(color.label2rgb(segments_f, RGB_ha, kind='avg'))
print("it took", ((time.time()-start)/60), "mins for segmentation/plotting")

from skimage import measure
regions = measure.regionprops(segments_f, intensity_image=RGB_gray)

region_means = [r.mean_intensity for r in regions]
plt.hist(region_means, bins=20)

from sklearn.cluster import KMeans
model = KMeans(n_clusters = 5)
region_means = np.array(region_means).reshape(-1,1)

# fit model
model.fit(region_means)
print(model.cluster_centers_)

# predict labels
features_labels = model.predict(region_means)
features_labels
```

```
# label raster appropriately
classified_labels = segments_f.copy()
for features, region in zip(features_labels, regions):
    classified_labels[tuple(region.coords.T)]=features
plt.figure(figsize=(15,15))
plt.imshow(color.label2rgb(classified_labels, image=RGB_ha,
                           bg_label=0))

#save
driver = gdal.GetDriverByName("GTiff")
driver.Register()
output = driver.Create("2020.tif", cols, rows, 1, gdal.GDT_Float32)
output.SetGeoTransform(gt)
output.SetProjection(proj)
output.GetRasterBand(1).SetNoDataValue(-99999)
output.GetRasterBand(1).WriteArray(classified_labels)
output.FlushCache()
output = None
```

Appendix C

Classification Report, GAMA

C.1 Image Classification Report - RF

Table C.1: RF Classification Report, GAMA 1991

	Precision	Recall	F1-Score	Support
Built-up	0.96	0.97	0.96	132
Water	1	0.99	0.99	76
vegetation	0.95	0.95	0.95	104
Transition	0.82	0.79	0.81	39
Confusion Matrix				
	Built-up	Water	vegetation	Transition
Built-up	128	0	1	3
Water	0	75	1	0
vegetation	1	0	99	4
Transition	5	0	3	31
Overall Accuracy	**0.9487179**			
Kappa Score	**0.927807**			

Table C.2: RF Classification Report, GAMA 2002

	Precision	Recall	F1-Score	Support
Built-up	0.94	0.97	0.95	153
Water	1	1	1	60
Vegetation	0.94	0.93	0.93	111
Transition	0.85	0.82	0.83	77
Confusion Matrix				
	Built-up	Water	Vegetation	Transition
Built-up	148	0	1	4
Water	0	60	0	0
Vegetation	1	0	103	7
Transition	8	0	6	64
Overall Accuracy	**0.906074**			
Kappa Score	**0.906074**			

Table C.3: RF Classification Report, GAMA 2013

	Precision	Recall	F1-Score	Support
Built-up	0.97	0.93	0.95	100
Water	1	1	1	37
Vegetation	0.88	0.95	0.92	87
Transition	0.8	0.74	0.77	47
Confusion Matrix				
	Built-up	Water	Vegetation	Transition
Built-up	93	0	2	5
Water	0	37	0	0
Vegetation	0	0	83	4
Transition	3	0	9	35
Overall Accuracy	**0.915129**			
Kappa Score	**0.880653**			

Table C.4: RF Classification Report, GAMA 2022

	Precision	Recall	F1-Score	Support
Built-up	0.93	0.95	0.94	109
Water	1	0.98	0.99	64
Vegetation	0.98	0.99	0.99	117
Transition	0.86	0.8	0.83	45
Confusion Matrix				
	Built-up	Water	Vegetation	Transition
Built-up	104	0	0	5
Water	1	63	0	0
Vegetation	0	0	116	1
Transition	7	0	2	36
Overall Accuracy	**0.916417**			
Kappa Score	**0.933241**			

C.2 Image Classification Report - SVM

Table C.5: SVM Classification Report, GAMA 1991

	Precision	Recall	F1-Score	Support
Built-up	0.97	0.94	0.95	120
Water	0.99	1	0.99	97
Vegetation	0.97	0.93	0.95	102
Transition	0.71	0.84	0.77	32
Confusion Matrix				
	Built-up	Water	Vegetation	Transition
Built-up	113	0	1	6
Water	0	97	0	0
Vegetation	1	1	95	5
Transition	3	0	2	27
Overall Accuracy	**0.945869**			
Kappa Score	**0.924596**			

Table C.6: SVM Classification Report, GAMA 2002

	Precision	Recall	F1-Score	Support
Built-up	0.97	0.94	0.95	154
Water	1	1	1	57
Vegetation	0.96	0.93	0.95	120
Transition	0.81	0.89	0.84	70
Confusion Matrix				
	Built-up	Water	Vegetation	Transition
Built-up	145	0	1	8
Water	0	57	0	0
Vegetation	1	0	112	7
Transition	4	0	4	62
Overall Accuracy	**0.93765586**			
Kappa Score	**0.912842761**			

Table C.7: SVM Classification Report, GAMA 2013

	Precision	Recall	F1-Score	Support
Built-up	0.92	0.98	0.95	98
Water	0.97	1	0.99	35
Vegetation	0.9	0.85	0.87	92
Transition	0.75	0.72	0.73	46
Confusion Matrix				
	Built-up	Water	Vegetation	Transition
Built-up	96	0	1	1
Water	0	35	0	0
Vegetation	3	1	78	10
Transition	5	0	8	33
Overall Accuracy	**0.8929889**			
Kappa Score	**0.848752**			

Table C.8: SVM Classification Report, GAMA 2022

	Precision	Recall	F1-Score	Support
Built-up	0.96	0.88	0.92	104
Water	1	1	1	68
Vegetation	1	0.99	1	124
Transition	0.73	0.9	0.8	39
Confusion Matrix				
	Built-up	Water	Vegetation	Transition
Built-up	92	0	0	12
Water	0	68	0	0
Vegetation	0	0	123	1
Transition	4	0	0	35
Overall Accuracy	**0.94925373**			
Kappa Score	**0.929248506**			

Appendix D

Map comparing RF, SMV and SLIC K-Means

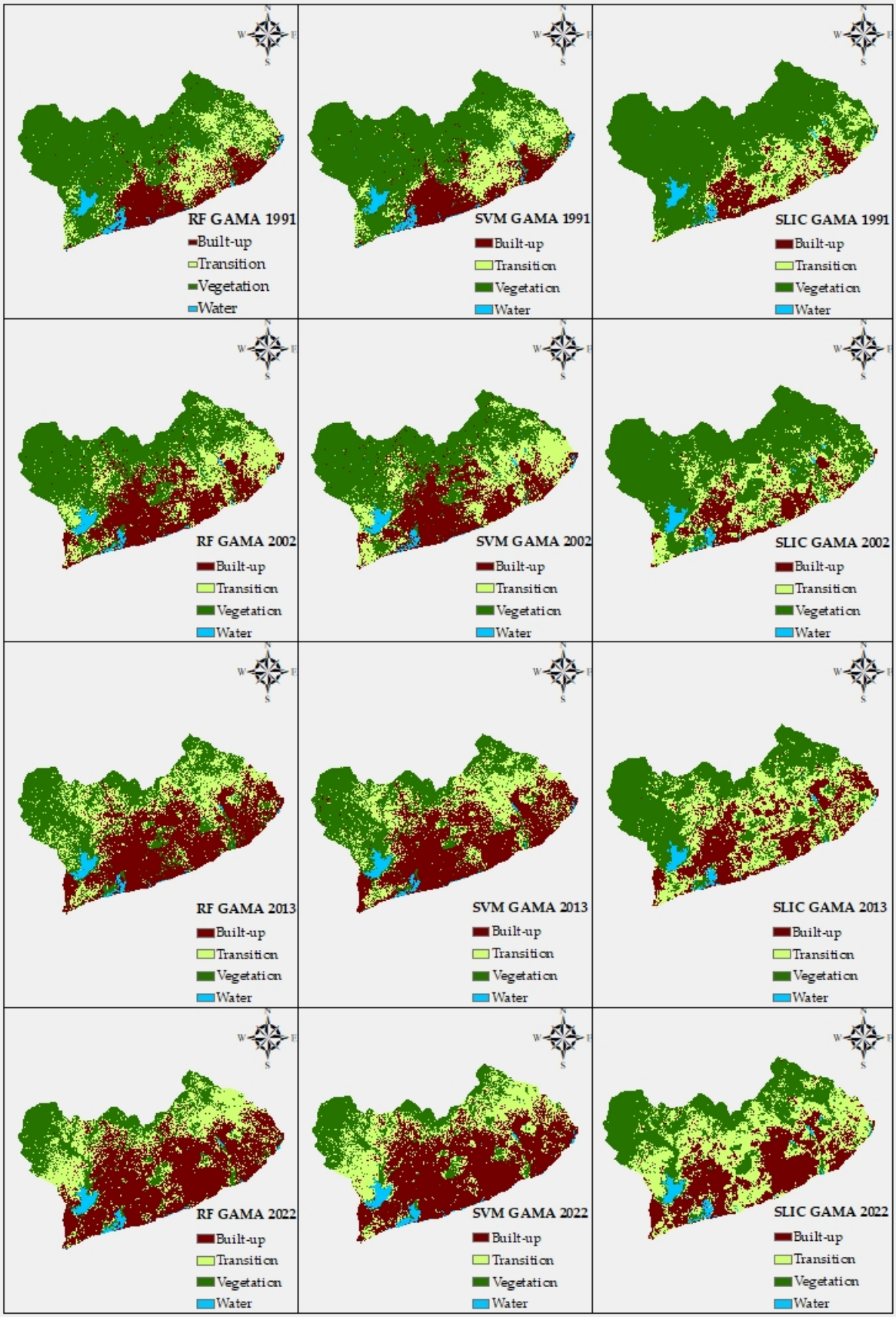

Figure D.1: Map comparing RF, SMV and SLIC K-Means

Appendix E

Fractal Dimension, Total Edge and Patch Number charts

E.1 Fractal Dimension, GAMA 1991, 2002, 2013 and 2023

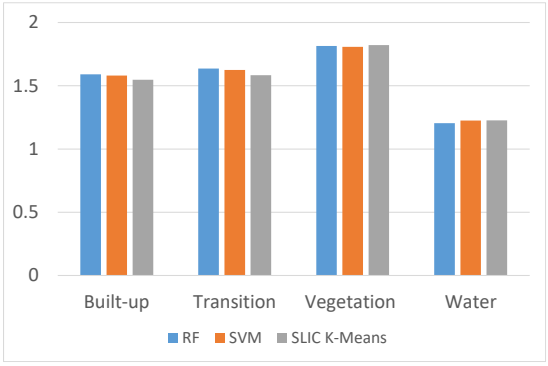

(a) FD GAMA 1991

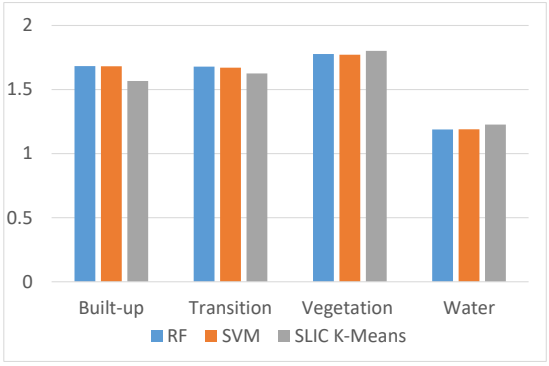

(b) FD GAMA 2002

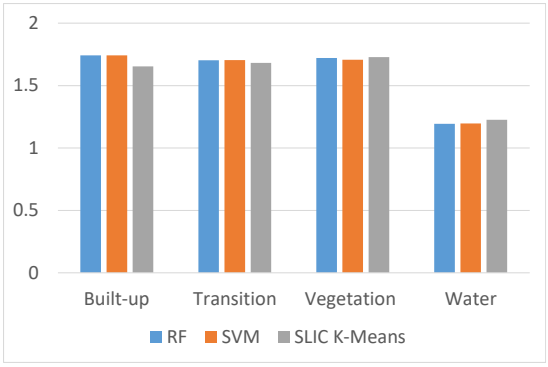

(c) FD GAMA 2013

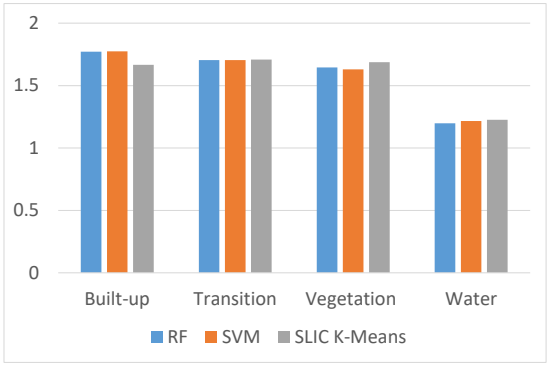

(d) FD GAMA 2022

Figure E.1: FD GAMA 1991, 2002, 2013 and 2022

E.2 Total Edge, GAMA 1991, 2002, 2013 and 2022

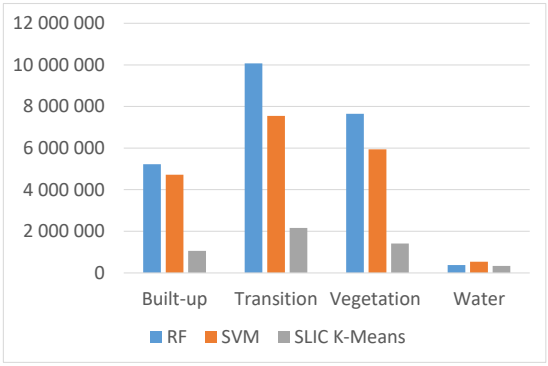

(a) TE GAMA 1991

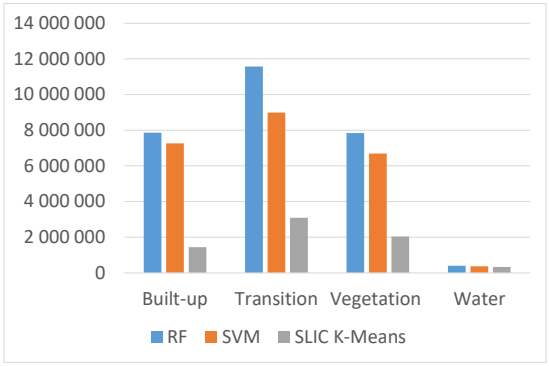

(b) TE GAMA 2002

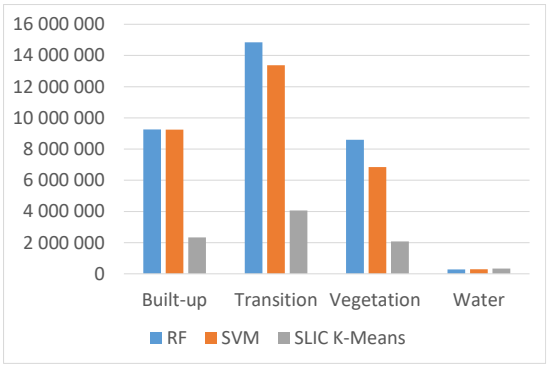

(c) TE GAMA 2013

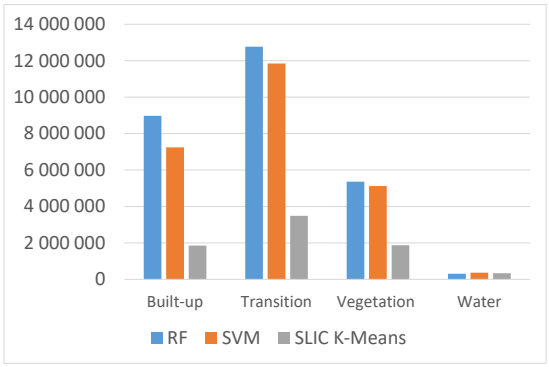

(d) TE GAMA 2022

Figure E.2: TE GAMA 1991, 2002, 2013 and 2022

E.3 Patch Number, GAMA 1991, 2002, 2013 and 2022

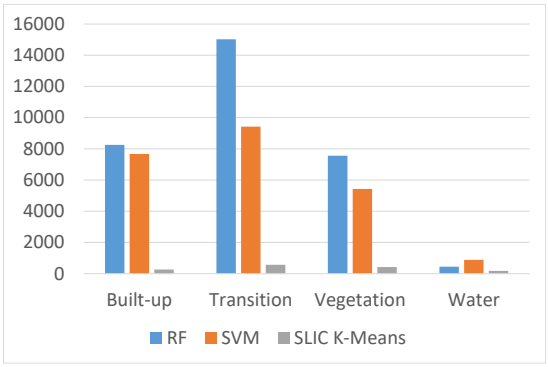

(a) PN GAMA 1991

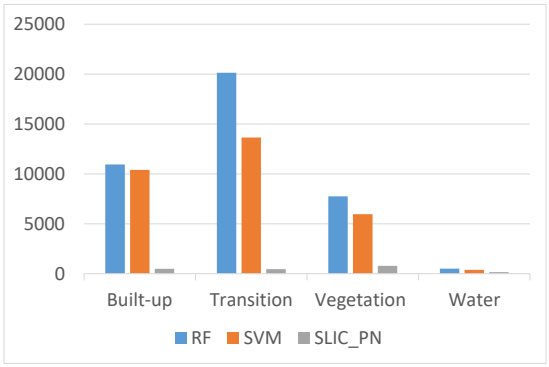

(b) PN GAMA 2002

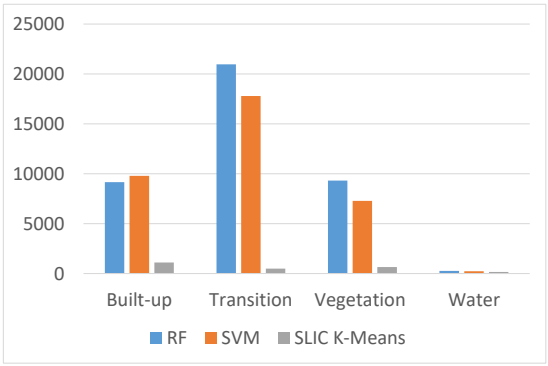

(c) PN GAMA 2013

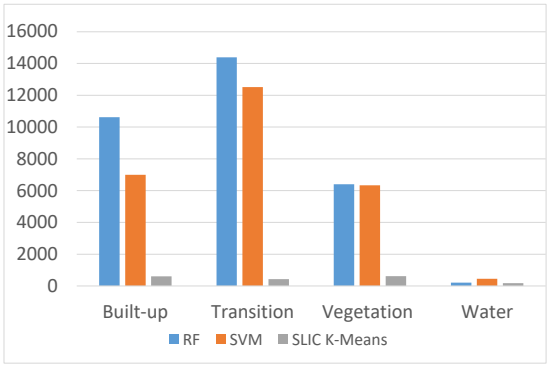

(d) PN GAMA 2022

Figure E.3: TE GAMA 1991, 2002, 2013 and 2022

Appendix F

Map of Section A, B and C

F.1 Section A, GAMA 1991, 2002, 2013 and 2022

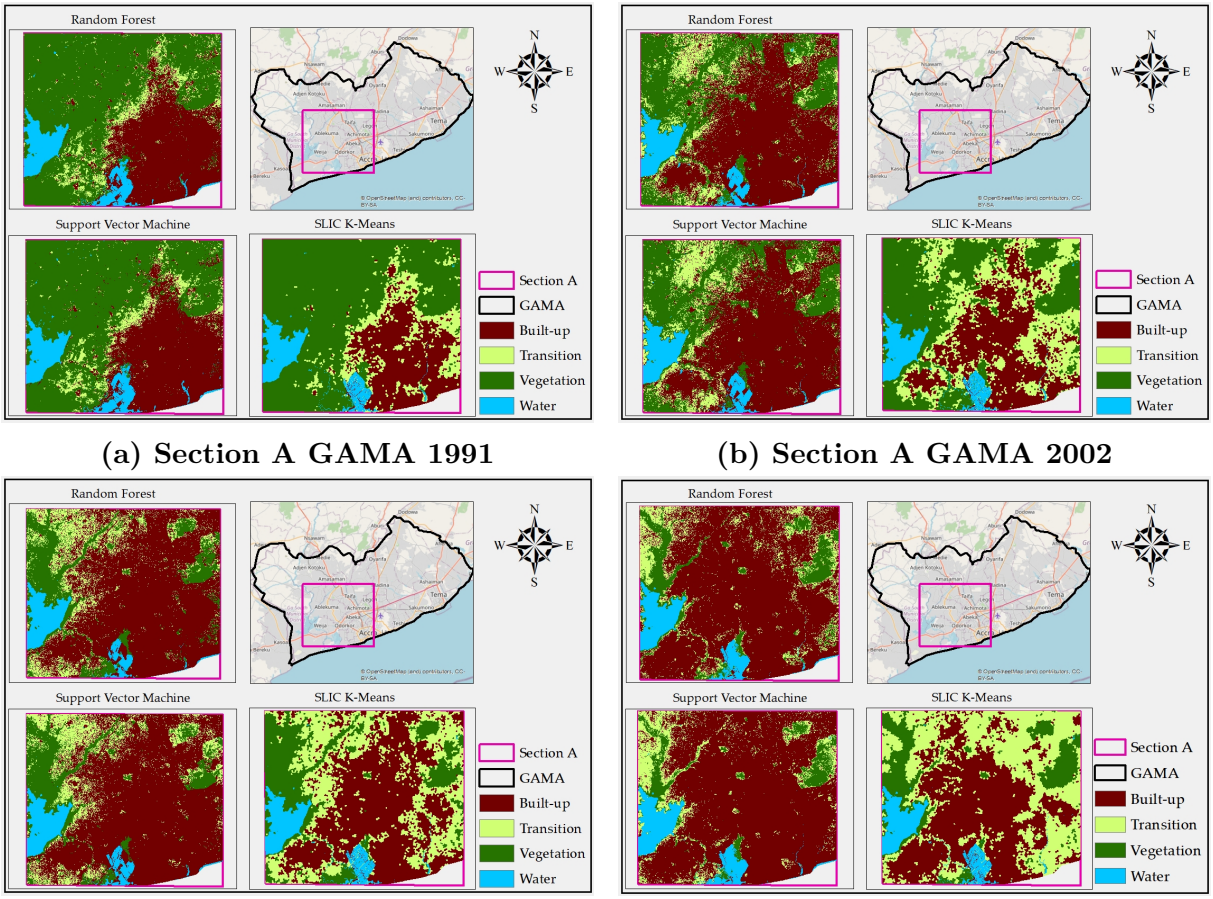

(a) Section A GAMA 1991

(b) Section A GAMA 2002

(c) Section A GAMA 2013

(d) Section A GAMA 2022

Figure F.1: FD GAMA 1991, 2002, 2013 and 2022

F.2 Section B, GAMA 1991, 2002, 2013 and 2022

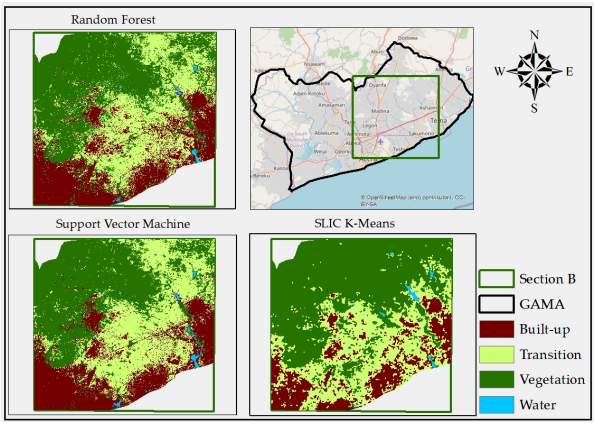

(a) Section B GAMA 1991

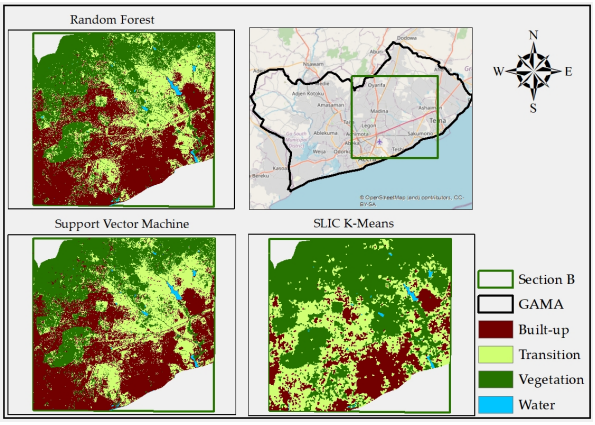

(b) Section B GAMA 2002

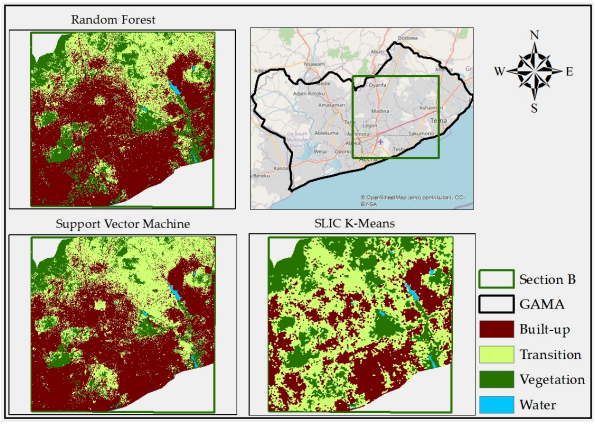

(c) Section B GAMA 2013

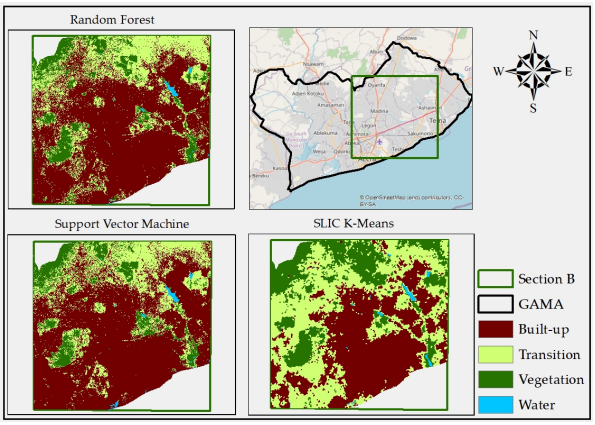

(d) Section B GAMA 2022

Figure F.2: FD GAMA 1991, 2002, 2013 and 2022

F.3 Section C, GAMA 1991, 2002, 2013 and 2022

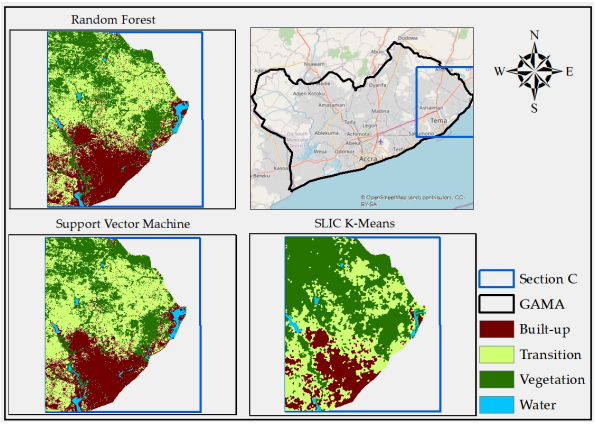

(a) Section C GAMA 1991

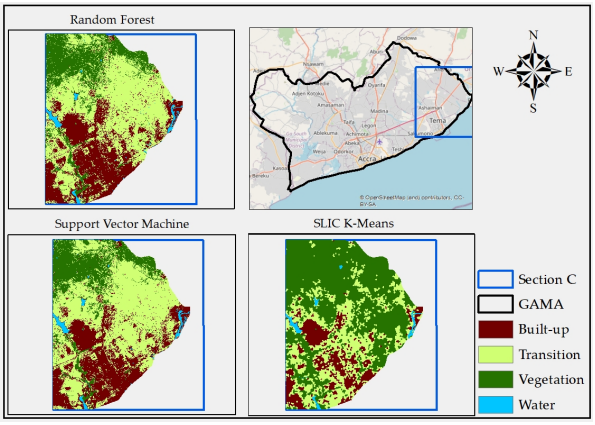

(b) Section C GAMA 2002

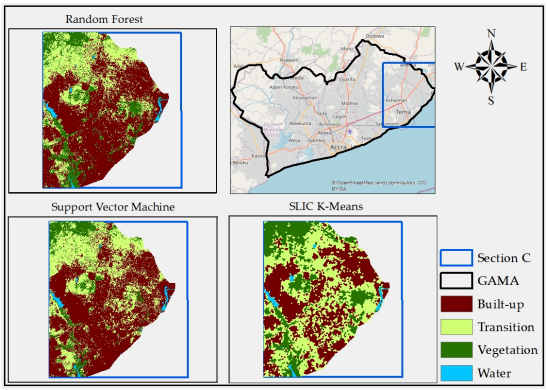

(c) Section C GAMA 2013

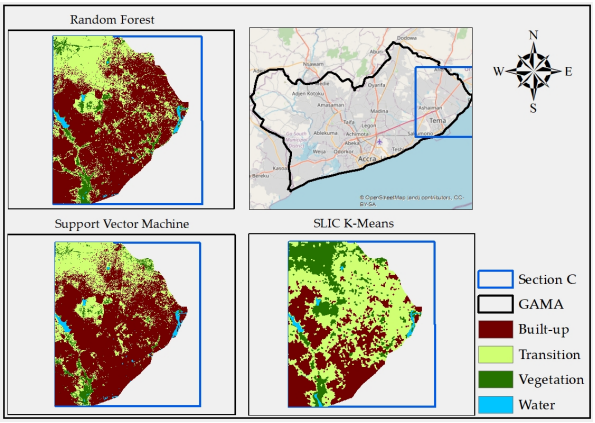

(d) Section C GAMA 2022

Figure F.3: FD GAMA 1991, 2002, 2013 and 2022

Appendix G

Fractal Dimension, Total Edge, and Patch numbers of Section A, Section B and Section C

Table G.1: FD, TE, and PN of Section A

Section A 1991									
Land Cover Type	**Random Forest**			**Support Vector Machine**			**SLIC K-Means**		
	FD	**TE**	**PN**	**FD**	**TE**	**PN**	**FD**	**TE**	**PN**
Built-up	1.693	1226610	1573	1.693	1157460	1563	1.661	392640	230
Transition	1.506	1758000	3787	1.465	1298160	2642	1.519	573240	303
Vegetation	1.822	1558740	1471	1.824	1278240	1113	1.833	359250	82
Water	1.414	170370	124	1.4	219480	294	1.435	221010	123
Section A 2002									
Land Cover Type	**Random Forest**			**Support Vector Machine**			**SLIC K-Means**		
	FD	**TE**	**PN**	**FD**	**TE**	**PN**	**FD**	**TE**	**PN**
Built-up	1.81	2499210	2591	1.813	2215080	2520	1.68	631170	203
Transition	1.618	2876580	6760	1.6	2169210	4444	1.675	1028010	335
Vegetation	1.722	2175930	2651	1.711	1925340	2167	1.72	601530	283
Water	1.388	150900	132	1.394	144090	105	1.435	221010	123
Section A 2013									
Land Cover Type	**Random Forest**			**Support Vector Machine**			**SLIC K-Means**		
	FD	**TE**	**PN**	**FD**	**TE**	**PN**	**FD**	**TE**	**PN**
Built-up	1.847	2435760	1729	1.848	2298930	1758	1.76	757110	262
Transition	1.624	2801400	5008	1.63	2647110	4345	1.694	1064010	327
Vegetation	1.608	1267170	1937	1.585	1143060	1649	1.595	449040	190
Water	1.436	123030	84	1.444	130380	70	1.436	221340	123
Section A 2022									
Land Cover Type	**Random Forest**			**Support Vector Machine**			**SLIC K-Means**		
	FD	**TE**	**PN**	**FD**	**TE**	**PN**	**FD**	**TE**	**PN**
Built-up	1.865	2067390	1170	1.869	1419840	726	1.765	686820	315
Transition	1.59	2498940	4243	1.576	1848180	3246	1.726	892470	217
Vegetation	1.499	785550	1023	1.419	579390	675	1.535	317520	96
Water	1.456	135720	80	1.413	167130	194	1.435	221010	123

Table G.2: FD, TE, and PN of Section B

Section B 1991									
Land Cover Type	**Random Forest**			**Support Vector Machine**			**SLIC K-Means**		
	FD	**TE**	**PN**	**FD**	**TE**	**PN**	**FD**	**TE**	**PN**
Built-up	1.719	3388650	4659	1.71	2968470	4318	1.63	667590	171
Transition	1.77	5519070	7327	1.761	3999390	4629	1.723	1271580	206
Vegetation	1.8	3616620	4646	1.784	2550420	3046	1.818	659910	134
Water	0.889	66360	128	0.986	131760	275	0.945	53280	51
Section B 2002									
Land Cover Type	**Random Forest**			**Support Vector Machine**			**SLIC K-Means**		
	FD	**TE**	**PN**	**FD**	**TE**	**PN**	**FD**	**TE**	**PN**
Built-up	1.791	3751020	4126	1.785	3428460	3692	1.623	726750	241
Transition	1.749	5137350	9019	1.743	4024410	6296	1.724	1522980	264
Vegetation	1.756	3177000	3887	1.745	2670120	2909	1.808	900510	164
Water	0.933	72510	121	0.948	72150	108	0.945	53280	51
Section B 2013									
Land Cover Type	**Random Forest**			**Support Vector Machine**			**SLIC K-Means**		
	FD	**TE**	**PN**	**FD**	**TE**	**PN**	**FD**	**TE**	**PN**
Built-up	1.858	4390020	4222	1.851	4096500	4101	1.717	1142670	295
Transition	1.747	5388300	8630	1.777	5114040	6835	1.801	1900170	291
Vegetation	1.648	2688030	4180	1.576	2009430	3242	1.652	837240	203
Water	0.913	42570	56	0.938	45870	61	0.945	53100	50
Section B 2022									
Land Cover Type	**Random Forest**			**Support Vector Machine**			**SLIC K-Means**		
	FD	**TE**	**PN**	**FD**	**TE**	**PN**	**FD**	**TE**	**PN**
Built-up	1.878	3821520	3869	1.883	3119580	2665	1.761	706290	148
Transition	1.733	4892070	5093	1.711	4286370	4597	1.771	1258230	151
Vegetation	1.545	1521300	2439	1.536	1364850	2173	1.629	578700	148
Water	0.923	43410	90	0.932	63600	132	0.945	53280	51

Table G.3: FD, TE, and PN of Section C

Section C 1991									
Land Cover Type	**Random Forest**			**Support Vector Machine**			**SLIC K-Means**		
	FD	**TE**	**PN**	**FD**	**TE**	**PN**	**FD**	**TE**	**PN**
Built-up	1.685	1671300	2917	1.671	1521750	2630	1.599	278310	74
Transition	1.793	3203190	3529	1.793	2570880	2073	1.713	733590	120
Vegetation	1.731	2279250	2703	1.706	1893480	2245	1.791	499020	87
Water	1.1	78540	122	1.167	137250	218	1.173	39540	8
Section C 2002									
Land Cover Type	**Random Forest**			**Support Vector Machine**			**SLIC K-Means**		
	FD	**TE**	**PN**	**FD**	**TE**	**PN**	**FD**	**TE**	**PN**
Built-up	1.698	1626000	2627	1.682	1456170	2002	1.555	319380	99
Transition	1.813	2495670	2472	1.817	2008680	1758	1.681	793590	178
Vegetation	1.622	1185840	1556	1.609	953190	1138	1.803	533070	90
Water	1.058	89370	176	1.08	76920	99	1.173	39540	8
Section C 2013									
Land Cover Type	**Random Forest**			**Support Vector Machine**			**SLIC K-Means**		
	FD	**TE**	**PN**	**FD**	**TE**	**PN**	**FD**	**TE**	**PN**
Built-up	1.833	2350590	1878	1.832	2490570	1940	1.724	638160	124
Transition	1.727	2812980	4786	1.755	2886390	4001	1.745	960420	171
Vegetation	1.58	1310910	2066	1.489	904770	1584	1.6	393450	128
Water	1.055	50280	44	1.08	53430	56	1.173	39330	8
Section C 2022									
Land Cover Type	**Random Forest**			**Support Vector Machine**			**SLIC K-Means**		
	FD	**TE**	**PN**	**FD**	**TE**	**PN**	**FD**	**TE**	**PN**
Built-up	1.847	1791300	1329	1.857	1773030	1341	1.699	452820	104
Transition	1.73	2188260	2547	1.716	2083740	2304	1.782	748050	95
Vegetation	1.361	511470	887	1.309	454530	902	1.572	328830	131
Water	1.092	57870	67	1.083	74460	99	1.173	39540	8

Appendix H

Fractal Dimension, Total Edge and Patch Number charts

H.1 Fractal Dimension, Section A 1991, 2002, 2013 and 2022

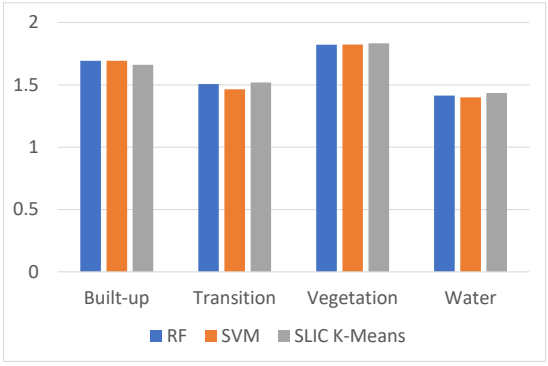

(a) FD Section A 1991

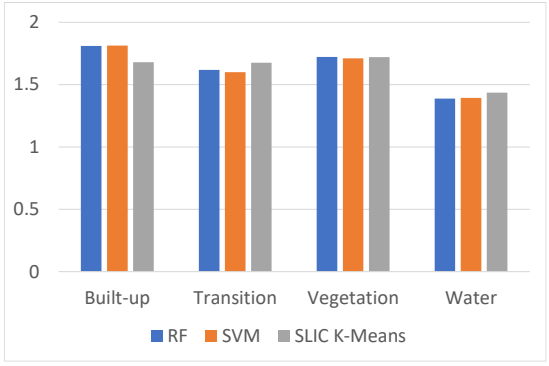

(b) FD Section A 2002

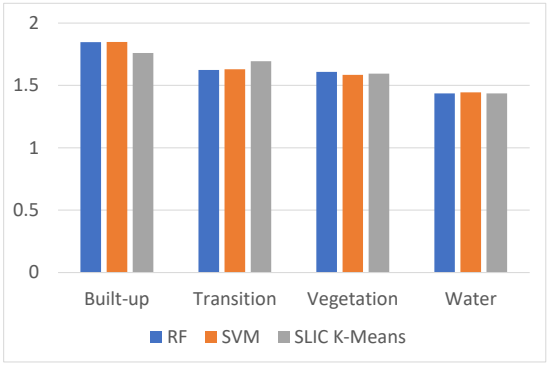

(c) FD Section A 2013

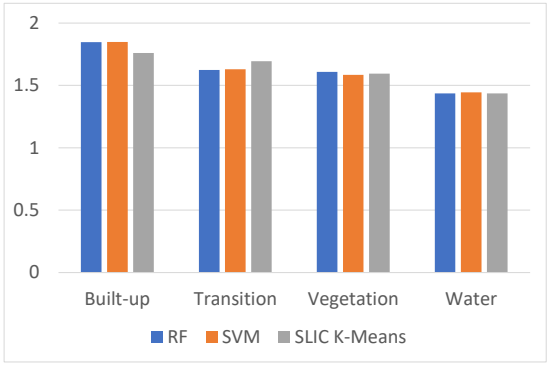

(d) FD Section A 2022

Figure H.1: FD, Section A 1991, 2002, 2013 and 2022

H.2 Total Edge, Section A 1991, 2002, 2013 and 2022

(a) TE Section A 1991

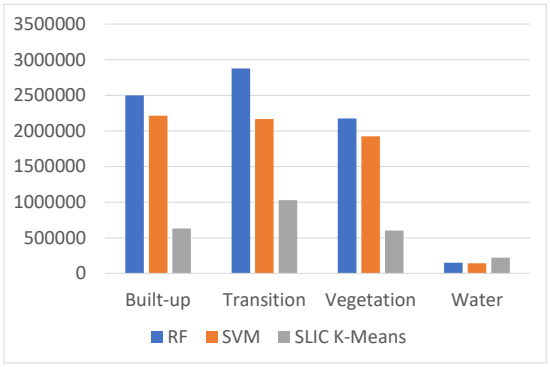

(b) TE Section A 2002

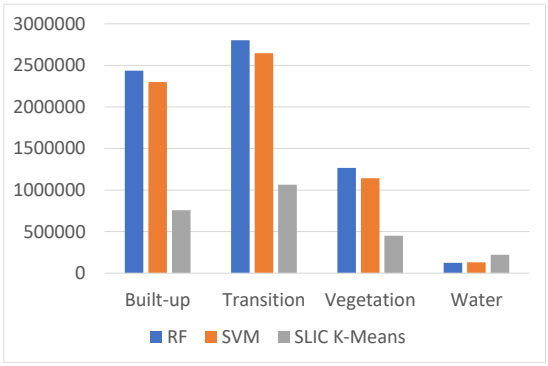

(c) TE Section A 2013

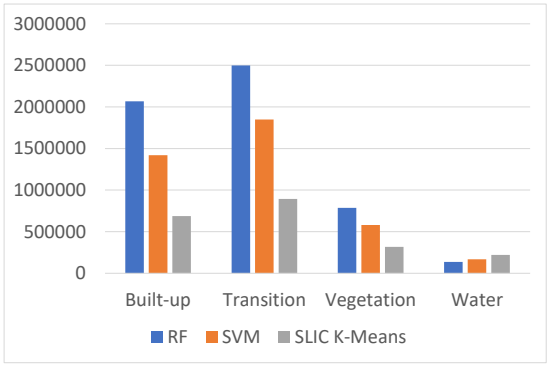

(d) TE Section A 2022

Figure H.2: TE, Section A 1991, 2002, 2013 and 2022

H.3 Patch Number, Section A 1991, 2002, 2013 and 2022

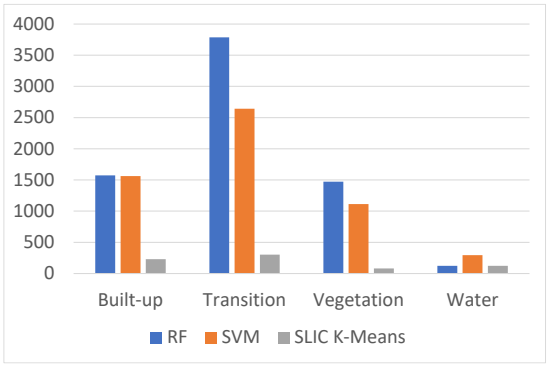

(a) PN Section A 1991

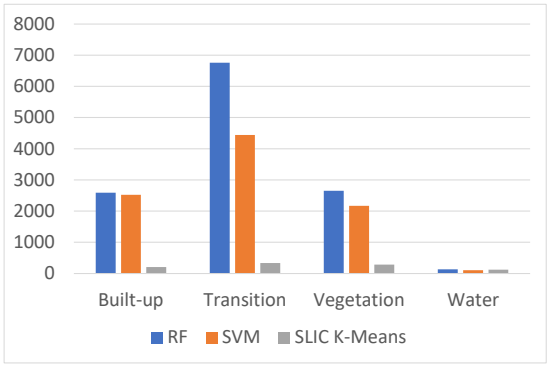

(b) PN Section A 2002

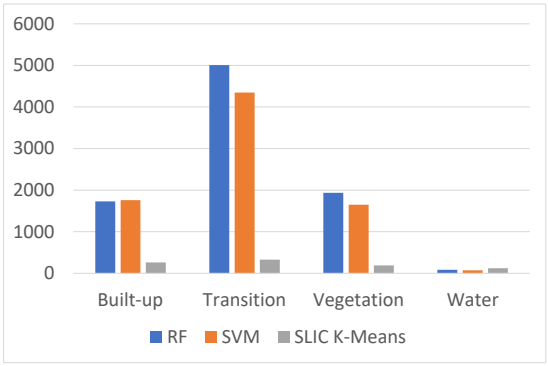

(c) PN Section A 2013

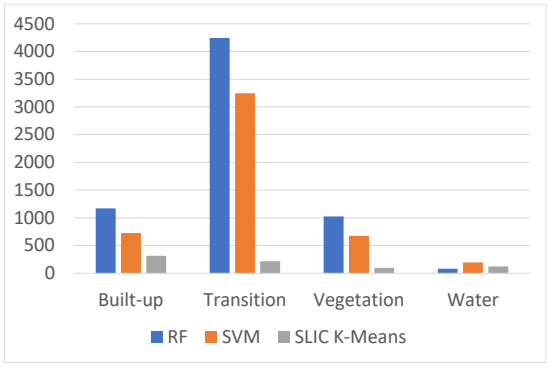

(d) PN Section A 2022

Figure H.3: PN, Section A 1991, 2002, 2013 and 2022

H.4 Fractal Dimension, Section B 1991, 2002, 2013 and 2022

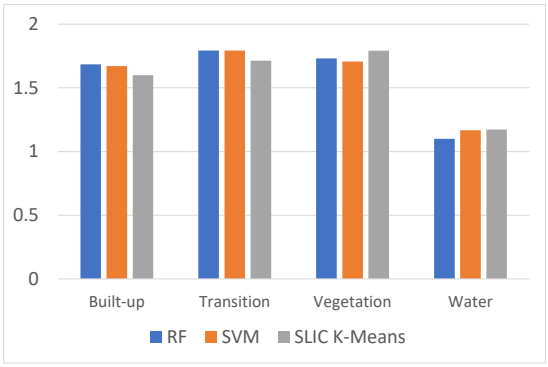

(a) FD Section A 1991

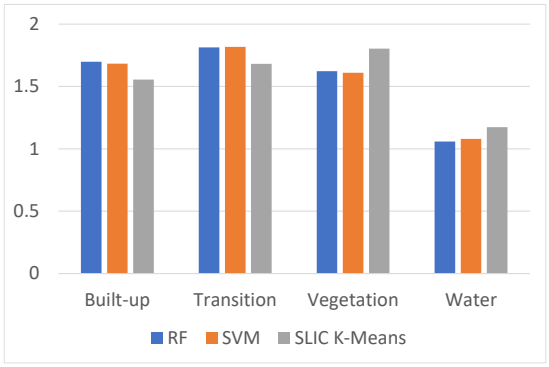

(b) FD Section B 2002

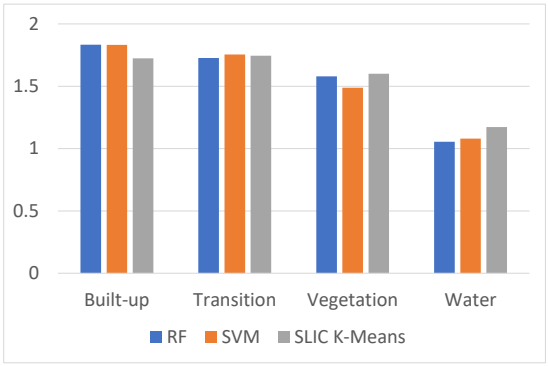

(c) FD Section B 2013

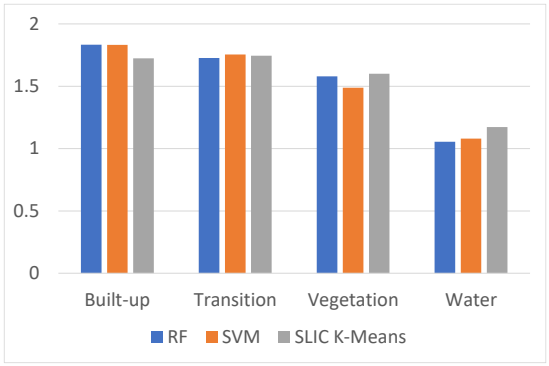

(d) FD Section B 2022

Figure H.4: FD, Section B 1991, 2002, 2013 and 2022

H.5 Total Edge, Section B 1991, 2002, 2013 and 2022

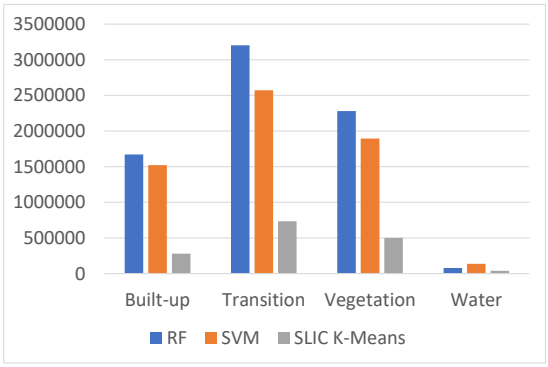

(a) TE Section B 1991

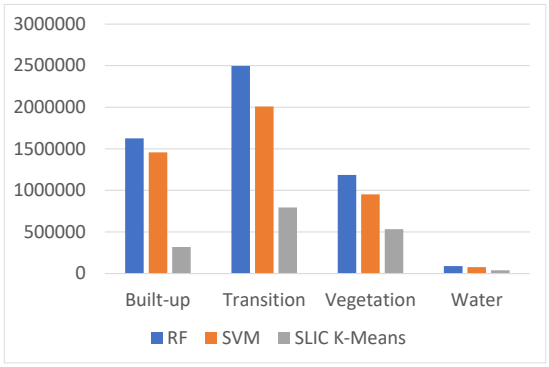

(b) TE Section B 2002

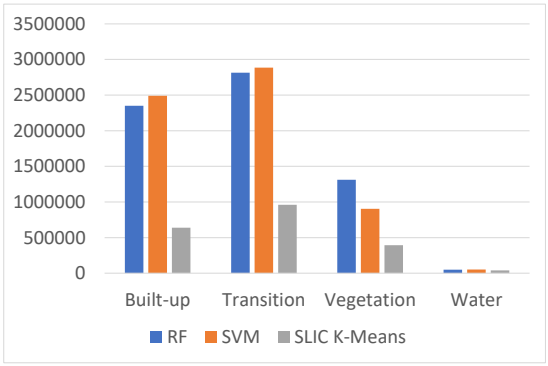

(c) TE Section B 2013

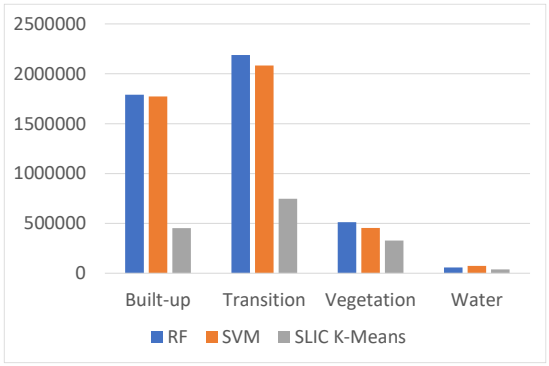

(d) TE Section B 2022

Figure H.5: TE, Section B 1991, 2002, 2013 and 2022

H.6 Patch Number, Section B 1991, 2002, 2013 and 2022

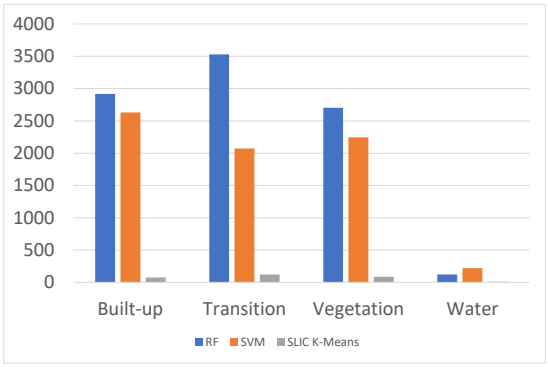

(a) PN Section B 1991

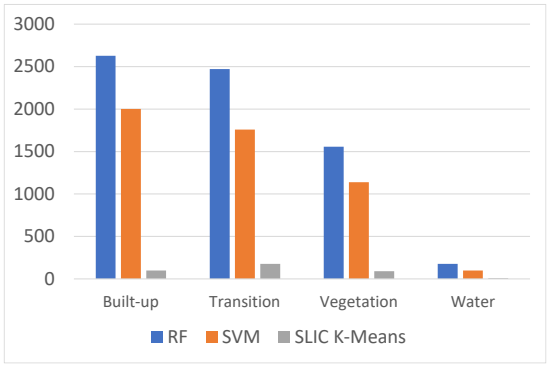

(b) PN Section B 2002

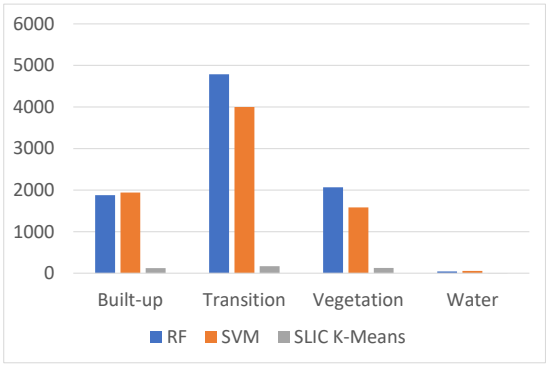

(c) PN Section B 2013

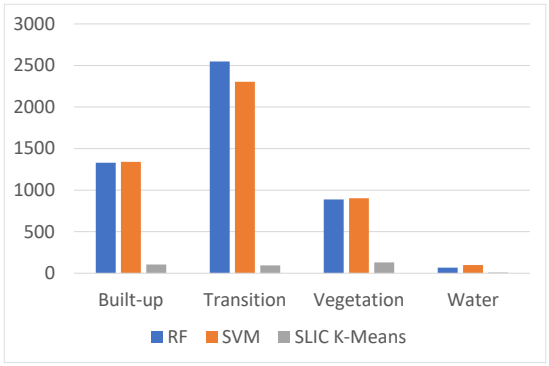

(d) PN Section B 2022

Figure H.6: PN, Section B 1991, 2002, 2013 and 2022

H.7 Fractal Dimension, Section C 1991, 2002, 2013 and 2022

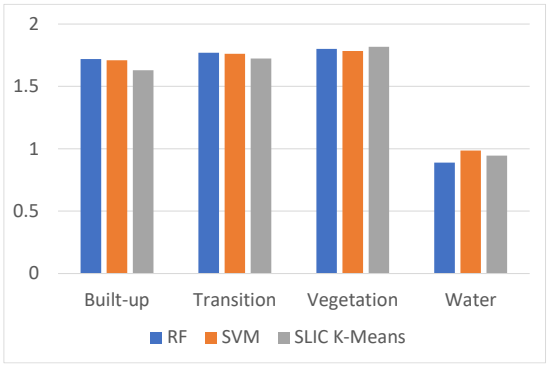

(a) FD Section C 1991

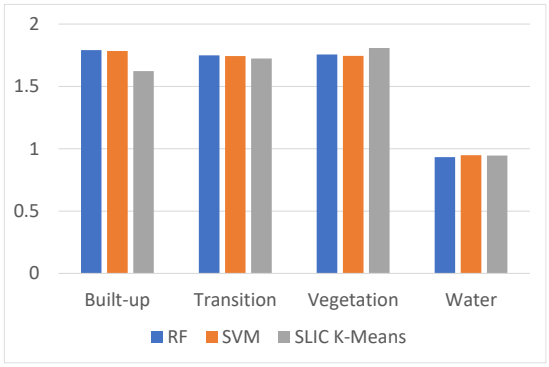

(b) FD Section C 2002

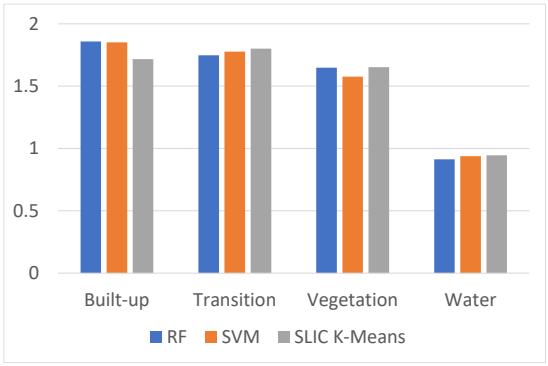

(c) FD Section C 2013

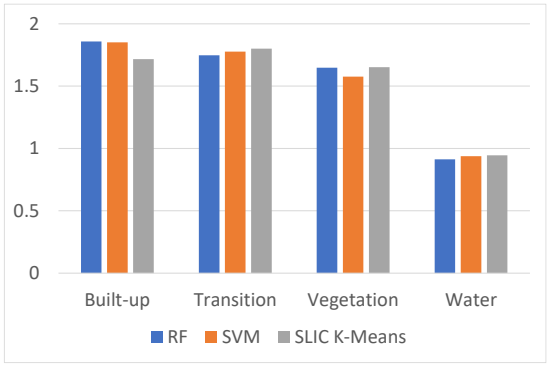

(d) FD Section C 2022

Figure H.7: FD, Section C 1991, 2002, 2013 and 2022

H.8 Total Edge, Section C 1991, 2002, 2013 and 2022

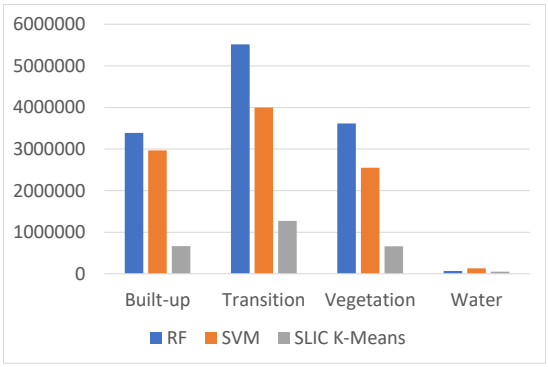

(a) TE Section C 1991

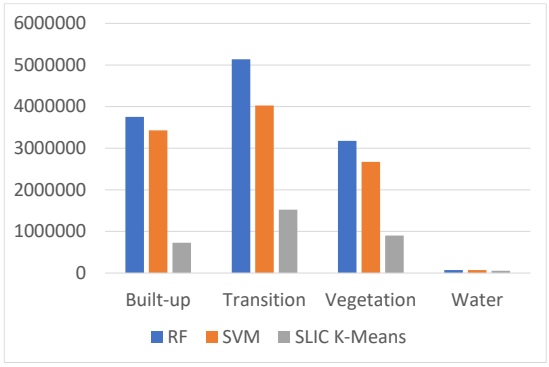

(b) TE Section C 2002

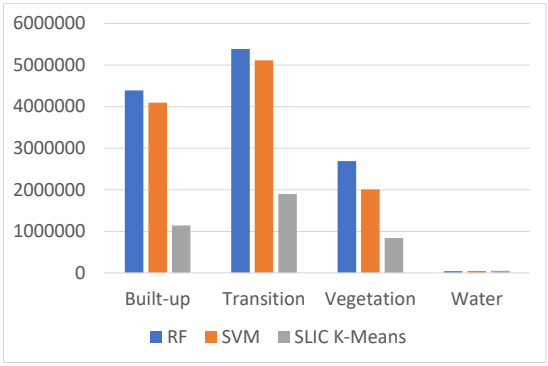

(c) TE Section C 2013

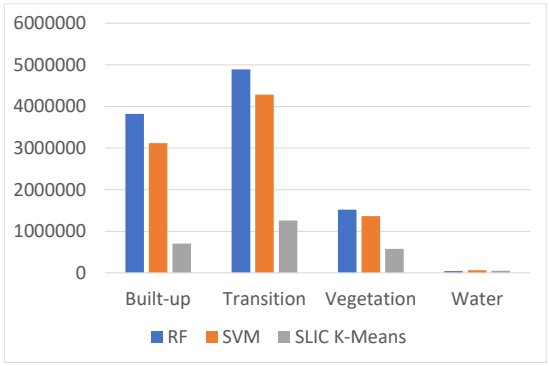

(d) TE Section C 2022

Figure H.8: TE, Section C 1991, 2002, 2013 and 2022

H.9 Patch Number, Section C 1991, 2002, 2013 and 2022

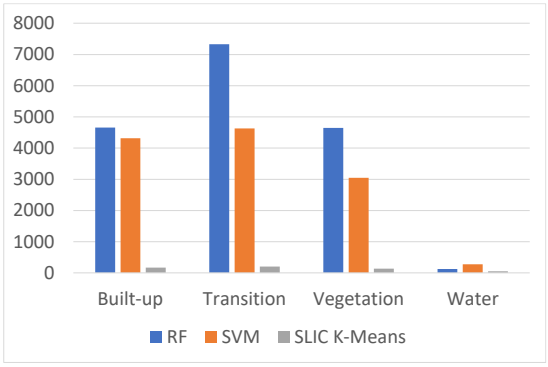

(a) PN Section C 1991

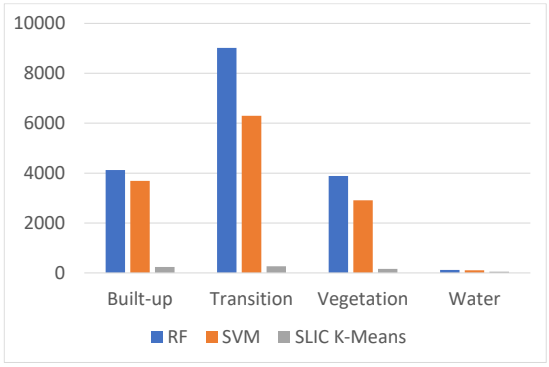

(b) PN Section C 2002

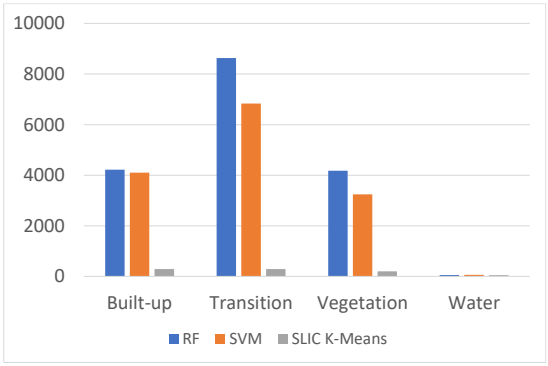

(c) PN Section C 2013

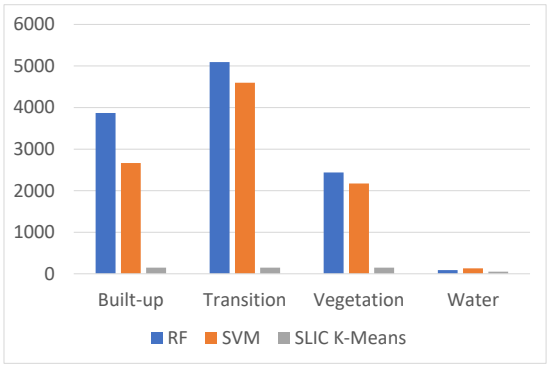

(d) PN Section C 2022

Figure H.9: PN, Section C 1991, 2002, 2013 and 2022

Appendix I

Box Counting Scaling Behavior

Table I.1: Scaling Behavior, 1991

Input: GAMA_1991_Built-up.tif-bin			
Method: Box counting			
Parameters: coef1.50000_min30.0000_max19710.0			
Dimension: 1.581			
b: 17.8991			
R^2: 0.999846			
p-value: 0.00000			
Confidence (95%): [1.569 - 1.592]			
Bootstrap confidence: [1.569 - 1.591]			
X	Y	Scaling behavior	Estim
30	288274	1.63046	274627
60	93108	1.63675	91819.8
90	47948	1.61778	48373.4
150	30983	1.60146	21575.1
240	9885	1.58245	10264.1
330	5972	1.56399	6204.7
510	3023	1.48426	3118.17
780	1609	1.53973	1593.09
1140	897	1.50344	874.464
1740	475	1.63964	448.202
2580	249	1.66786	240.481
3900	125	1.65102	125.156
5850	64	1.71676	65.9358
8760	32	1.28568	34.831
13140	19	1.58301	18.35
19710	10	NaN	9.66735

Table I.2: Scaling Behavior, 2002

Input: GAMA_2002_Built-up.tif-bin			
Method: Box counting			
Parameters: coef1.50000_min30.0000_max19710.0			
Dimension: 1.687			
b: 18.8766			
R^2: 0.999752			
p-value: 0.00000			
Confidence (95%): [1.672 - 1.703]			
Bootstrap confidence: [1.673 - 1.707]			
X	Y	Scaling behavior	Estim
30	499410	1.66195	507617
60	157819	1.67317	157609
90	80081	1.68091	79514.8
150	33933	1.68199	33581.8
240	15392	1.67325	15194.1
330	9034	1.68781	8877.77
510	4333	1.66035	4258.86
780	2140	1.71797	2079.36
1140	1115	1.7234	1096.05
1740	538	1.75968	536.971
2580	269	1.81643	276.242
3900	127	1.69017	137.561
5850	64	1.71676	69.4004
8760	32	1.28568	35.1141
13140	19	1.58301	17.7153
19710	10	NaN	8.93745

Table I.3: Scaling Behavior, 2013

Input: GAMA_2013_Built-up.tif-bin			
Method: Box counting			
Parameters: coef1.50000_min29.9900_max19703.4			
Dimension: 1.738			
b: 19.2875			
R^2: 0.999431			
p-value: 0.00000			
Confidence (95%): [1.714 - 1.762]			
Bootstrap confidence: [1.710 - 1.768]			
X	Y	Scaling behavior	Estim
29.99	677082	1.72432	645201
59.98	204913	1.75427	193443
89.97	100614	1.77393	95617.1
149.95	40655	1.80099	39354.8
239.92	17438	1.79361	17388.8
329.89	9850	1.79704	9998.21
509.83	4505	1.77629	4692.16
779.74	2118	1.77722	2242.33
1139.62	1079	1.70363	1159.54
1739.42	525	1.77423	556.085
2579.14	261	1.76249	280.445
3898.7	126	1.67067	136.774
5848.05	64	1.79539	67.6058
8757.08	31	1.20737	33.5164
13135.6	19	1.58301	16.5668
19703.4	10	NaN	8.1888

Table I.4: Scaling Behavior, 2022

Input: GAMA_2022_Built-up.tif-bin			
Method: Box counting			
Parameters: coef1.50000_min30.0000_max19710.0			
Dimension: 1.777			
b: 19.6394			
R2: 0.999238			
p-value: 0.00000			
Confidence (95%): [1.748 - 1.805]			
Bootstrap confidence: [1.744 - 1.816]			
X	Y	Scaling behavior	Estim
30	870550	1.79232	803585
60	251335	1.80916	234545
90	120691	1.82833	114126
150	47431	1.84189	46052.5
240	19957	1.84157	19981
330	11102	1.83564	11347.8
510	4993	1.83151	5236.44
780	2293	1.80934	2461.57
1140	1154	1.7698	1254.34
1740	546	1.82563	591.771
2580	266	1.7703	293.923
3900	128	1.78781	141.07
5850	62	1.56191	68.6425
8760	33	1.36157	33.5021
13140	19	1.58301	16.3016
19710	10	NaN	7.93214

Appendix J

Transition Variables

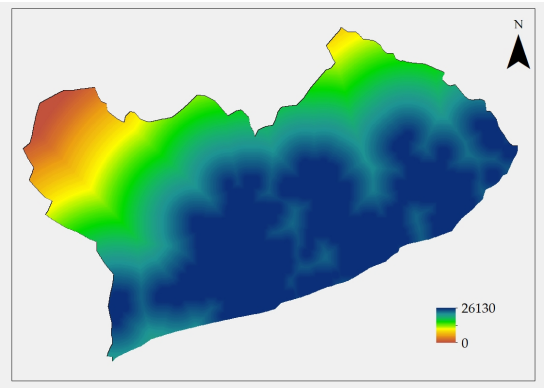

(a) Distance to CBD 2013

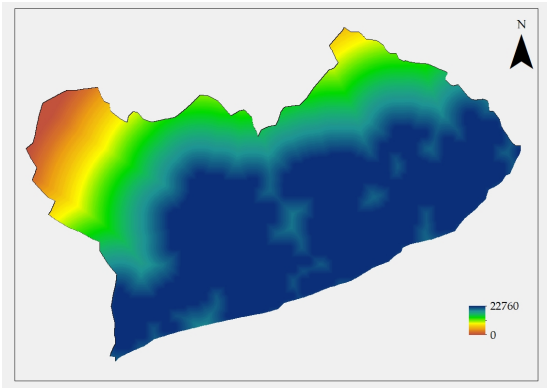

(b) Distance to CBD 2022

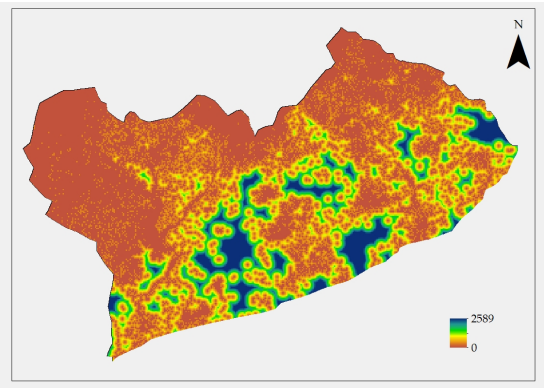

(c) Distance to vegetation 2013

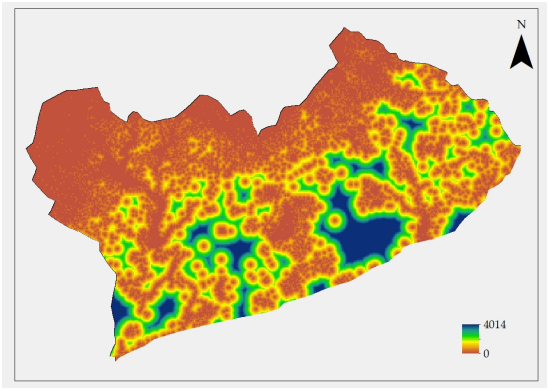

(d) Distance to vegetation 2022

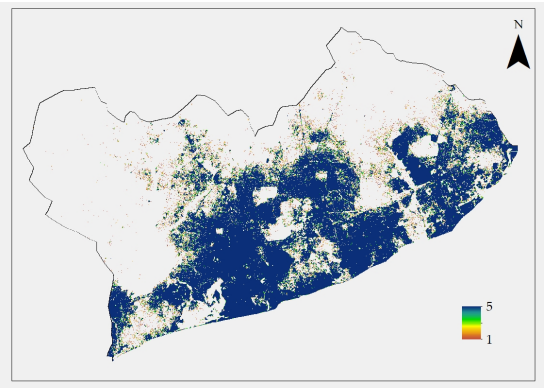

(e) Fractal Dimension 2013

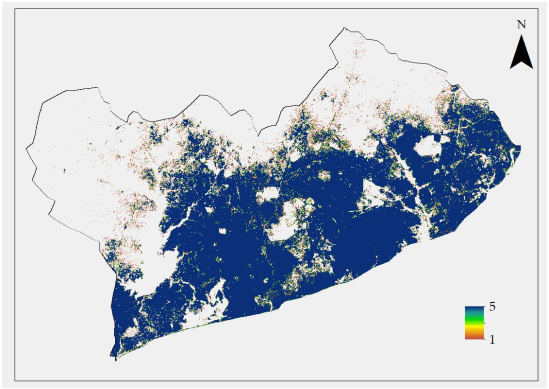

(f) Fractal Dimension 2022

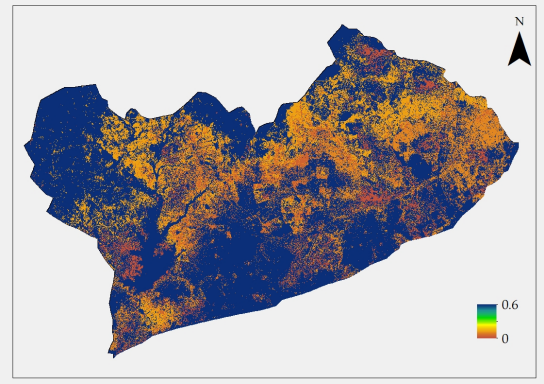

(g) Evlikelihood 2013

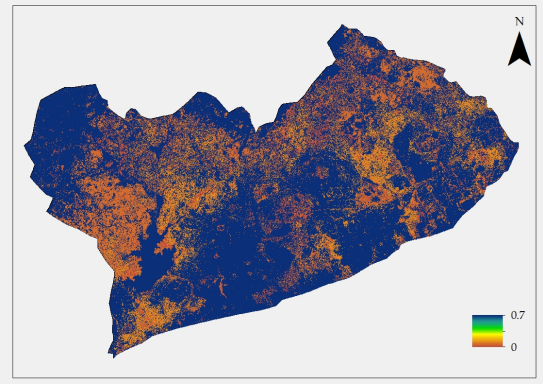

(h) Evlikelihood 2013

Figure J.1: Transition areas

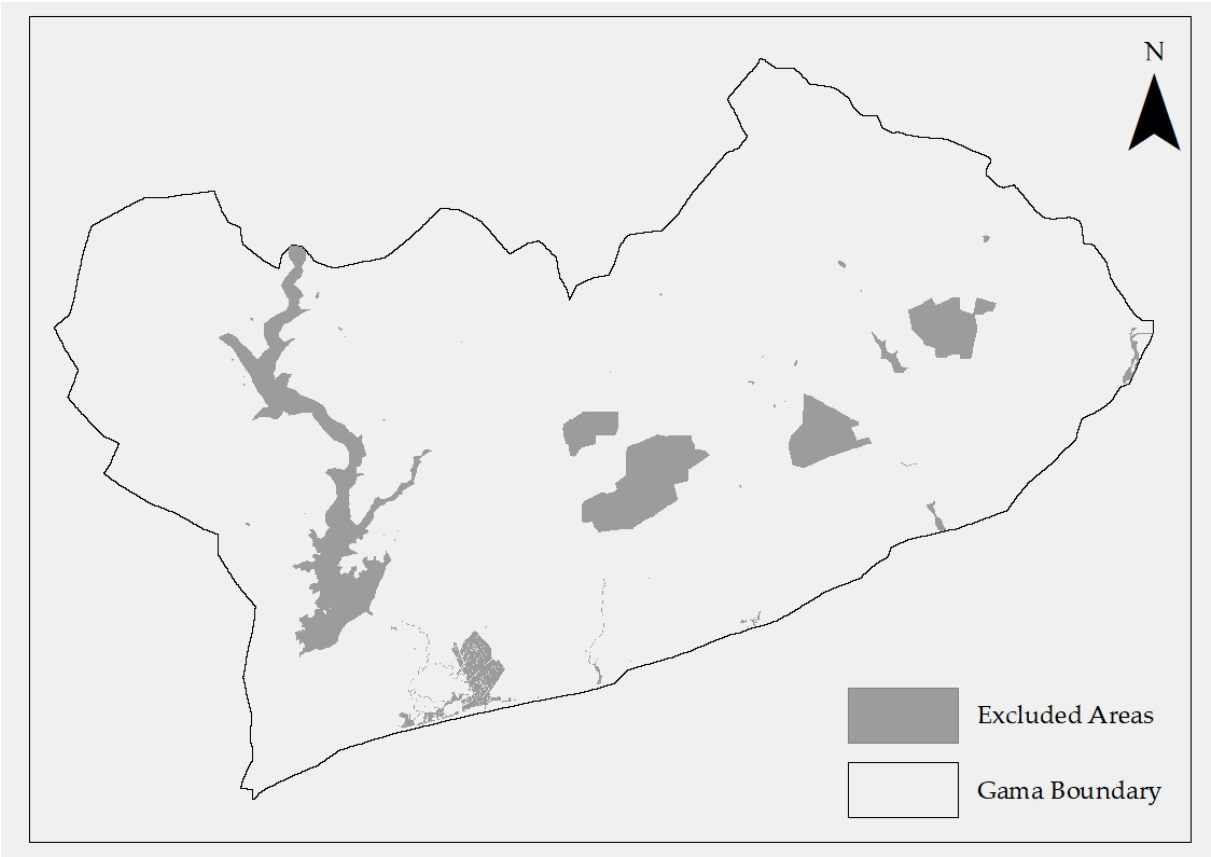

Figure J.2: Excluded areas

Appendix K

Land Change Modeler MLP Model Results

K.1 Urbanisation Sub model

1. General Model Information

    1) Input Files

Table K.1: Input Files

Independent variable 1	Evlikelihood2002-2013
Independent variable 2	2013_frac
Independent variable 3	Dist_veg_2013
Independent variable 4	Dist_urb_2013
Training site file	ch4_pred_Train_Urbanisation

    2) Parameters and performance

    3) Model Skill Breakdown by Transition and Persistence

2. Weights Information of Neurons across Layers

    1) Weights between Input Layer Neurons and Hidden Layer Neurons

    2) Weights between Hidden Layer Neurons and Output Layer Neurons

3. Sensitivity of Model to Forcing Independent Variables to be Constant

    1) Forcing a Single Independent Variable to be Constant

Table K.2: Parameters and performance

Input layer neurons	4
Hidden layer neurons	5
Output layer neurons	5
Requested samples per class	10000
Final learning rate	0
Momentum factor	0.5
Sigmoid constant	1
Acceptable RMS	0.01
Iterations	10000
Training RMS	0.2123
Testing RMS	0.2101
Accuracy rate	86.78%
Skill measure	0.8347

Table K.3: Model skill breakdown by transition and persistence

Class	Skill measure
Transition : Vegetation to Transition	0.8974
Transition : Vegetation to Built-up	1
Transition : Transition to Built-up	0.7916
Persistence : Vegetation	0.6285
Persistence : Transition	0.8555

Table K.4: Weights between input layer neurons and hidden layer neurons

Neuron	h-Neuron 1	h-Neuron 2	h-Neuron 3	h-Neuron 4	h-Neuron 5
i-Neuron 1	-15.0064	11.979	11.0173	-15.1586	0.5081
i-Neuron 2	-7.301	-1.0642	1.0303	4.4292	0.1636
i-Neuron 3	-1.6095	0.546	-1.6145	5.2878	-0.5174
i-Neuron 4	13.4831	-0.6015	-3.3518	-3.4671	3.0182

Table K.5: Weights between hidden layer neurons and output layer neurons

Neuron	o-Neuron 1	o-Neuron 2	o-Neuron 3	o-Neuron 4	o-Neuron 5
h-Neuron 1	9.7176	8.6705	-11.3918	5.5396	-11.822
h-Neuron 2	0.3593	-12.9177	2.5852	-3.6545	2.9132
h-Neuron 3	-6.803	-13.3452	-1.621	3.0526	4.9523
h-Neuron 4	-12.5072	6.7141	7.289	-10.7864	-0.2356
h-Neuron 5	-3.9226	-2.4568	-3.5285	-1.7953	-3.0675

Table K.6: Forcing a Single Independent Variable to be Constant

Model	Accuracy (%)	Skill measure	Influence order
With all variables	86.78	0.8347	N/A
Var. 1 constant	34.91	0.1863	1 (most influential)
Var. 2 constant	40.33	0.2542	2
Var. 3 constant	86.78	0.8347	4 (least influential)
Var. 4 constant	75	0.6876	3

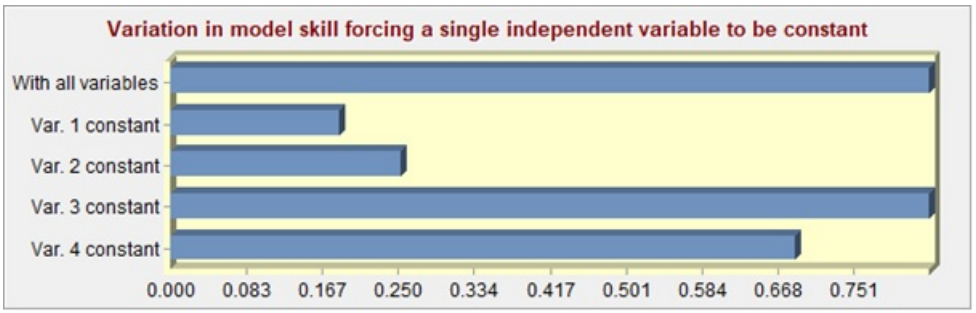

Figure K.1: Variation in model skill forcing a single independent variable to be constant

2. Forcing All Independent Variables Except One to be Constant

Table K.7: Forcing All Independent Variables Except One to be Constant

Model	Accuracy (%)	Skill measure
With all variables	86.78	0.8347
All constant but var. 1	40.1	0.2512
All constant but var. 2	34.91	0.1863
All constant but var. 3	20.04	0.0005
All constant but var. 4	12.07	-0.0991

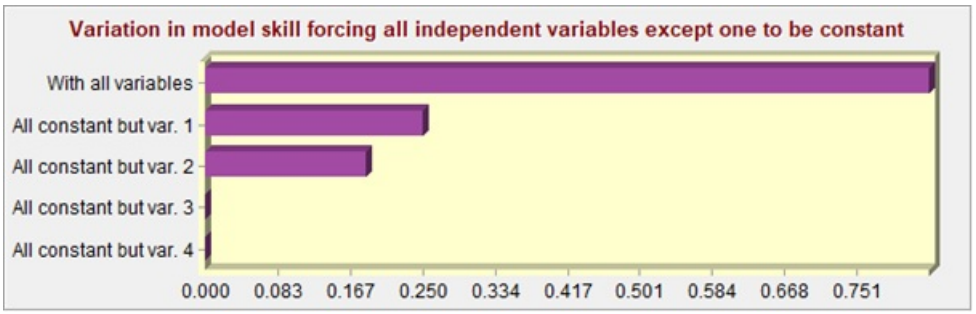

Figure K.2: Variation in model skill forcing all independent variables except one to be constant

3) Backwards Stepwise Constant Forcing

Table K.8: Backwards Stepwise Constant Forcing

Model	Variables included	Accuracy (%)	Skill measure
With all variables	All variables	86.78	0.8347
Step 1: var.[3] constant	[1,2,4]	86.78	0.8347
Step 2: var.[3,4] constant	[1,2]	75	0.6876
Step 3: var.[3,4,2] constant	[1]	40.1	0.2512

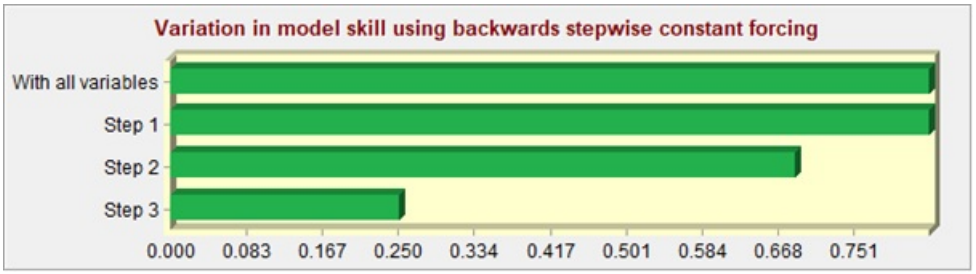

Figure K.3: Variation in model skill using backwards stepwise constant forcing

K.2 Afforestation Sub model

1. General Model Information

1) Input Files

Table K.9: Input Files

Independent variable 1	Evlikelihood2002-2013
Independent variable 2	2013_frac
Independent variable 3	Dist_veg_2013
Independent variable 4	Dist_urb_2013
Training site file	ch4_pred_Train_Afforestation

2) Parameters and performance

3) Model Skill Breakdown by Transition and Persistence

Table K.10: Parameters and Performance

Input layer neurons	4
Hidden layer neurons	4
Output layer neurons	4
Requested samples per class	10000
Final learning rate	0.0001
Momentum factor	0.5
Sigmoid constant	1
Acceptable RMS	0.01
Iterations	10000
Training RMS	0.229
Testing RMS	0.2285
Accuracy rate	86.15%
Skill measure	0.8154

Table K.11: Model Skill Breakdown by Transition and Persistence

Class	Skill measure
Transition : Transition to Vegetation	0.7494
Transition : Built-up to Transition	0.8083
Persistence : Transition	0.7856
Persistence : Built-up	0.9181

2. Weights Information of Neurons across Layers

1) Weights between Input Layer Neurons and Hidden Layer Neurons

Table K.12: Weights between input layer neurons and hidden layer neurons

Neuron	h-Neuron 1	h-Neuron 2	h-Neuron 3	h-Neuron 4
i-Neuron 1	-11.0221	-0.7713	7.4612	1.9104
i-Neuron 2	-0.9747	-0.6502	-3.482	0.3592
i-Neuron 3	2.8321	-7.5729	-15.206	16.2359
i-Neuron 4	1.2936	8.0707	15.7859	-17.795

2) Weights between Hidden Layer Neurons and Output Layer Neurons

3. Sensitivity of Model to Forcing Independent Variables to be Constant

1) Forcing a Single Independent Variable to be Constant

Table K.13: Weights between hidden layer neurons and output layer neurons

Neuron	o-Neuron 1	o-Neuron 2	o-Neuron 3	o-Neuron 4
h-Neuron 1	6.7628	8.6903	-10.0777	-8.3956
h-Neuron 2	3.2304	-3.892	0.5528	-7.6366
h-Neuron 3	-0.5786	-15.8761	7.8819	-5.2153
h-Neuron 4	-15.8032	0.1971	-6.4455	6.5447

Table K.14: Forcing a Single Independent Variable to be Constant

Model	Accuracy (%)	Skill measure	Influence order
With all variables	86.15	0.8154	N/A
Var. 1 constant	44.74	0.2632	1 (most influential)
Var. 2 constant	61.37	0.4849	2
Var. 3 constant	81.37	0.7516	3
Var. 4 constant	84.94	0.7992	4 (least influential)

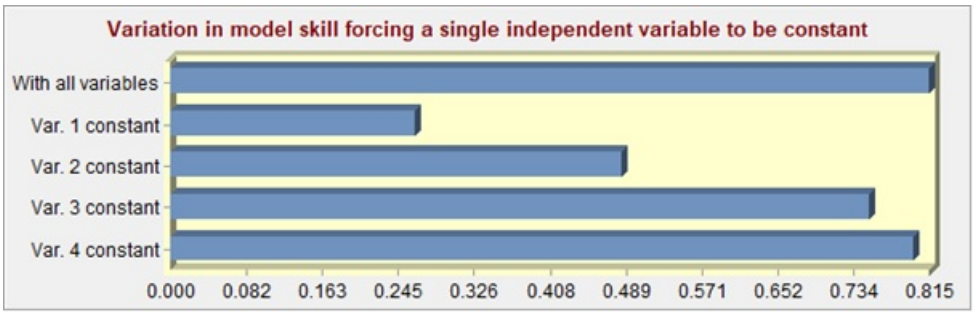

Figure K.4: Variation in model skill forcing a single independent variable to be constant

2. Forcing All Independent Variables Except One to be Constant

Table K.15: Forcing All Independent Variables Except One to be Constant

Model	Accuracy (%)	Skill measure
With all variables	86.15	0.8154
All constant but var. 1	50.03	0.3337
All constant but var. 2	44.39	0.2586
All constant but var. 3	37.12	0.1617
All constant but var. 4	38.12	0.1749

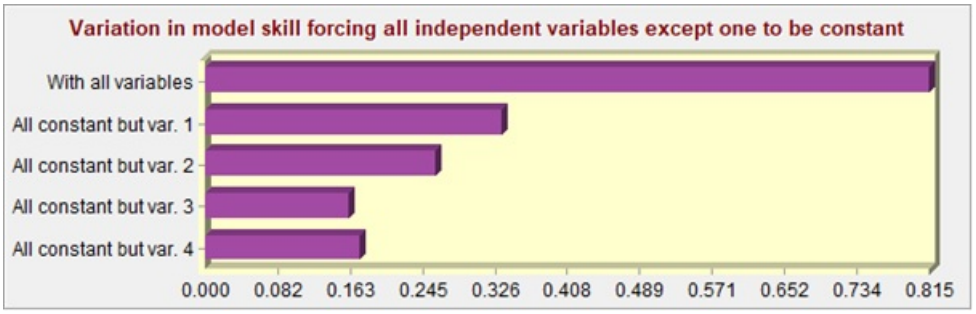

Figure K.5: Variation in model skill forcing all independent variables except one to be constant

3) Backwards Stepwise Constant Forcing

Table K.16: Backwards Stepwise Constant Forcing

Model	Variables included	Accuracy (%)	Skill measure
With all variables	All variables	86.15	0.8154
Step 1: var.[4] constant	[1,2,3]	84.94	0.7992
Step 2: var.[4,3] constant	[1,2]	69.4	0.592
Step 3: var.[4,3,2] constant	[1]	50.03	0.3337

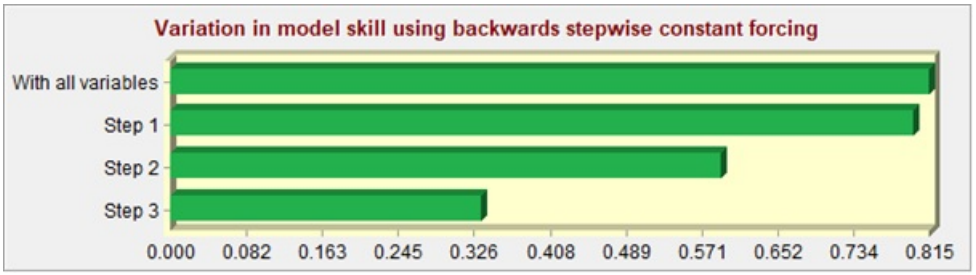

Figure K.6: Variation in model skill using backwards stepwise constant forcing

Appendix L

Classification Report, STMA

L.1 Image Classification Report - RF

Table L.1: Error Matrix, Random forest classification, STMA 2016

	Water	Vegetation	Built-up	Transition	User Accuracy
Water	33	0	1	0	0.970588235
Vegetation	0	103	0	1	0.990384615
High Urban	0	0	81	1	0.987804878
Low Urban	0	0	0	17	1
Producer Accuracy	1	1	0.987805	0.8947368	
Overall Accuracy	0.987342				
Kappa Coefficient	0.980932				

Table L.2: Error Matrix, Random forest classification, STMA 2022

	Water	Vegetation	Built-up	Transition	User Accuracy
Water	35	0	0	0	1
Vegetation	0	33	0	0	1
High Urban	0	0	131	0	1
Low Urban	0	0	1	82	0.987951807
Producer Accuracy	1	1	0.992424	1	
Overall Score	0.996454				
Kappa Coefficient	0.99469				